BOTSWANA INTERNATIONAL UNIVERSITY OF SCIENCE AND TECHNOLOGY, PALAPYE

FACULTY OF ENGINEERING AND TECHNOLOGY

DEPARTMENT OF MINING AND GEOLOGICAL ENGINEERING

A THESIS REPORT ENTITLED

SLOPE STABILITY MODELLING OF SLURRY DAMS THROUGH CONE PENETRATION DATA INTERPRETATION

BY

THUTO CHAMPI

(Student ID. No.: 12000399)

SUBMITTED IN FULFILLMENT OF THE REQUIREMENT FOR THE AWARD OF THE DEGREE OF MASTER OF ENGINEERING IN GEOLOGICAL ENGINEERING

THESIS SUPERVISORS

……	……
DR. RAHUL VERMA	**DR. GABATSOSWE LEBITSA**

PALAPYE, BOTSWANA

August 2021

DECLARATION

I declare that this thesis is my own work. It is being submitted for the degree of Master of Engineering in Geological Engineering in the Botswana International University of Science and Technology (BIUST), Palapye. It has not been submitted for any degree or examination in any other University.

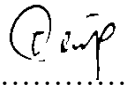

……

(Signature of candidate)

24th day of August, 2021

ABSTRACT

This research entailed slope stability analysis of Orapa Mine Slurry Dam 2, located at Orapa in Botswana. The Finite Element (FE) Strength Reduction Technique was used and findings were compared with results from three Limit Equilibrium analysis techniques, namely Bishop Simplified, Spencer's and Morgenstern-Price methods. The FE analysis was executed using the geotechnical engineering Rocscience software often referred to as Phase 2 or RS2 and the LE analysis was executed using the geotechnical engineering Rocscience software called Slide. The main purpose was to assess the geotechnical performance of the slurry dam. The LE and FE analysis results were observed to be in agreement with an average difference of 5.28%. The overall probability of failure of the slurry dam was zero and the overall reliability of the slurry dam has proven to be satisfactory with factors of safety for all slurry dam walls averaging at 1.65. The most important governing parameter in the stability of the dam is the friction angle. Furthermore, this study involved a regression analysis through supervised machine learning using MATLAB. This was to investigate any possible ways in which Cone Penetration Test (CPTu) measured variables (Cone Tip Resistance, Sleeve Friction, and Pore Pressure) could be predicted using depth as input into a function in a MATLAB workspace. The Gaussian Process Regression algorithm has responded well to the slurry dam data and produced good models.

ACKNOWLEDGEMENT

My foremost deepest gratitude and praises are directed towards the Almighty God, for his unlimited blessings, strength and divine wisdom during my entire Master of Engineering research journey.

My extreme gratitude is directed towards Botswana International University of Science and Technology (BIUST) for providing a conducive platform in carrying out my research and for supporting every aspect of my research journey.

My sincere appreciation towards my research supervisors, Drs. Rahul Verma and Gabatsoswe Lebitsa. They both provided invaluable guidance throughout this research and helped me put the presented ideas to higher levels above simplicity, into a solid and quality framework.

I am overwhelmed with all humbleness to acknowledge the Barclays FG Mogae Scholarship foundation in paying for my tuition fees and funding my research work. My research would not have been completed successfully without their financial support.

I am grateful to the management of Debswana Orapa Diamond Mine for giving me access to their slurry dams' data and allowing me to collect data from the slimes dam.

I also express my deepest gratitude to my parents for their support, prayers, love and for the sacrifices they made in raising me and preparing me for the future. I thank my husband and son for their continuous support and understanding in completing this research work.

TABLE OF CONTENTS

LIST OF FIGURES

LIST OF TABLES

LIST OF ABBREVIATIONS

A_c – Projected Area of the cone

ANCOLD – Australian National Committee of Large Dams

ASCII – American Standard Code for Information Interchange

CPT – Cone Penetration Test

CPTu – Cone Penetration Test with Pore Pressure Measurements

E – Elevation

ESCS – European Soil Classification System

EXP – Exponential

FD – Finite Difference

FE – Finite Element

FFNs – Feed Forward Neural Networks

f_s – Sleeve Friction

FS/FoS/FOS – Factor of Safety

GI – Gravity Increase

GLE – General Limit Equilibrium

GPR – Gaussian Process Regression

GPS – Global Positioning System

HD – Horizontal Distance

I_c – SBT Index

IMU – Inertial Measurement Unit

LE – Limit Equilibrium

LIDAR – Light Detection and Ranging

MAE – Mean Absolute Error

MATLAB – Matrix Laboratory

MSE – Mean Square Error

Phi – Internal Angle of Friction

q_s – Cone Tip Resistance

RI – Reliability Index

RLA – Regression Leaner App

RMSE – Root Mean Square Error

RQ – Rational Quadratic

R-Squared – Coefficient of Determination

SBT – Soil Behavior Type

SBTn – Normalised Soil Behavior Type

SRF – Strength Reduction Factor

SSR – Shear Strength Reduction

TIN – Triangulated Irregular Network

TSFs – Tailings Storage Facilities

u – Pore Water Pressure

USCS – Unified Soil Classification System

CHAPTER 1

INTRODUCTION

Products of the extractive industry are very important to modern society, they provide employment opportunities, social and community developments. On a global scale, their demand is very high and ever increasing. The extraction and processing of the targeted resources produce waste material end product such as tailings/slurry, and the volume is normally far in excess of the recovered resource. This type of waste is very hazardous to human life and the environment. Therefore, it is normally stored behind impoundments/dams. The role of these dams is to isolate this waste and stop them from entering freshwaters, destroying community developments and human life. These dams frequently fail due to a combination of multiple factors that can yield enormous amounts of waste into the environment (Kossoff, *et al*., 2014). These types of events are a serious threat, and best safety practices regarding these structures are very crucial.

Recent tailings dam failures and their causes have resulted in substantial research efforts focused on slope stability analysis of tailings dams (Thygesen, 2017). Significant research continues to focus on techniques of evaluating the stability of dams. Several scientists have used and evaluated different simulation approaches for modeling tailings dams and evaluating their stability. A large percentage of published work focuses on Limit Equilibrium (LE), Finite Element (FE) and Finite Difference (FD) slope stability analysis methods (Serra, 2013). Due to its simplicity, the LE method is very common and has been used extensively in engineering design. This method computes a single numerical value (called the Factor of Safety) to signify the safety margin of the slope, which simplifies the interpretation of the slope stability analysis results (Bolton *et al.*, 2010). However, researchers including Chiwaye and Stacey (2010) have observed that the LE evaluation approach is not entirely reliable as it underestimates the expected amount of failure unlike the FE and FD analytical methods. Due to recent technological advances, the use of FE and FD analysis methods continue to increase because of their capabilities in allowing for a wide range of geometries and gradually computing the stress and strain as well as the Factor of Safety on the model.

There are generally two approaches to carrying out an FE slope stability analysis. One approach is referred to as Gravity Increase (GI), it assumes that the external forces increase due to increase in gravity until the slope becomes unstable and equilibrium conditions no longer exist (Sternik, 2013). The second approach is referred to as Shear Strength Reduction (SSR), it decreases the strength parameters of a slope until it becomes unstable and equilibrium conditions no longer exist (deWolfe *et al.*, 2011). According to Sternik (2013), the GI method leads to a significant overestimation of a Factor of Safety as compared to the SSR method, as such the SSR method is the most frequently used for slope stability analysis.

There are several LE analysis methods in place, the most common is the method of slices which involve different approaches including the Ordinary Method of Slices (Fellenius Method), Bishop's Simplified/Modified, Janbu's Simplified, Janbu's generalized, Spencer, Chugh, Morgenstern-Price and Fredlund-Krahn (General Limit Equilibrium, GLE) (CIVILAX, 2018). All these approaches involve discretizing the sliding mass into slices and considering equilibrium conditions through equations involving all forces acting on each slice with different assumptions on inter-slice forces and moments. They differ according to assumptions that are put in place in terms of interslice forces for each approach. An approach which considers all contributing forces in the analysis may be more reliable than those that do not, but when used properly this approach will yield very similar factors of safety as those that ignore some of the forces. Therefore, the best approach is to use more than two methods and comparing the results to verify the accuracy and precision in the results obtained (Mosquera *et al.*, 2013).

Generally, Limit Equilibrium methods are based on force and moment equilibrium while Finite Element use stress-strain relationships to define model behaviour. Researchers such as Memon (2018) have concluded that these two methods are a powerful combination in any form of analysis. They observed that each method has its own merits and limitations, furthermore, when used comparatively the results are generally in good agreement.

Cone Penetration Testing with pore pressure measurements (CPTu) has been used extensively in research. It has been relied upon as a powerful, time and cost efficient in-situ technique (Steiner *et al.*, 2015). Application of CPTu in Tailings Storage Facilities (TSFs) has been to delineate their complex stratigraphy. According to Lunne *et al.* (1997), CPTu has exceptional logging capabilities in delineating complex stratigraphy of TSFs. Its

usefulness in slope stability is mainly for construction of geometric sections of slopes being analysed. CPTu measurements and Machine Learning have been the most powerful combination for some researchers providing convenience in data analysis and prediction. For example, Reale *et al.* (2018) presented capabilities of Artificial Neural Networks in automating soil classification according to USCS and ESCS guidelines using sleeve friction and cone resistance as inputs. Their approach proved adept in predicting such classifications correctly classifying almost 90% of soils while incorrectly classified soils were only partially misclassified. Yabbarova *et al.* (2021) discussed the use of Machine Learning in predicting of CPTu test data. They concluded that the use of Machine Learning allows to obtain realistic CPTu parameters based on the physical and mechanical properties of soils of various genesis.

1.1 Study Area – Orapa Diamond Mine Slurry Dams

Orapa Diamond Mine is one of the world's largest diamond mine and Debswana's oldest operating mine (De Beers UK, 2019). It is situated at Orapa (Figure 1.2), in eastern Botswana's Boteti sub-district, 240 km west of Francistown. This mine covers a surface area of 118 km^2 and has been ranked as the world's largest open pit diamond mine by area. The Orapa kimberlite was discovered in 1967, just one year after Botswana gained independence and it was declared a major discovery by DeBeers geologists the following year. Operations began in 1971 and capacity expanded to double its production in 2000. Emplacement of this kimberlite has been estimated to be of Late-Cretaceous. It intruded basement and cover rocks of the Orapa Mine area. Local basement is also consisting of igneous rocks that intruded the area during Archean while local cover rocks consist of volcano-sedimentary rocks (Chiomba, 2015). Table 1.1 represents a stratigraphic model of the country rocks that host the Orapa kimberlite with age increasing from top to bottom.

Table 1.1 Stratigraphic Model of Orapa Mine Area Country Rock (Chiomba, 2015)

Lithology Name	Lithological Code	Stratigraphic Formation	Geological Age	Thickness (m)
Basalt	BAS	Stormberg	Jurassic	95 - 110
Sandstone	SST	Ntane	Triassic	20 - 60
Red Mudstone	RMST	Mosolotsane	Triassic	55 - 110
Laminated Sandstone	LSST	Mosolotsane	Triassic	55 - 110
Mudstone	MST	Thlabala	Triassic	90
Carbonaceous Mudstone	CMST	Tlapana	Permian	155
Arkosic Sandstone	ASST	Mea	Permian	15 - 20
Granite-Gneiss	GG	Basement	Archaean	N/A

Figure 1.1 shows the top part of Karoo deposits exposed on the mining face of Orapa mine open pit. Exposure of Orapa mine country rocks remains poor due to a thick layer of unconsolidated Kalahari sediments covering the area. Current information and understanding on the stratigraphy is derived from mapping exposed mining faces and logging data from boreholes.

Figure 1.1 Exposed Karoo Deposits on Orapa Mine Open Pit Mining Face (Photo by Orapa Mine)

Orapa mine was established on the A/K1 kimberlite which is among a cluster of kimberlite bodies known as the Orapa kimberlite cluster. Currently operating as a conventional open pit, it is expected to transition to an underground mining operation after almost doubling its current depth. This mine is a significant producer of diamonds in Botswana and continues to contribute to economic growth (De Beers UK, 2019).

Orapa Diamond Mine Slurry Dams (Figure 1.2 (B)) were constructed for the Orapa 2000 project intended in increasing the tonnage output. They were constructed for containment of a large amount of slurry that would be produced during execution of the expansion project. Slurry dam 1 is the older of the two dams, it was commissioned in 2000. Ever since it's commissioning, there were issues and challenges with regard to its safety and stability (Jones & Wagener, 2016).

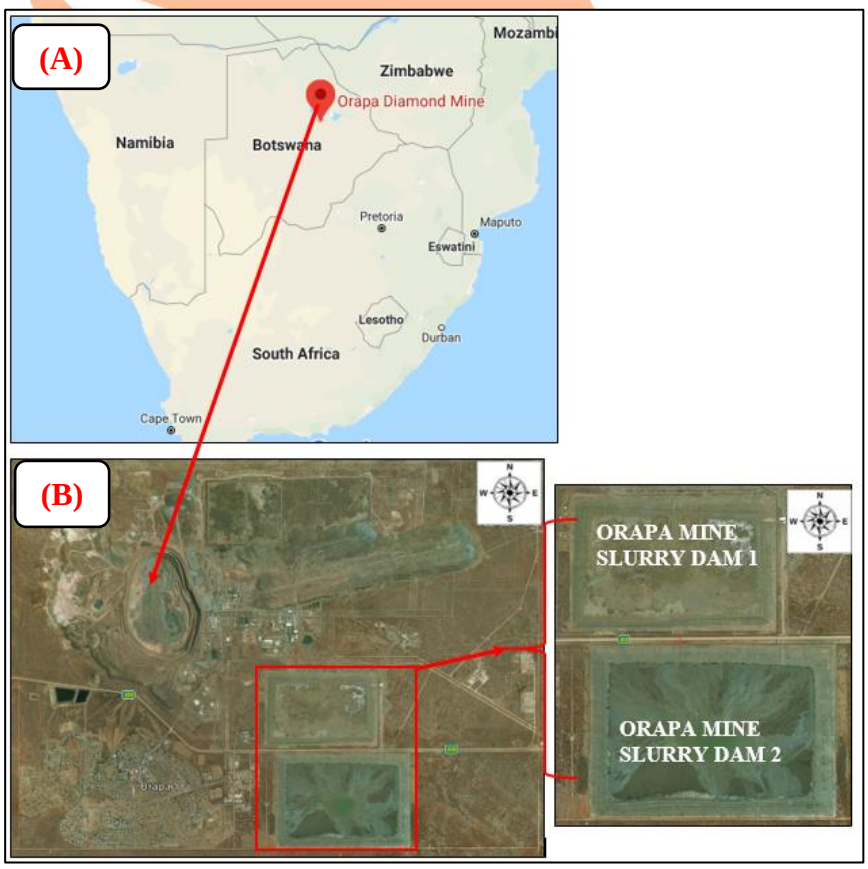

Figure 1.2 (A) Location of Botswana in Southern Africa; (B): Mining Area and Two Slurry Dams

Orapa mine was currently operating two plants (Plant 1 and Plant 2) for the processing of ore and extraction of diamonds. These plants have inter-connected disposal systems for the three waste streams (tailings, grits and slimes) (Table 1.2).

Table 1.2 Orapa Mine Waste Streams (Golder Associates Africa (Pty) Ltd, 2002)

Waste Product	**Aspect**	**Plants 1 and 2**
Tailings	Grading	1.6 – 25 mm
	Deposition	End tipped on tailings dump.
Grits	Grading	0.3 – 1.6 mm
	Deposition	To tailings dam or pumped to slurry dams with slime for cyclone split and deposition.
Slimes	Grading	< 0.3 mm
	Deposition	To slimes dam or pumped to slurry dams with grits for cyclone split and deposition.

The capacity of Slurry Dam 1 was too small to accommodate the tonnage of waste delivered from both plants. This led to poor geotechnical performance, including piping through dam body, a high rate of rise (the required freeboard could not be maintained) led to high pore water pressure and hence dam instability. By May 2001 this came as a matter of urgency at the mine regarding slurry disposal. To reduce the risks inherent in its continued operation another slurry dam was proposed as a matter of urgency. The new dam was referred to as Slurry Dam 2, as shown in Figure 1.3, it was positioned to the south of Slurry Dam 1, within the constraints of the main access road to the north, the AK-20 pipe to the east, the mining concession boundary to the south and the existing township to the west. A part of this dam called a temporary dam was commissioned in July 2002, by this time Slurry Dam 1 needed to rest and consolidate (Golder Associates Africa (Pty) Ltd, 2002).

However, for the lifespan of these two dams to increase, the tonnage of waste had to be split between the two. In summary, the tonnage of waste delivered form either plant 2 only or both plant 1 and plant 2 was opposed to the recommended maximum tonnage to be delivered to the two dams. Figure 1.4 summarises the events of slurry deposition from 2015 until 2019, only one month chosen from each year. As seen from the graph and according to the design recommendations by Golder Associates Africa (Pty) Ltd (2002), the target amount of slurry delivered from both plants was 680,000 tons per day (500,000 tons from Plant 2 and 180,000 tons from Plant 1).

Figure 1.3 Orapa Mining Concession Boundary (Google, 2020)

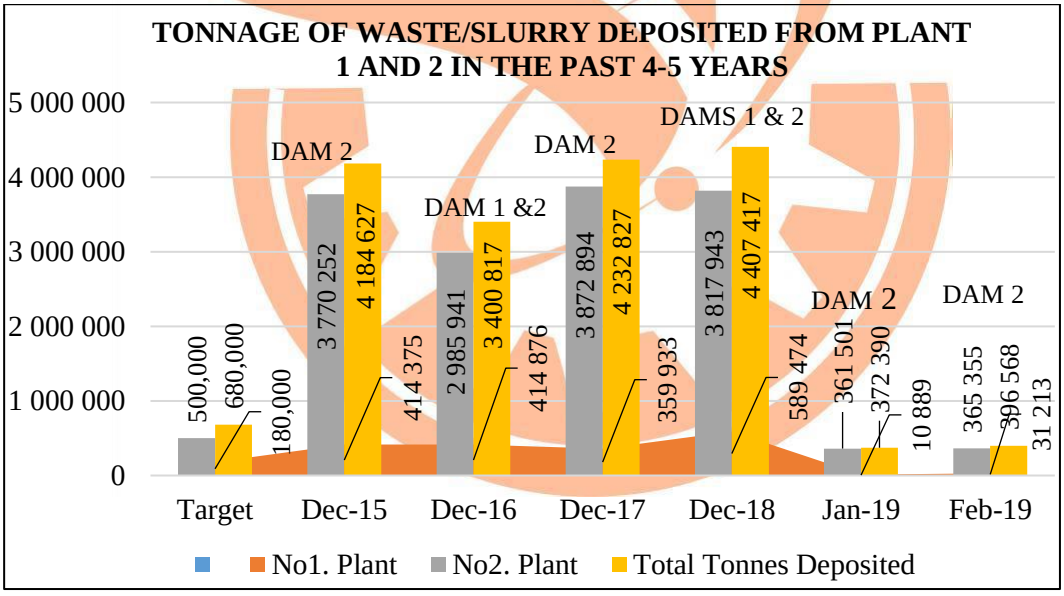

Figure 1.4 Tonnage of Slurry Deposited from December 2015 until Feb 2019

However, every year this recommended maximum amount was exceeded except in 2019 when the use of these two dams was minimal. For example:

i. In December 2015 slurry from both plants was deposited in Dam 2 alone, the total tonnage delivered (colored yellow) in a day was 3,504,627 tons (4,184,627 – 680,000 tons) in excess of the recommended maximum amount.

ii. In December 2018, tonnage output per day from the two plants was split between the two dams, and the total tonnage deposited was 3,727,417 tons (4,407,417 - 680,000 tons) in excess of the recommended maximum amount.

This high amount of slurry deposited over the years could only mean that the dams were over-stressed during this period. Therefore, caution had to be practiced and priority had to be given to stability analysis and monitoring.

Slurry Dam 2 was the basis of this study, it was chosen based on the implications concerning its location, size, history and the topography of the area. As shown in Figure 1.3, this dam is located in the confines of roads and residences, therefore in the event of failure the impact will be higher as compared to Slurry Dam 1, as many lives will be lost including property damage. In terms of topography, Golder Associates Africa (Pty) Ltd. (2002) discovered that the Orapa area is dipping in a north-easterly direction, therefore in an event of failure the slurry would flow in the same direction. This implies that, the north and east dam walls may be overstressed due to high seepage as the slurry will tend to segregate towards the north-eastern corner. Therefore, a slope stability analysis of each dam wall was necessary to determine the overall safety margin of this slurry dam.

This research incorporates a slope stability analysis of Orapa Mine Slurry Dam 2, located at Orapa in Botswana. The FE Strength Reduction Technique was used and findings were compared with results from three LE analysis techniques; namely Bishop Simplified, Spencer's and Morgenstern-Price methods. The FE analysis was executed using the geotechnical engineering Rocscience software often referred to as RS2 2019 and the LE analysis was executed using the geotechnical engineering Rocscience software called Slide 2019. In addition, a regression analysis was carried out to assess any possible relationship between the slurry dam wall depth and the variables measured through a Cone Penetration Test with pore pressure measurements (Piezocone test or CPTu). The piezocone test yielded Cone Tip Resistance, Sleeve Friction and Pore Pressures with respect to depth. This analysis was carried out through the use of machine learning tools in MATLAB R2020a. It was meant to assess any suitable model that could allow a prediction of the CPTu variables with depth as an input variable.

1.2 Statement of the Problem

Orapa Diamond Mine Slurry Dam 2 is located in eastern Botswana's Boteti sub-district. It was constructed in support of the expansion project which was meant to increase tonnage output in 2000. This dam measures approximately 1.30 km (North-South) by 2.04 km (East-West), giving a total area of 265 ha (Golder Associates Africa (Pty) Ltd, 2002). Slurry Dam 2 is currently at an elevation of ~1000 meters above mean sea level. Attributed to inappropriate deposition practices in its history, it has been undergoing instability problems caused by a high rate of rise, seepage and erosion. A northeasterly dipping topography of the area also caused segregation towards the northeastern corner causing distress on the east and north dam walls in terms of stability (Jones & Wagener, 2016).

With recent advances in technology, mining operations are growing rapidly. This has become an environmental concern as low-grade ores can now be mined and processed producing significantly high amounts of mining waste (Naeini and Akhtarpour, 2018). This has led to the development of large tailings dams containing vast amounts of waste and higher dam systems. Large tailings dam systems require large quantities of quality construction materials. However, the almost entirely flat nature of the mining environment in Botswana often calls for the use of large volumes of low quality construction materials such as mine tailings. In the absence of such quality reliable materials, contractors tend to use the readily available materials (mine tailings) for construction to avoid the costs associated with materials from borrow pits and other reliable areas. Tailings dam stability is dependent on the properties of the available dam construction materials and the condition of the foundation soil. Due to the lack of quality construction materials, the heterogeneity of natural soils and other contributing factors, there is a risk of stability problems and dam failure (EPA, 1994).

Although a tailings dam needs a large investment in resources, it is a very important part of the operations of a mine. In the performance of a mining operation and its industrial processes, its management plays a pivotal role. However, there is no direct financial return on the expense of planning, building, running, maintaining and rehabilitating a tailings dam, therefore, it may be tempting to give their safety and maintenance a low priority. Neglecting the safety of the tailings dam has proven to be a seriously flawed strategy and has proved to be a leading factor in contributing to the poor global record of dam failures and incidents (Alkalaj, 2014).

Continuous stability analysis of tailings dams during and after the mine's lifespan is very crucial as their stability is very pivotal in protecting the environment. This role can be achieved cost-effectively through stability analysis and continuous management, thus providing long-term stability of both the dam and the waste for long-term environmental protection (Ponce-Zambrano and Gordon, 2014).

1.3 Research Questions

i. What is the safety margin of Orapa Mine Slurry Dam 2?
ii. Which parameter affects the outcome of Orapa Mine Slurry Dam 2 Factor of Safety?
iii. Which measures are vital in controlling, preventing and/or mitigating possible instability problems?
iv. How useful is CPTu in slurry dam stability analysis?
v. Is machine learning applicable in CPTu data analysis?

1.4 Research Aim

The main aim of this research was to perform an LE and FE slope stability analyses of Orapa Mine Slurry Dam 2 so as to identify a key parameter which affected the outcome of the Factor of Safety with a further assessment on the applicability of machine learning in CPTu data analysis.

1.5 Research Objectives

i. To execute CPTu testing as part of a large geotechnical site investigation programme for proper definition of the geotechnical properties of the slurry storage facility materials and the foundation soil.
ii. To carry out dissipation tests and analysis during CPTu testing in order to determine the phreatic surface level in the investigated dam-slurry-foundation system.
iii. To perform stability analyses on Orapa Mine Slurry Dam 2 by the Finite Element Strength Reduction Technique and comparing the results with those obtained from three Limit Equilibrium methods namely; Bishop Simplified, Spencer’s and Morgenstern-Price.

iv. To adopt the use of machine learning tools in studying the relationship between CPTu measured variables and slurry dam wall depth, to assess any possibility of prediction.

1.6 Expected Outcomes

i. CPTu derived geotechnical parameters of materials making up Orapa Slurry Dam 2.
ii. The phreatic surface depth on each slurry dam wall.
iii. Critical Factors of Safety and Strength Reduction Factors for each slurry dam wall.
iv. The best predictive supervised machine learning algorithm or model for Orapa Slurry Dam 2 CPTu data.

1.7 Thesis Structure

This thesis is made up of five chapters. Chapter 1 has the introduction to the research background, in which the problems faced by the mining sector globally in terms of tailings dam slope stability are described. An insight into existing research work on slope stability analysis methods is also presented as well as research questions, research aim and research objectives.

Chapter 2 incorporates a literature review which gives basic concepts that were used throughout this project. It presents and describes the theory behind all the analysis methods and software used. It also includes a background summary of Orapa Mine Slurry Dams including their operational history.

Chapter 3 comprises of the methodology adopted for this study. It describes the procedure for CPTu testing, slope stability analysis and regression analysis. It also incorporates procedures for data analysis and measures used for data interpretation.

Chapter 4 incorporates discussions and analysis of piezocone testing results, stability analysis results and regression analysis results while Chapter 5 comprises of findings, conclusions and recommendations from this research.

CHAPTER 2

LITERATURE REVIEW

2.1 Introduction

Tailings dams have evolved in the late 1900s, they are huge physical structures which serve the dual purpose of impounding tailings and recycling the water for reuse. Tailings are defined in this research as fine-grained waste material that results from the extraction and recovery of target minerals. Tailings are rejected at the 'tail end' of the ore milling and separation process in slurry form with a particle size range of ~0.001 mm to ~1.0 mm (EPA, 1994). This type of waste is considered to be very hazardous as it contains metals and other elements that may be harmful to human life and the environment. Therefore, it is normally stored behind embankments/dams normally referred to as tailings dams with the goal of isolating it from the environment. Tailings dams are constructed either from the coarse particle fraction of tailings or earth-fill materials (Penner, 2014). A representative layout of a tailings disposal system comprises of different components as shown in Figures 2.1 and 2.2. The main components are described below (McPhail and Wagner, 1989):

i. Toe wall - Normally referred to as a starter wall, it is constructed in the early stages of tailings dam construction, its main purpose is to confine the tailings (labelled in Figures 2.1 and 2.2).
ii. Drainage system – This system comprises of filter drains (labelled 'under drainage' in Figure 2.2), these are trenches lined with a geotextile or similar material and filled with gravel material to allow only passage of runoff water. The main purpose of these drains is to lessen and control the amount of seepage within the dam.
iii. Draw-off system – This comprises a system of pipes that help in removing water accumulated on the body of the dam.
iv. Delivery system - Comprises of a system of pipes, valves and points of discharge to transport and deliver the slurry.
v. Drainage water system – This system comprises of pumps, pipelines and dams for transporting and storing excess water (including storm water) from the tailings dam to the plant.

vi. Storm water system – This system comprises of a series of trenches around the embankment to manage and redirect storm water from and around the impoundment (shown in Figure 2.1).

vii. Catchment paddocks – Designed as walls around the downstream side of the impoundment to catch, manage and retain storm water and sediments eroded from the side slopes of the tailings dam (Figure 2.2).

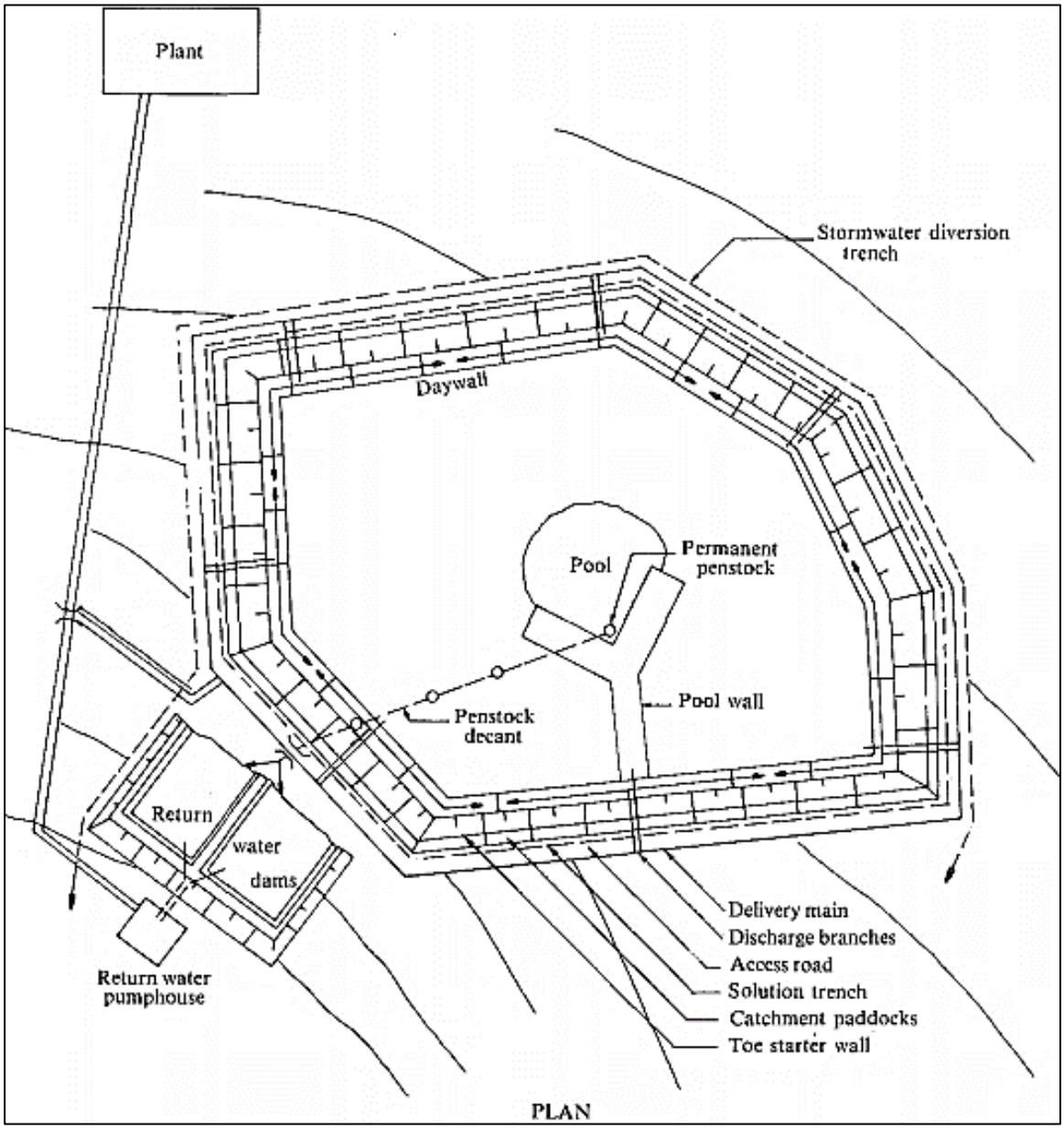

Figure 2.1 Plan View of Tailings Dam (McPhail and Wagner, 1989)

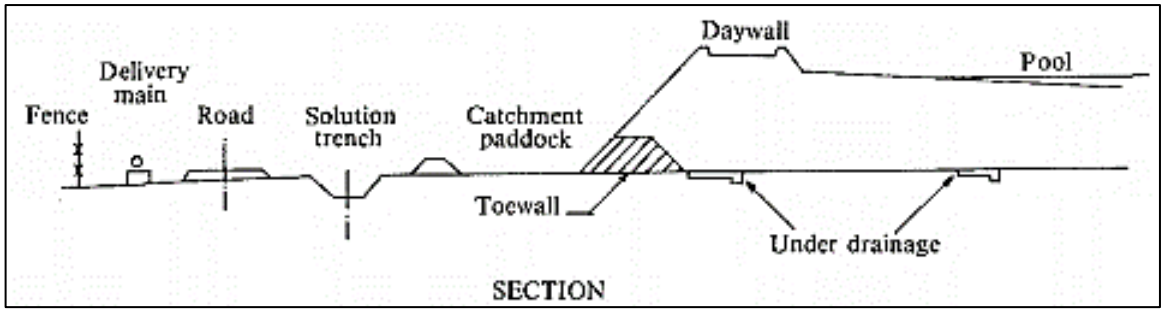

Figure 2.2 Cross-section of a Typical Tailings Dam (McPhail and Wagner, 1989)

2.2 Tailings Dam Construction

Tailings dam design and construction is dependent on different factors, including mine preference, geology, seismicity, nature of tailings, site conditions, climatic conditions, regulations and environmental constraints in the vicinity of the mine and the location of the processing plant. All these factors are very important in site selection and in the actual design of a tailings dam (EPA, 1994).

The most commonly used material for constructing tailings dams is tailings, this is considered the most economical method of construction. Nevertheless, the use of tailings as a construction material has its disadvantages, these include high susceptibility to piping through the body of the dam and high susceptibility to liquefaction under seismic shocks. For improvement purposes, only the coarse particles of tailings may be used for construction and compacted to produce a dense mass with increased resistance to liquefaction (EPA, 1994).

Separation of tailings is usually carried out through a process called cycloning. Cycloning is the most common method of tailings deposition in which the coarse particles of tailings are used to construct the dam during deposition. This method adopts the use of cyclones (Figure 2.3), these are mechanical devices used to separate the slurry into coarse and fine particles. The cyclones adopt the concept of centrifugal acceleration to separate coarse particles from fine particles (normally referred to as slime). As the slurry enters the cyclone at high pressure, the fine particles plus water rise to the top outlet and the coarse particles spiral downwards and exit at the bottom outlet (illustrated in Figure 2.3). The fine particle fraction is called overflow and the coarse particle fraction is called the underflow. The underflow is used for construction of the embankment during active deposition while the overflow is deposited inside the embankment for containment (EPA, 1994).

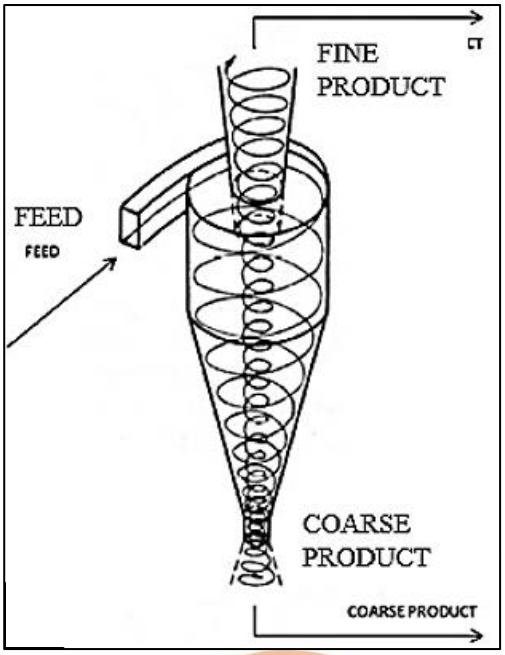

Figure 2.3 Principle of Centrifugal Acceleration Adopted by a Cyclone (Kujawa, 2011)

The three most common construction methods are upstream, downstream and centerline. These methods utilise tailings as a construction material, they are briefly described below.

2.2.1 Upstream Method

This is the most common and economical method of tailings dam construction. The starting point is construction of a starter dam/dyke at the base (dyke numbered 5 in Figure 2.4). This starter dyke should be capable of directing seepage water away from the embankment. Tailings are deposited from the crest of the starter dyke peripherally using cyclones, this deposition develops a dyke (the second dyke after the starter dyke in Figure 2.4) and a beach area made up of coarse material. After drying, the beach becomes the foundation of the following dyke (the third dyke in Figure 2.4). In the application of this method, the ability of the beach to effectively support the next dyke is of utmost importance. According to Vick (1990), the coarse fraction making up the beach should contain more sand particles (40-60%) in order to achieve a strong foundation. Tailings dams built using the upstream method typically have a low relative density and a high water saturation. This increases the liquefaction susceptibility in the event of an earthquake. Different other factors restrict the applicability of this method including the rate of dam raise which is restricted by the accumulation of excess pore pressures in the deposited tailings. Pore pressure build-up may result in overall dam failure (EPA, 1994).

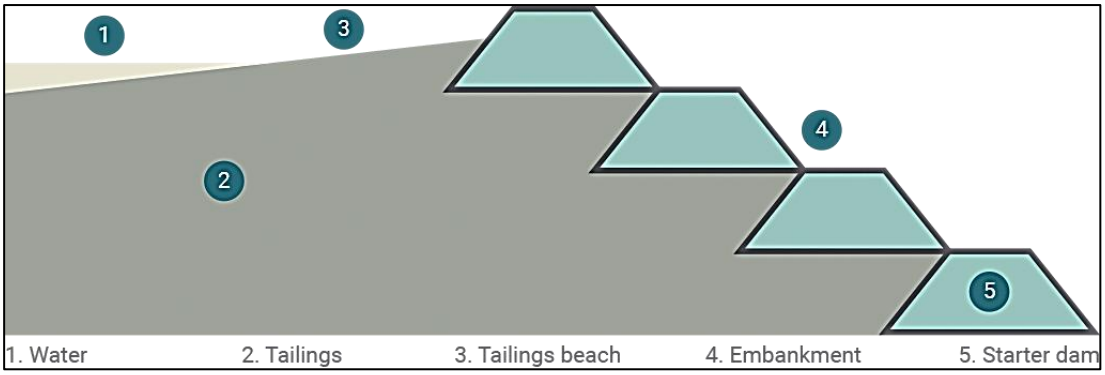

Figure 2.4 Upstream Tailings Construction Method (ICMM, 2020)

2.2.2 Downstream Method

The downstream method starts with construction of a starter dyke (numbered 4 in Figure 2.5) which should have the ability of minimize seepage through the body of the dam (should be impervious). During cyclone separation and deposition, the fine fraction of the tailings is deposited in the dam while the coarse fraction is used to raise the dam wall with each wall built and supported above the downstream slope of the previous dyke. In this method, the dam crest moves downstream as the dam is gradually raised. In comparison to the upstream method, the downstream method provides more stability as it allows for easy compaction, installation of phreatic surface control measures and dam raising is not dependent on the deposited tailings for a strong foundation (EPA, 1994).

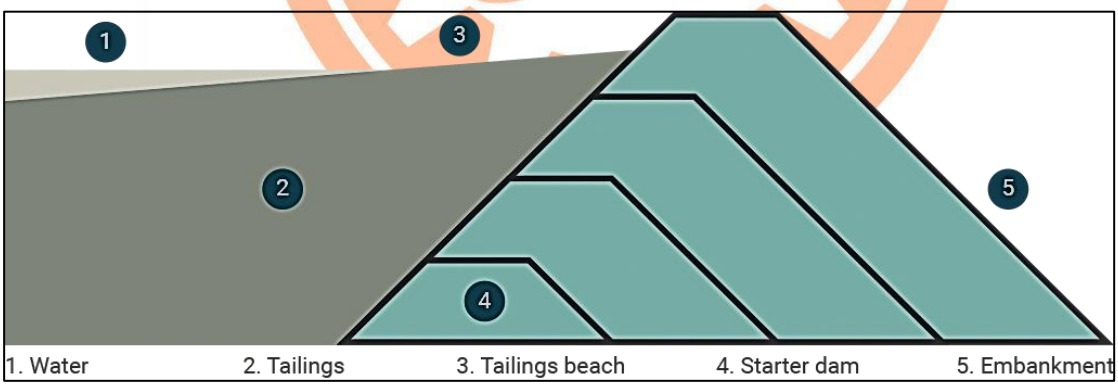

Figure 2.5 Downstream Tailings Construction Method (ICMM, 2020)

2.2.3 Centerline Method

This method is similar to both downstream and upstream methods as embankment construction starts with starter dam construction at the toe (labelled 4 in Figure 2.6) and the tailings are deposited at the dam crest to form a beach. The unique feature of this method is

that the centerline of the embankment is maintained during progressive dam raising and the coarse material is deposited both on the beach and on downstream slope during deposition to build the embankment. The centerline construction method is favorable to some extent as it mitigates some of the disadvantages experienced in both upstream and downstream methods (EPA, 1994).

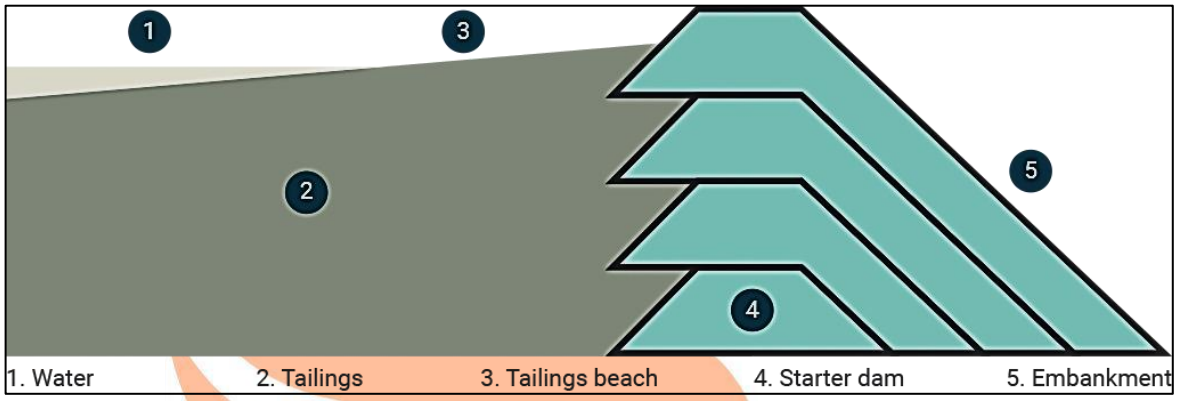

Figure 2.6 Centerline Tailings Construction Method (ICMM, 2020)

2.3 Tailings Dam Failures

The mining industry has been growing rapidly in recent years, this is due to the ever-increasing demand and an advancement in equipment used to mine and process ore minerals. These contributing factors have led to the mining of large low-grade ores through the use of advanced equipment and technology from the manufacturing industry (Naeini and Akhtarpour, 2018). In the mining and processing of large low-grade deposits, the amount of tailings produced usually far exceeds the recovered resource. The ever-increasing amounts of tailings produced by the mining industry is of great concern, as it has led to the development of huge impounding structures reaching a height of 200m and containing vast amounts of tailings. These tailings impoundments are usually constructed using tailings material (most economical method) which is associated with seepage and overall stability problems (EPA, 1994). Concerns on the stability and environmental performance of tailings dams have been raised. These are in line with recent tailings dam failure events which are listed in Table 2.1 including the Brumadinho Brazil iron ore tailings dam failure of 2019 (Luiz *et al.*, 2020).

On a global scale, there is a long list of tragic tailings dam failures and incidents that have occurred over the years, recent failure events have been outlined chronologically by Rico *et*

al. (2018). It was discovered that dams used for impounding tailings are more prone to fail than dams used for water storage due to their distinctive characteristics. These include:

i. Tailings dams constructed using fill material such as soil, tailings and waste material from mining operations.
ii. Multi-stage embankment raising meant to increase storage capacity.
iii. Absence of regulation on specific design criteria.
iv. A requirement of continuous control and management.
v. A high cost of remediation measures after mine closure.

All these characteristics label tailings dams as vulnerable to stability problems such as liquefaction and slides, therefore, they are more susceptible to failure.

The mining industry has been affected by several significant dam failure events in recent history, Table 2.1 summarises basic information regarding dam failures from 1928 to 2015.

Table 2.1 Baseline Information on Tailings Dam Failures (Lyu et al., 2019)

Year	Name (location)	Dam height (m)	Dam type	Failure cause (fatalities)
1928	Barahona (Chile) [31]	61	Upstream	Earthquake (54)
1937	Dos Estrellas (Mexico) [32]	UN	Upstream	Seepage (70)
1948	Kimberley (Canada) [33]	UN	Upstream	Seepage (UN)
1962	Huogudu (China) [26]	UN	Upstream	Foundation failure (171)
1965	El Cobre (Chile) [34]	36	Upstream	Earthquake (>300)
1966	Aberfan (UK) [35]	UN	Water retention	Seepage (144)
1966	Mirolubovka (Bulgaria) [36]	45	Upstream	UN (488)
1970	Mufulira (Zambia) [37]	50	Unknown	Mine subsidence (89)
1972	Buffalo Creek (USA) [38]	14–18	Upstream	Seepage (125)
1974	Bafokeng (South Africa) [39]	20	Upstream	Seepage (14)
1974	GCOS (Canada) [40]	61	Upstream	Seepage (UN)
1975	Mike Horse (USA) [37]	18	Upstream	Overtopping (UN)
1976	Dashihe (China) [41]	37	Upstream	Earthquake (UN)
1978	Syncrude (Canada) [42]	UN	Centerline	Foundation failure (UN)
1978	Mochikoshi Nos. 1 and 2 (Japan) [43]	28, 19	Upstream	Earthquake (1)
1978	Arcturus (Zimbabwe) [44]	25	Upstream	Overtopping (1)
1979	Union Carbide (USA) [30]	43	Upstream	Seepage (UN)
1985	Stava (Italy) [45]	29.5	Upstream	Seepage (268)
1985	Chenzhou (China) [46]	UN	Upstream	Overtopping (49)
1985	Cerro Negro No. 4 (Chile) [47]	40	Upstream	Earthquake (UN)
1986	Huangmeishan (China) [32]	UN	Upstream	Seepage (19)
1988	Lixi (China) [48]	40	Upstream	Overtopping (20)
1991	Sullivan (Canada) [49]	21	Upstream	Seepage (UN)
1993	Marsa (Peru) [32]	UN	Upstream	Overtopping (6)
1994	Tapo Canyon (USA) [50]	24	Upstream	Earthquake (UN)
1994	Merriespruit (South Africa) [51]	31	Upstream	Overtopping (17)
1995	Omai (Guyana) [52]	44	Unknown	Seepage (UN)
1995	Surigao (Philippines) [53]	UN	Upstream	Foundation failure (12)
1996	Porco (Bolivia) [6]	UN	Upstream	Overtopping (UN)
1996	Sgurigrad (Bulgaria) [54]	45	Upstream	Seepage (107)
1998	Los Frailes (Spain) [15]	27	Upstream	Foundation failure (UN)
2000	Baia Mare and Baia Borsa (Romania) [55]	7	Downstream	Overtopping (UN)
2002	San Marcelino Zambales (Philippines) [56]	UN	Unknown	Overtopping (UN)
2004	Pinchi Lake (Canada) [57]	12	Water retention	UN (UN)
2009	Karamken tailing plant (Russia) [58]	20	Unknown	UN (1)
2010	Ajka (Hungary) [59]	22	Downstream	Seepage (10)
2011	Kayakari (Japan) [60]	UN	Unknown	Earthquake (UN)
2012	Padcal No. 3 (Philippines) [61]	UN	Upstream	Overtopping (UN)
2014	Mount Polley (Canada) [62]	40	Unknown	Foundation failure (UN)
2015	Fundão (Brazil) [63]	90	Upstream	Seepage (19)

Note: UN = unknown.

Every failure event results in extensive damage to property, downstream pollution and loss of many lives. These failures have raised concerns of the environmental protection authorities, the mining sector and the public at large. Tailings dam failures are often due to a combination of multiple factors and are primarily influenced by the external environment, e.g. by seismic events, increased dam loading and flooding. These factors cause changes in stress and seepage conditions which result in the overall instability of the dam (Lyu *et al.*, 2019). The following common causes are outlined in connection to the resulting failure:

i. Slope instability (Static failure) – Failure is often facilitated by partial saturation of the dam and occurs as a result of induced deformation which drives the dam to a point of failure.
ii. Foundation conditions – Failure results from weak foundation soil (e.g. clay soil).
iii. Structural inadequacies – Failure results from design errors or functionality errors.

iv. Overtopping – Failure results from erosion caused by overflowing of water at the top of a dam.

v. Mine subsidence – Failure is due to failure of an underground mine beneath the dam.

vi. Seepage – Failure is due to internal erosion of the dam caused by seepage water within the body of the dam.

vii. External erosion – Failure is due to external erosion of the dam face normally caused by precipitation runoff.

viii. Earthquake – Failure is caused by a seismic event when the earthquake magnitude is larger than the one incorporated in the design (Thygesen, 2017).

Figure 2.7 summarises these causes in connection with 206 tailings dam failure events that occurred between 1915 and 2016, each cause is assigned a number to show the number of failures triggered by such. It can be noted from this pie chart that the causes of most failure events remain unknown (~25.2%). Overtopping (~21.4%) is the leading cause followed by slope instability (~14.6%) and seismic events (~13.1%), this means that they take considerable responsibility in triggering tailings dam failures. Overtopping, slope instability and failure due to earthquakes symbolise the importance of proper design, periodic stability assessments, continuous monitoring and management of tailings storage facilities (Thygesen, 2017).

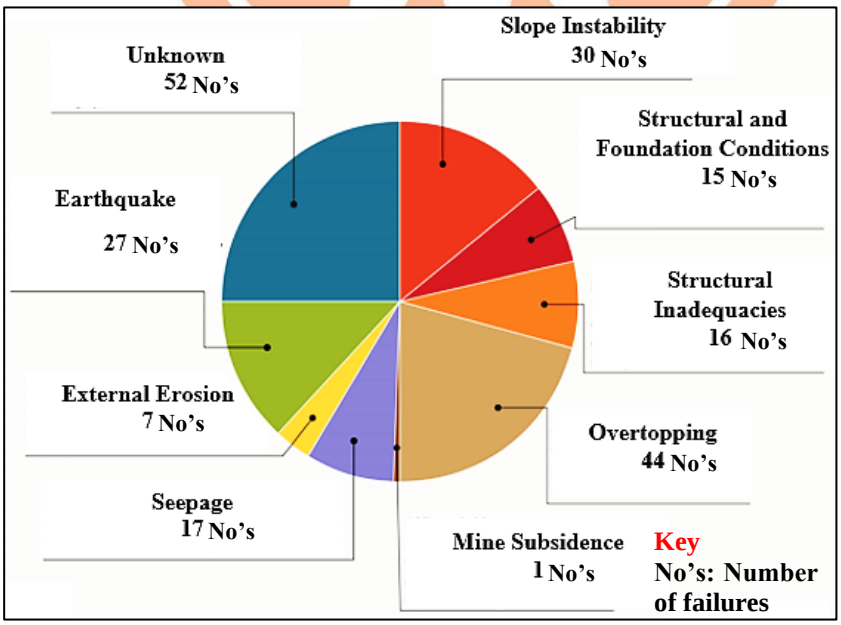

Figure 2.7 Causes of Tailings Dam Failures 1915-2016 (Thygesen, 2017)

According to Yin *et al.* (2011), research has shown that tailings dams are one of the main sources of risk in the mining sector. A mining organization must be reasonable and responsible enough to prioritize on proactively isolating tailings to prevent contamination of the environment (Kossoff *et al.*, 2014). Tailings dam management requires effective maintenance of a high level of structural stability, therefore, stability assessments on new, active and decommissioned dams remain a requirement. According to Souza (2010), Limit Equilibrium and Stress-Deformation stability analysis methods are the most common methods used in engineering.

2.4 Slope Stability Analysis

Slope stability is the potential of an engineered or naturally occurring slope to withstand ground movements. Slope stability analysis encompasses methods for the analysis and evaluation of slope safety. The basic fundamentals of slope stability analysis enclose slope deformations and slope stability analysis methods, slope failure mechanisms, slope design parameters, methods for determination of strength properties, phreatic surface estimations and mitigation measures (Huang, 2014). The main purpose of stability analysis is to assist in safely designing slopes, to assess the possibilities of slope failures, to understand failure mechanisms, to investigate and redesign failed slopes, to prepare and design remedial/preventative measures (Abramson *et al.*, 2002). Slope stability analysis can be carried out in two ways, that includes the deterministic and probabilistic approaches. These are briefly outlined below.

2.4.1 Deterministic Approach

In a deterministic approach, the stability of a slope is measured using the Factor of Safety which is computed using fixed values of input parameters. The Factor of Safety is the ratio of the shear strength to the shear stress using the mean values of input parameters. This approach has been adopted for many years due to its simplicity, however recent research work has highlighted the need to include inconsistency and uncertainty in input variables (Queiroz, 2016). Slope stability analysis is associated with uncertainties, examples of these uncertainties are listed as follows:

i. Limited representative data.
ii. Constant changes in environmental conditions.
iii. Spatial variability of soil characteristics.
iv. Non-homogeneity of slopes.

v. The dispersion of test results.
vi. Unexpected failure mechanisms.
vii. Human error in design and construction.

As a result, the input parameters are not known with complete accuracy and precision. The deterministic approach does not incorporate inconsistency and uncertainties in the input parameters, therefore it introduces inaccuracies to stability assessments (deWolfe *et al.*, 2011). To account for uncertainties when using the deterministic approach, the Factor of Safety is selected and used in accordance with variability or uncertainty in the test results. One example is using a high Factor of Safety when there is a low level of reliance in the accuracy and precision of input parameters.

2.4.2 Probabilistic Approach

A probabilistic approach incorporates randomness of key parameters and evaluates stability on the basis of Probability of Failure (PF) and a Reliability Index (RI). In this type of analysis one or more input variables must be established as random variables and assigned a statistical distribution (Queiroz, 2016). A random variable is a parameter e.g. angle of internal friction, which does not have a single fixed value, but may take up any number of values. The exact value of any one of these variables at a specific location cannot be predicted, hence the name 'random variable'. Based on the assigned statistical distributions, input data samples are generated, producing N values for each random variable (N is the number of samples generated). As shown in Figure 2.8, a single iteration of the analysis is carried out by loading an array of random variable samples and reiterating the analysis.

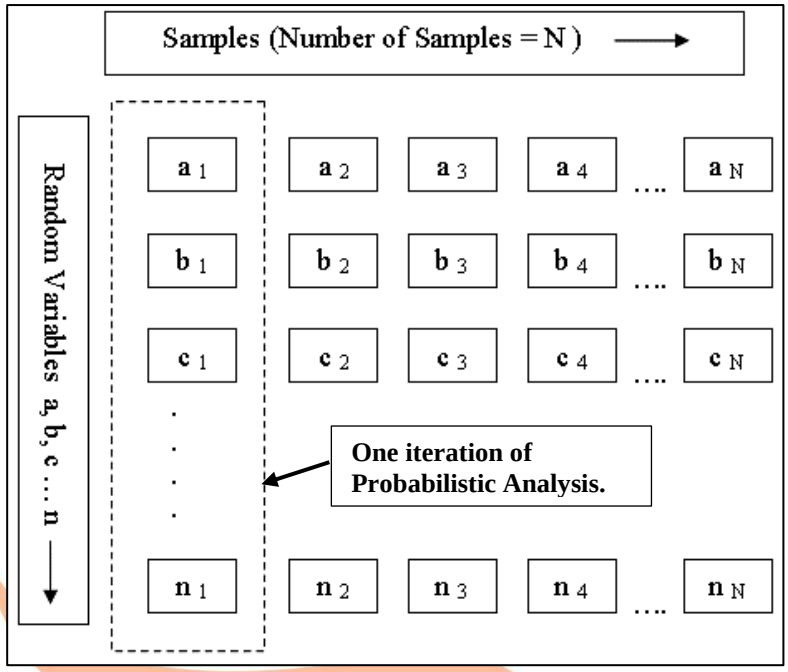

Figure 2.8 Random Variable Samples in a Probabilistic Analysis (Rocscience, 2018)

In each simulation, the Factor of Safety is computed, giving varying values of the Factor of Safety for a failure surface. This results in a distribution of factors of safety which are used for computing the Probability of Failure (PF) (Rocscience, 2018). This process is summarised in a flow chart in Figure 2.9.

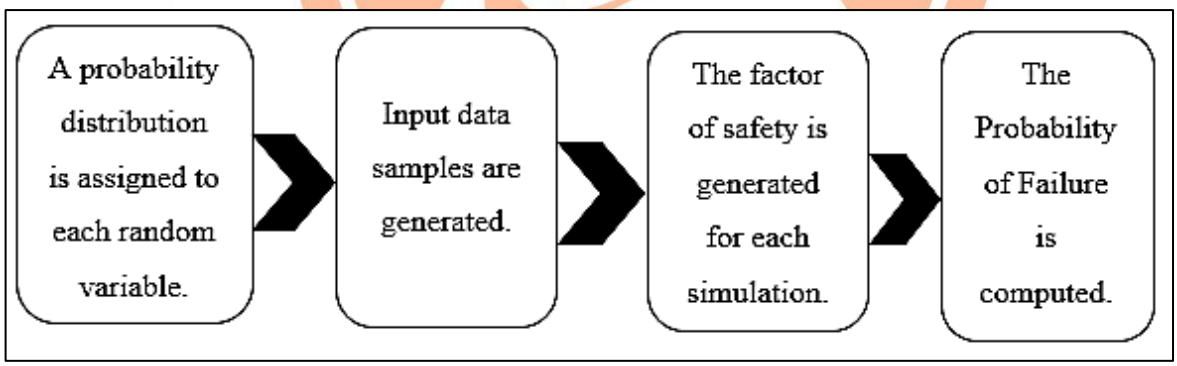

Figure 2.9 Workflow of the Probabilistic Slope Stability Analysis Method

Another important safety measure used in the probabilistic approach is the Reliability Index (RI). It is used to amount to the number of standard deviations separating the average Factor of Safety from the critical Factor of Safety (FoS = 1). To ensure a reasonable level of satisfaction, the RI should be equal or greater than 3 (Rocscience, 2018).

In a probabilistic approach, it is common practice to incorporate a Sensitivity Analysis. This method is another reliability-based approach that intends to determine how the changes in input variables affect the outcome of the dependent variable. It is used as a measure of the level of confidence on the analysis of results in connection with the uncertainties/variabilities of the input variables. In a sensitivity analysis, input variables are varied across a range of values and an observation is made on how this affects the calculated factors of safety.

According to Leao (2019), a probabilistic approach does not eliminate the problem of uncertainties but in essence provides a consistent working method that accounts for uncertainties. Laçasse (1994) further highlighted that this approach is useful addition to the deterministic approach and not a replacement. Therefore, the probabilistic approach has been used extensively in research to complement the conventional deterministic approach.

2.4.3 Slope Stability Analysis Methods

Traditionally, slope stability analysis has been based upon computation of a Factor of Safety(FoS). The FoS is a numerical value, commonly used to express the 'safety' against 'failure' of a slope. It is expressed as the ratio between the forces resisting movement (shear strength) and those driving it (shear stress). When the shear strength exceeds the shear stress, the slope is considered stable. As a general rule, the FoS adopted for permanent slope should equal or exceed 1.5 depending on the required safety level and the level of confidence in the material parameters used (Gonzalez De Vallejo and Ferrer, 2011). The FoS has an advantage of simplifying results interpretation of a stability analysis, since a single quantitative value is used to indicate the overall stability of a slope being analyzed. Therefore, it has been used for many decades in engineering design, its use continues despite the new developments in design tools and understanding of material behavior (Herza *et al.*, 2017).

According to Chiwaye and Stacey (2010), relying entirely on methods founded on the FoS only has been proven to be inaccurate as they only rely on equations of statics. Therefore, they do not account for the displacement of materials involved as well as the distribution of stress and strain. Therefore, for more advanced slope stability analyses, numerical methods have been introduced as a more reliable tool (Kanda and Stacey, 2016). There are different methods in engineering practice used to analyze stability of slopes. Among others, the Limit

Equilibrium (LE) and Finite Element (FE) techniques are the most widely used methods in slope stability analysis.

Limit equilibrium analysis methods

The fundamental assumption in the LE analysis method is that failure of a slope occurs through sliding along a surface within the slope, usually referred to as a critical/slip surface (Figure 2.10). The LE method uses static equilibrium equations to locate slip surfaces and compute the Factor of Safety. The critical slip surface is a sliding surface with the lowest Factor of Safety. The LE method requires assumptions with regard to the location and shape of a slip surface. Shear stresses are computed in accordance with the Mohr coulomb failure criterion and compared with the available resistance (shear strength of the soil), this comparison brings forward a Factor of Safety as the first measure of the overall slope stability (CIVILAX, 2018). There are different limit equilibrium methods in practice, and the most common method is the method of slices (illustrated in Figure 2.10). This method discretizes the sliding mass into slices and equilibrium conditions are considered through equations involving all forces acting on each slice with different assumptions on inter-slice forces and moments. The different methods of slices differ according to assumptions that are put in place (CIVILAX, 2018). Table 2.2 summarises these assumptions for the most common methods of slices.

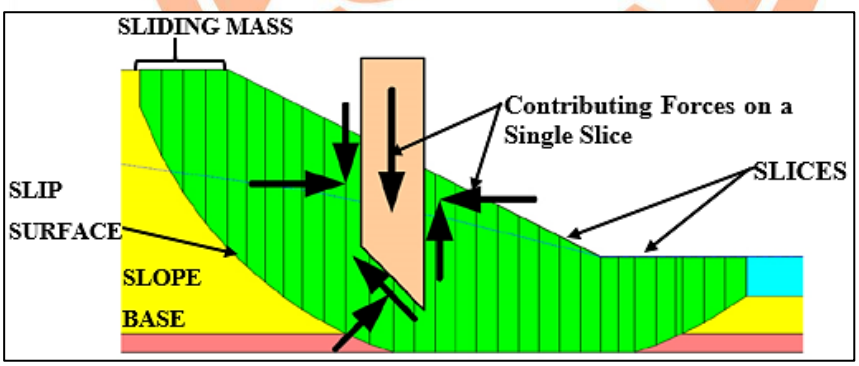

Figure 2.10 Limit Equilibrium Method of Slices Used in Slope Stability Analysis (CIVILAX, 2018)

Methods which consider all the contributing forces in the analysis may be more reliable than those that do not, but when used properly these methods will yield very similar factors of safety as those that ignore some of the forces. Therefore, the best approach is to use more

than two methods and comparing the results to verify the accuracy and precision in the results obtained (Mosquera *et al.*, 2013).

Table 2.2 Common Limit Equilibrium Methods of Slices Alongside Assumptions

Limit Equilibrium Method	Assumptions
Ordinary Method of Slices (Fellenius Method)	Neglects interslice forces.
Bishop's Simplified/Modified	Resultant interslice forces are assumed to be horizontal. Neglects interslice shear forces.
Janbu's Simplified	Resultant interslice forces are assumed to be horizontal. Uses an empirical correction factor in accounting for interslice shear forces.
Janbu's generalized	Uses a line of thrust assumption in defining the interslice normal force location.
Spencer	The resultant interslice forces have a slope throughout the sliding mass. The line of thrust is a degree of freedom.
Chugh	Similar to Spencer's method, however, a constant acceleration force is applied on each slice.
Morgenstern-Price	An arbitrary function is used to define the direction of resultant interslice forces. Requires computation of the fractions of the function value needed to balance force and moment.
Fredlund-Krahn (General Limit Equilibrium, GLE)	Similar to Morgenstern-Price

Finite element analysis method

The Finite Element analysis method is a numerical approach to analyzing structures/slopes. It involves discretizing the structural system/slope into a finite collection of simple geometric shapes called elements (Figure 2.11). Material properties and governing relationships are considered and expressed for each of these elements in terms of unknown values at element corners (called nodes). All these equations are assembled with considerations on constraints and loading giving a set of equations, solving these equations gives an approximation of the behavior of the continuous mass/slope (Ashcroft, 2011). There are generally two main approaches to FE slope stability analysis (namely Gravity Increase and Shear Strength Reduction) as mentioned in Chapter 1 Section 1.0. Sternik (2013) discovered that the Gravity Increase (GI) method leads to a significant

overestimation of a Factor of Safety as compared to the Shear Strength Reduction (SSR) method, as such the SSR method is the most frequently used for slope stability analysis. The SSR Method involves a finite element analysis in which material strength properties are reduced by a factor until a critical factor that induces instability is attained (Rocscience, 2018). This factor is called the Strength Reduction Factor (SRF) and sometimes called the Factor of Safety, it is the main output of the analysis. Unlike the Limit Equilibrium analysis methods, this method requires no assumptions for either locating the failure surface, approximating its shape or the contributing forces. It allows the critical failure modes and mechanisms to assume any shape and location (Chiwaye & Stacey, 2010).

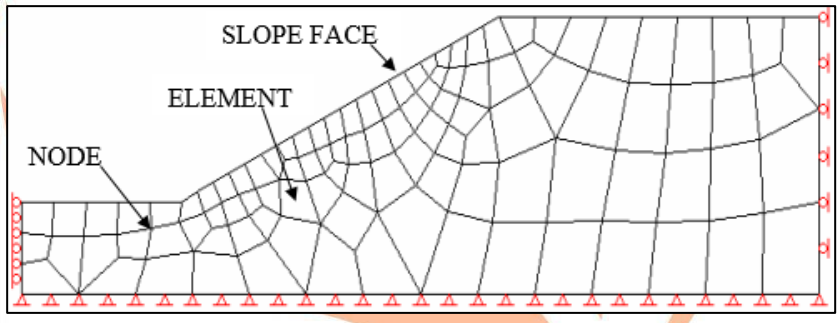

Figure 2.11 Finite Element Analysis Method (Rocscience, 2018)

2.5 Slope Stability Software Programmes

This study adopted the use of Slide 2018 for the LE analysis and RS2 2019 (Rock and Soil 2-dimensional analysis programme) for the FE analysis. These software programmes were developed by Rocscience. However, there are a number of other available software programmes for the analysis of slope stability through LE and FE analyses. These include the following:

a) PLAXIS - Finite Element Approach
b) SLOPE/W - Limit Equilibrium Approach
c) GSLOPE - Limit Equilibrium Approach
d) STABLE WV - Limit Equilibrium Approach
e) FLAC/Slope - Finite Difference Approach
f) GALENA - Limit Equilibrium Approach
g) SVSlope - Limit Equilibrium Approach
h) CLARA-W - Limit Equilibrium Approach
i) CRISP 2D - Finite Element Approach
j) HYDRUS - Limit Equilibrium Approach

k) GEO FEM Finite Element Approach

2.5.1 Slide 2018

Slide 2018 has a user-friendly graphical interface with good modelling and overall data interpretation efficiency. It computes factors of safety for both circular and non-circular failure slip surface using various limit equilibrium analysis methods such as the Bishop method, the Morgenstern-Price method, Janbu, Spencer and the General Limit Equilibrium method (GLE). The user-friendly editing and analysis tools in Slide make it a convenient platform for performing parametric studies that are underpinned by sound geotechnical engineering practice (Rocscience, 2018).

Critical slip surface search is one of the most important aspects in slope stability analysis, it helps locate weak surfaces where slopes experience the lowest factors of safety. Slide has proven slip surface search methods for both circular and non-circular surfaces (Rocscience, 2018). The circular slip surface methods are of interest to this study, they include *Grid Search*, *Slope Search* and *Auto-refine Search*, these methods automate the search for potential circular slip surfaces.

Grid search method

In grid search definition of a grid of slip centers is required (Figure 2.12), each center in this grid represents a center of rotation of slip circles. By default, Slide uses radius increment and slope limits to determine radii for slip circles as shown in Figure 2.12. The slope limits are used to define the slope surface, then depending on the distances between the slip centers and the surface of the slope, maximum and minimum radii are determined. Thereafter, at each slip center, the radius increment is used to determine the number of equally spaced circles between the maximum and minimum radii. This is repeated for all slip centers to generate slip circles at each point on the grid (Rocscience, 2018).

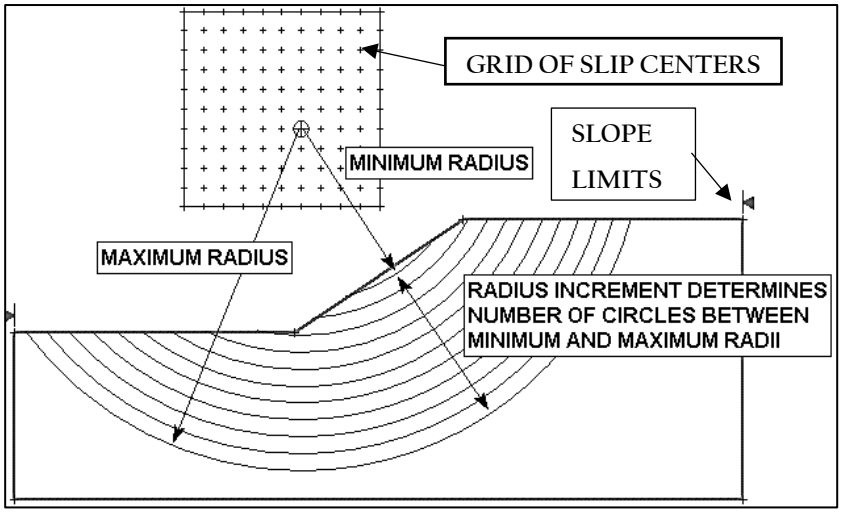

Figure 2.12 Grid Search Method Implementation (Rocscience, 2018)

Slope search method

This method offers an alternative to carry out a circular slip surface search on chosen areas of a slope surface instead of using a slip center grid. It allows the user to choose areas on a slope surface through which slip surfaces should pass (Rocscience, 2018).

Auto-refine search method

In this method, an iterative approach is used in searching for critical slip surfaces. Results obtained from a single iteration are used to refine and narrow down the slope search area in the next iteration. In many instances, for an equal number of slip surfaces generated, this method will locate slip circles with lower factors of safety than those located by both grid and slope search methods (Rocscience, 2018).

According to Rocscience (2018), it is good practice to experiment and compare results obtained from different search methods. Similarity in the location and Factor of Safety of the critical slip surface indicates that a true critical slip surface has been located.

2.5.2 RS2 2019

RS2 2019 an FE analysis programme used for analyzing geotechnical structures and designing both underground and surface excavations including their support. Excavations ranging from simple to complex orientations can be easily created and edited through a combination of multiple stages. RS2 2019 has the capabilities of determining groundwater pore pressure through a steady-state finite element groundwater seepage analysis.

Groundwater conditions like pressures gradients and flows are computed based on hydraulic conditions defined by the user. The Shear Strength Reduction (SSR) Method (Section 2.4.3) is featured in RS2 2019 to automatically run finite element analyses using either Mohr-Coulomb or Hoek-Brown strength parameters.

2.6 Cone Penetration Test (CPTu) Method

Cone Penetration Test (CPT) is a very common method for field measurements of various sub-surface characteristics such as geological regime, hydrological regime, and sub-surface strata properties. It has been one of the methods commonly used and accepted worldwide to assess the properties of the sub-surface strata (EPA, 1994).

This test is conducted in-situ and involves a series of one-meter rods with a steel cone at the end continuously pushing into the ground. A continuous measurement of resistance to penetration of the cone tip and surface sleeve is done. The total force acting on the cone, divided by the projected area of the cone, A_c, gives the cone tip resistance q_c, and the total force acting on the friction sleeve divided by the surface area of the friction sleeve A_s, gives the friction sleeve f_s (Robertson and Cabal, 2010). A piezocone (CPTu) contains a pore pressure transducer which measures the pore pressure in addition to measurements with a CPT. The terminology used for description of CPTu steel cone and its measured parameters are shown in Figure 2.13.

Cone tip resistance is indicative of the undrained (i.e. including in-situ moisture) shear strength of the soil. Sleeve friction measurement represents the variation in lateral ground pressure and can be used to investigate the effect of soil compaction on the stress state. Measuring the excess pore water pressure with CPTu detects layers and seams of fine-grained material (silt and clay). More detailed information on soil permeability is possible, therefore soil stratification and seepage conditions can also be obtained (El-Reedy, 2017).

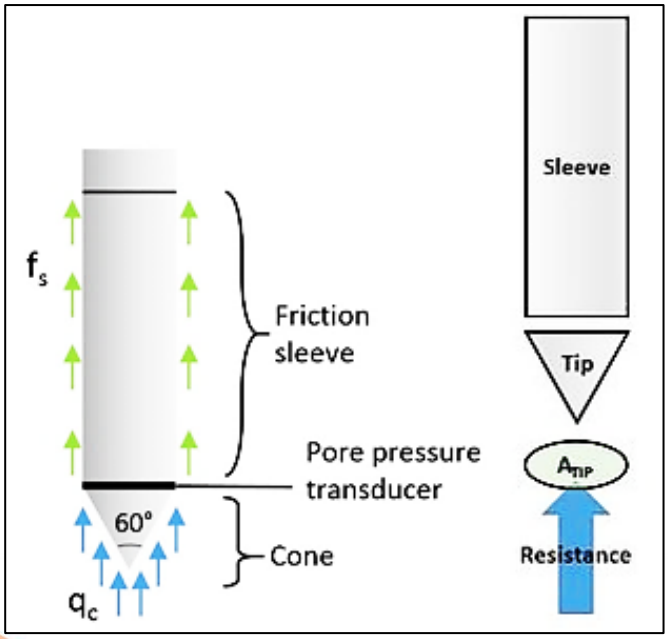

Figure 2.13 Terminology for CPTu Steel Cone (Robertson and Cabal, 2010)

2.6.1 Instrument Description

CPTu equipment is normally mounted on a heavy truck or a trailer rig, this is to ensure that the required reaction force to drive through hard soils is provided. The equipment (Figure 2.14) consists of 1 m long rods and the information gathering equipment (including a laptop and a work bench).

The one-meter rods are continuously inserted into the soil, one rod at a time until the soil offers total resistance to penetration of the cone. Cone tip resistance, sleeve friction along with pore water pressure are measured and recorded with respect to depth of penetration. With CPTu testing, thin less permeable layers (clay) sandwiched between thick high permeable layers (silty/sandy) are easily detected. This is very crucial in the design of slopes and foundations of engineering structures.

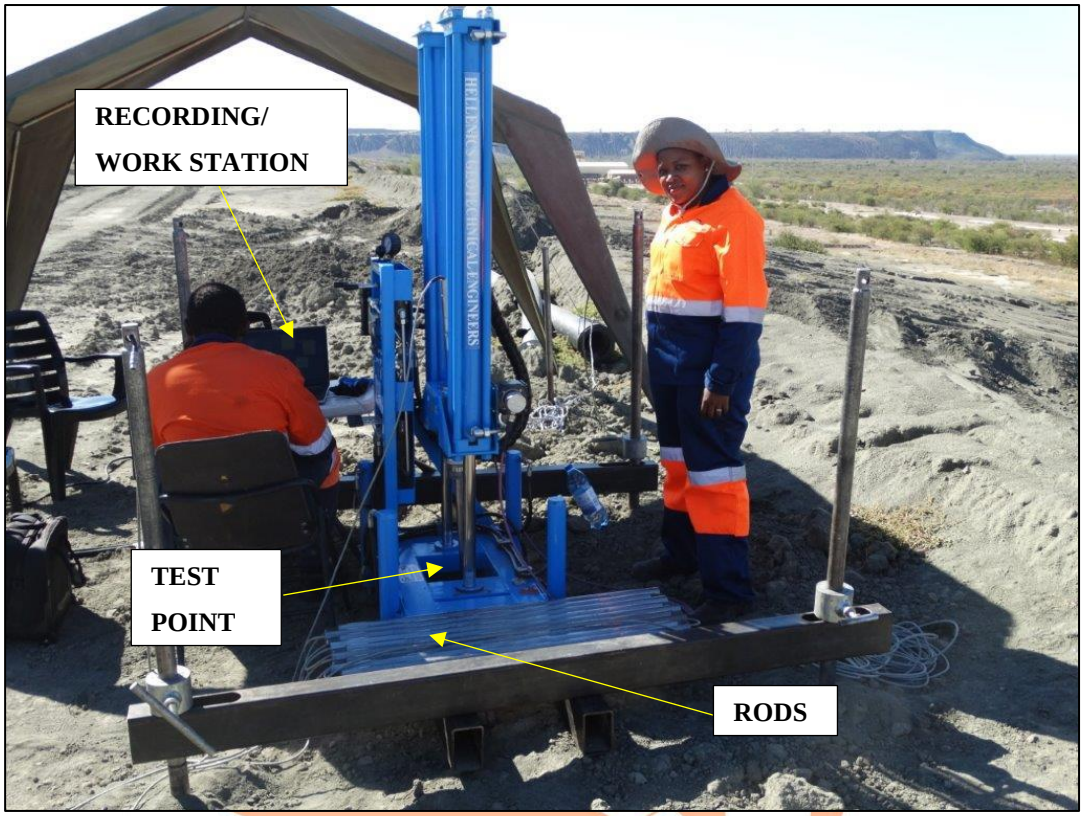

Figure 2.14 Envi-20 Ton Pusher CPTu Equipment on Slurry Dam 2

2.6.2 Measured Variables

Cone penetration testing with pore pressure measurements, measures and records three types of variables as described below.

Cone tip resistance (q_c)

This is given as the ratio of the total axial load on the tip of the cone to the circular projected area of the cone. As the tapered cone advances causing a failure of the soil about 15 inches ahead of tip, the cone tip resistance is measured by the embedded load cells located just behind the tapered cone (location '2' in Figure 2.15) (Spring, 2004).

Sleeve friction (f_s)

Sleeve friction is measured by 4 inches long tension load cells located behind the cone tip on the sleeve of the cone (location '4' in Figure 2.15). It is given as the ratio of the total frictional force on the sleeve to the measured area of the sleeve. Theoretically, sleeve friction is related to the friction of the region being penetrated (Spring, 2004).

*Pore water pressure (**u**)*

Pore pressure is given as the sum of the hydrostatic pore pressure and the change in pore pressure (Δu) as a result of pushing the cone into the ground. Hydrophilic polypropylene porous plastic insert is usually employed by piezometers just behind the conical point (location '1' in Figure 2.15) for measuring the pore pressure (Spring, 2004).

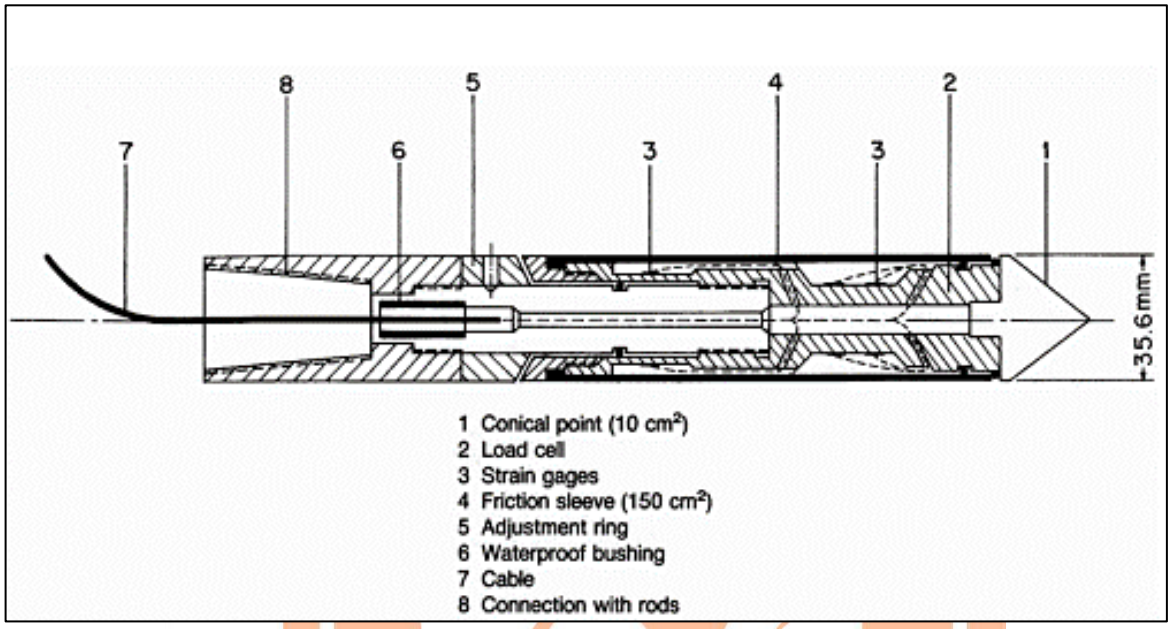

Figure 2.15 Electric Friction-Cone Penetrometer Tip (Spring, 2004)

A number of researchers have explored the reliability and accuracy of the measured CPTu variables and also explored correlations between CPTu results and results from numerical, physical and laboratory experiments. Ryzhko and Isaev (2015) carried out both numerical and physical experiments to study the mechanism in which the soil resists the insertion of the cone at the sleeve. It was reported that sleeve friction decreases away from the cone tip, confirming that the length of the friction sleeve is influential on the recorded sleeve friction. Moreover, it was noted that sleeve friction measurements are less accurate and less reliable as compared to cone tip resistance measurements because of the manufacture imprecision and the friction sleeve surface wear. However, according to Lunne *et al.* (1997), recent improved designs regarding cone penetrometer manufacturing have made it possible to acquire sleeve friction measurements with improved accuracy.

2.6.3 Cone Penetration Test and Soil Classification

For many years, extensive work has been carried out on soil classification using CPTu. The most comprehensive work was from Douglas and Olsen (1981), who produced a chart based on correlations observed from the extensive data obtained from areas in western United States of America. Some of the observations from the studies are as follows:

i. Sandy soils have a tendency to generate a high resistance to penetration of the cone tip and a low friction ratio.
ii. Soft clay soils have a tendency to generate a low resistance to penetration of the cone tip and a high friction ratio.
iii. Soils with high horizontal stress (having a high Over Consolidation Ratio) have a tendency to produce higher resistance to penetration of the cone tip and a higher friction ratio.

One of the most important observation by Douglas and Olsen (1981) was that, CPTu classification charts are unable to accurately classify soils based on grain size distribution, but that such charts are only able to provide information about Soil Behavior Type (SBT). Recently, researchers have been able to bring forward new observations and improved charts (Robertson *et al.*, 1986). The recent observations have emphasized the importance of the design of a cone and water pressure effects on the measured cone tip resistance and sleeve friction as a result of unequal end areas. Therefore, cones designed differently can give different values of cone tip resistance and sleeve friction. It was noted that corrections for water pressure are essential for controlling these effects. Another observation made with CPTu soil classification charts was that use of cone tip resistance and friction ratio with increasing depth increases cone tip resistance. This is simply because of overburden stress; all the three measured variables increase with increasing overburden stress. In light of this, errors can be expected with measurement obtained at greater depths when using charts that use these measured variables. However, there are approaches that have been put into place to normalize the acquired data (Lunne *et al.*, 1997), but these approaches involve a very complex iterative procedure that can only be carried out with the help of a computer programme.

Robertson (1990) proposed modified Soil Behavior Type (SBT) chart that incorporates the CPTu measured variables to predict soil behavior type. The SBT chart uses the recorded values of cone tip resistance q_c and sleeve friction f_s, to make reasonable predictions of soil

behviour type for CPT data. It plots cone tip resistance against Friction Ratio; Friction Ratio is the ratio between sleeve friction and cone tip resistance, expressed as a percentage. The chart only predicts the Soil Behaviour Type (SBT), this means that it classifies the soil according to their mechanical behavior. This is because, the cone does not respond directly to grain size distribution or plasticity but responds to the mechanical behavior of the soil. However soil classification methods based on grain size distribution and plasticity relate very well to in-situ soil behaviour, therefore Unified Soil Classification System (USCS) often agrees with CPT/SBT classification charts (Robertson, 2010).

Sleeve friction and cone tip resistance increase with depth as a result of an increase in overburden stress, therefore there is a need to normalize or correct CPT data for overburden stress for very shallow and/or very deep soundings (Robertson and Cabal, 2010) . Results on a normalized chart are more reliable than those on non-normalized charts. SBTn refers to a normalised SBT chart as shown in Figure 2.16.

Each data point is colored and plotted according to its representative soil layer to help in identification of which types of soils are available in the medium under investigation. Soil types are represented by 9 zones within the plot, each zone represents a soil type which is identified through different colours as shown by the SBTn legend in Figure 2.16. The application of the SBT chart can be simplified through a combination of cone tip resistance and friction ratio into one SBT index (I_c), where I_c represents the concentric circle boudaries separating the nine zones. The SBT boundaries are approximated based on the SBT index I_c. It has been suggested that these charts are global in nature and their use is in the form of a guide in defining soil behavior type based on cone penetration data.

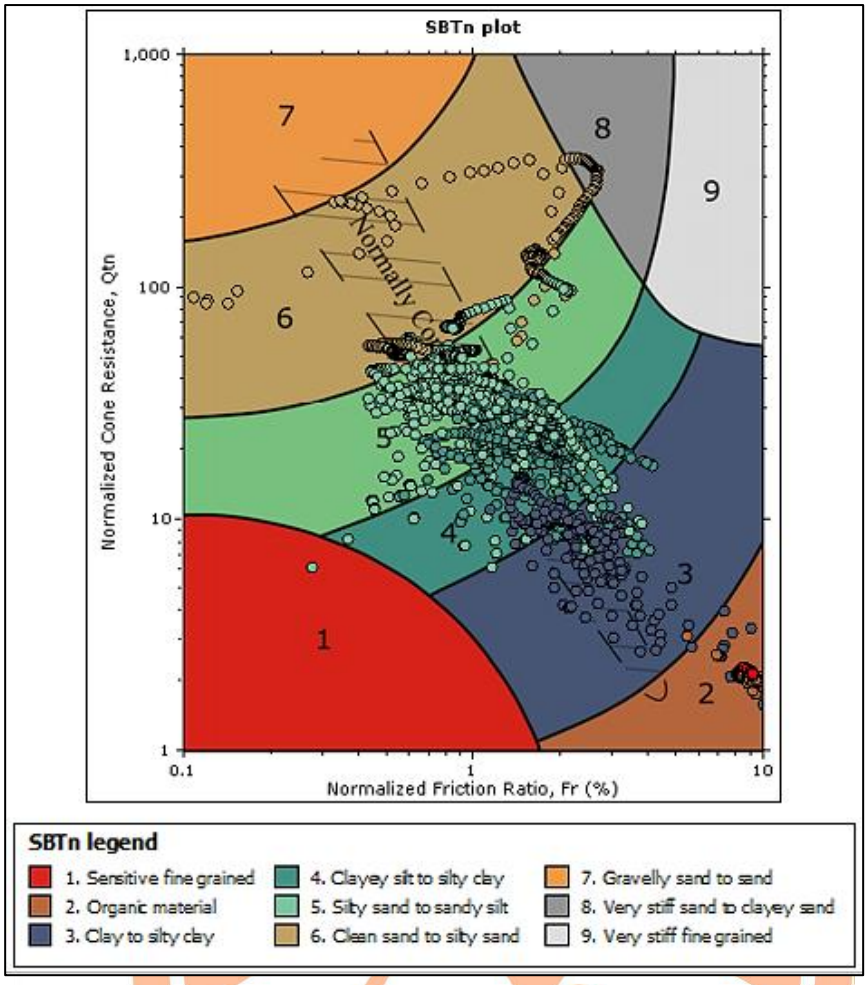

Figure 2.16 Normalized-Modified SBT Chart (Robertson, 1990)

2.6.4 Cone Penetration Test and Mine Tailings

The stability of mine Tailings Storage Facilities (TSFs) are a major challenge in geotechnical engineering. By their nature, TSFs are normally very stratified and layered with very thin fine-grained beds trapped between thick beds of medium grained beds. One of the most important applications of CPTu is the delineation of the nature and sequence of subsurface strata (Lunne *et al.*, 1997). This is achieved by reasonable predictions of the Soil Behavior Type (SBT) (Section 2.6.3). The cone is sensitive to soil mechanical behavior, and therefore it detects and responds to it, leaving behind data that suggests a type of soil that behaves in the same manner under loading conditions. Mine tailings vary in particle size from coarse to clay size, CPTu is only applicable in fine tailings or in very weak coarse waste rock e.g. chalk. According to Lunne *et al.* (1997), CPTu has exceptional logging capabilities in delineating complex stratigraphy of TSFs.

A sample CPT geotechnical section of Orapa Slurry Dam 2 with a plot of depth against cone tip resistance and the SBT index (I_c) obtained from field work results of this study, is shown in Figure 2.17. The cone tip resistance plot demonstrates the resistance of the soil to the cone tip with increasing depth while the index plot classifies each soil layer according to its mechanical behavior. The SBT index plot (yellow plot) in this section is used in the same way as in the SBT plot to classify soils accordingly into different colored zones. The graph plots across soil behavior type boundaries to depict the types of soils detected with increasing depth.

Figure 2.17 demonstrates capabilities of CPTu in delineating thin layers of clay (colored in blue) trapped between sand and silt (colored in green). These types of weak beds are very important in engineering design as they affect the structure's response to stresses.

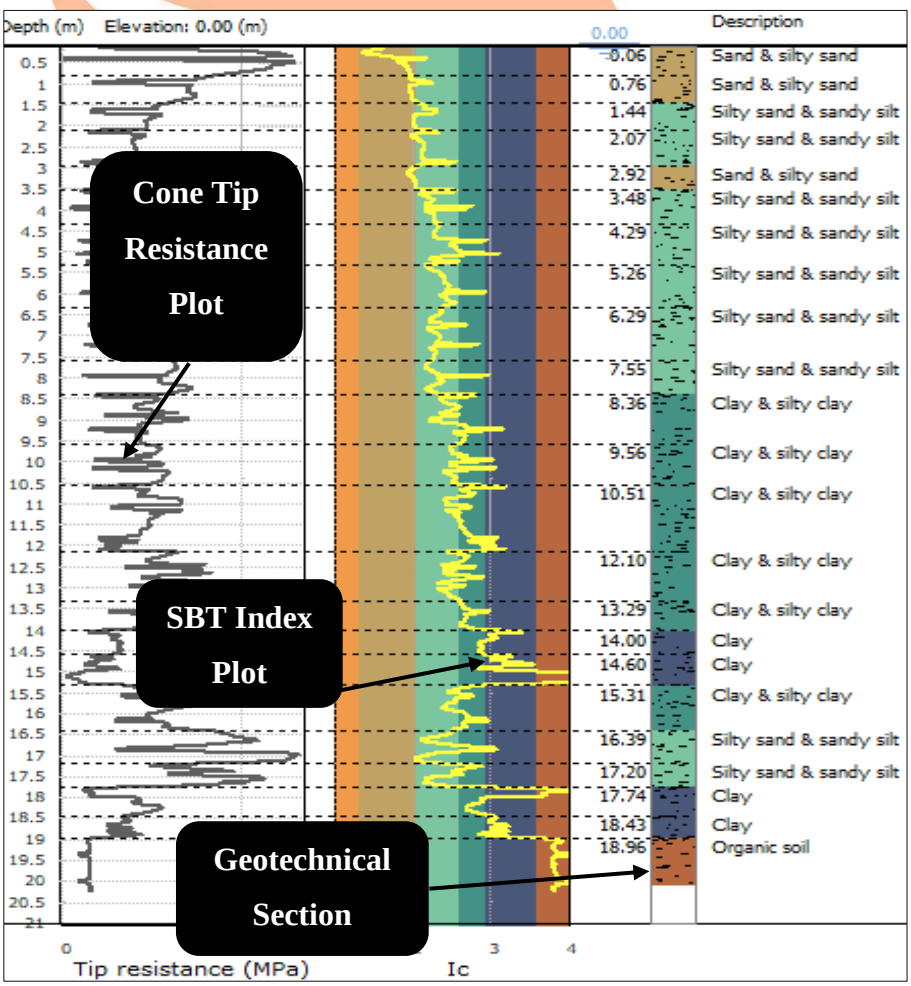

Figure 2.17 CPT Thin Fine Beds Delineation Capability from Orapa Mine Slurry Dam 2

2.6.5 Seepage Control and Dissipation

Seepage is a continuous flow of water from an upstream slope face to a downstream slope face as shown by the arrows in Figure 2.18. Figure 2.18 shows that the upper part of this watercourse has a pore pressure equals to atmospheric pressure and is referred to as a phreatic surface. A phreatic surface is a level of saturation within an embankment (normally referred to as the water table). Water is the most important part of a tailings disposal system and a principal variable in dam stability. Therefore, the principles applied to water flow through and around the dam dominate many rules that regulate tailings dam design (EPA, 1994).

Maintaining the safest level of a phreatic surface within the embankment is one of the most important principles used in design. The phreatic surface dictates to a large extent the stability of the tailings dam, the major principle in design is to keep it as low as possible. A low phreatic surface means that the pore water pressure at the face of the embankment is less than the atmospheric pressure thereby holding the dam stable. The most effective way to maintain a low phreatic surface is to increase the relative permeability in flow direction (Lindquist and Törnqvist, 2015). As shown in Figure 2.18, increasing relative permeability downstream is achieved by constructing an embankment with a lower permeability zone in the upstream area (for example, through the use of cores or fine grained material) and a high relative permeability zone in the downstream area (for example, through the use of drainage zones). This technique allows the downstream drainage zones to speed the removal of water from the embankment and helps in avoiding high pore water pressures within the embankment that may cause instability problems.

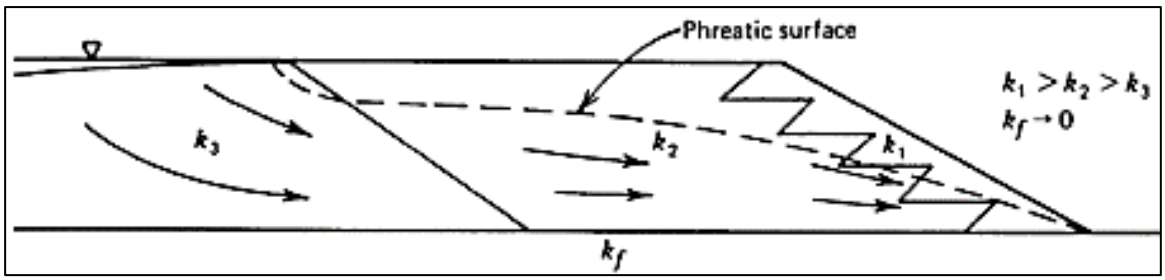

Figure 2.18 Phreatic Surface through a Tailings Dam (EPA, 1994)

In seepage analysis, the estimation of hydraulic conditions/parameters is normally carried out through the use of *dissipation tests*. A dissipation test is conducted at different intervals

during a piezocone test to measure equilibrium pore pressure. This test is conducted by pausing penetration at specific intervals and measuring pore pressure variation with time until pore pressure reaches equilibrium. The time recorded is normally referred to as t_{100} which is the point at which 100% of excess pore pressure has dissipated. A typical curve obtained when conducting a dissipation test is shown in Figure 2.19, t_{100} is obtained as ~13mins and equilibrium pore pressure is recorded as ~7psi (EPA, 1994).

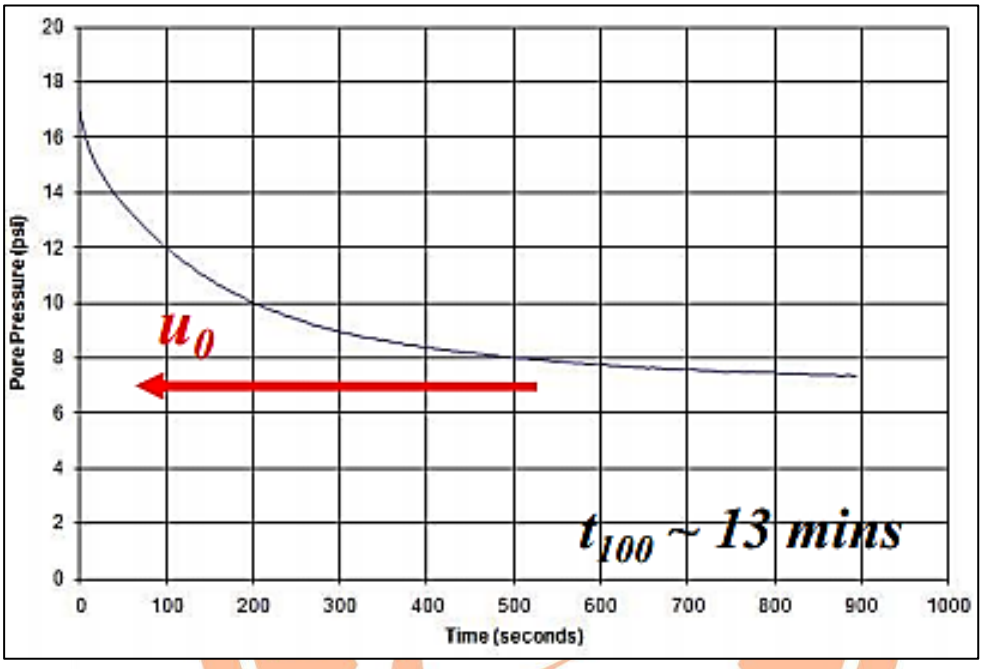

Figure 2.19 Pore Water Pressure Response during Cone Penetration Testing (Robertson and Cabal, 2010)

A dissipation test data is used in engineering design for estimating the phreatic surface, atmospheric pressure, coefficient of consolidation and coefficient of permeability. Therefore, this test can be used to estimate among other parameters, the hydraulic conductivity of soil needed to predict time-dependent settlement.

2.6.6 CPTu Software Programmes

This study adopted two CPTu software programmes for data collection, recording and interpretation. Envi logger C1/CS1 R1B software was used for data collection and recording while CpeT-IT 3.0 software was used for CPTu data interpretation.

The Envi logger C1/CS1 R1B software is a logger system where all data is stored in a computer installed database. Raw values are recorded and stored from rig sensors with continuous digitization of analogue data before storage. This software allows for continuous data collection and storage during each CPTu sounding, resulting in a very robust data collection mechanism where data can be retrieved any time. It allows the user to select parameters to view and include in the files to be created during each a CPTu sounding (Envi, 2012). The Envi logger C1/CS1 R1B system is made up of two program modules as follows:

a) EnviPackage – This is a foundation software that handles transducer data collection and database interaction.
b) CPTApplication – This module allows the user to choose tests between CPTu and Standard Penetration Test.

CpeT-IT 3.0 is a user-friendly yet detailed software package that is used to interpret raw CPTu data in terms of Soil Behavior Type (SBT) and other geotechnical parameters. It was developed in collaboration with Professor Peter Robertson a co-author of an extensive textbook on CPTu together with Greg Drilling and Testing Inc., a leading company in site investigation including CPTu. CpeT-IT 3.0 uses current published correlations based on reviews by Lunne, *et al.* (1997) and Professor Robertson's recent updates (Geologismiki, 2018). Some of its main properties and data output are:

i. Import raw CPT data from any ASCII text file.
ii. Presentation of all interpretation results in tables and graphs.
iii. Overall analysis reports.
iv. Interpretation of dissipation data.
v. Creation of a typical geotechnical section.

CpeT-IT 3.0 uses the common CPT Soil Behaviour Type (SBT) charts by Robertson *et al.* (1986). It has a proven track record in easy to use yet detailed CPTu data interpretation tools for geotechnical engineers (Geologismiki, 2018). It has been used in engineering for site characterization, soil classification and stability analysis.

2.6.7 LIDAR Survey

LIDAR stands for Light Detection and Ranging, it consists of a laser rangefinder that operates on an airborne platform (for example, a drone or an airplane) to take continual measurements from this platform to the ground surface. A laser rangefinder is a device that

measures distances from the observer to an object through the use of a laser (laser stands for Light Amplification by Stimulated Emission of Radiation) beam. As shown in Figure 2.20, the LIDAR system operates with a combination of the of the following instruments to continuously record elevation data (Sabatini, 2015).

i. *Laser device* which consists of an Inertial navigation measurement unit (IMU) – that progressively records the orientation of the drone/airplane, and a High precision airborne Global Positioning System (GPS) – which records the position of the drone/airplane in three dimensions.
ii. *Computer interface* for communication control and management among devices and data storage.

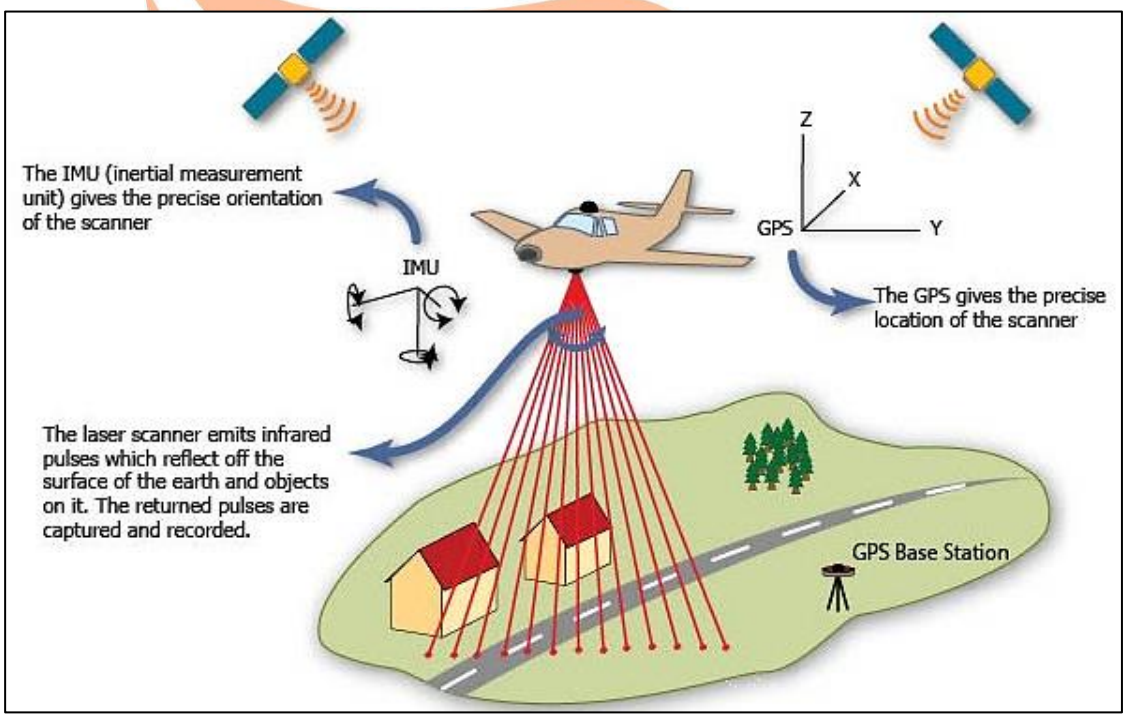

Figure 2.20 Schematic Diagram showing Airborne LIDAR survey (Elprocus, 2020)

The LIDAR system requires a GPS base station within ~50 km of the measurement area to continuously operate, correct and improve the airborne GPS precision.

LIDAR has been used extensively in surveying and engineering for acquisition of elevation data. It has proven capabilities in producing extremely high accuracies and point densities,

hence allows precise and realistic three-dimensional presentations of elevation data (Carter *et al.*, 2012).

LIDAR survey data contains a lot of data points which require a lot of memory and excellent processing capabilities. Without the necessary tools, LIDAR survey data cannot be used effectively as a design resource. However, with recent three-dimensional modelling applications, new methods have been introduced to help in filtering and reducing the initial data into a manageable size (Sabatini, 2015).

AutoCAD Civil3D 2019 (normally referred to as Civil3D) is a civil infrastructural design and documentation software featured with a rich set of tools that provide a fast and efficient way to process, visualize and analyze surveyed data (Autodesk, 2021). In preliminary design, Triangulated Irregular Network (TIN) surfaces can be created using LIDAR survey point data in AutoCAD Civil3D 2019. A TIN surface consists of triangles forming an irregular triangulated network as shown in Figure 2.21 (Autodesk, 2019).

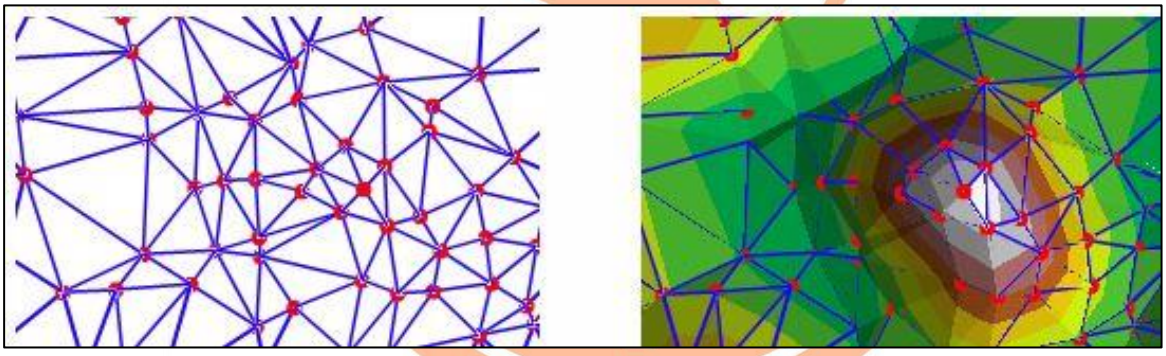

Figure 2.21 Example of a TIN Surface (ArcMap, 2016)

In Civil3D 2019, the TIN lines are created by connecting surface points that are closer to each other, this eventually results in a TIN model which represents a topographical surface consisting entirely of triangular facets. TIN surfaces are used in generating topographical surfaces from surveyed point data. Civil3D 2019 offers a fast and effective way of computing volumes and creating alignment profile cross sections using polyline drawn on top of TINs. These profile cross sections aid in obtaining slope geometries to help in site layouts and designs (Autodesk, 2019).

2.7 Regression Analysis in Machine Learning

Regression analysis involves a statistical technique that describes a relationship between variables. In this type of analysis, a statistical procedure called a **regression model** is used to estimate the relationship between two or more quantitative variables. In a two variable regression model, one variable is a **dependent** variable (y) while the other variable is an **independent** variable (x). The values of a dependent variable depend on the values of the independent variable (however not implying that y is directly caused by x). The independent variable may be known to cause changes in the dependent variable or may occur prior to the dependent variable in time (Tiemann & Mahbobi, 2010).

On a scatter diagram, a straight line cannot possibly pass through all the data points, therefore a line of best fit called the regression line is necessary. Statistically, a measure called R-Squared is used in measuring the closeness of observed known values to the fitted line (a measure of goodness-of-fit for a regression model). It evaluates the scatter of the data points around the regression line and measures the strength of a relationship between the dependent variable and the model on a scale of 0 - 100%. A higher R-squared denotes smaller differences between the observed data points and the fitted values (Tiemann & Mahbobi, 2010). However, according to Ellis *et al.* (2013), in some fields where processes are difficult to predict (e.g. geological, geotechnical, health), low R-Squared values are entirely expected. It was highlighted that low R-squared values do not affect the interpretation of the significant variables and important conclusions can be drawn.

Regression models are widely used models in *machine learning* for predicting target variables. The term *machine learning* is used to refer to an automatic identification of significant patterns in data (Shai & Shai, 2014). It is a type of *Artificial Intelligence* that allows systems to learn from data to improve, describe and make predictions without the need for explicit programming. Machine learning uses different algorithms to iteratively learn from data (Expert.ai, 2020). An algorithm is a problem-solving procedure carried out in accordance with a sequence of specified actions.

A machine learning model is the output produced when the machine learning *algorithm* is trained with data to learn from. An algorithm is trained with data and in the process it identifies patterns in the training data, mapping the input data attributes to the response to be predicted and generates a predictive (machine learning) model capturing these patterns

(Amazon Web Services, 2020). Thereafter, when the predictive model is provided with data, it produces a prediction based on the data that trained the model.

Machine learning algorithms have two most common categories; Supervised and Unsupervised machine learning algorithms.

2.7.1 Supervised Learning

The basic concept behind supervised learning is that data offers examples of situations and a specified result for each example. Then a machine (e.g. a computer) uses this data to build the model (the mapping function), which is then used to predict outcomes of the new data set based on the past examples. Technically supervised machine learning is where there is an input variable (a) and an output variable (b) and an algorithm is used to approximate a function that maps (a) onto (b) (Equation 2.1). The raw data required to train the model (or approximate the function) is (a) and (b), this means that input and output data is known but the mapping function is unknown (Brownlee, 2016).

$$b = f(a) \quad (2.1)$$

The outcome is a mapping function f(a), approximated as accurate as possible such that output variables (b) can be predicted from new input data (a). In Figure 2.22, three apples are used as raw data to train the model (or approximate f(a)) so that underlying patterns and relationships are detected. This results in a model/function (as shown by a human head), through which output variable 'It's an apple!' can be predicted from an unknown/new input variable '?' as shown.

Supervised learning can be further classified into *Regression* and *Classification*. With regression, the output variable is a numerical value (for example, mass, friction angle, cohesion) normally referred to as an independent variable while the input variables are referred to as dependent variables. There are different types of regression which include linear regression, multiple regression and polynomial regression. With classification the output variable is a unique group/class/category of similar objects (for example, spam email or not spam email) (Brownlee 2016).

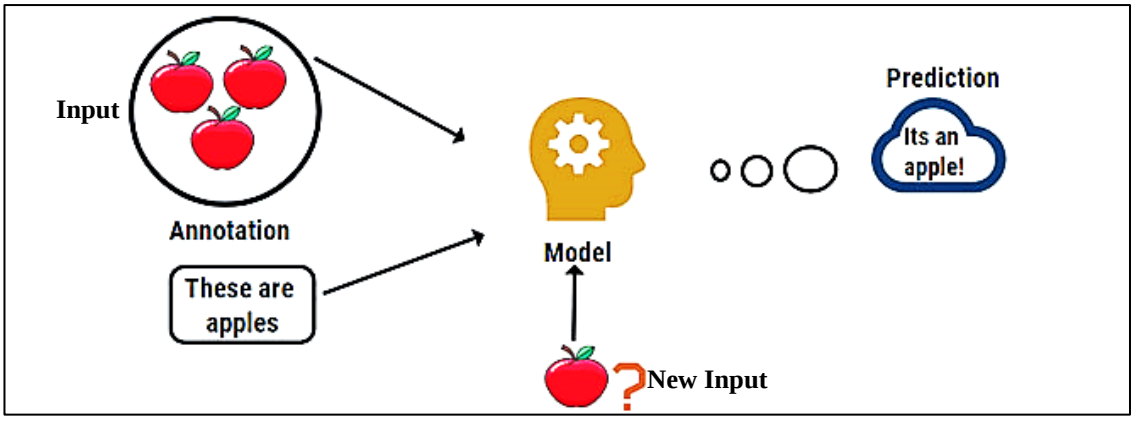

Figure 2.22 Illustration of how Supervised Machine Learning Works (Educba, 2020)

Supervised machine learning algorithms have the opportunity of measuring prediction accuracy called algorithm performance. This is due to the existence of a labelled full data set (known input and output variables) that is used to train the model. The answers are known, and the algorithm is used to correct the training data predictions iteratively. Consequently, this is considered the most accurate, reliable and simple method (Vaseekaran, 2018).

2.7.2 Unsupervised Learning

This type of learning is used when the problem requires a large amount of unlabeled data. Technically, this is where there is an input variable (a) and the corresponding output variable is unknown. The goal is to model the underlying patterns or clusters, structures and/or distribution in the training data with an intention to learn from the data. The algorithms used in unsupervised machine learning are able to use input data to search for rules, find patterns, summarize and group data points in an attempt to derive meaningful insights for better description of data to the user. In Figure 2.23, a combination of bananas and apples are used to represent input data which is introduced directly into the machine/computer and the output is in the form of apples and bananas in two separate clusters. Unsupervised learning problems can be further grouped into *Clustering* and *Association*. Clustering problems require a search for inherent groupings in data, while association problems require a search from rules that provide a description of large portions of data (Brownlee, 2016).

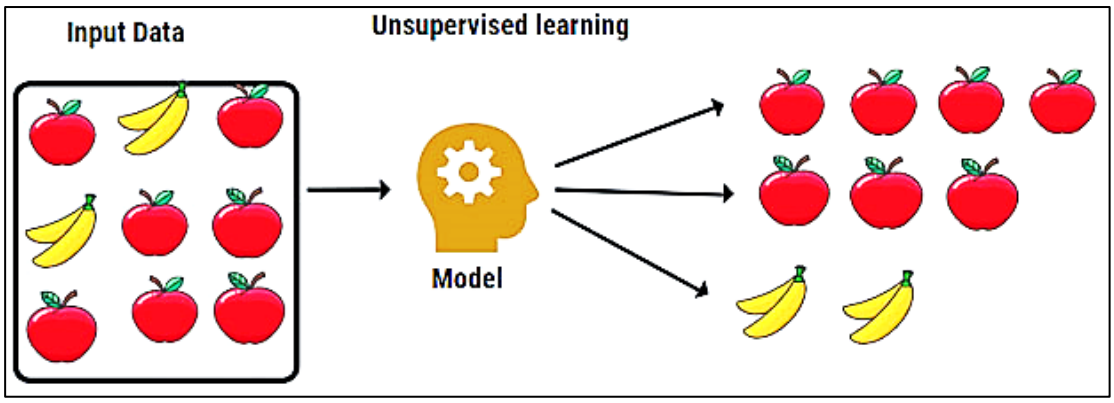

Figure 2.23 Unsupervised Machine Learning Simplification (Educba, 2020)

2.7.3 Machine Learning Software Programme

This study adopted the use of MATLAB as the basis for regression analysis. MATLAB (Matrix Laboratory) is a programming language and numerical analysis environment developed by an American privately held corporation called MathWorks. It was specifically designed for engineers and scientists to analyze data, build algorithms, construct models as well as applications. MATLAB has been used extensively in engineering for analyzing data, solving problems, experimentation and algorithm development. Its extensive use has been attributed to a friendly programming environment, easily used graphics, and powerful built in operators (Schreiber, 2007). There are several *Apps* embedded in MATLAB, these Apps are self-contained MATLAB programmes in which tasks or calculations are automated. All operations concerning the task are performed within the App, these include importing data, analyzing data and generating results. Among others, the *Regression Learner App* (RLA) is of interest to this study.

Regression learner App

This App is featured in MATLAB to allow the user to carry out iterative regression model training to predict data using supervised machine learning. Training a machine learning model is carried out by providing a machine learning algorithm with data to learn from. The regression model is a predictive model that results from the training process. The Regression Learner App leads into a step-by-step regression analysis from which various algorithms can be chosen for training and validating regression models. The following flow chart (Figure 2.24) provides a summary of the steps used in training regression models in Regression Learner App (MathWorks Inc., 2020).

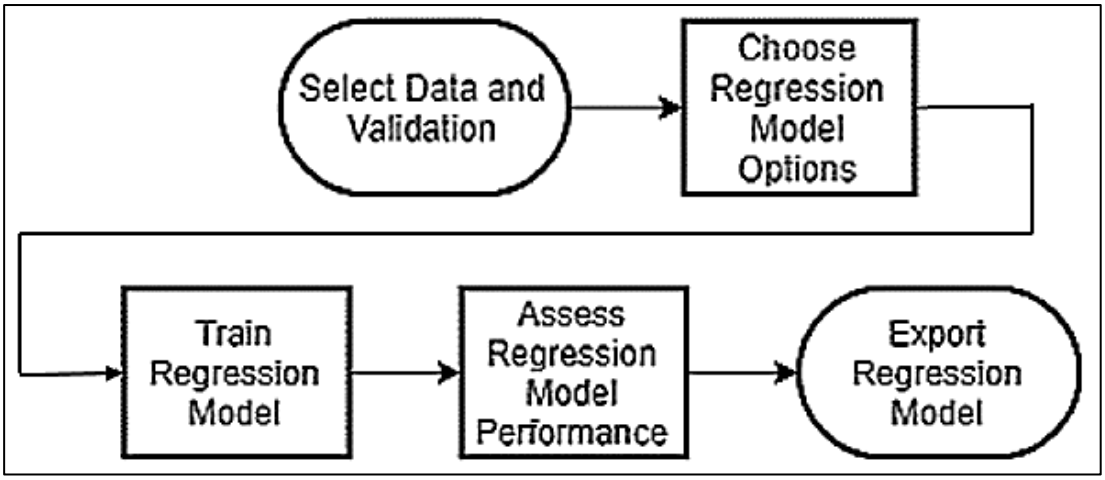

Figure 2.24 Workflow for Training Regression Models in Regression Learner App (MathWorks Inc., 2020)

Machine learning regression models in regression learner App

The Regression Learner App consists of different regression models that use training data to produce different types of predictive models. These are listed as follows:

a) *Linear regression models*: A relationship between two quantitative variables is modelled by applying a linear equation to observed data. The equation is presented in the form $y = mx + c$, where y is a dependent variable, m is the slope of the line, x is an independent variable and c is a y-intercept (the y value when $x = 0$) (Hayes, 2021).

b) *Regression trees*: This is a regression method that allows an output variable to be predicted from a mixture of continuous and categorical input variables. The goal is to predict the output variable based on a number of input variables (FrontlineSolvers, 2021).

c) *Gaussian process regression models*: A Gaussian Process is a random process that involves a combination of random variables indexed by space and time. Any finite linear combination of these random variables is normally distributed. Gaussian Process regression models use a Gaussian Process to predict values of unknown points from training data through measurements of similarities between points (kernel functions) (Bachoc, 2017). The theory of Gaussian Process Regression is shown in Appendix E1 for depicting an in-depth description on training a GPR model and performing prediction.

d) *Support vector machines*: A support vector machine is a linear model used in regression and classification. It involves creating a line or a plane across data to separate it into classes (Pupale, 2018).

e) *Ensembles of regression trees*: This is a predictive model consisting of a mixture of weighted regression trees. A combination of multiple regression trees typically improves model efficiency and makes predicted responses more accurate (FrontlineSolvers, 2021).

Model performance evaluation

After model training the RLA presents the regression analysis results in three types of plots for assessment of model performance:

i. Response plot.
ii. Predicted versus Actual plot.
iii. Residuals plot.

Response plot: The Response plot is a graph of response/output variables plotted against input variables. An example of a response plot is shown in Figure 2.25. The blue-point markers in Figure 2.25 represent the response obtained when plotting input dataset $\{(a_1, b_1); (a_2, b_2); \ldots\ldots; (a_i, b_i)\}$ that is used to train the model. In this plot, (a) is represented as Horsepower and (b) is represented as the response (in MPG) in the figure. The plot represented by the blue markers is referred to as the true response (the observed known values), it is obtained when plotting training/imported data. The orange plot markers represent a predicted response; this is the predictive regression model which results from training. The red bars represent the error bars, the length of each bar represents the difference between the predicted response and the true response (MathWorks Inc., 2020).

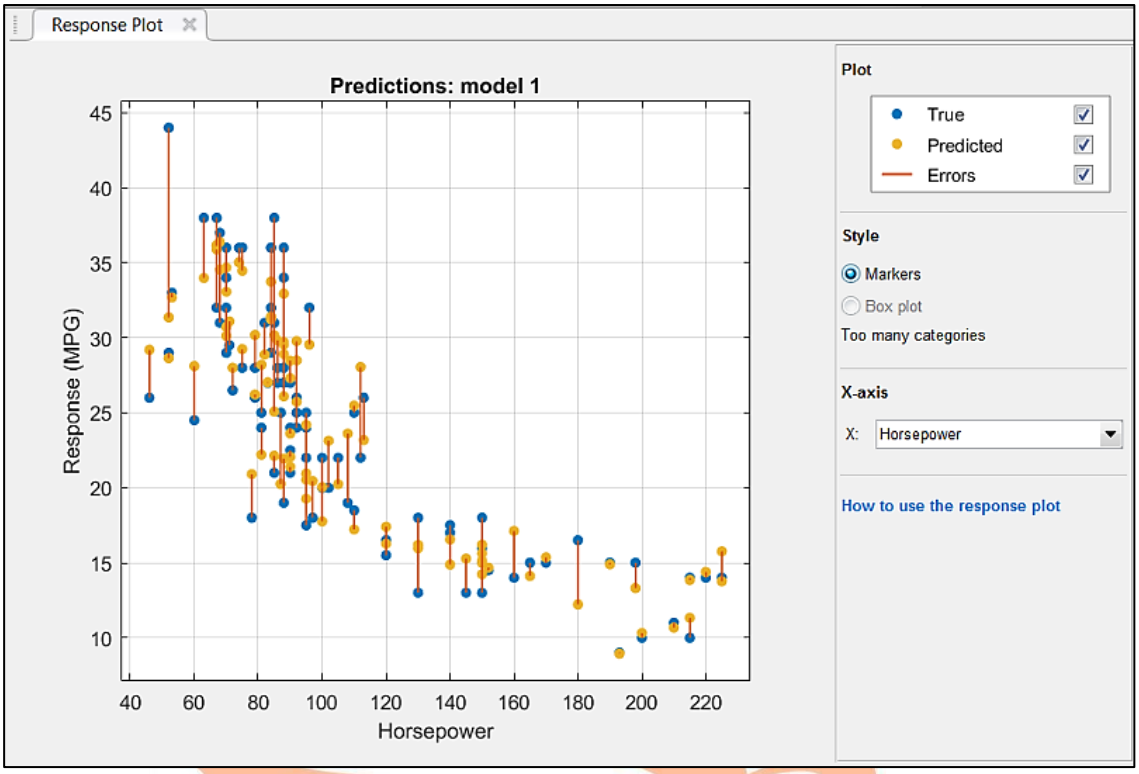

Figure 2.25 Response Plot from MATLAB Regression Learner App (MathWorks Inc., 2020)

The Response plot is used for viewing the regression analysis results and assessment of the model performance. The performance of the model is assessed based on the following model statistics summarised in Table 2.3.

i. Root Mean Square Error (RMSE).
ii. Mean Square Error (MSE).
iii. Mean Absolute Error (MAE).
iv. Coefficient of Determination (R-Squared).

The Regression Learner App has the capability to accommodate more complex regression curves (like that of Gaussian processes) without specifying the relationship between the response and predictor variables with a predetermined regression function. With these types of models, responses for new data can be predicted using the trained model after being exported to MATLAB workspace (MathWorks Inc., 2020).

Table 2.3 Model Statistics Description

Statistic	Description	Tip
RMSE	Measures the error of prediction. It represents the mean difference between the observed values and the predicted values.	Smaller values are better.
MSE	Represents the average squared difference between the observed values and the predicted values.	Smaller values are better.
MAE	Represents the magnitude of errors of prediction without consideration of direction.	Smaller values are better.
R-Squared	Lies between 0 and 1. Indicates the goodness of fit of the model.	Values closer to 1 (or 100%) are better.

Predicted versus actual plot: A predicted versus actual plot is another measure of model performance whereby the model's predicted response is plotted against the actual response. The predicted response is equal to the actual response in a perfect regression model as thus the values are presented diagonally as shown by a black solid line in Figure 2.26. The predictive error for any point of observation is a vertical distance from the black solid line to that specific point of observation (the blue marker) (MathWorks Inc., 2020). A successful model has minor errors, so the observation points (predictions) should be scattered along the black line as shown in Figure 2.26.

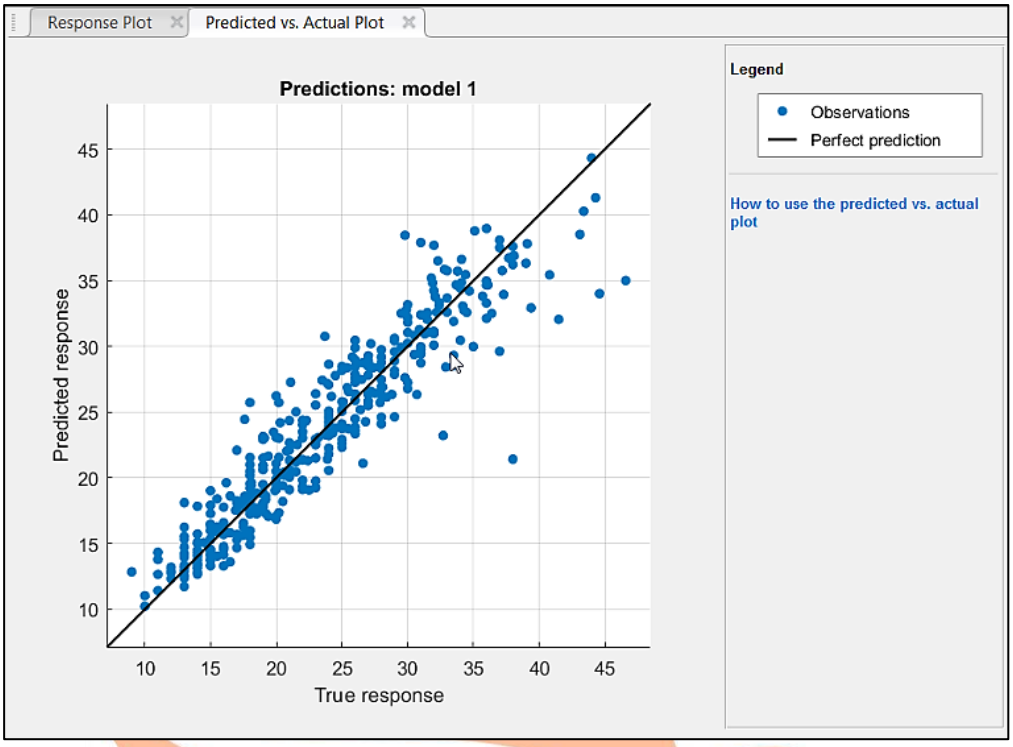

Figure 2.26 Predicted Versus Actual Plot Using MATLAB Regression Learner App (MathWorks Inc., 2020)

Residuals plot: A residual value measures the extent to which a regression line misses a data point (errors). A regression line provides a best fit to the data points, however other data points lie within the line that others do not. A Residual plot has the residuals (residual values) on the vertival axis and the independent variable or the true response or the predicted response or the record number on the horizontal axis. It is also used for model performance evaluation, it shows differences between the predicted and actual responses (MathWorks Inc., 2020). A good model has residuals roughly and symmetrically scattered around zero as shown by a black solid line in Figure 2.27.

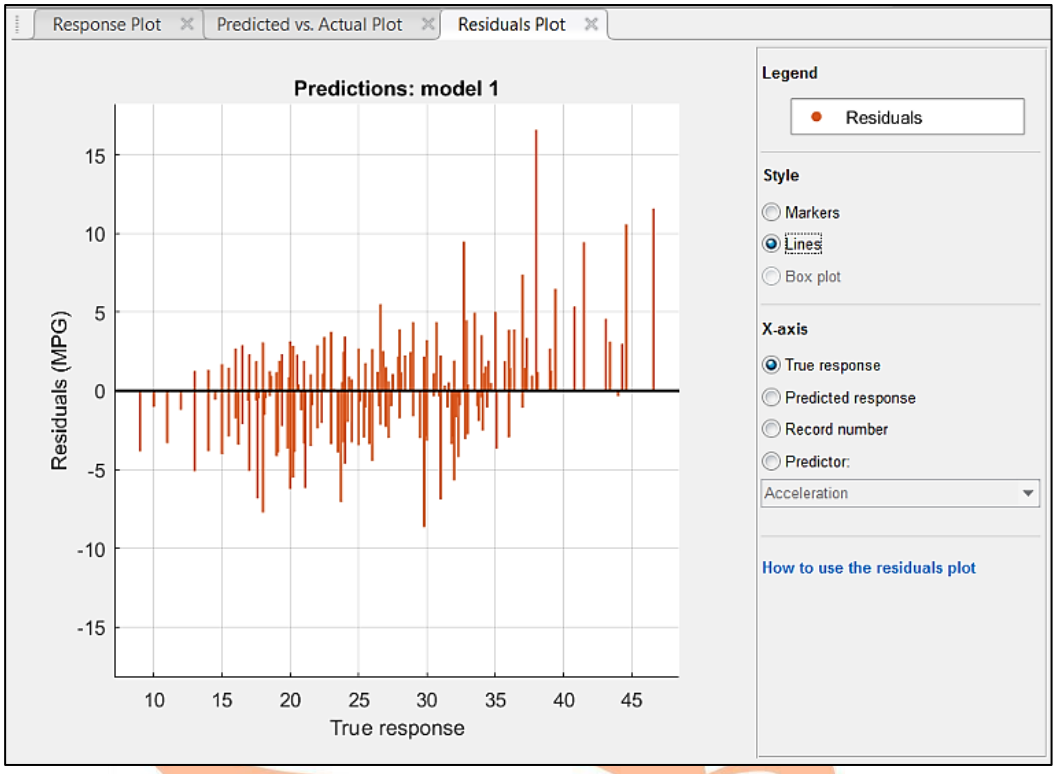

Figure 2.27 Residuals Plot Using MATLAB Regression Learner App (MathWorks Inc., 2020)

2.7.4 Machine Learning Applications in Geotechnical Engineering

Machine learning has been used effectively in geotechnical engineering, to develop powerful predictive models for soil and foundation engineering parameters/behaviors. This approach allows for the estimation of geotechnical parameters from empirical or numerical correlations that are developed from regression fitting to a dataset (Fallah & Yousefpour, 2018). Several studies have focused on these types of applications, and they continue to grow in the geotechnical engineering field. Researchers such as (Mustafa *et al.*, 2013) have tested machine learning algorithms for modeling responses of pore water pressure to rainfall. The algorithms were assessed to determine the best algorithm to model the dynamics of the soil pore water pressure response to the rainfall. It was found that training time and prediction accuracy were related to the appropriate type of training algorithm.

Taormina *et al.* (2012) employed the Feed Forward Neural Networks (FFNs) for predicting and forecasting in a coastal unconfined aquifer system. The model was initialized with observations of groundwater elevations at specified times, the built FNN was expected to produce variations in water level using only the extended input variables, identified as

rainfall and evapotranspiration. As part of their findings, they discovered that the developed FNN could reproduce accurate groundwater levels for several months. The algorithm was proven a reliable tool for modelling aquifer responses or reconstructing missing data.

With machine learning techniques, geotechnical engineering parameters are not always directly obtained from laboratory and field tests, rather often obtained through regression fitting to a dataset (Fallah & Yousefpour, 2018). This approach saves both time and money, because when a more accurate model is in place more output variables can be generated, eliminating the need for conducting tests.

CHAPTER 3

METHODOLOGY

3.1 Introduction

This study involved the use of different methods, both for slope stability analysis and regression analysis. This chapter contains a description of the methods that were used in studying the Orapa Mine Slurry Dam 2 including those that were adopted during construction of the dam. Analysis methods are listed as follows:

i. In-Situ Testing: Cone Penetration Testing with Pore Pressure measurements (CPTu).
ii. Stability Analysis: Limit Equilibrium Method - Deterministic, Probabilistic and Sensitivity analysis methods; Finite Element Method – Deterministic analysis method.
iii. Regression Analysis: Supervised machine learning.

3.2 Deposition Methodology (Cycloning System) and Dam Construction

The slurry was deposited through a cyclone separation method throughout the lifespan of Slurry Dam 2 (Figure 3.1). This method is described in detail in Section 2.3, it involved building free draining outer impounding walls using the cyclone coarse underflow (coarse fractions/grits), within which the fine overflow (fines content/slime) could be stored.

Cyclones adopt a principle of centrifugal acceleration to separate the fines content from the coarse content and the sizes of the three openings (the feed/entry, the overflow/fine product opening and the underflow/coarse product opening) have an influence on the separation characteristics achieved by the cyclone (see Figure 2.3). The coarse underflow was used to construct the dam within which the fine overflow would be stored (Figure 3.1).

A progressive downstream deposition method was used and the numbers in Figure 3.2 show the sequence in which the dam was constructed. The most important aspect of this method is to maintain an adequate freeboard, this could be achieved by spending more time in building the outer wedge (wedge 3 and 6). This allows for containment of the overflow and

the drying of the beach before proceeding to wedge 1, 2, 5 or 4 hence preventing issues of overtopping and piping failure.

Figure 3.1 Cyclone Deposition of Underflow for Embankment Construction at Orapa Mine Slurry Dam 2 (Golder Associates Africa (Pty) Ltd, 2002)

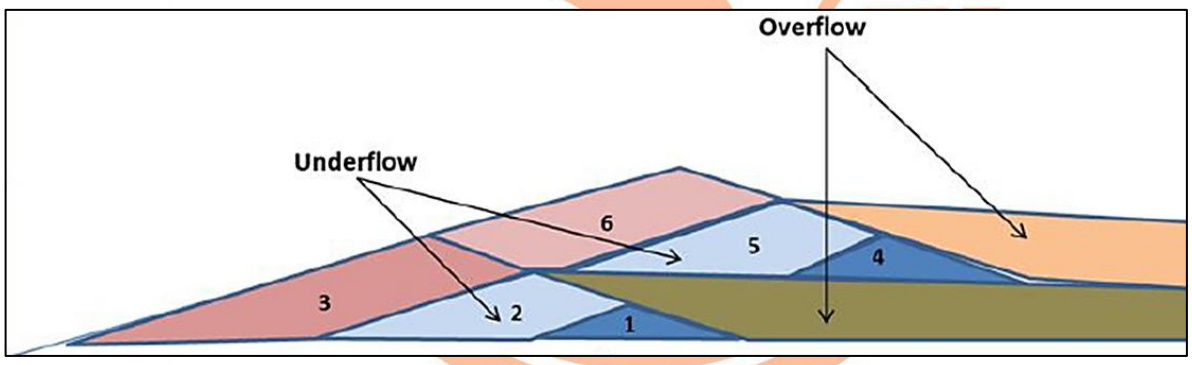

Figure 3.2 Dam Construction Methodology (Golder Associates Africa (Pty) Ltd, 2002)

3.3 Cone Penetration Test (CPTu) Method

This study involved the use of the Envi 20-ton pusher (shown in Figure 3.3) equipped with an Envi-logger G1 software for CPTu data acquisition on the Orapa Mine Slurry Dam 2. This rig was manufactured in Sweden, it is small and portable enough to be transported on a pick-up truck or a trailer.

Figure 3.3 The Envi 20-ton Pusher

3.3.1 Cone Penetration Testing Procedure

CPTu was carried out using the ISO 22476-1:2012 standard of geotechnical and field testing. The procedure started with rig setup, which was carried out at each sounding spot/test point to get the rig fully secured on the ground and ready for testing. It involved marking the sounding spot and drilling to secure four anchors into the ground. The ground anchors were screwed into the ground through the use of an anchoring unit operated by at least two people (see Figure 3.4). The main purpose of ground anchors was to hold the rig down during CPT sounding by providing enough reaction force to hold the rig in place. For an increased reaction force, extension rods were used to increase the length of the anchors.

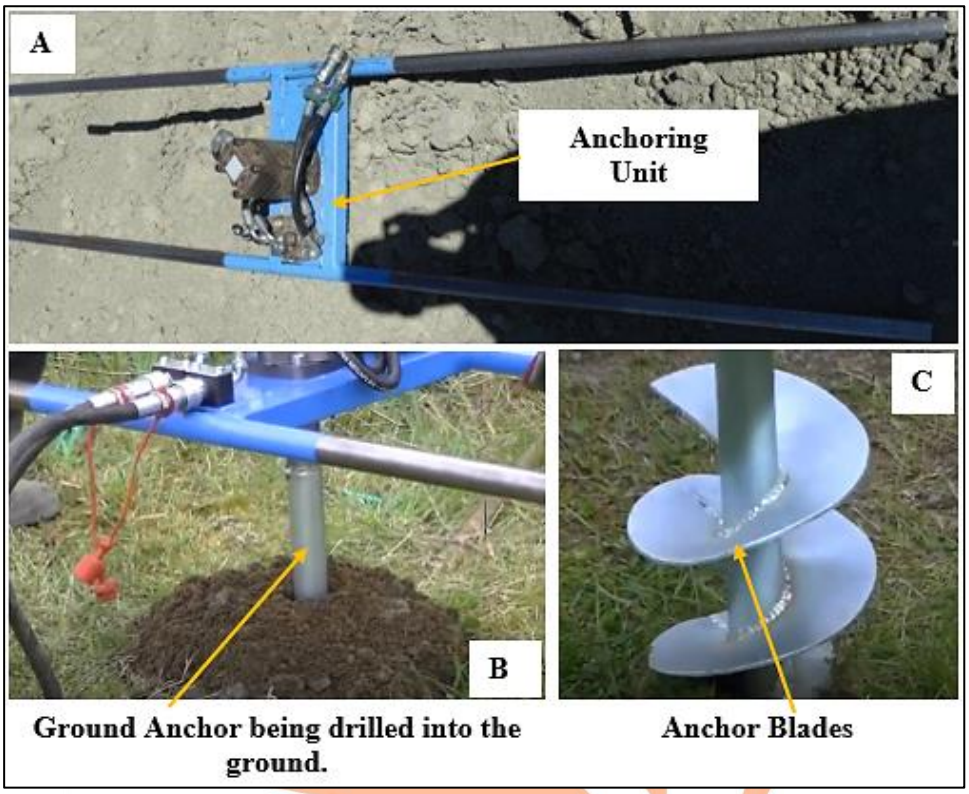

Figure 3.4 Insertion of Ground Anchors during a CPTu Rig Setup

After securing the four ground anchors, the rig was placed at the center of the ground anchors and dismantled from the trailer/carrier as shown in Figure 3.5.

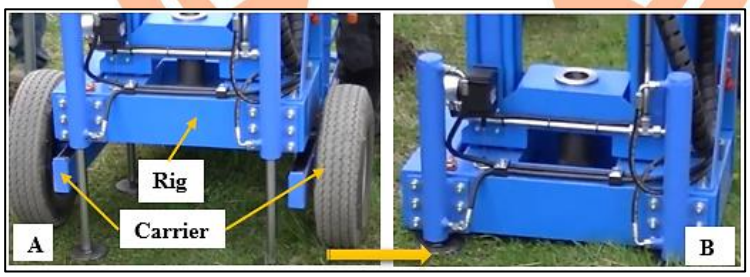

Figure 3.5 A - Placement of Rig at the Center of Four Ground Anchors;
B - Removal of Trailer, Leaving the Rig Resting on the Ground

Confirming the verticality of the pusher is one of the most important aspects during rig setup, it should be levelled and set to as near vertical as possible (at 90^0 to the ground). The verticality of the pusher and the straightness of the extension rods ensured that the thrust direction did not deviate from the vertical path so that correct readings were obtained during testing. This was done using the two bubbles shown in Figure 3.6 (Picture A), which level

the pusher in two Cartesian planes. Four beams were used as shown in Figure 3.6 (Picture B) to connect the rig to the ground anchors and secure it on the ground with beam locks (Picture C).

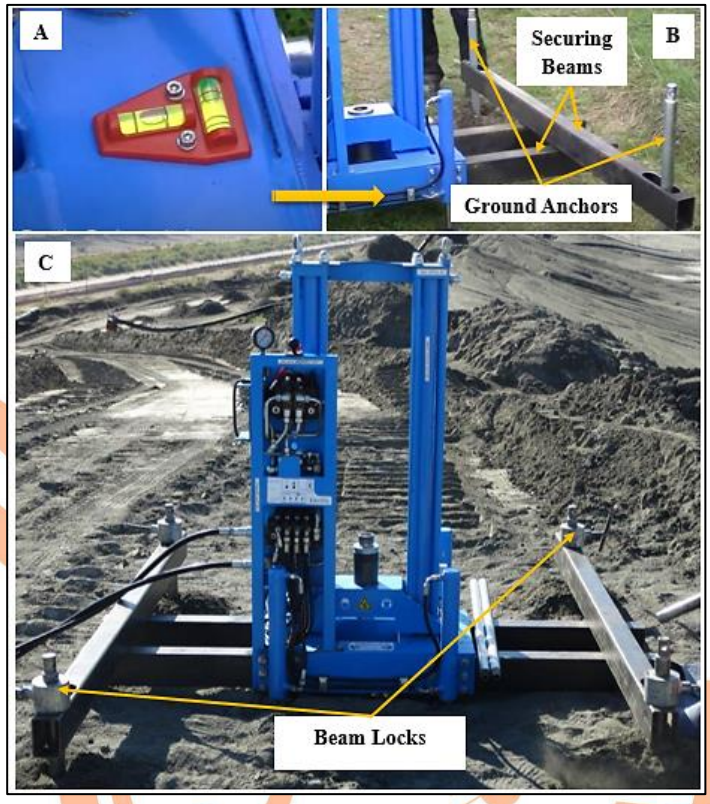

Figure 3.6 Picture A - Rig levelling; Picture B - Installation of Securing Beams; Picture C – Locking of Securing Beams with Beam Locks

The Envi 20-ton pusher contains two hydraulic cylinders with a stroke of one meter allowing to push one-meter extension rods in one stroke. Its data transfer system consists of a data transfer cable/cord threaded through the extension rods for data transmission to the computer and voltage supply to the penetrometer (see Section 2.6 for penetrometer description). The rate of penetration of 20mm/second was used in one-meter increments (extension rod length). Dissipation tests were carried out at selected one-meter rod breaks to monitor the pore water pressure decay with time. The same procedure was used for all tests carried out on the Orapa Slurry Dam 2. A complete setup of the rig is shown in Figure 3.7.

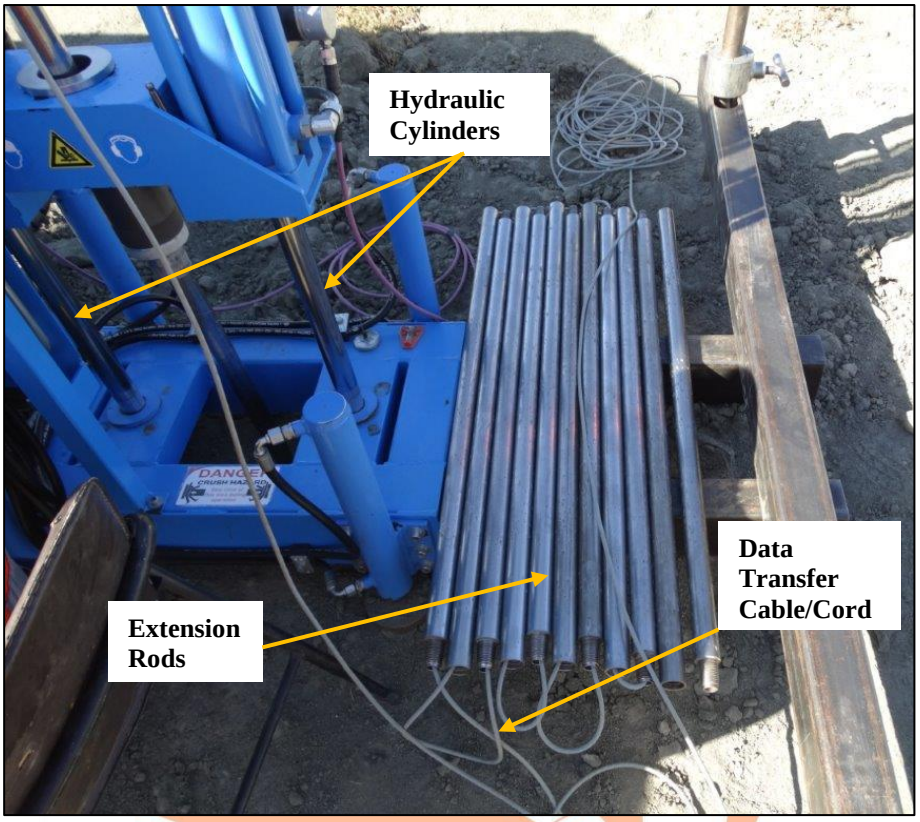

Figure 3.7 Complete Setup of the Rig, Depicts Readiness to Start the Test

3.3.2 Test Point Geographic Locations

A total of fifteen CPTu tests were carried out on the Orapa Mine Slurry Dam 2, five (test points 3, 6, 8, 12 and 13) were located on the beach, five (test points 2, 5, 7, 9 and 15) at the top of dam wall and five (test points 1, 4, 10, 11 and 14) on the downstream side of the embankment. Data was collected from the geographic locations shown in Figure 3.8 on Orapa Slurry Dam 2 and was analyzed and interpreted using a software called CpeT-IT. CpeT-IT is a detailed software package used to interpret raw CPTu data in terms of Soil Behavior Type (SBT) and other geotechnical parameters. It uses current published correlations based on reviews by Lunne, Robertson and Powell (1997) and Professor Robertson's recent updates (Geologismiki, 2018), (see details in Section 2.6.6). The tests involved continuous measurements and recording of cone tip resistance, friction sleeve, pore pressure and conducting dissipation tests at required depths to attain equilibrium pore pressure.

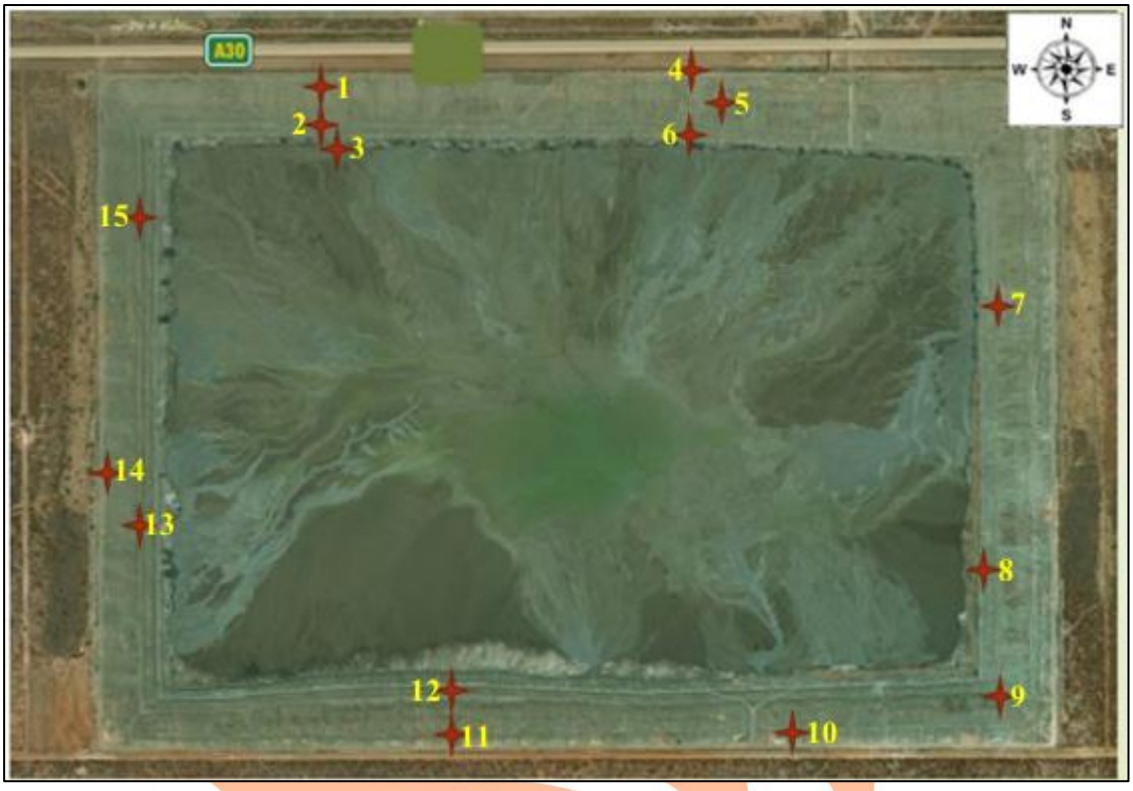

Figure 3.8 Geographic Locations (shown by ✦) of Fifteen Tests carried out on Orapa Mine Slurry Dam 2

3.3.3 CPTu Data Interpretation

The CpeT-IT 3.0 software programme described in detail in Section 2.6.6 was used for interpreting CPTu data which was saved in American Standard Code for Information Interchange (ASCII) data files normally referred to as text files. The input parameters required by the software were as follows:

i. Depth.
ii. Cone Tip Resistance.
iii. Sleeve Friction.
iv. Pore water Pressure.
v. Unit Weight.

CpeT-IT 3.0 utilizes established correlations for computations of important geotechnical parameters. These parameters include Permeability, Modulus of Elasticity, Relative Density, Friction Angle, Shear Modulus, Undrained Shear Strength and Over Consolidation Ratio. Some of these correlations use a range of specified values, which depend on factors such as soil type and geology. However, the software uses default values that have been

selected to produce generally low estimates of the computed parameters. The output geotechnical parameters were presented in the form of labelled graphs, stratigraphic sections and tables (see Section 4.2). The predicted geotechnical parameters were used in slope stability analysis to define the materials adding up to the slurry dam slope model. Mean values were used as input for both the Limit Equilibrium and Finite Element Deterministic analyses, and the range and standard deviation of these values were used for the Probabilistic-Sensitivity analysis.

3.4 Lidar Survey Data Interpretation

LIDAR survey was imported in the form of a topographic map and interpreted using Civil 3D 2019 design software (see Section 2.6.7). Alignments (the purple lines) labelled in Figure 3.9 designate cross section lines. They were used to cut across slopes in order to generate and present slopes in the form of profiles (with elevation on the vertical axis).

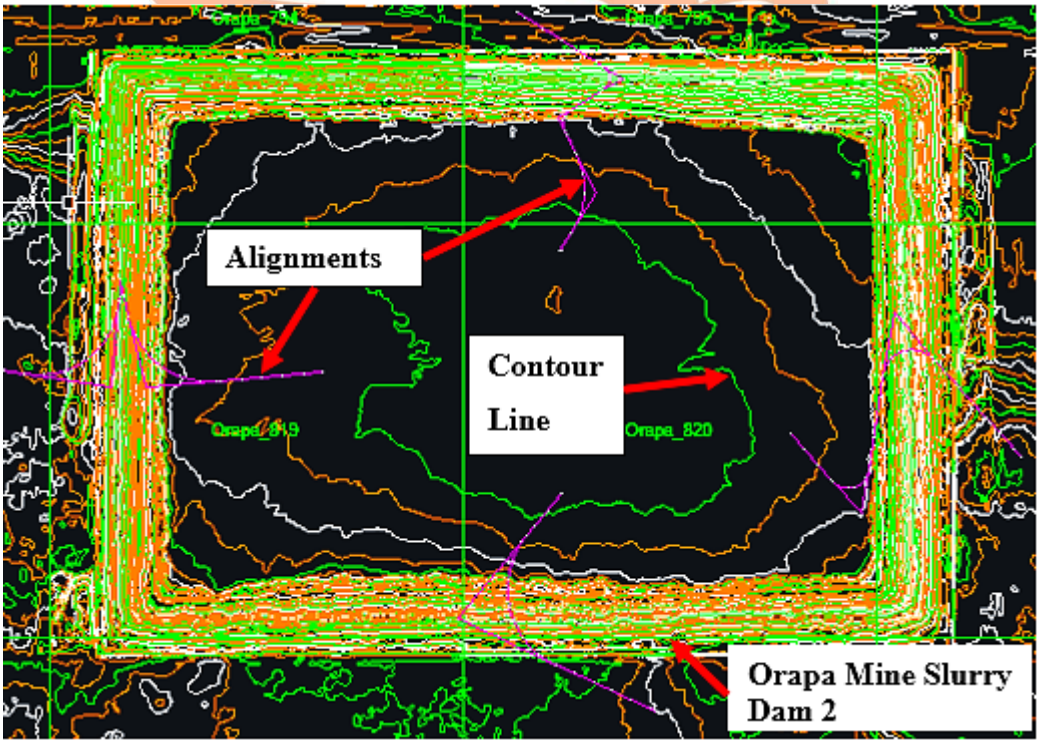

Figure 3.9 Topographic Map of Orapa Mine Slurry Dam 2, using Civil 3D

A profile view of the slope helped in viewing elevation changes of the slope (z-axis), therefore profile views were used in determining the slope geometry. Profile views obtained for the four dam walls are shown in Figure 3.10 to Figure 3.13 with elevations presented in feet above mean sea level. Coordinates of the slope boundary were exported to an excel file

and used as input in Slide software as external boundary coordinates. The external boundary coordinates obtained from Civil 3D 2019 design software were used in conjunction with CPTu geotechnical sections to produce complete slope geometries through interpolation showing material boundaries.

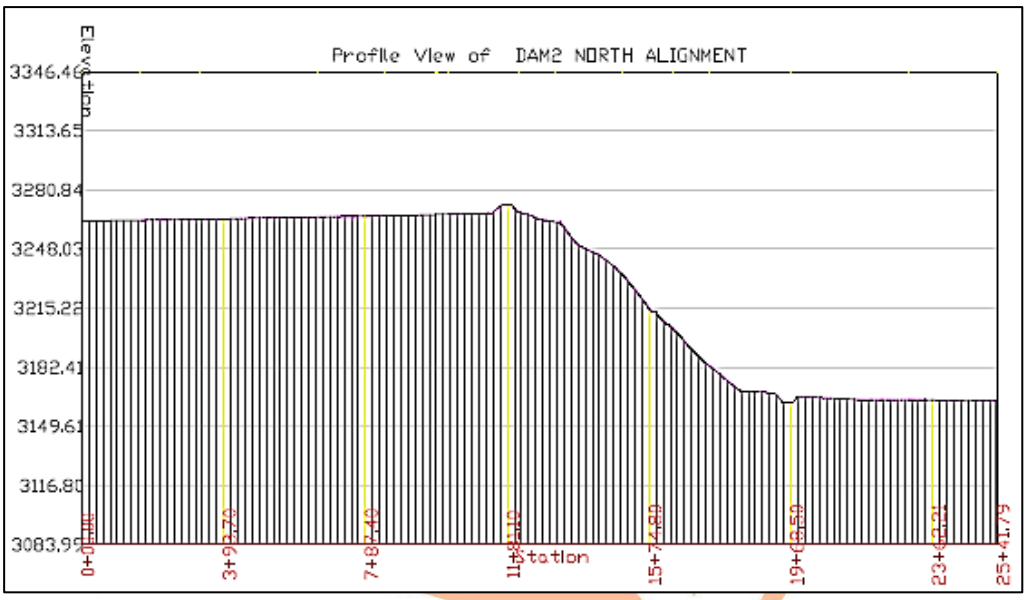

Figure 3.10 Profile View of Orapa Slurry Dam 2 North Dam Wall

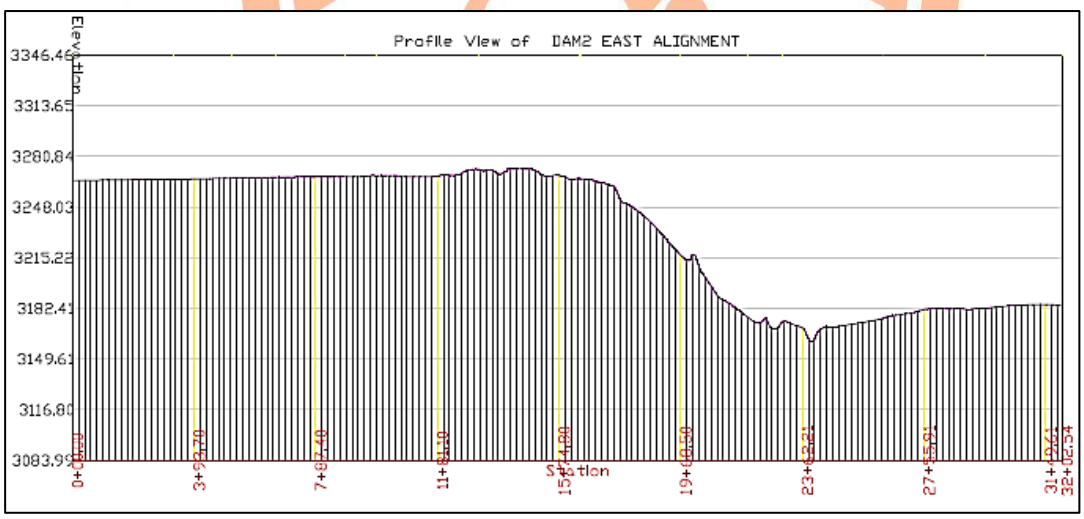

Figure 3.11 Profile View of Orapa Slurry Dam 2 East Dam Wall

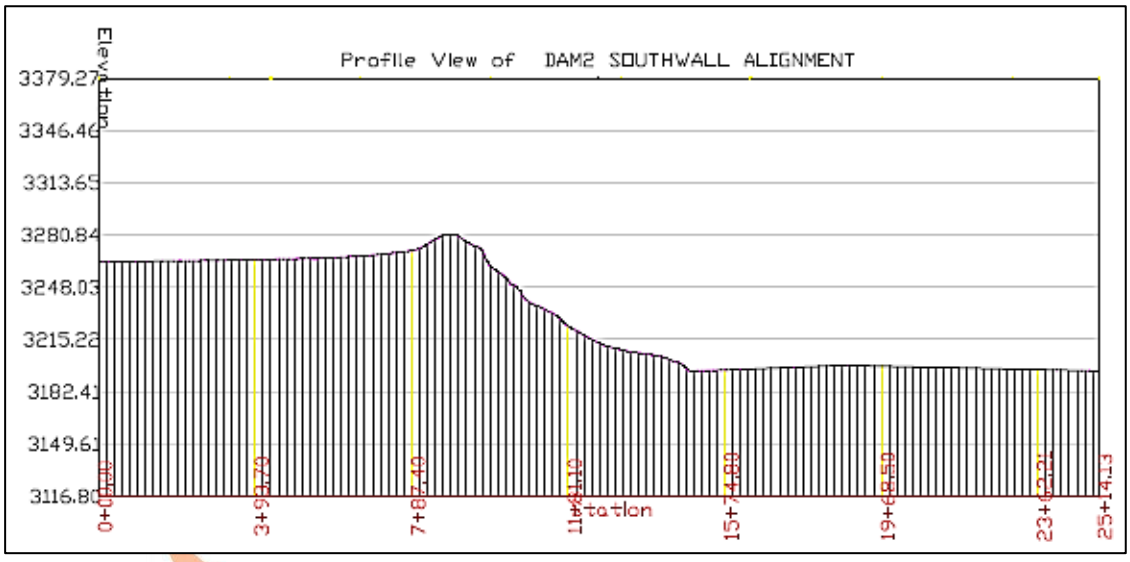

Figure 3.12 Profile View of Orapa Slurry Dam 2 South Dam Wall

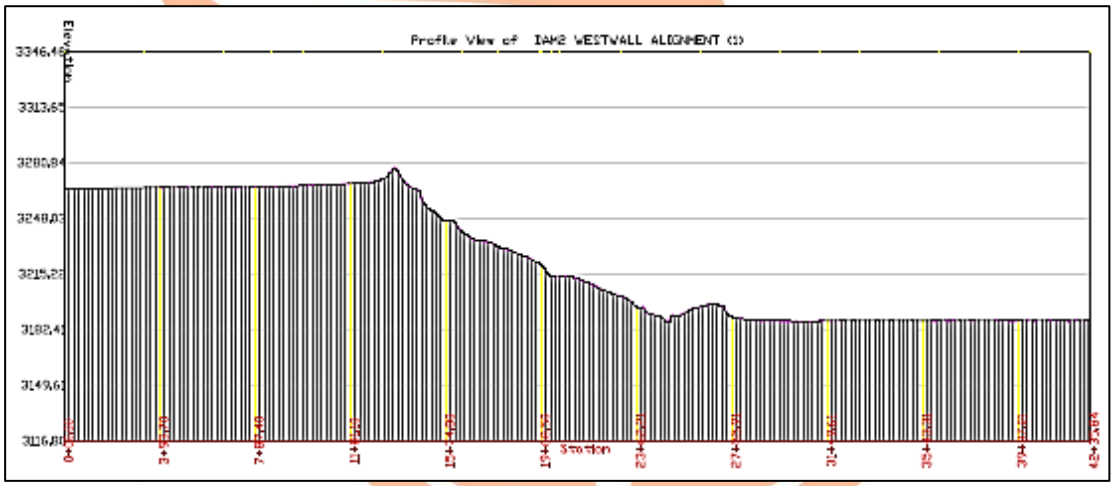

Figure 3.13 Profile View of Orapa Slurry Dam 2 West Dam Wall

3.5 Stability Analysis

Piezocone testing involved the establishment of shear strength properties including friction angle, cohesion, elastic modulus and Poisson's ratio. Afterwards, geotechnical modelling followed, which involved the use of Limit Equilibrium and Finite Element analysis methods.

A model was used to appropriately simplify the complex nature of reality. The skill in modelling was to establish the correct degree of simplification, that was to analyze the

nature of the problem and recognize the key features that needed to be considered and be included in the design. In dam modelling, the first aspect that was required was geometry.

For this study, the geometry of the slopes was acquired from CPTu and Lidar survey data. Lidar survey data provided the slope profiles described in Section 3.4 to define the external boundary of the slope. The geotechnical sections obtained from CPTu provided information about the stratigraphy, they were used for defining the material properties and boundaries. The pore pressure dissipation test results (pore pressure against time) were used to approximate the depth at which pore pressure equals equilibrium pore pressure. Equilibrium pore pressure was the pore pressure obtained at t_{100} on a pore pressure versus time graph (see Section 2.6.5). The blue linear graph shown in Figure 3.14 represents a change in equilibrium pore pressure with respect to depth. It was obtained when superimposing dissipation test results (plotting (depth-of-dissipation-test; equilibrium pore pressure) coordinates) on a depth versus pore pressure plot. The depth at which pore pressure equals zero when extrapolating from the blue linear graph is representative of the approximate phreatic surface depth.

During CPTu data recording, positive values of pore pressure were encountered at an elevation of approximately 978m (±5 m) above mean sea level. This depth marks the beginning of this pore pressure log, therefore, 0 meters in this log represents 978m above mean sea level as labelled in Figure 3.14. This is labelled by a blue groundwater level sign in Figure 3.14, this depth is the approximate phreatic surface depth. Each CPTu test line (with respect to depth) was composed of at least three dissipation tests, this offered assistance towards attaining an accurate equilibrium pore pressure linear graph.

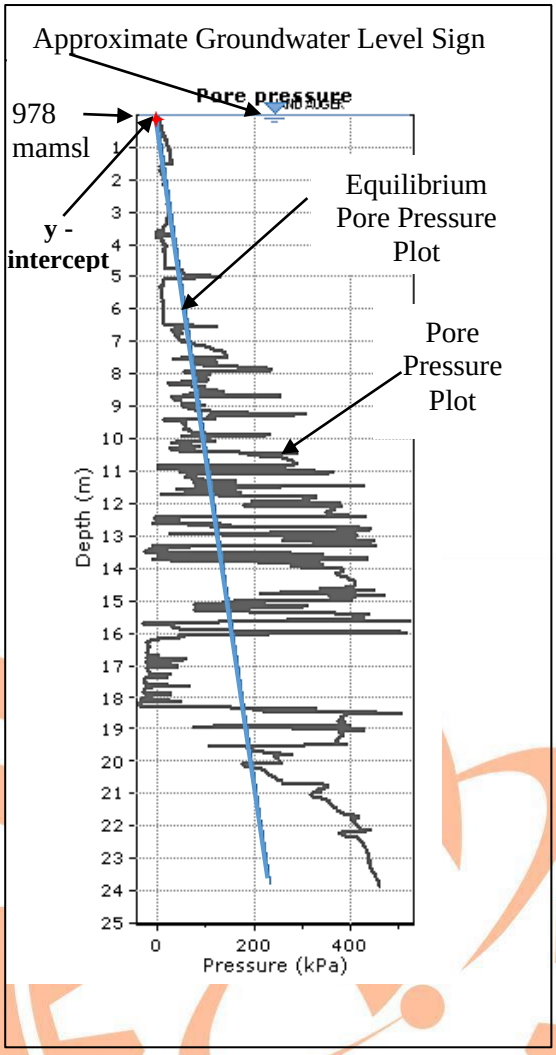

Figure 3.14 Dissipation Test Results for North Dam Wall Test Point 009 showing Pore Pressure vrs. Depth

The approximated phreatic surface level for each piezocone test point was used as input in a finite element groundwater seepage analysis model. It was used collectively with permeability to compute pore pressures for each slope in both Slide and RS2 analysis packages (see Figures 4.10 to 4.13).

The main purpose of stability analysis had been to investigate failure phenomenon and the overall current stability of Slurry Dam 2. In the design of tailings dams, the stability of the downstream slope was of utmost importance because the most critical failure modes and factors of safety occur along and towards the downstream slope as shown by the arrows in Figure 3.15. Therefore, the failure direction was chosen to be towards the downstream side of each slope.

Figure 3.15 Arrows showing Critical Failure Direction Considered in this Study

The average height of Orapa Slurry Dam 2 is currently at ~1000 meters above mean sea level (equivalent to ~3265 feet above mean sea level. The stability assessment was conducted along four sections of the dam (A, B, C and D) as shown in Figure 3.16. Each cross section had its unique slope angle and geometry.

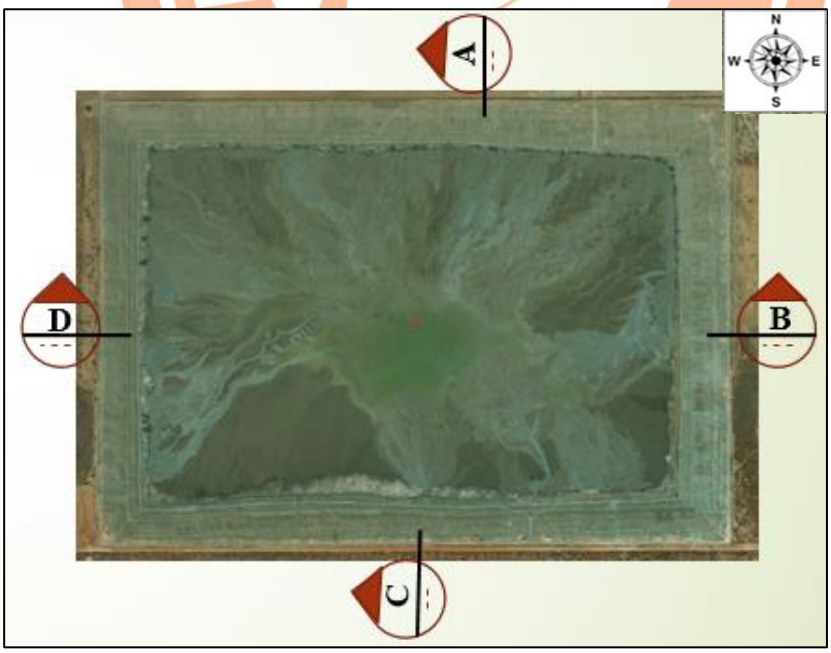

Figure 3.16 Locations of Cross Sections on Slurry Dam 2

Slide 2018 slope stability analysis package was the basis of the equilibrium analysis for this study. The Bishop simplified, Spencer and Morgenstern-Price methods were used and the results were compared. Four models shown in Figure 4.6 to 4.9 were analyzed based on circular mode (circular slip surface analysis), using Grid, Slope and Auto-Refine slip search methods (see Section 2.5.1).

For the Finite Element analysis, the geometries of the four slopes were simply imported from Slide after the limit equilibrium analysis was completed. All the necessary geotechnical parameters were input into RS2 2019 for each slope and the materials making up the slope. After both the limit equilibrium and finite element analyses, further analysis involved regression analysis between depth and the three CPTu measured variables (cone tip resistance, sleeve friction and pore pressure).

3.6 Regression Analysis

Regression analysis involved an investigation of the relationship between CPTu measured variables of Orapa Slurry Dam 2 (cone tip resistance, sleeve friction and pore pressure) and depth along the dam walls. The main idea behind this investigation was the possibility of a prediction of these variables with any selected depth as input. This was associated with a rigorous use and selection of suitable supervised machine learning algorithms for use in modelling these variables against depth.

The Regression Learner Application (RLA) through MATLAB R2020a was the basis for this investigation. Figure 2.24 shows a summary workflow for training regression models in RLA. The procedure for building regression models involved importing data in the form of a table into the App. Imported data was made up of cone tip resistance, sleeve friction and pore pressure alongside recorded depth. It was first exported from ASCII text files and imported into excel files for sorting, outlier analysis and the removal of duplicates. A single circle of analysis (regression model training involving a single dataset of Depth versus a CPTu variable for each test point) required a two-column table with a chronologic collection of depth values on the left column and CPTu variables (cone tip resistance, pore pressure or sleeve friction) on the right column. This data was used for training at least five regression models in the Regression Learner App to find a model that best predicts unknown values to the highest possible accuracy. As explained in Section 2.7.3, a training session involves approximating a mapping function (a predictive model) such that unknown values can be

approximated to the highest possible accuracy. In each training session, performance of the resultant model was evaluated based on R-Squared and validation errors presented in Table 2.3.

The RLA has the capability to accommodate more complex regression curves (like that of Gaussian processes) without specifying the relationship between the response and predictor variables with a predetermined regression function. With these types of models, responses for new data can be predicted using the trained model after being exported to MATLAB workspace.

Four CPTu test lines were sampled, one from each dam wall for use in this analysis. Data was imported into the Regression Learner App as a table with each CPTu variable independently being analyzed against depth. This data was used for training multiple models including regression trees, linear regression models, gauss process regression models, and vector support vehicles to look for the best regression model type. The best model was chosen and exported into the MATLAB R2020a workspace to check the predictions produced when using different values of depth.

CHAPTER 4

RESULTS, ANALYSIS AND DISCUSSIONS

4.1 Introduction

In summary, a total of three methods were used to analyze Orapa Mine Slurry Dam 2, and these were:

i. Limit Equilibrium Analysis Methods (LE).
ii. Finite Element Strength Reduction Method (FE).
iii. Regression Analysis.

The LE analysis method incorporates a deterministic analysis (using three Slide 2018 circular slip search methods), a probabilistic analysis and a sensitivity analysis. For all these three methods, Cone Penetration Testing (CPTu) was the basis for data collection. Section 4.2 is a presentation of CPTu data in interpreted form and a description on how this data was used to bring accurate and meaningful results.

4.2 Cone Penetration Test (CPTu) Data

The output data from in-situ measurements (CPTu) was cone tip resistance, sleeve friction and pore pressure. This data was used as input into CpeT-IT for computation of other important parameters such as permeability, modulus of elasticity, relative density, friction ratio, undrained shear strength, and for plotting of graphs for data presentation and interpretation. As shown in Figure 4.1, the north dam wall had six CPTu test points (marked as ✦1 through ✦6) and the other three dam walls had three test points each, giving a total of fifteen test points. Samples of the results from the four dam walls were used in this section to illustrate how they were used to draw conclusions about the state of Orapa Mine Slurry Dam 2.

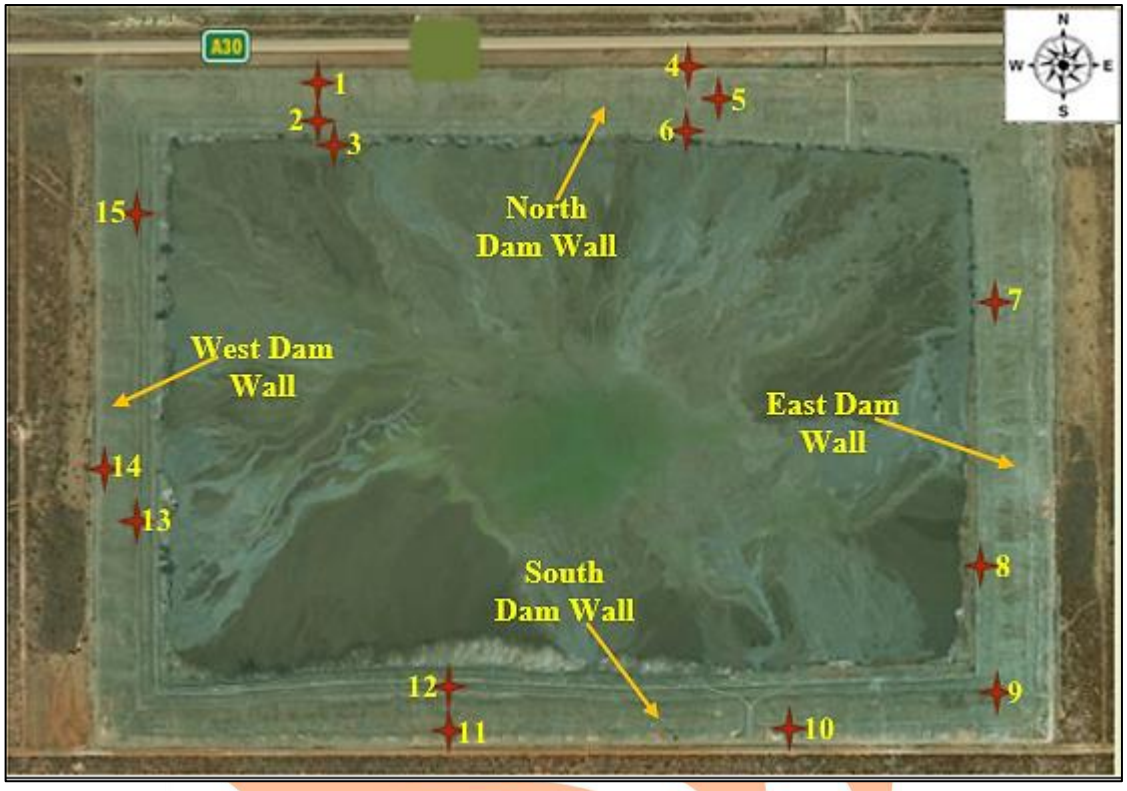

Figure 4.1 CPTu Test Points on Orapa Slurry Dam 2

4.2.1 Pore Water Pressure and Stratigraphy

Graphs of CPTu measured parameters, Soil Behavior Type plots and geotechnical sections obtained from CpeT-IT are almost similar on all dam walls under analysis. This similarity arises despite their different positions, geometries and elevations because they were constructed on the same foundation soil, using the same method of separation and deposition. They therefore acquired almost the same stratigraphy with the same soil types and pore water pressure (depending on the depth of weak layers). Two test points were chosen from north dam wall (010 and 004, as shown by arrows in Figure 4.2) to illustrate how interpretation of results was carried out. The remaining test point results are given in Appendix A and summarised as mean values of stability analysis input parameters, from CpeT-IT 3.0 shown in Table 4.1. From the 15 piezocone test points, two from north dam wall were chosen (upstream point 010 and downstream point 004) to only provide a description on how pore water pressure and stratigraphy results were interpreted during the analysis.

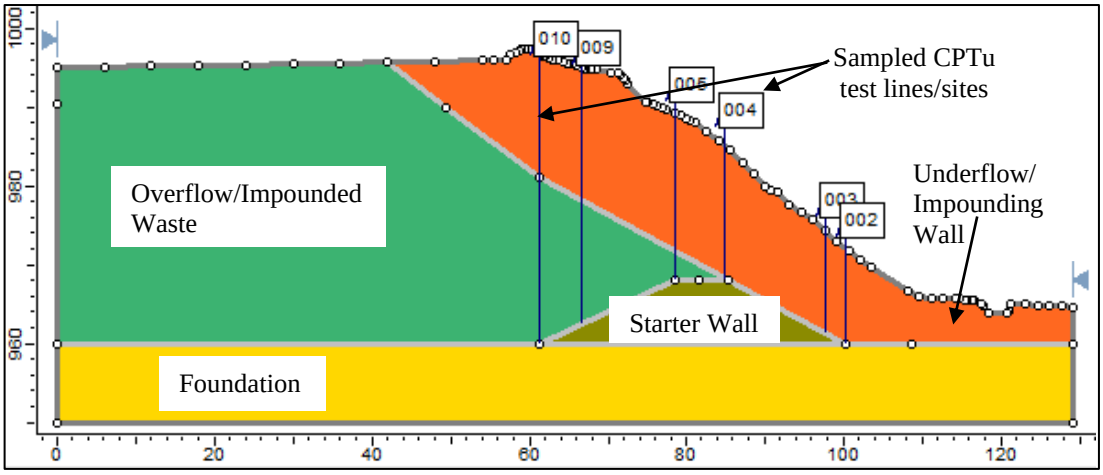

Figure 4.2 North Dam Wall Cross Section from Slide with CPTu Test Lines

CPTu results were superimposed onto these two chosen test lines in order to assist in the description and interpretation of the results. The initial location of the CPTu profiles was the phreatic surface elevation (~1000 meters above mean sea level) which started at the underflow region on all cross-sections. Pore pressure profile was used to identify and explain areas with high pore water pressures along test lines, and the geotechnical section was put in place to show the stratigraphy of the dam. One most important feature of CPTu is its capability in delineating thin weak layers hidden between other layers. As shown in Figures 4.3 and 4.4, a clay layer is trapped beneath a mixture of silt, sand and clay. Generally, clay has a very low permeability, therefore it tends to trap water molecules between clay particles, creating water pressure within pores. There is a record of concern for this type of behavior in geotechnical engineering since pore water pressure causes slope instability (Ural, 2018).

Matching pore pressure graphs in Figures 4.3 and 4.4 with their corresponding geotechnical sections, shows that pore water pressure through the dam wall is mostly equal to or slightly less than equilibrium pore pressure (shown by the cross-cutting blue line). However, layers made of clay and clay mixed with silty clay depict a pore water pressure higher than equilibrium pressure. To illustrate this pore pressure-clay layer relation, two separate sections labelled ‘1’ and ‘2’ in Figures 4.3 and 4.4 are selected and highlighted using bold dotted lines. These sections highlight randomly sampled depths at which pore pressure is higher than equilibrium pore pressure. All the highlighted sections contain clay material, in consequence, high pore pressures are experienced at these depths.

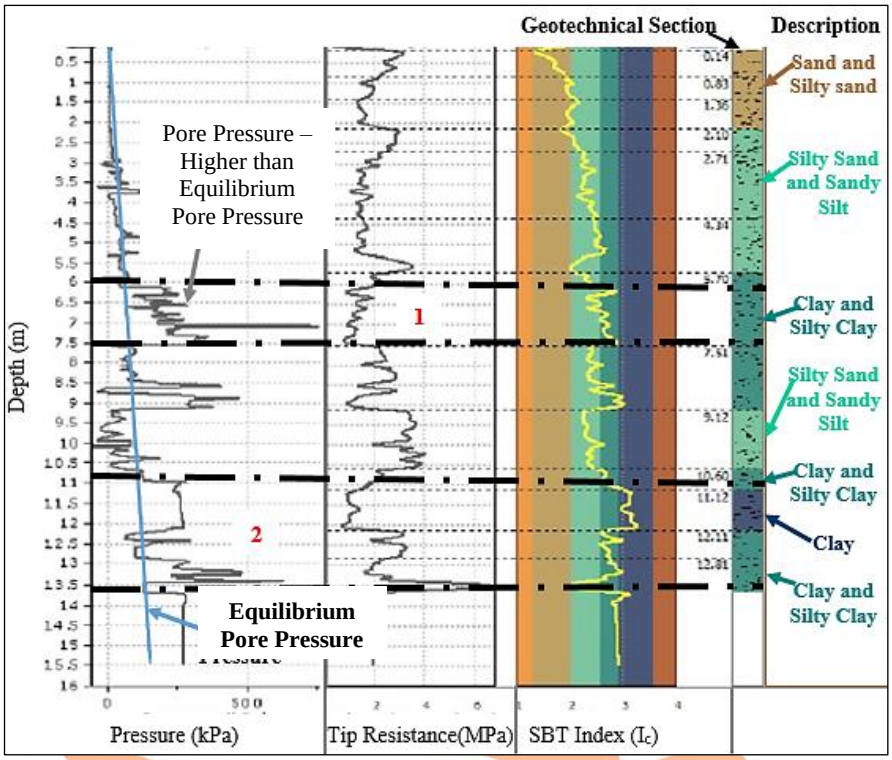

Figure 4.3 Pore Pressure Profile, Tip Resistance Profile and a Geotechnical Section of Test Line 004 from CPTu

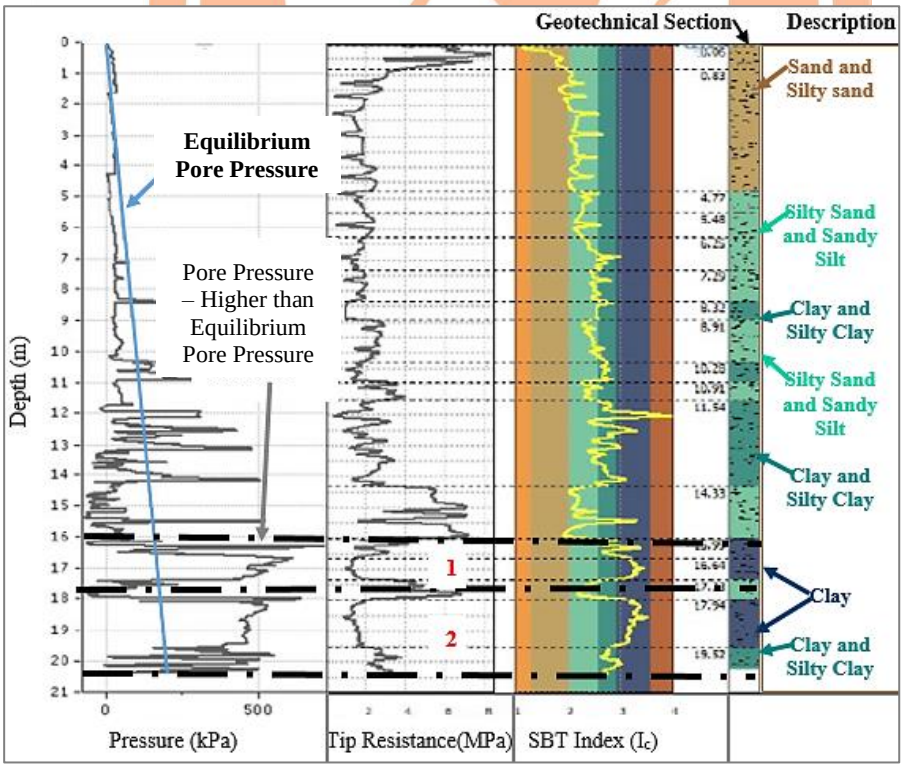

Figure 4.4 Pore Pressure Profile, Tip Resistance Profile and a Geotechnical Section of Test Line 010 from CPTu

4.2.2 Classification

CpeT-IT software uses the popular CPT Soil Behavior Type chart (SBT), proposed by Robertson (1990). This chart is global in nature, it uses CPT parameters like tip resistance and friction ratio to reasonably predict Soil Behavior Type for CPT soundings. It is made up of 9 zones each separated by a boundary line, each zone represents a specific type of soil (see Section 2.6.3). This chart is presented in Figure 4.5 for the chosen CPTu test lines in the north dam wall.

SBT charts presented in Figure 4.5 show data points plotted on a plane of normalised cone tip resistance versus normalised friction ratio. The data points are plotted in different zones and colored accordingly to show types of soils encountered throughout the depth of penetration of a CPTu penetrometer. Normalized SBT charts plot in zones 3 to 6 and when the depth of foundation material has been reached during probing they also plot in zone 2.

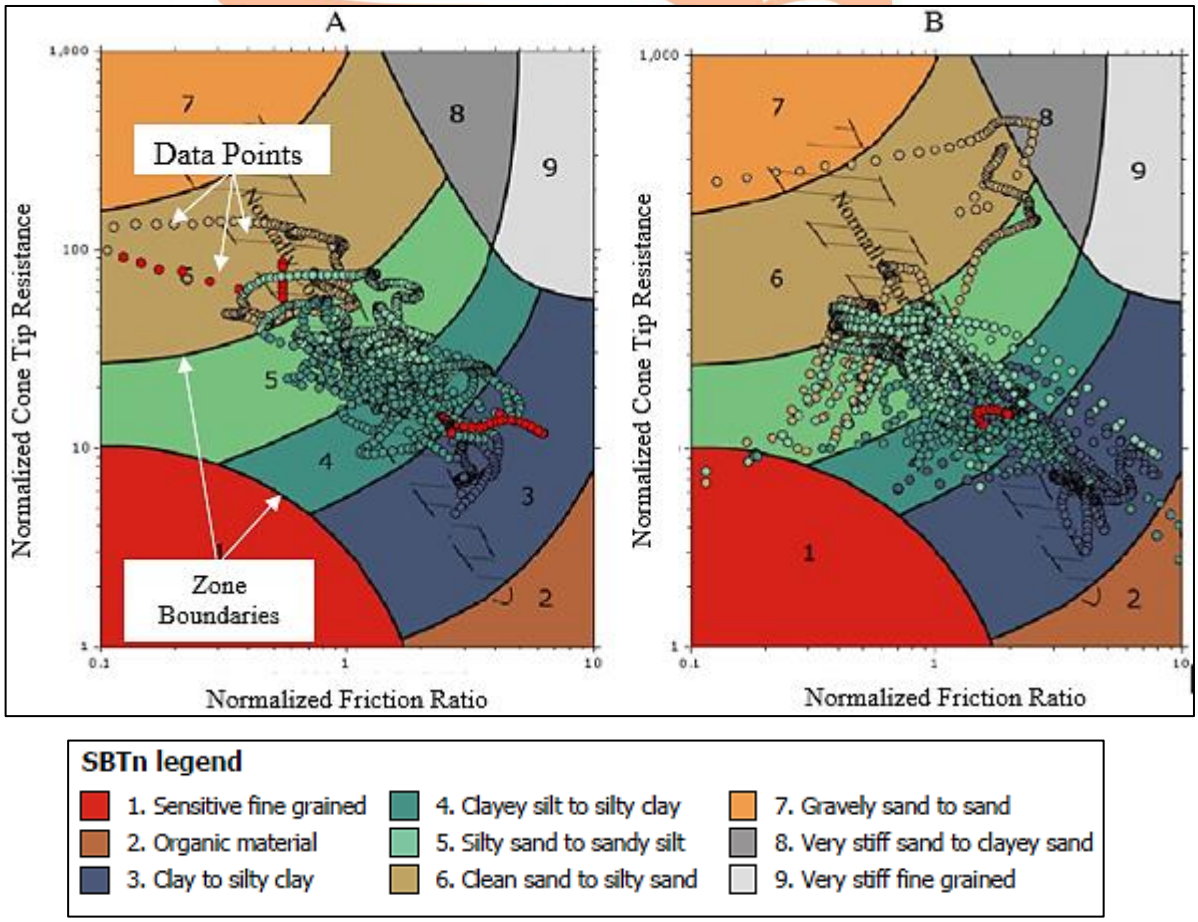

Figure 4.5 SBT Plots for (A): North Dam Wall 004 and (B): North Dam Wall 010

The method used to plot points on the SBT chart is the same as the method used in constructing geotechnical sections (Figures 4.3 and 4.4) hence the similarity in resultant soil types. So along the depth of the dam wall there is clay to silty clay (zone 3), clayey silt to silty clay (zone 4), silty sand to sandy silt (zone 5) and clean sand to silty sand (zone 6, at ground level). It is difficult to classify the soil throughout the depth of the dam wall as one type of soil, since it is made up of layers of different soil types, therefore this study will only highlight those soil types that were identified.

4.3 Limit Equilibrium Analysis Results

This analysis involved the use of Slide 2018 from Rocscience, Slide runs both deterministic and probabilistic analyses. It uses different slip search methods to search for potential slip circles, compute their mean safety factors, locate the most critical slip circle (the one with the lowest safety factor) and refer to it as the *Global Minimum*.

A probabilistic analysis locates a critical probabilistic surface; this surface is not necessarily the same as a global minimum, it represents a slip surface that is most likely to fail. Both deterministic and probabilistic analyses in Slide 2018 require geometry of the slope as input which encompasses the external boundary, material boundaries and their properties. External boundary coordinates were acquired from Lidar survey data carried out at Orapa in 2018. This data provided topography data of Orapa and it was through this data that elevations (in the form of profiles) of the four slurry dam walls were obtained. The topographic map is presented in detail in Appendix B1. CPTu geotechnical sections superimposed onto the Lidar survey profiles produced a complete geometry of slopes as shown in Figures 4.6 to 4.9.

4.3.1 Deterministic Analysis

Four main layers were identified in the slurry dams through CPTu, these are given alongside with their representative colors in the models below. The average elevation of the dam walls averaged at ~1000 meters above mean sea level, which is equivalent to ~3264 feet above mean sea level.

- ✓ Underflow (Sand, Silty Sand and Sandy Silt) - **Orange**
- ✓ Overflow (Clay and Silty Clay) - **Green**
- ✓ Starter dyke (Sand and Silty Sand) – **Military Green**
- ✓ Foundation (Organic soil) – **Yellow**

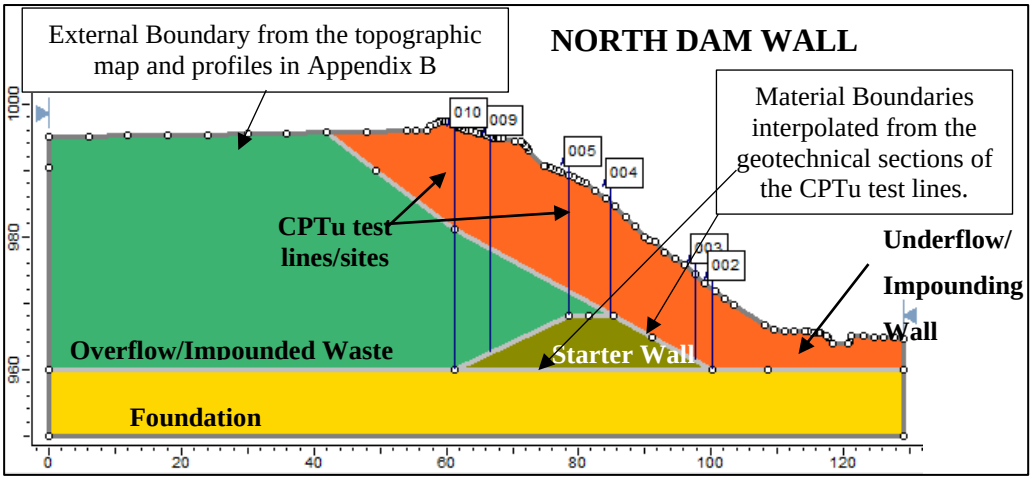

Figure 4.6 North Dam Wall Geometry from Slide 2018 used for Stability Analysis

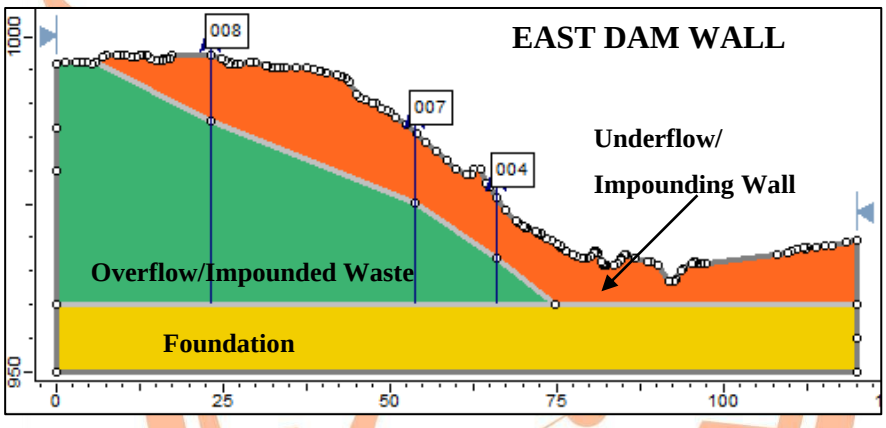

Figure 4.7 East Dam Wall Geometry from Slide 2018 used for Stability Analysis

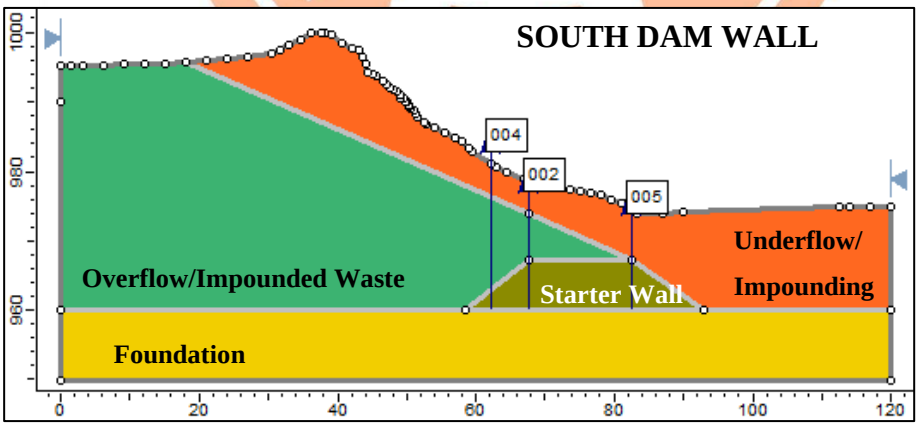

Figure 4.8 South Dam Wall Geometry from Slide 2018, used for Stability Analysis

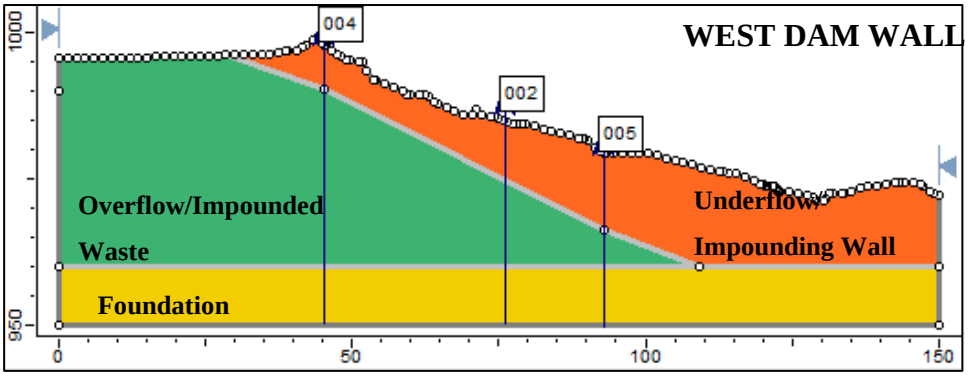

Figure 4.9 West Dam Wall Geometry from Slide 2018, used for Stability Analysis

Input parameters were mechanical properties of these layers (friction angle, cohesion and unit weight). They were entered as shown in Table 4.1.

Table 4.1 Input Parameters from CPTu, used for Modelling Slurry Embankments

Property	Foundation	Over Flow	Under Flow	Starter Dyke
Color				
Strength Type	Mohr-Coulomb			
Unit Weight (kN/m^3)	19.5	16.0	20.4	19.5
Cohesion (kPa)	0.0	5.0	1.0	0.0
Friction Angle (degrees)	37.0	23.0	30.0	37.0
SBT Material Type	Organic Soil	Clay and Silty Clay	Sand, Silty Sand and Sandy Silt	Sand and Silty Sand

Parameters in Table 4.1 were used in Slide to define materials embodied in the dam walls so that a circular failure analysis could be executed using three Slide circular slip search methods (Grid search, Slope search and Auto-refine search). Bishop simplified, Spencer and Morgenstern-Price limit equilibrium methods were chosen for safety factor computations. Factor of Safety is widely used as an overall measure of the safety of slopes. According to Herza *et al.* (2017), a back-calculation of the Factor of Safety of existing dams was carried out in the United States of America during the 20th century in order to determine the minimum acceptable Factor of Safety. A Factor of Safety of 1.5 was found to provide enough flexibility and was generally considered acceptable. The recommended minimum Factor of Safety for embankment dams was also discussed and stated by ANCOLD (1969). The recommended minimum Factor of Safety for failures towards the downstream slope of

a dam under steady-state seepage condition was stated as 1.5. Therefore, a minimum design Factor of Safety of 1.5 was considered to be reliable for use in this study. This has been considered to take into account uncertainties associated with many factors influencing slope stability and it is generally considered acceptable.

All four slope geometries used in the analysis were subjected to a finite element groundwater seepage analysis in Slide. This type of analysis allows for definition and computation of pore pressures in a slope stability problem.

Two sets of hydraulic parameters were used to estimate the location of a phreatic surface. These were dam material permeability and the depth of a pore pressure transition point where pore pressure equals zero (P = 0). Throughout the CPTu test, recordings began at this pore pressure transition when pore pressures started recording values greater than zero. The average elevation of a pressure transition point encountered at all CPTu test points was 978 meters above mean sea level (± 5 m). The phreatic surface was inferred automatically as shown in Figures 4.10 to 4.13 using these input hydraulic parameters. It is represented as a purple line to represents the pore pressure transition (P = 0) in each slope. In a groundwater seepage analysis, results consist of slope geometries colored with respect to change in pore pressure head (in meters). Pressure head is representative of pore pressure measured in units of length with respect to the phreatic surface (P = 0). A closer look into the pressure head legend in conjunction with pressure head contours in Figures 4.10 to 4.13, shows that pore pressure increases from the ground surface downwards towards overflow in a diagonal direction as shown in Figure 4.10. Flow vectors labelled in Figure 4.10, represent direction of flow of water through the body of the dam. This flow path is used by water molecules that were trapped in between overflow material particles. Continuous movement of these water molecules is called seepage as described in Section 2.6.5.

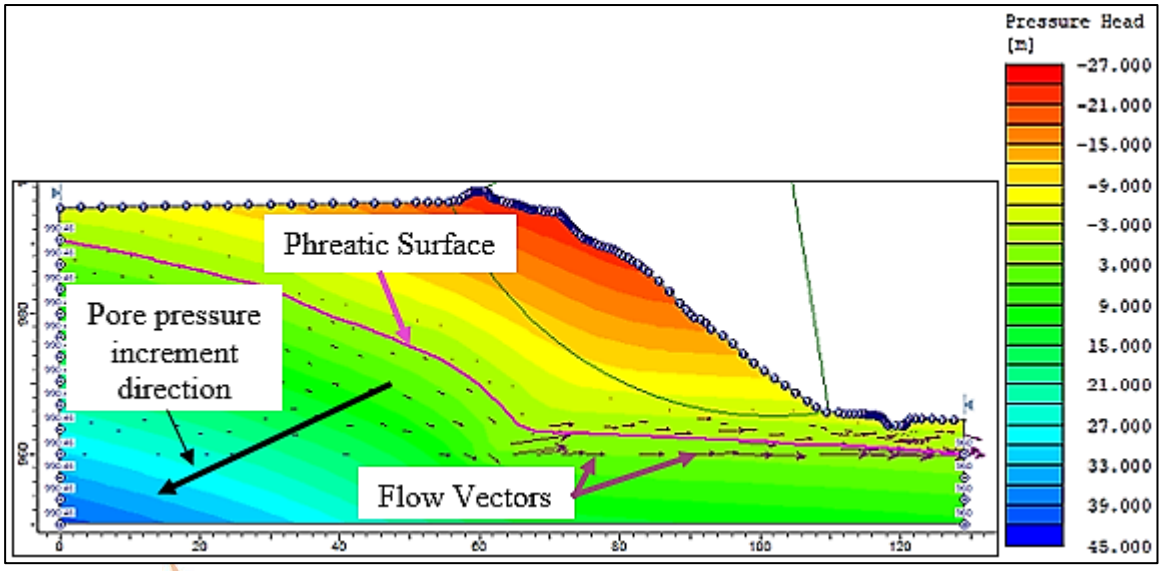

Figure 4.10 North Dam Wall Finite Element Groundwater Seepage Analysis Model from Slide

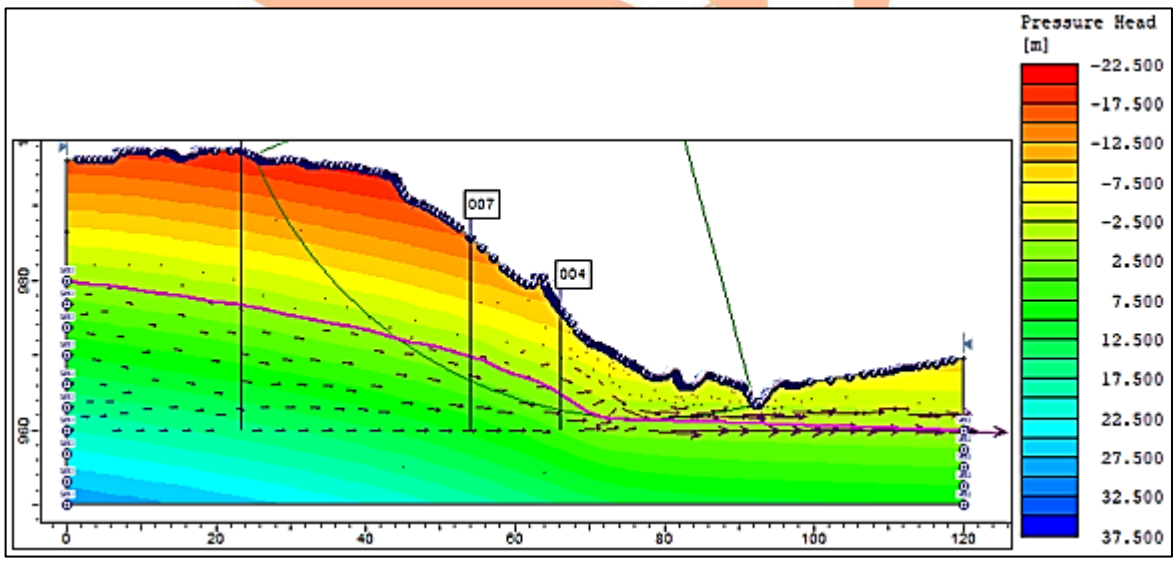

Figure 4.11 East Dam Wall Finite Element Groundwater Seepage Analysis Model from Slide

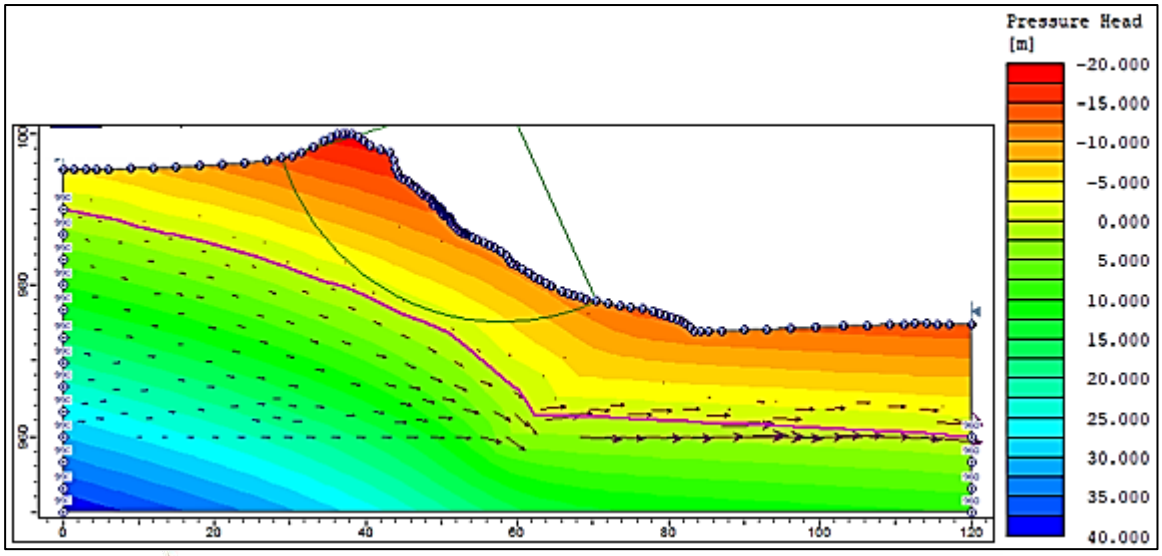

Figure 4.12 South Dam Wall Finite Element Groundwater Seepage Analysis Model from Slide

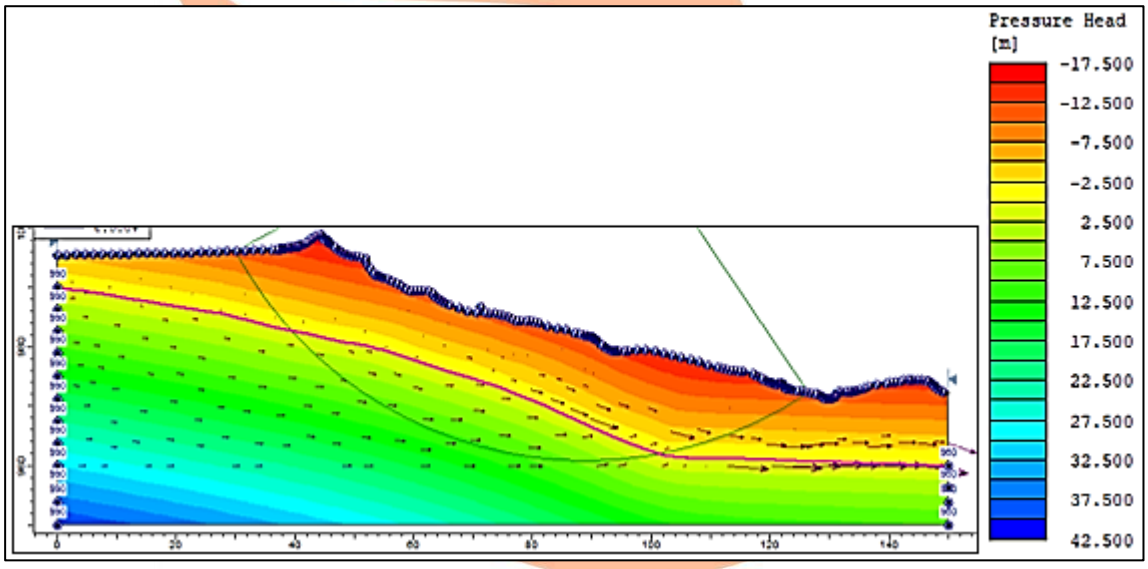

Figure 4.13 North Dam Wall Finite Element Groundwater Seepage Analysis Model from Slide

In Slide, groundwater seepage analysis boundary conditions are defined only once and used for both groundwater seepage analysis and slope stability analysis. Figures 4.14 to 4.25 show model results obtained from a limit equilibrium deterministic analysis of the four slurry dam walls. Circular slip surface search methods used in this analysis are Grid search, Slope search and Auto Refine search described in detail in Section 2.5.1. These methods were used collectively as a way of ensuring accuracy in a search for critical slip circles.

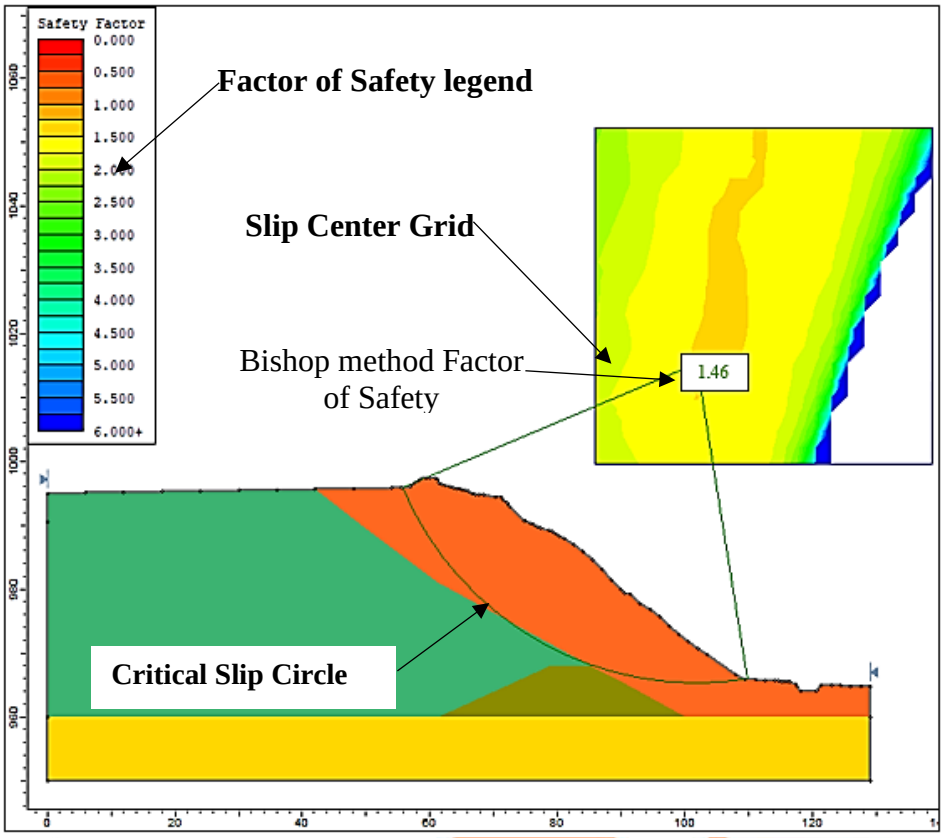

Figure 4.14 Limit Equilibrium Grid Search Results for North Dam Wall

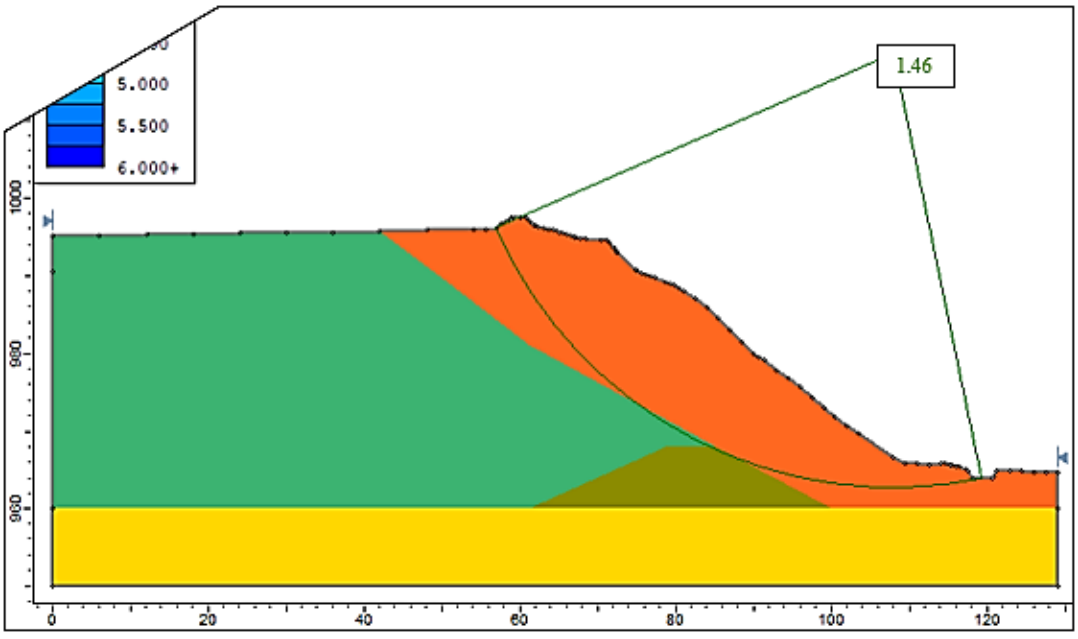

Figure 4.15 Limit Equilibrium Slope Search Results for North Dam Wall

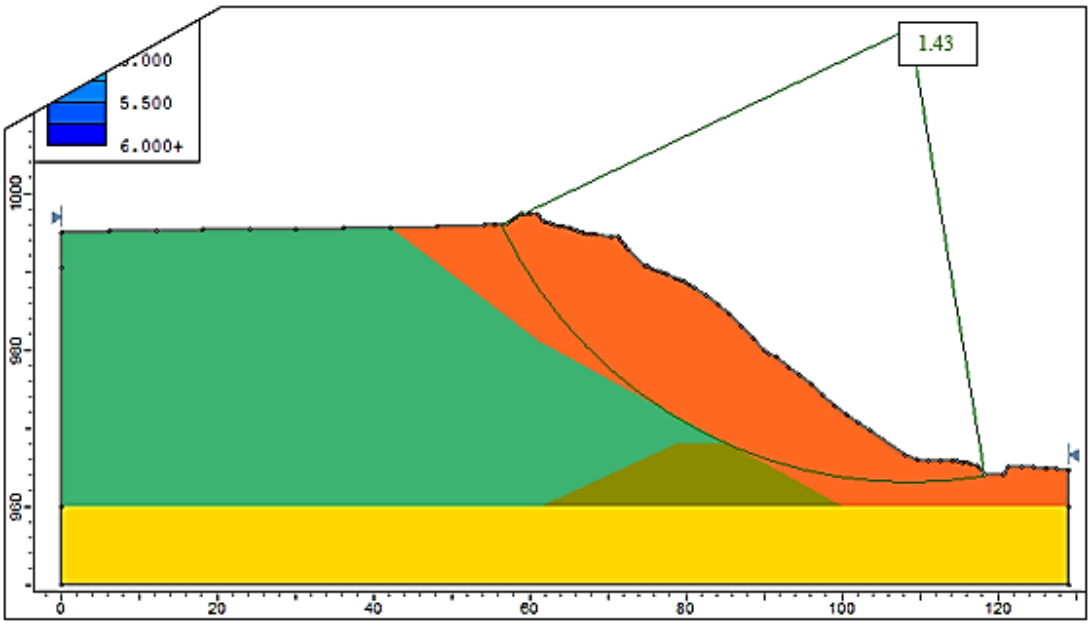

Figure 4.16 Limit Equilibrium Auto Refine Search Results for North Dam Wall

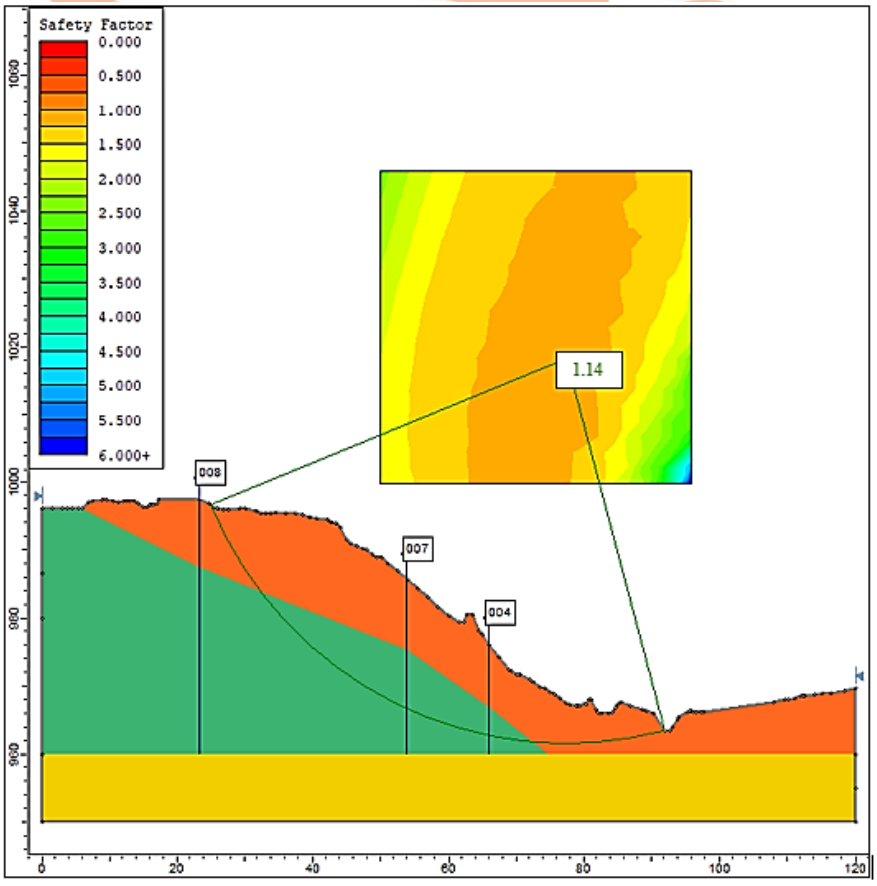

Figure 4.17 Limit Equilibrium Grid Search Results for East Dam Wall

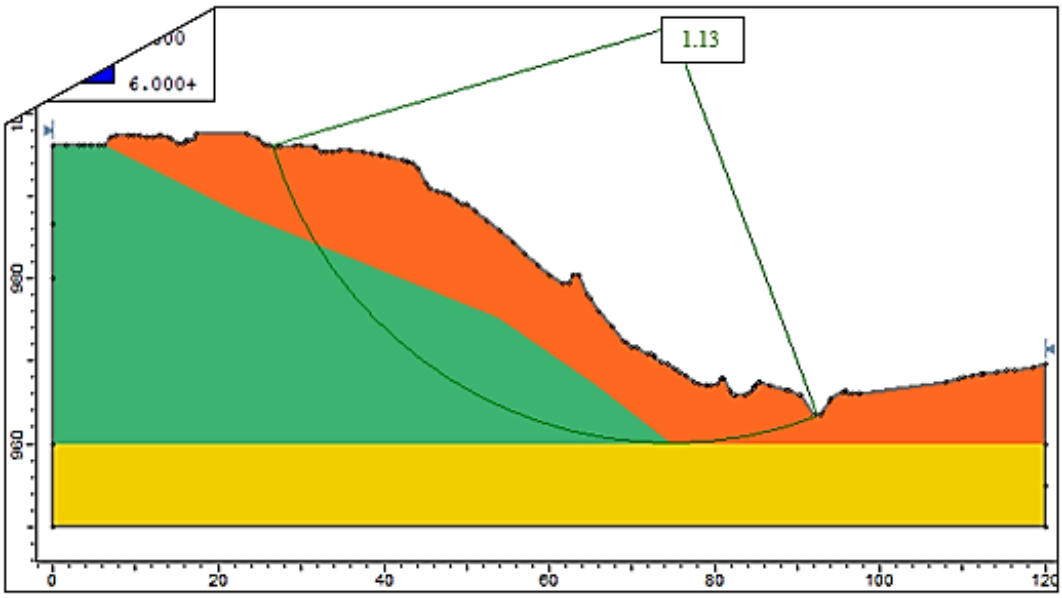

Figure 4.18 Limit Equilibrium Slope Search Results for East Dam Wall

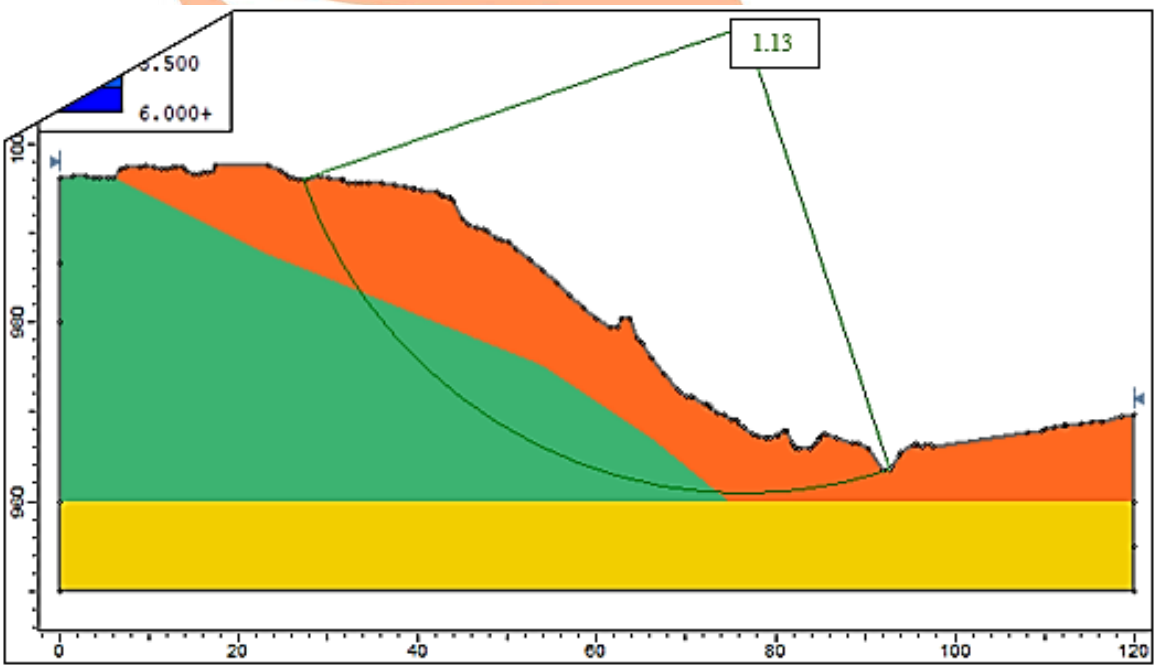

Figure 4.19 Limit Equilibrium Auto Refine Search for East Dam Wall

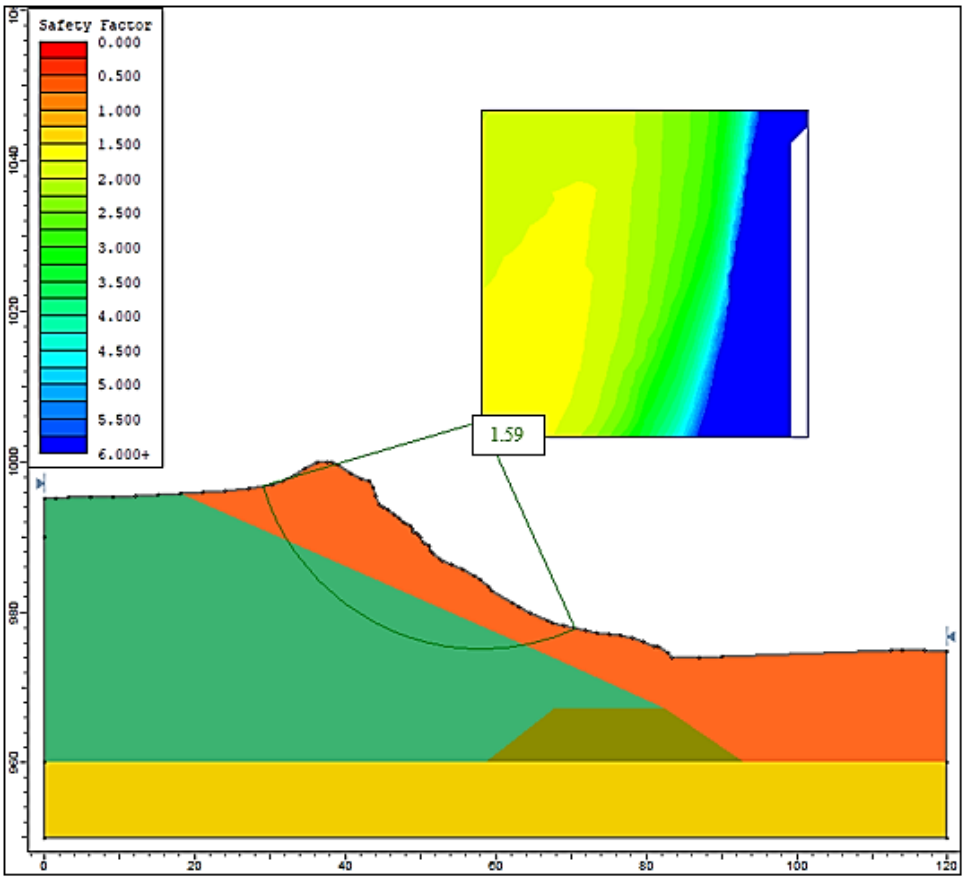

Figure 4.20 Limit Equilibrium Grid Search Results for South Dam Wall

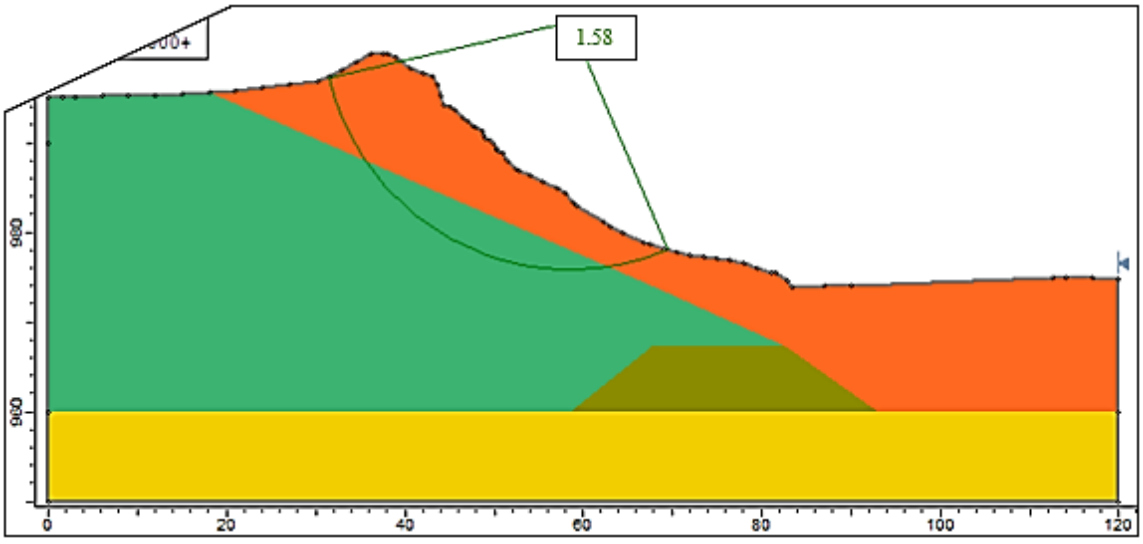

Figure 4.21 Limit Equilibrium Slope Search Results for South Dam Wall

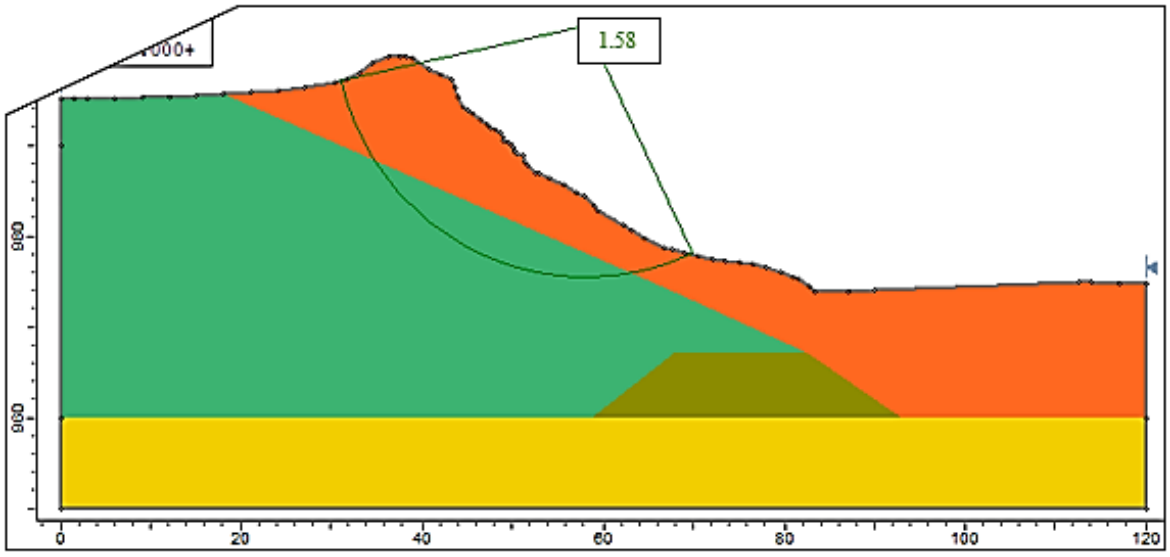

Figure 4.22 Limit Equilibrium Auto Refine Search Results for South Dam Wall

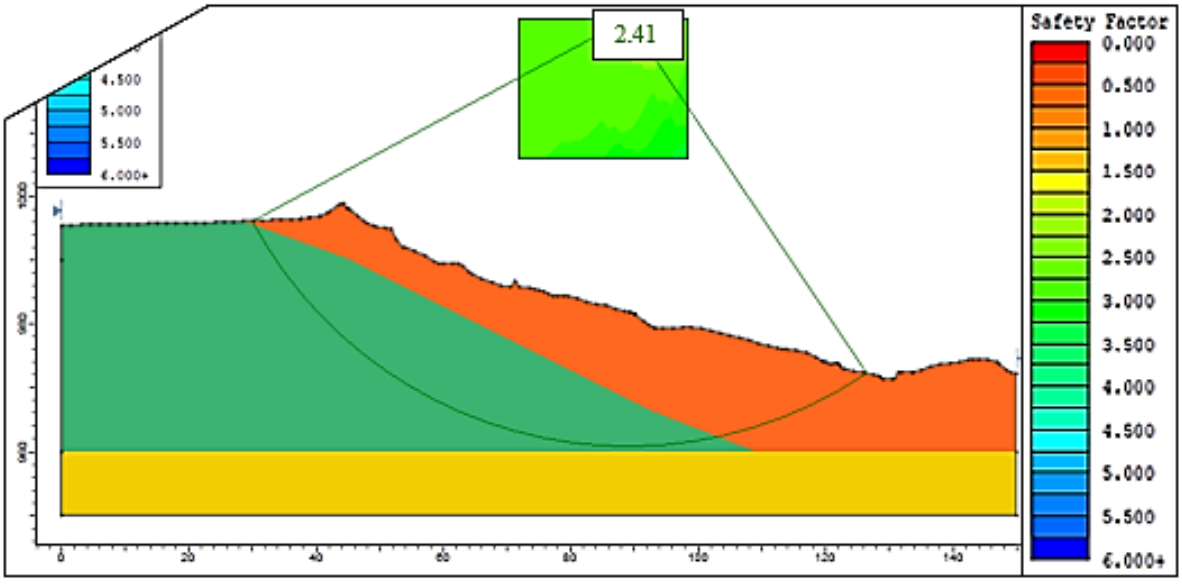

Figure 4.23 Limit Equilibrium Grid Search Results for West Dam Wall

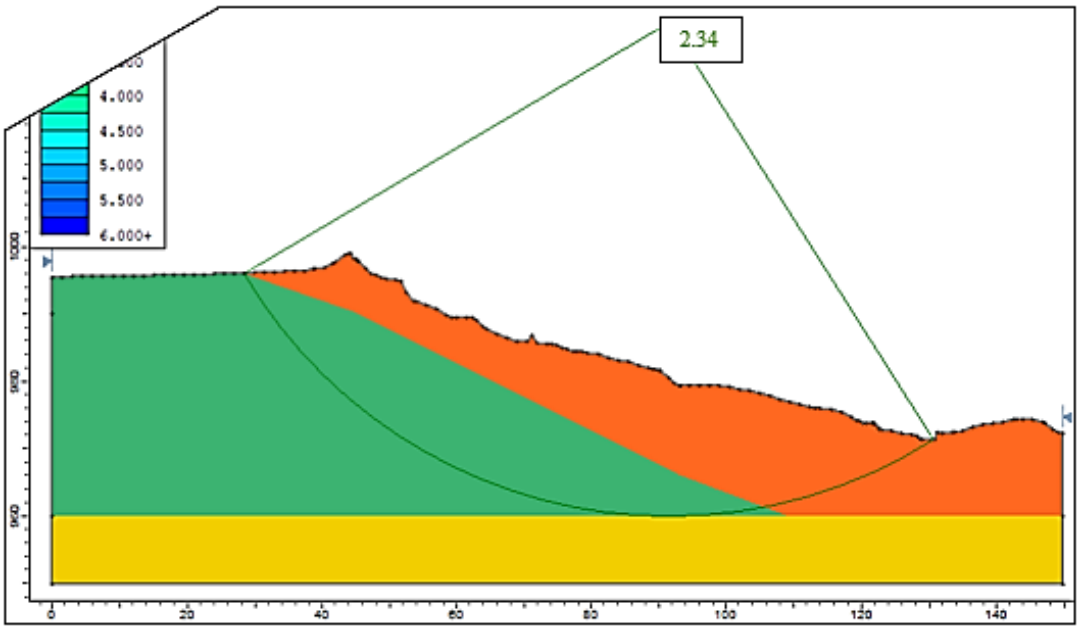

Figure 4.24 Limit Equilibrium Slope Search Results for West Dam Wall

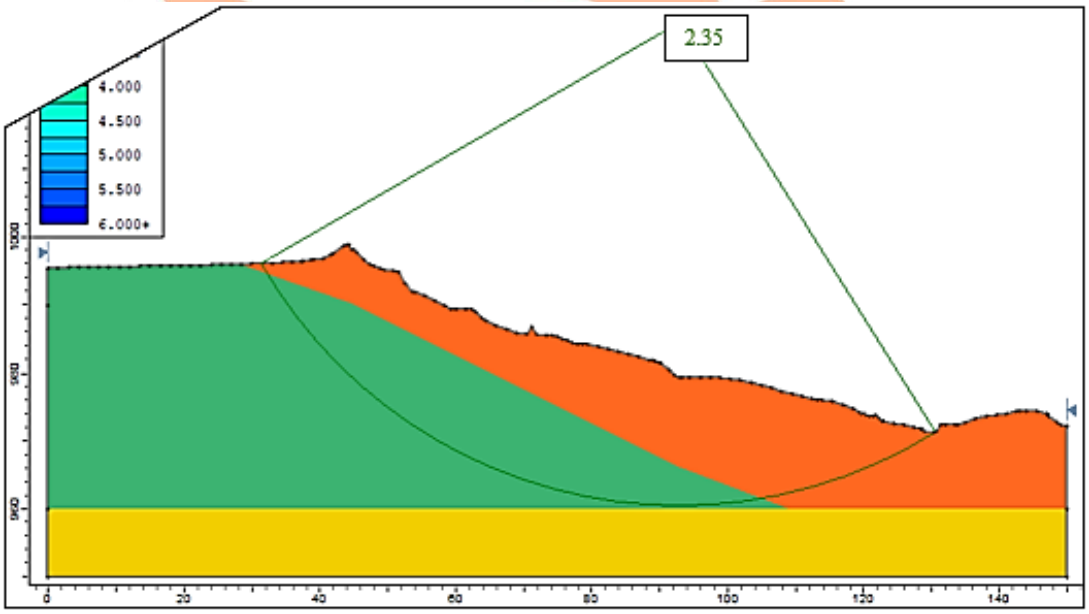

Figure 4.25 Limit Equilibrium Auto Refine Search Results for West Dam Wall

As observed from Figures 4.14 to 4.25, the arc that points towards the slip center grid (the color contoured square) is the critical slip circle located during a grid search. This arc represents a path of a circular failure surface with the lowest Factor of Safety. The slip center grid consists of slip circle centers; it is contoured according to the Factor of Safety of each slip circle as shown by the Factor of Safety legend. In comparison, the slip circle locations and Factors of Safety obtained from all three slip circle search methods are very similar. In

essence, Auto Refine search method is known to have the capability of locating critical slip circles with the lowest Factors of Safety. This capability can be noticed from north dam wall and west dam wall factors of safety obtained. However, differences between Factors of Safety obtained from the Auto Refine search method and those from Grid and Slope search methods are very small (≤ 0.03). Therefore, these differences are considered insignificant and obtained slip circle paths and factors of safety are considered accurate and reliable.

Table 4.2 shows Factors of Safety obtained from three limit equilibrium methods displayed for each dam wall. It is noticeable that there is an agreement between the three Slide search methods and between the three limit equilibrium methods. Factor of Safety(FoS) values can be used as an important standardized way for comparing reliability and strength between different methods (Pricop *et al.*, 2013). In case of this analysis, the Factor of Safety has confirmed that results obtained from three search methods adopted here, and three limit equilibrium methods can be regarded as reliable for use in rating the stability of the dam walls.

Table 4.2 Orapa Slurry Dam 2 Deterministic Analysis Results

Section	Critical Factors of Safety				Total Slice Area (Grid Search) (m^2)
	Method	Grid Search FoS	Slope Search FoS	Auto Refine Search FoS	
North	GLE	1.46	1.47	1.44	645.7
	Spencer	1.46	1.47	1.44	
	Bishop	1.46	1.46	1.43	
East	GLE	1.15	1.15	1.14	819
	Spencer	1.15	1.15	1.14	
	Bishop	1.14	1.13	1.13	
South	GLE	1.59	1.58	1.58	432.7
	Spencer	1.60	1.59	1.59	
	Bishop	1.59	1.58	1.58	
West	GLE	2.43	2.37	2.36	1609.6
	Spencer	2.43	2.37	2.36	
	Bishop	2.41	2.35	2.34	

A Factor of Safety of 1 means that shear resistance along a particular shear surface is in equilibrium with the forces and/or moments driving the slope to failure. It means the slope is at a brink of failure, and any additional load added will cause failure. Table 4.2 shows that all Factors of Safety obtained from limit equilibrium analysis are above 1. A graphical presentation of the Factors of Safety is shown in Figure 4.26 for ease of comparison. However, only south and west dam walls are in compliance with the Australian National Committee of Large Dams (ANCOLD) Factor of Safety regulations that recommend a minimum Factor of Safety of 1.5. The Auto refine search method displays low factors of safety in comparison to both Grid search and Slope search. This is in line with the ability of this method in finding surfaces with a lower Factor of Safety for an equal number of surfaces generated than both of these methods. East and north dam wall analysis results presented Factors of Safety less than 1.5, this can be a result of a number of reasons that may range from geometry to geotechnical parameters used in the analysis. Sensitivity analysis results that follow later in this chapter will provide information on which geotechnical parameter is influential on the stability of each dam wall. South dam wall presented a Factor of Safety of 1.59, the safety of this slope may be rated as 'moderate', as any additional load will render it unsafe.

Even though a Factor of Safety is not entirely reliable and has little meaning in terms of slope stability, it is useful when generally assessing the safety margin of a slope and in finding out whether there is a need to perform analyses for further assessments (Herza *et al.*, 2017). In case of Orapa Mine Slurry Dam 2 limit equilibrium deterministic analysis results, appropriate measures are required to improve strength/stability of east, north and south dam walls and/or assess the cause of the acquired low Factors of Safety.

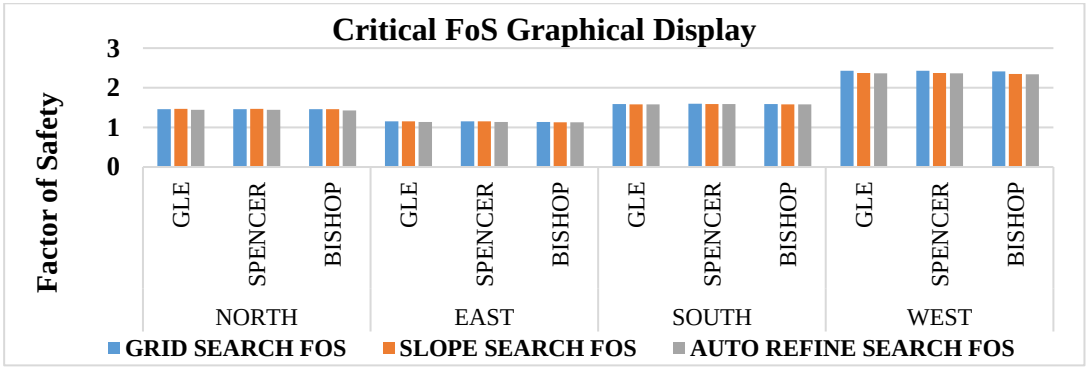

Figure 4.26 Factor of SafetyGraph from Deterministic Analysis

4.3.2 Probabilistic Analysis

For this analysis, random variables were chosen to be cohesion, friction angle and unit weight for all material types. They were defined as shown in Table 4.3 using a uniform probability density function which simulates random variation between two values (minimum and maximum values) where all values in the range are equally probable (Rocscience, 2018). These data sets are representative of all the CPTu test points considering variation for all soil types being analysed.

Table 4.3 Random variables entries

Material Name	Property	Distribution	Mean	Rel. Min	Rel. Max
Foundation	Phi	Uniform	37	2	2
	Unit Weight	Uniform	19.5	0.5	0.5
Overflow	Cohesion	Uniform	5	1	1
	Phi	Uniform	23	3	3
	Unit Weight	Uniform	16	2	2
Underflow	Cohesion	Uniform	1	1	1
	Phi	Uniform	30	5	5
	Unit Weight	Uniform	20.4	0.5	0.5
Starter Dyke	Phi	Uniform	37	2	2
	Unit Weight	Uniform	19.5	0.5	0.5

As observed from the results in Table 4.4, a *Deterministic* Factor of Safety is a Factor of Safety computed for the Global minimum slip surface (a slip surface with the minimum Factor of Safety) in a non-probabilistic (deterministic) slope stability analysis (Rocscience, 2018). This Factor of Safety is computed with mean values of input parameters. It is shown in this section as a comparison to results obtained from a probabilistic analysis.

A closer look into Table 4.4, shows that a deterministic Factor of Safety is not necessarily equal to a probabilistic Factor of Safety, and in all the four cases the probabilistic Factor of Safety is more than the deterministic Factor of Safety. This is because a deterministic analysis searches for a slip surface with the lowest Factor of Safety while the probabilistic analysis searches for a slip surface with the highest probability of failure (a slip surface that

is most likely to fail). Both the probabilistic and the deterministic factors of safety of the slurry dam walls are more than 1.5 (the recommended minimum Factor of Safety by ANCOLD) except for east dam wall which is sitting at 1.2.

Table 4.4 Limit Equilibrium Probabilistic Analysis Results for Orapa Mine Slurry Dam 2

Dam Wall	Overall Slope			Critical Probabilistic Surface			Critical Deterministic Surface		
	FS	PF	RI	FS	PF	RI	FS	PF	RI
North Dam Wall	1.4	0	5.1	1.5	0	3.8	1.5	0	5.0
South Dam Wall	1.6	0	6.9	1.7	0	6.5	1.6	0	6.8
West Dam Wall	2.4	0	8.6	2.6	0	8.2	2.4	0	8.5
East Dam Wall	1.2	0	2.8	1.2	0	2.8	1.2	0	2.9

In overall probability of failure is 0, which means out of 1000 samples, no sample produces a Factor of Safety less than 1. A reliability index (RI) measures overall slope stability after probability of failure, it indicates the number of standard deviations separating the mean safety factor from the critical Factor of Safety (=1). As a minimal assurance of a safe slope design, a reliability index of 3 is usually recommended (Rocscience, 2018). From the presented results all the RI values are well above 3 with the east dam wall as an exception. This implies that the slope safety of south, north and west dam walls is at a more satisfactory level, and measures are required towards stabilizing the east dam wall to improve its safety.

4.3.3 Sensitivity Analysis

This analysis was conducted through Slide 2018 using the same input variables that were used in the probabilistic analysis. Sensitivity of the safety factor to unit weight, cohesion, and friction angle was being analysed for each layer of slurry dam walls. In a sensitivity analysis each parameter is varied with equal increments between the minimum and maximum values while other parameters are held constant at their mean values (Rocscience, 2018). When the Factor of Safetyis plotted against all input variables, the horizontal axis is in terms of Percent of Range (as seen from Figure 4.27). A Percent of Range of 0 represent a minimum value of each variable, that of 100 represents a maximum value of each variable while a 50 percent of range represents a mean value of each variable. The Bishop Simplified method's sensitivity plot for north dam wall in Figure 4.27 shows that all the curves of the

variables are overlapping in a flat trend except for those of the Underflow and Overflow friction angles. This implies that varying parameters of both the starter dyke and foundation material have no influence on the Factor of Safety.

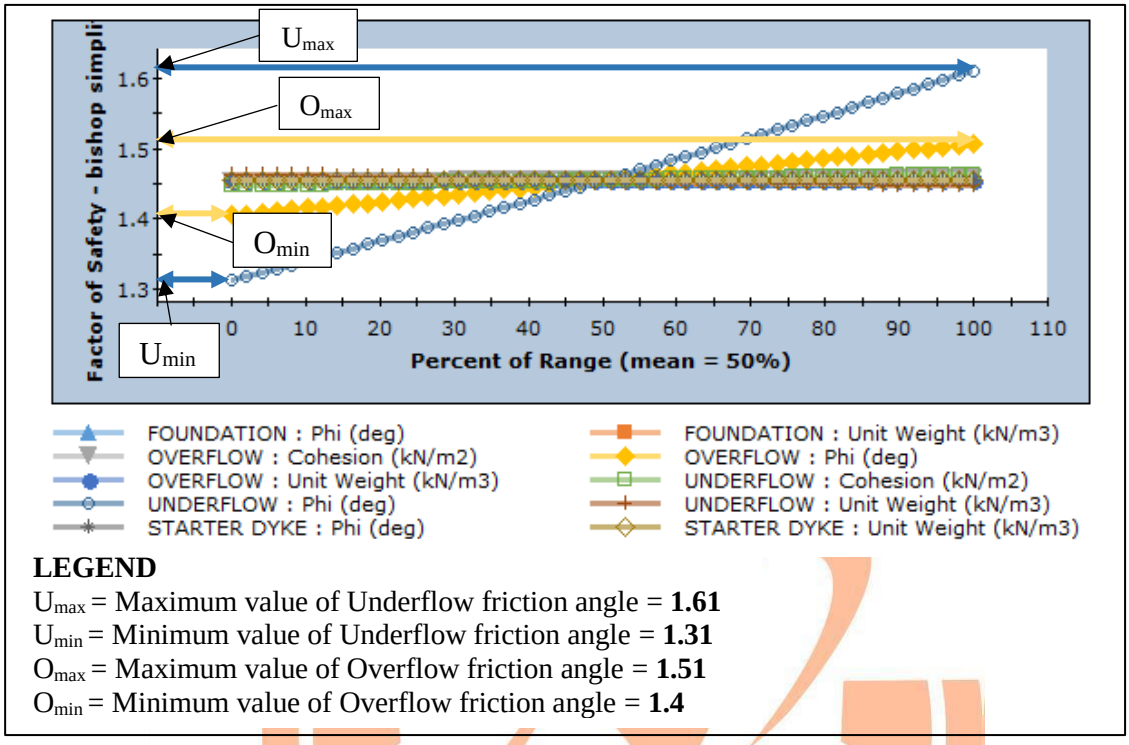

LEGEND

U_{max} = Maximum value of Underflow friction angle = **1.61**

U_{min} = Minimum value of Underflow friction angle = **1.31**

O_{max} = Maximum value of Overflow friction angle = **1.51**

O_{min} = Minimum value of Overflow friction angle = **1.4**

Figure 4.27 Bishop Simplified Method Sensitivity Plot for North Dam Wall

The insensitivity of the Factor of Safety towards varying parameters of the starter dyke and the foundation material can be explained better with a closer look at Figure 4.28. This figure shows that a path taken by the critical slip surface does not pass through these materials. However, it passes through the Underflow and a small portion of the slip surface passes through the Overflow. Therefore, the Factor of Safety is only influenced by varying parameters of both the Underflow and the Overflow.

North dam wall's deterministic Factor of Safety (Grid search – Bishop Simplified) obtained was 1.46. Figure 4.27 shows that the Underflow friction angle has the highest effect on the Factor of Safety than the Overflow friction angle. Maximum Underflow friction gives a 10.3% change in the Factor of Safety and the minimum value gives a 10.3% change. Percent change effect caused by maximum and minimum values of any chosen parameter is calculated as shown in Equations 4.1 and 4.2 respectively.

$$\%C_{max} = \frac{Y_{max} - F.S_{ave}}{F.S_{ave}} \times 100 \quad (4.1)$$

$$\%C_{min} = \frac{F.S_{ave} - Y_{min}}{F.S_{ave}} \times 100 \quad (4.2)$$

where: $\%C_{max}$ = the percent change given by the maximum value of a specific parameter.

$\%C_{min}$ = the percent change given by the minimum value of a specific parameter.

Y_{max} = the maximum value of a specific parameter.

Y_{min} = the minimum value of a specific parameter.

$F.S_{ave}$ = the average Factor of Safety obtained from the limit equilibrium analysis.

For example, percent change caused by the maximum value of the underflow friction angle is calculated as:

[(1.61 – 1.46)/1.46] = 10.3%

and percent change caused by the minimum value of the underflow friction angle is calculated as:

[(1.46 – 1.31)/1.46] = 10.3%

In contrast, overflow friction angle has displayed a low level of influence on the Factor of Safety, the maximum value giving a 3.4% change and the minimum value giving a 4.1% change in the Factor of Safety. However, based on Figure 4.28, just a small arc is submerged into the overflow material while the remaining large portion of the slip arc is completely submerged in the underflow material. Therefore, dam wall stability will be more dependent on underflow strength parameters than those of the overflow material.

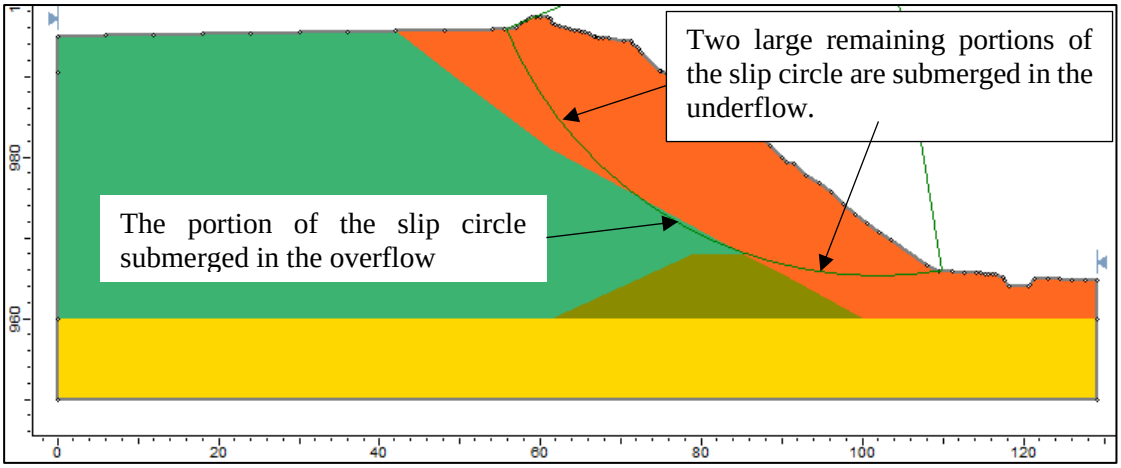

Figure 4.28 Critical Slip Surface of Orapa Slurry Dam 2 North Dam Wall

South dam wall's deterministic Factor of Safety is 1.59 (Grid Search – Bishop Simplified). On the south dam wall sensitivity plot in Figure 4.29, overflow friction angle gives a highest influence on the Factor of Safety. Maximum and minimum values of the overflow friction value both give an 8.8% change in the Factor of Safety. All curves of other varying parameters are overlapping in a flat trend, showing that they have no influence on the Factor of Safety.

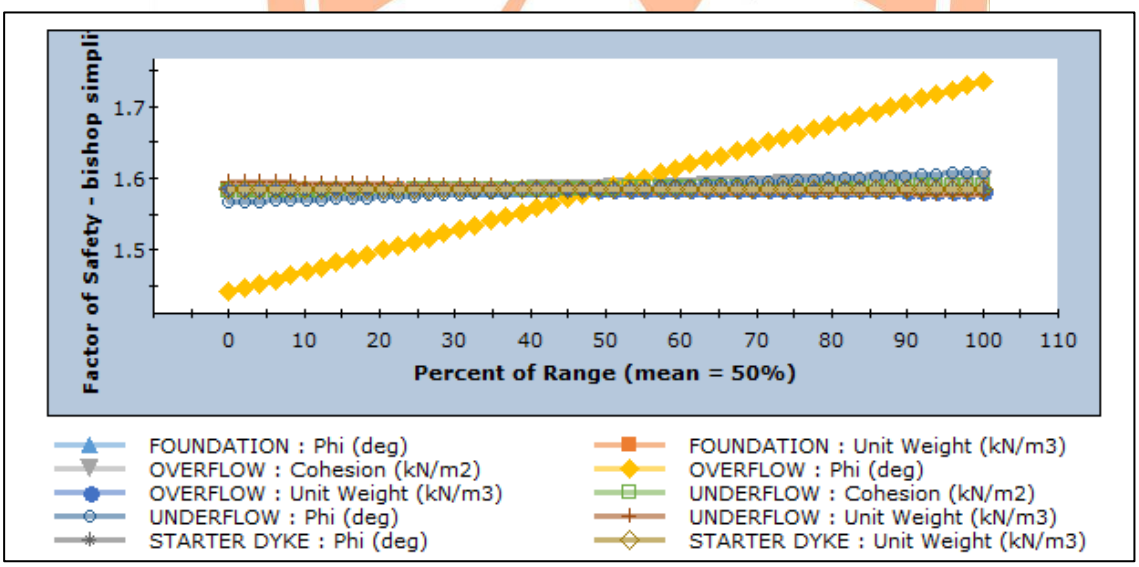

Figure 4.29 Bishop Simplified Method's Sensitivity Plot for South Dam Wall

Critical slip surface location in Figure 4.30 explains results displayed by the curves in Figure 4.29. The base of the slip surface is sitting within the overflow material; this implies that the ability of that slip surface in resisting failure is dependent on the strength of the overflow

material. According to the Mohr-Coulomb criterion which was adopted for this analysis, shear strength of the material is described in two components, which are the cohesive component and the frictional component. However, in this analysis the Factor of Safety is more responsive to changes in friction angle than cohesion, this may be due to values of cohesion being too small to contribute towards the shear strength of the material.

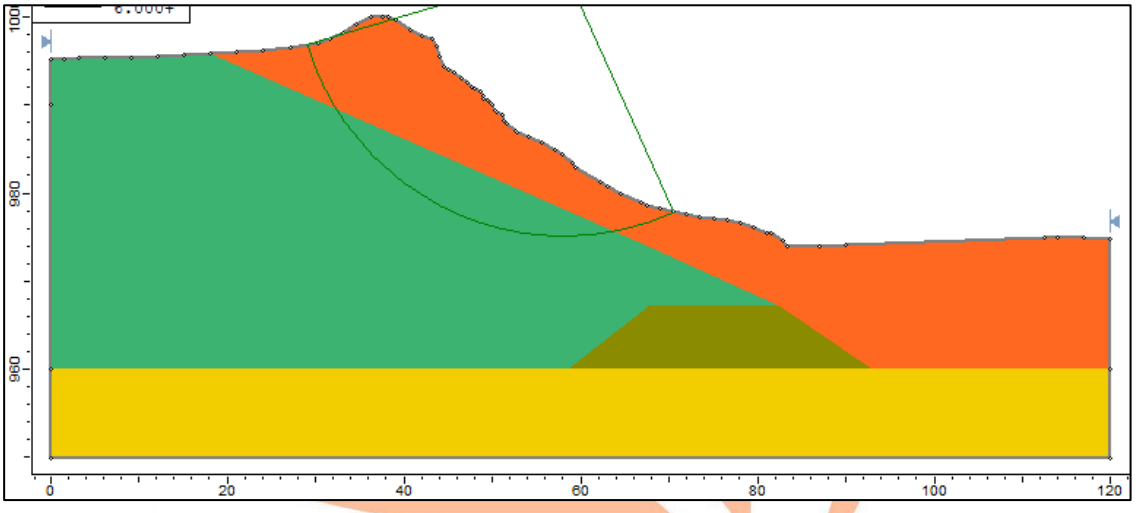

Figure 4.30 Critical Slip Surface of Orapa Slurry Dam 2 South Dam Wall

As calculated from the deterministic analysis, the critical Factor of Safety of the west dam wall is 2.41 from all limit equilibrium methods used. West dam wall's sensitivity plot in Figure 4.31 shows that all other varying parameters have no influence on the Factor of Safety except for Overflow unit weight, Overflow friction angle and Underflow friction angle. Overflow unit weight has shown a significant influence to change in the Factor of Safety, with the minimum value giving a 5.8% change and the maximum value giving a 4.6% change. According to this plot, the Factor of Safety is inversely proportional to the unit weight of a material. This may be caused by an increase in the total vertical force which may overpower friction resistance of the material thereby increasing its susceptibility to failure at the critical slip surface. Overflow friction angle gives the highest change in the Factor of Safety, with the maximum value giving a 10% change and the minimum value giving an 8.7% change. Furthermore, the Underflow friction angle has caused the least significant influence on the Factor of Safety, with the maximum value giving a 4.6% change and the minimum value giving a 4.6% increase.

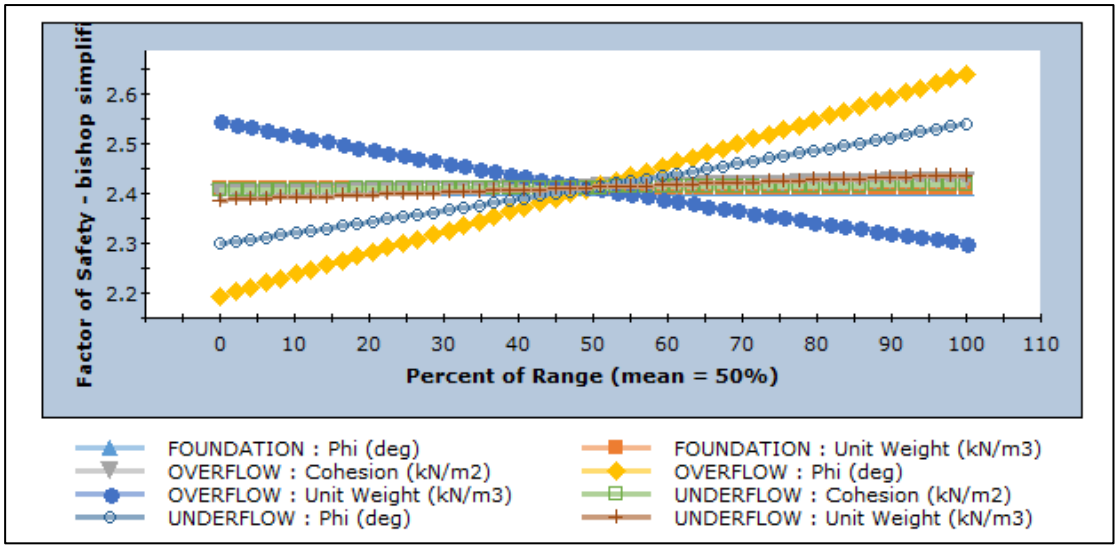

Figure 4.31 Bishop Simplified's Sensitivity Plot for West Dam Wall

As shown in Figure 4.32, the base of the critical slip surface is deep seated, almost coming into contact with the foundation material. This location has led to sensitivity of the Factor of Safetytowards Overflow unit weight since the total vertical force has increased. An increase in the total vertical force causes the shear strength of the overflow at the slip surface position to be dependent on the unit weight of the material overlying the slip surface path.

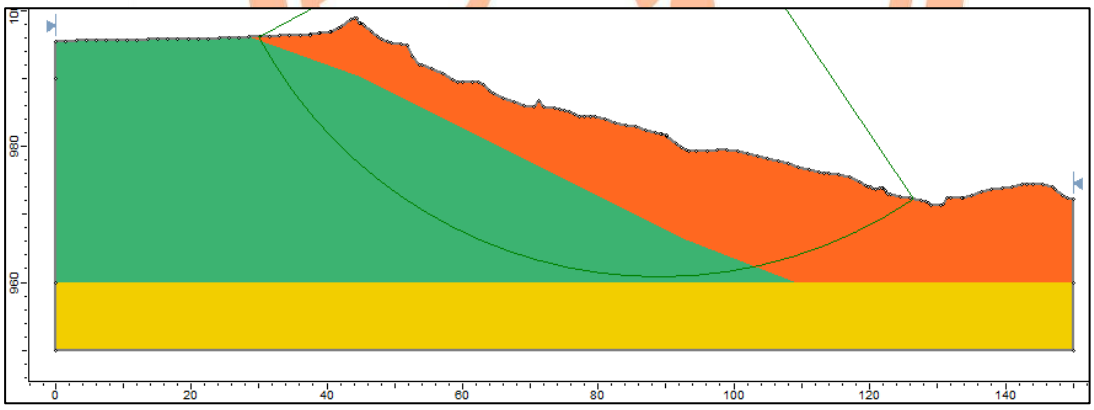

Figure 4.32 Critical Slip Surface of Orapa Slurry Dam 2 West Dam Wall

East dam wall's deterministic Factor of Safety is 1.14 as computed by grid Search-Bishop Simplified method. Figure 4.33 shows that friction angle of the overflow material gives the highest influence to change in Factor of Safety and the Underflow friction angle gives the least significant change in the Factor of Safety. The highest influence of the Overflow friction angle is easily explained by the location of the base of the slip surface as shown in Figure 4.34. It is located in the overflow material, therefore, the forces necessary for

resisting shear failure are mostly located in the overflow material. As a result, the Factor of Safety will be more sensitive to strength of the overflow material than that of the underflow material.

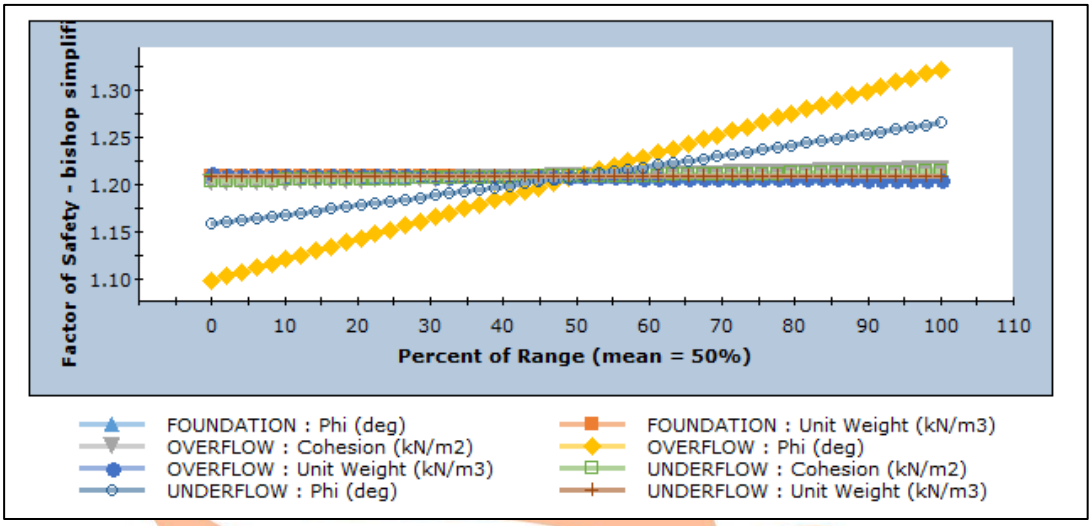

Figure 4.33 Bishop Simplified's Sensitivity Plot for East Dam Wall

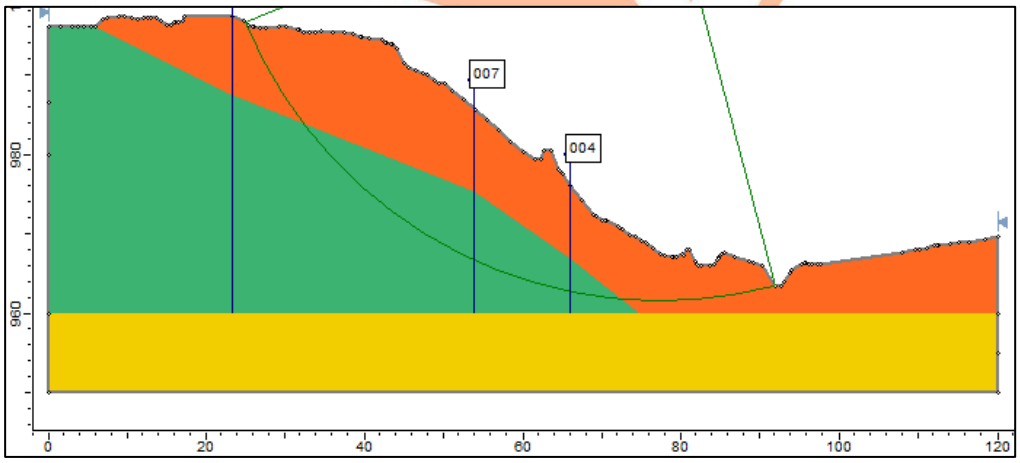

Figure 4.34 Critical Slip Surface of Orapa Slurry Dam 2 East Dam Wall

Sensitivity analysis results presented in this section were in accordance with Mohr-Coulomb criterion, nevertheless, this condition only applies at a location where the slip surface is passing. Parameters at other locations besides the slip surface path have insignificant influence on the Factor of Safety.

One of the major objectives of this study was to determine the variables that govern the stability of the Orapa Mine Slurry Dam 2. The sensitivity analysis section addresses this

objective. Therefore, it can be concluded that the performance/stability of the Orapa Mine Slurry Dam 2 is determined by underflow and overflow strength parameters, specifically the friction angle. Improving the strength of the underflow material (e.g. introduction of a buttress) and the overflow material (e.g. densification) will improve the stability of the slurry dams.

4.4 Finite Element Analysis Results

This analysis involved the use of a computer software called RS2 2019 from Rocscience sometimes called Phase2. A Strength Reduction method was used to analyze dam walls using the same geometries that were used in Slide 2018.

4.4.1 Deterministic Analysis

For this type of analysis, Mohr-Coulomb failure criterion was applied and entries shown in Table 4.5 were made for computation of the strength reduction factor (SRF). Two more parameters were added for the FE analysis (Elastic Modulus and Poisson's Ratio), these entries were presented as mean values of parameters obtained from CPTu.

Similarly, a finite element groundwater seepage analysis was carried out in RS2 2019 for pore pressure computations. Figures 4.35 to 4.38 were used in this section to compare seepage analysis results obtained from RS2 2019 and Slide 2018. The procedure for definition of hydraulic properties used in Slide 2018 was also applied in RS2 2019. The phreatic surface locations and seepage directions obtained from limit equilibrium and finite element methods are in good agreement as shown in Figures 4.35 to 4.38. This not only validates groundwater seepage results but also a good agreement between results of two different methods based on different concepts and thus gives confidence that the analysis results are correct.

Table 4.5 Input Parameters used for Finite Element Deterministic Analysis

Parameter	Section/Layer			
	Foundation	**Overflow**	**Underflow**	**Starter Dyke**
Cohesion (kN/m^2)	0	5	1	0
Friction Angle (^{0})	37	23	30	37
Poisson's Ratio	0.4	0.4	0.4	0.4
Elastic Modulus (MPa)	50	38.2	39.4	49.5
Unit Weight (kN/m^3)	19.5	16	20.4	19.5
SBT Material Type	Organic Soil	Clay and Silty Clay	Sand, Silty Sand and Sandy Silt	Sand and Silty Sand

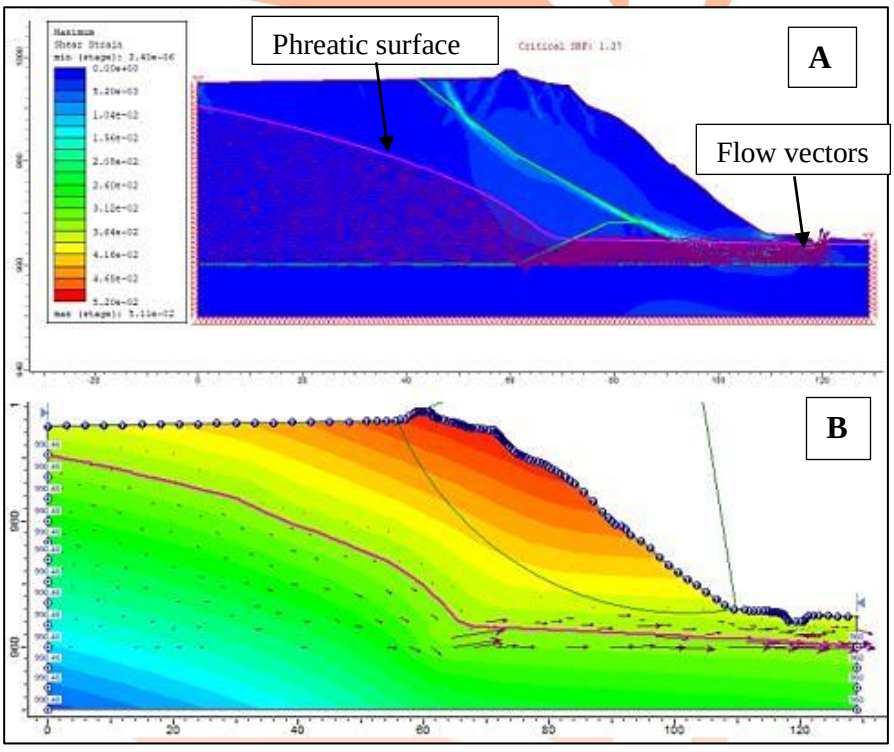

Figure 4.35 Finite Element Groundwater Seepage Analysis Results for North Dam Wall, from RS2 (Picture A) and Slide (Picture B)

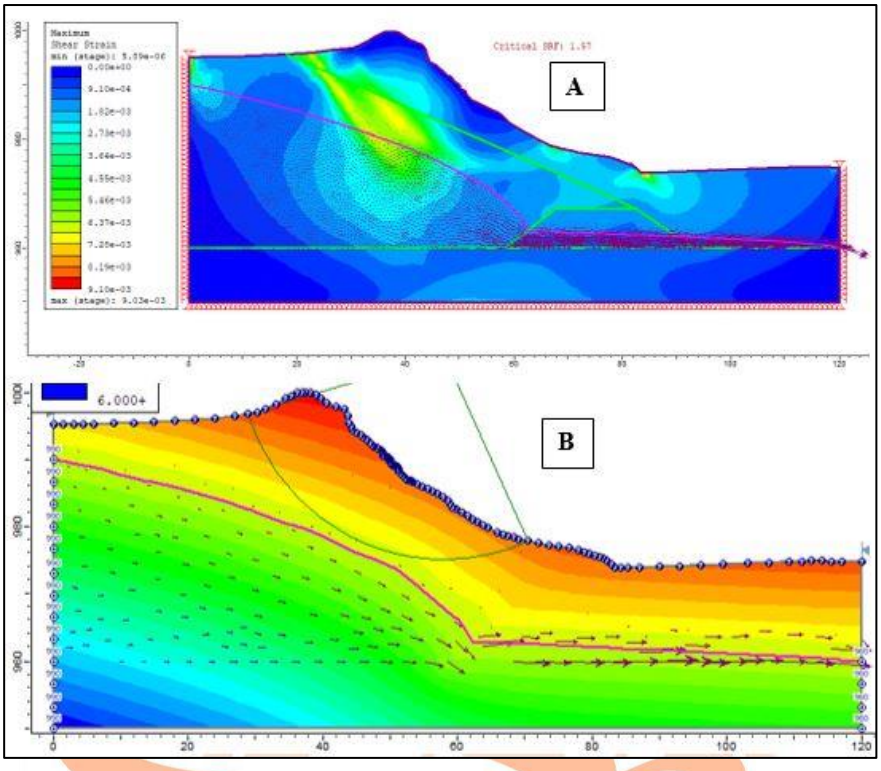

Figure 4.36 Finite Element Groundwater Seepage Analysis Results for South Dam Wall, from RS2 (Picture A) and Slide (Picture B)

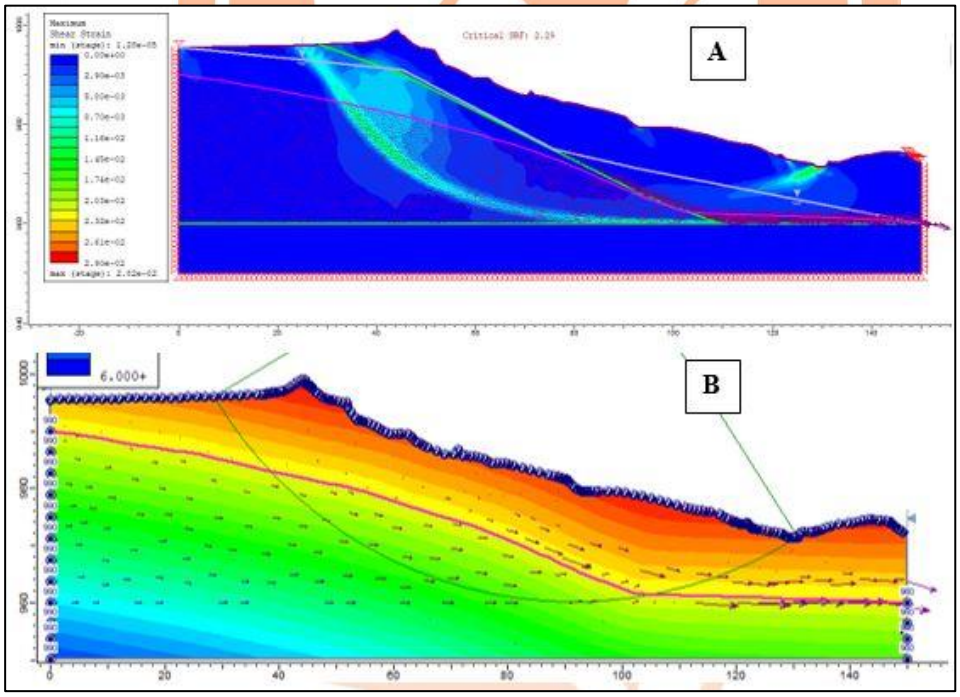

Figure 4.37 Finite Element Groundwater Seepage Analysis Results for West Dam Wall from RS2 (Picture A) and Slide (Picture B)

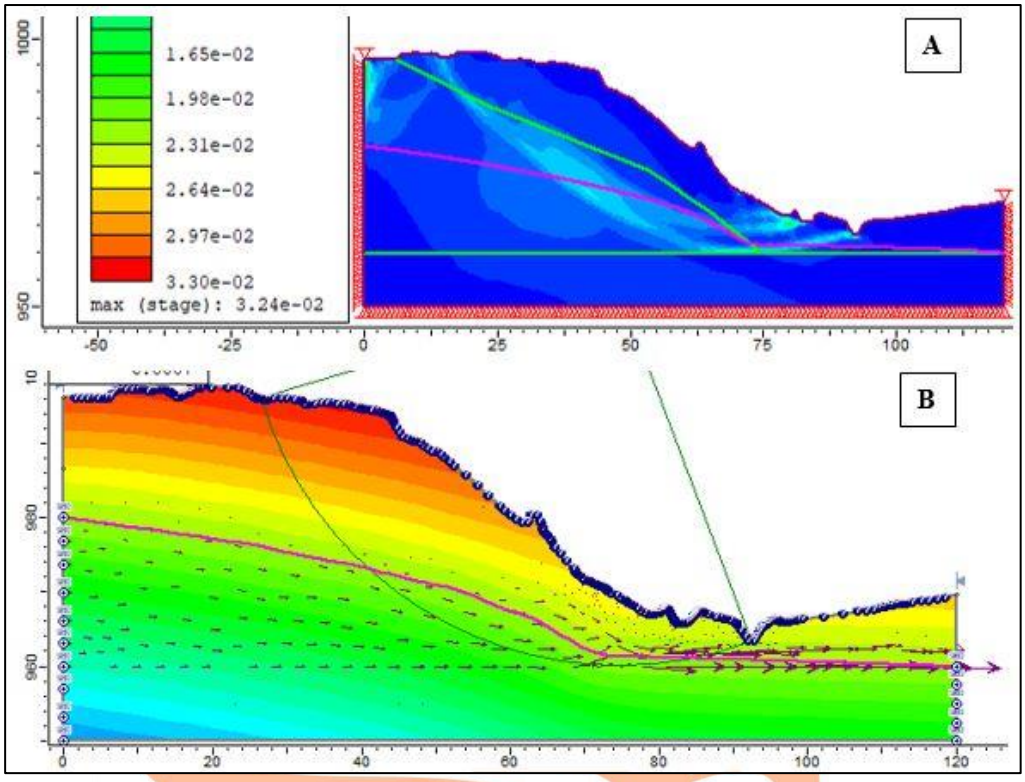

Figure 4.38 Finite Element Groundwater Seepage Analysis Results for East Dam Wall, from RS2 (Picture A) and Slide (Picture B)

Maximum shear strain gives a good indication of where slip will take place. Maximum shear strain dataset is contoured accordingly in Figures 4.39 to 4.42. The shear strain legend (for example as labelled in Figure 4.39) shows that shear strain increases downwards from the blue color at the top to the red color at the bottom. Red contours signify maximum shear strain and blue contours signify minimum shear strain. Therefore, in Figure 4.39 to 4.42, green contours represent areas of maximum shear strain in the model.

When the model is viewed with a higher Strength Reduction Factor (SRF), the slip surface path becomes more visible as shown in Figure 4.43 (Picture A). This picture depicts a slip circle path and it indicates that failure will occur along a weak boundary that exists between the north dam wall underflow and overflow. Limit equilibrium deterministic critical slip circle path in Figure 4.43 (Picture B) also sits on the underflow-overflow boundary, indicating that failure will occur along that boundary. This shows good agreement between the two methods in locating the slip circle path. More evidence is shown in Figures 4.44 to 4.46, where the limit equilibrium critical slip circle path is compared to the finite element slip circle path (defined by the maximum shear strain contour pathway).

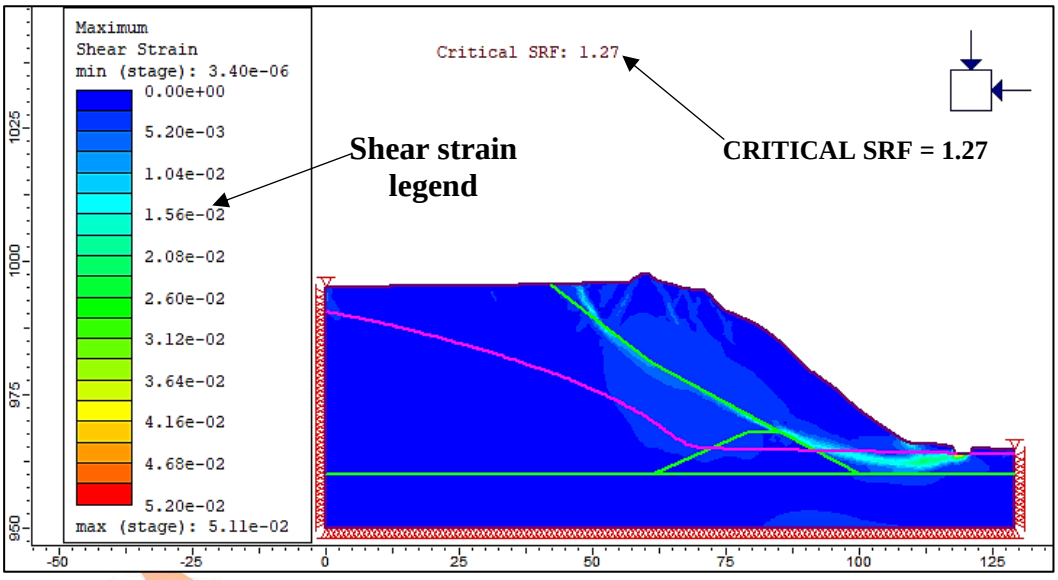

Figure 4.39 Critical SRF Maximum Shear Strain Contours for North Dam Wall

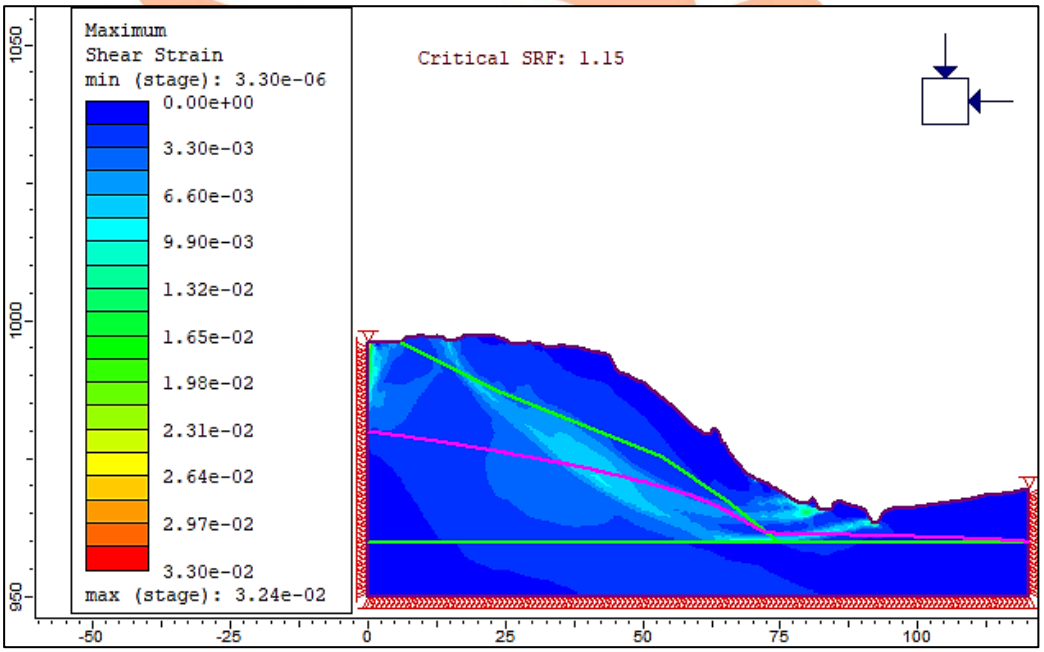

Figure 4.40 Critical SRF Maximum Shear Strain Contours for East Dam Wall

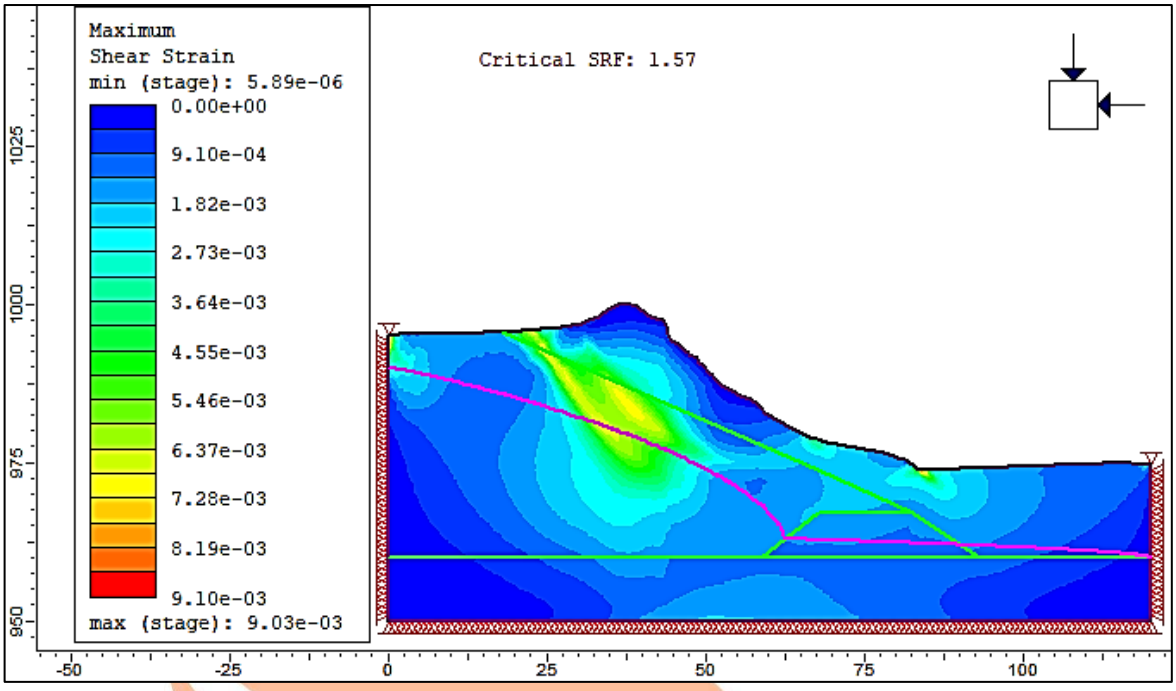

Figure 4.41 Critical SRF Maximum Shear Strain Contours for South Dam Wall

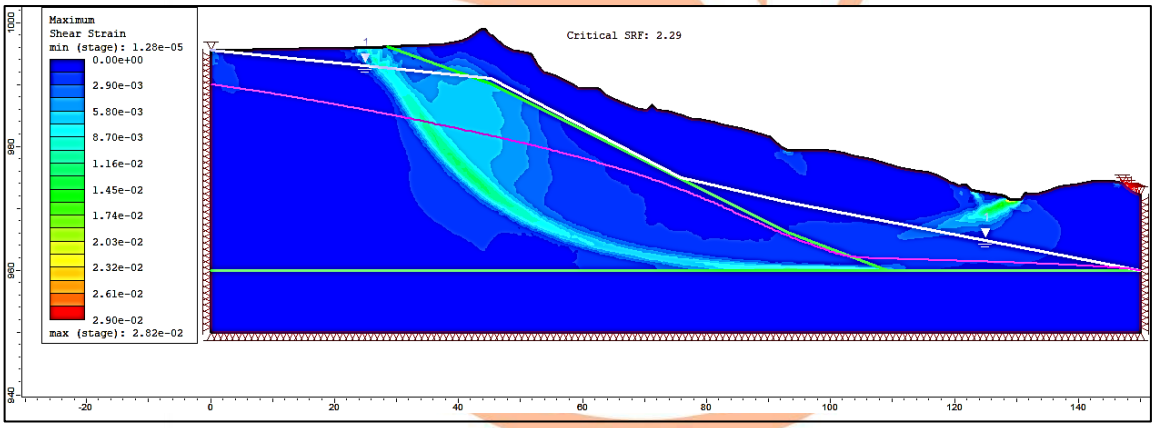

Figure 4.42 Critical SRF Maximum Shear Strain Contours for West Dam Wall

In Figure 4.44 more than one slip paths can be observed, the limit equilibrium slip path assumes a similar path but in between the two finite element slip paths. However, general trend and location are very similar and looking at Table 4.6, east dam wall's SRF and Factor of Safety are both 1.15. This means that the two methods located a critical slip path with a safety margin of 1.15. The east dam wall's Factor of Safety and SRF are below the recommended minimum value of 1.5. This could possibly be explained by the geometry since the dam wall is very steep and at the toe it has two visible depressions. These two depressions could provide a path for seepage water to escape to the ground surface after

leaving the dam. This could cause erosion at the toe of the slope and therefore destabilize the slope. It is also shown that the two slip circles in Figure 4.44 terminate at these two depressions, the same also applies in the LE model results. This is a clear indication that these two depressions may negatively affect the stability of the slope.

Furthermore, the finite element critical slip circle path located for south dam wall shows two downstream daylight positions as shown in Figure 4.45 (Daylight 1 and Daylight 2). This could also mean that two separate paths were located, however, the position of high shear strain zones shown coincide with the limit equilibrium slip circle path. A dotted arc that connects the two high shear zones is shown in the same figure and this path coincides with the path in Picture B.

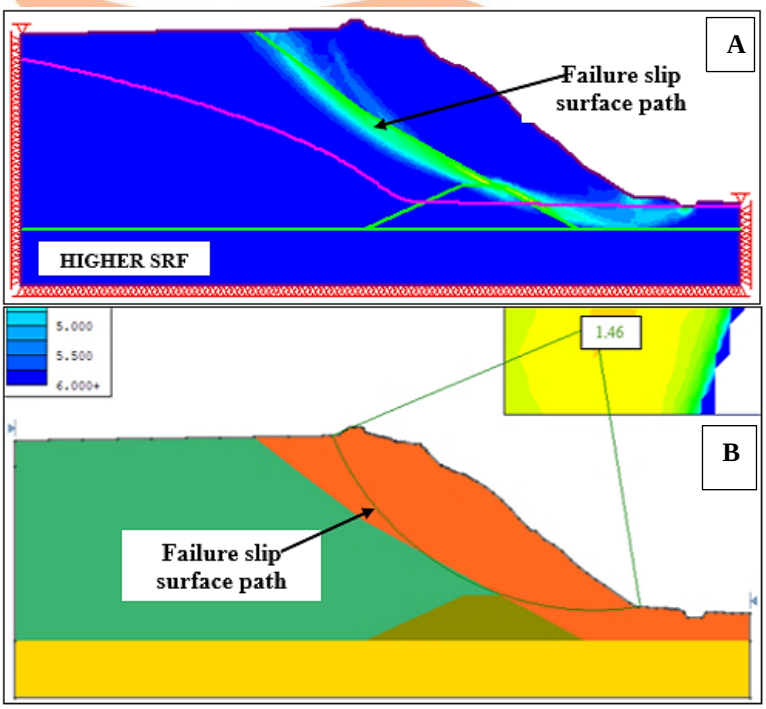

Figure 4.43 A - Maximum Shear Strain Contours for North Dam Wall; and B – Critical Failure Slip Path from Grid Search Method in Slide

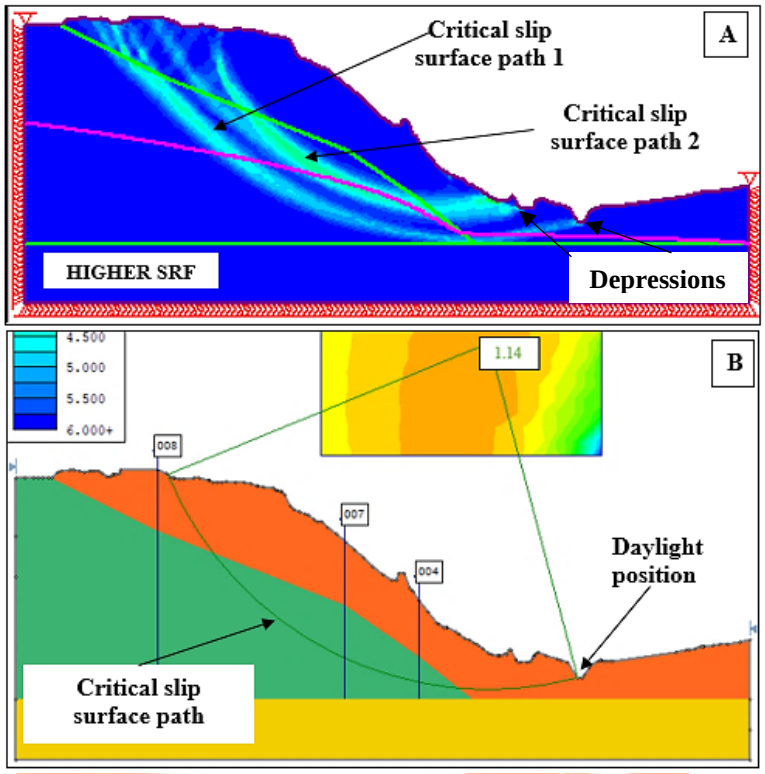

Figure 4.44 A - Maximum Shear Strain Contours for East Dam Wall; and B – Critical failure Slip Path from Grid Search Method in Slide

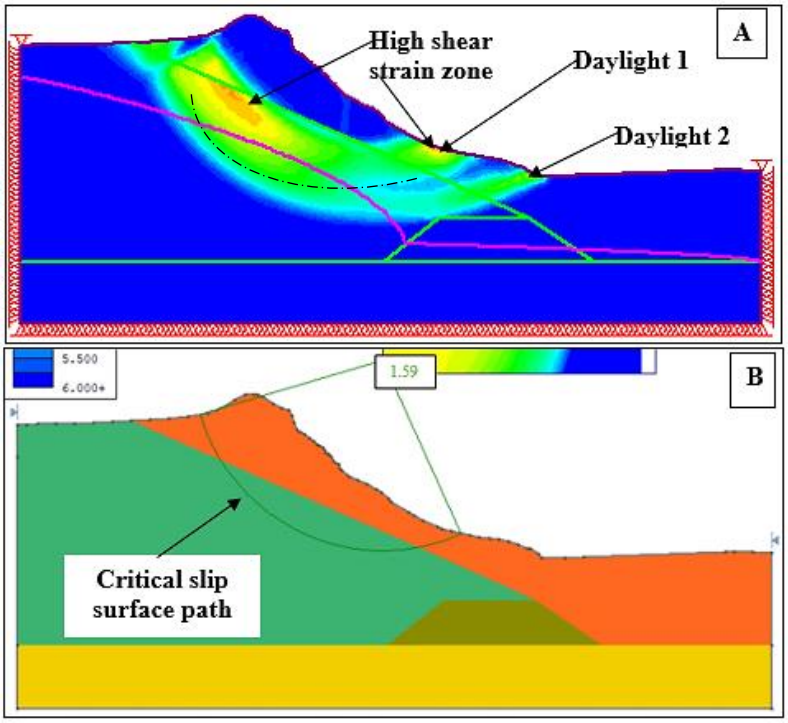

Figure 4.45 A - Maximum Shear Strain Contours for South Dam Wall; and B - Critical Failure Slip Path from Grid Search Method in Slide

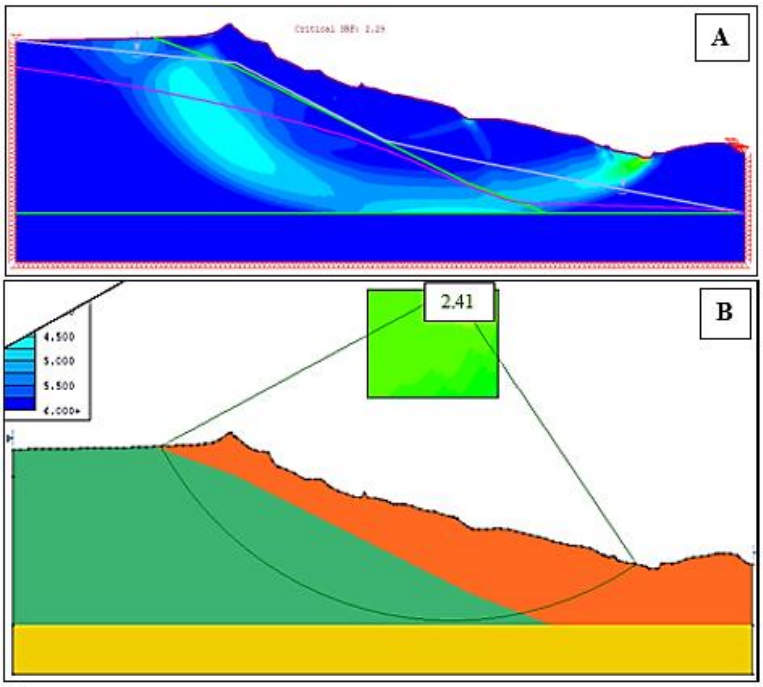

Figure 4.46 A - Maximum Shear Strain Contours for West Dam Wall; and B – Critical failure slip path from grid search method in Slide

Figures 4.47, 4.48 and 4.49 show a deformed mesh of three slurry dam walls. A deformed mesh highlights zones susceptible to displacement, direction in which the displaced material will move and resulting geometry. From the total displacement scale, red colored dataset represents areas with maximum displacement. Therefore, according to the shape of the mesh, in an event of failure, dam material would move downwards in a downstream direction. Soil particles in the maximum displacement contours will possess more kinetic energy and travel further as compared to those contoured in low/minimum displacement contours.

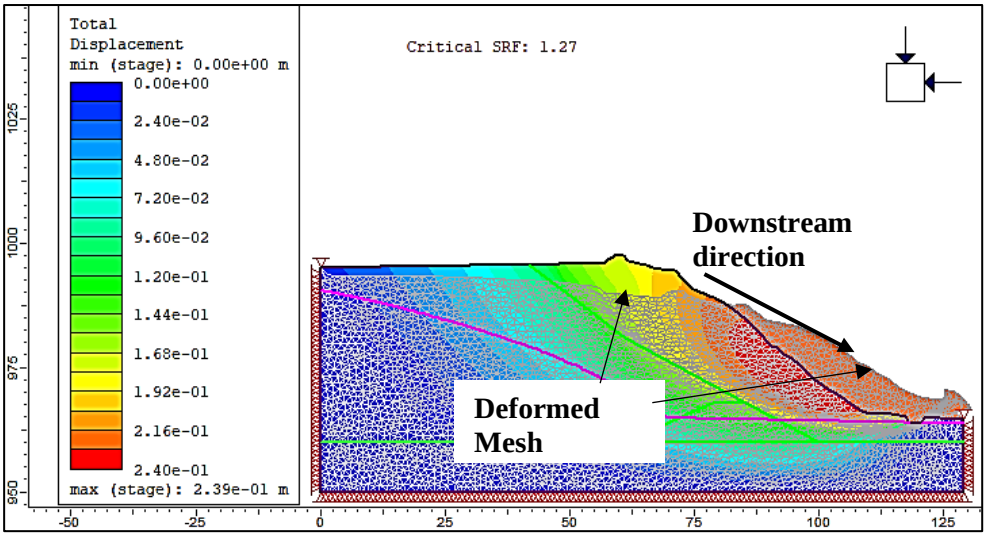

Figure 4.47 Total Displacement Contours and Deformed Mesh for North Dam Wall

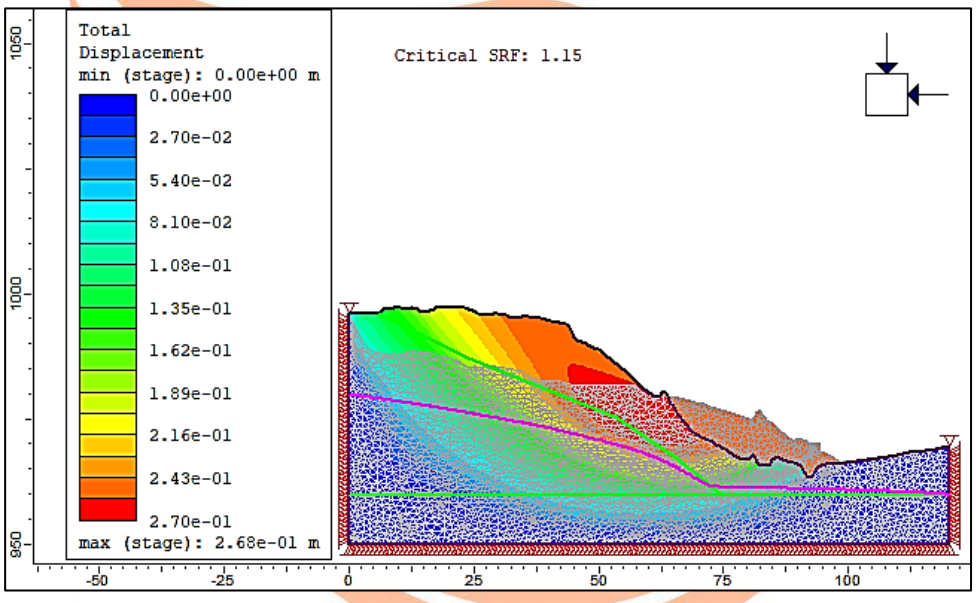

Figure 4.48 Total Displacement Contours and Deformed Mesh For East Dam Wall

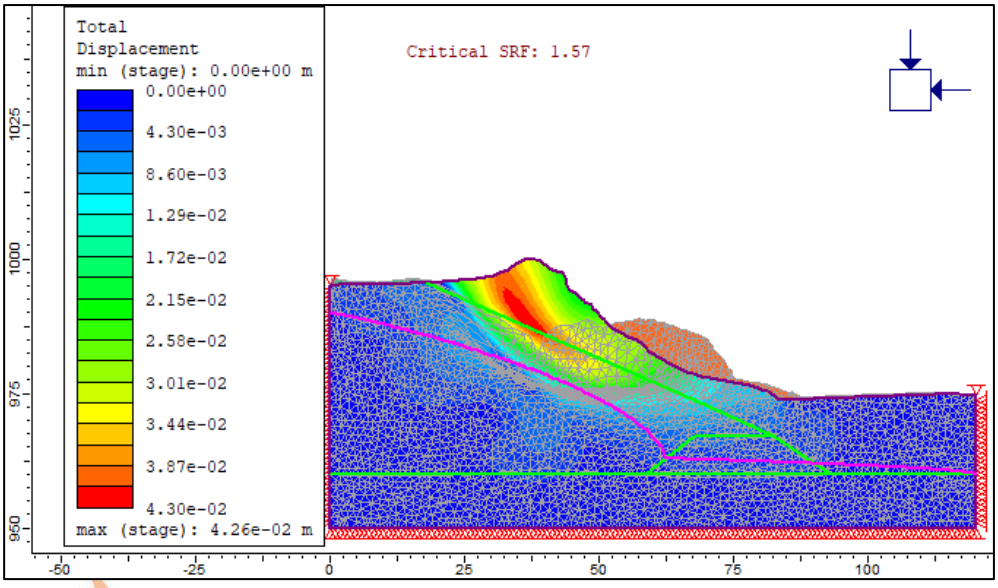

Figure 4.49 Total Displacement Contours and Deformed Mesh For South Dam Wall

Above models provide a clear indication of the state of the Orapa Mine Slurry Dam 2. Limit equilibrium analysis results are in good agreement with the finite element analysis results as shown in the above models and more precisely in Table 4.6. In comparison with limit equilibrium deterministic Factor of Safety, the computed SRF is lower (see Table 4.6). Researchers such as Krahn (2003) have stated that limit equilibrium analysis methods are lacking the fundamental physics of stress-strain relationship, therefore, they are unable to compute a more realistic stress distribution. A finite element analysis requires no assumptions for the computation of the strength reduction factor, it emerges naturally from the analysis without having to commit to any particular form of mechanism. Therefore, results obtained from this type of analysis are more likely to present lower values of the Factor of Safety.

It can be observed that both the north and the east dam walls present unsatisfactory SRFs as compared to the south and west dam walls. Perhaps this could be explained by observations that can be drawn from topographic data presented in Appendix B1, which has shown that the area is dipping towards a North-East direction. A report by Jones and Wagener (2016) has highlighted that in the event of a dam failure, the slurry would take a north-easterly channel and continue flowing in that direction.

Table 4.6 Strength Reduction Factors and Limit Equilibrium Factors of Safety for Orapa Mine Slurry Dam 2

Dam Wall	Strength Reduction Factor (SRF)	Limit Equilibrium Factor of Safety(FS) (GLE – Grid Search)	Differences	Percent Difference (%)
North	1.27	1.46	0.19	13.9
East	1.15	1.15	0	0
South	1.57	1.59	0.02	1.3
West	2.29	2.43	0.14	5.9

4.5 Regression Analysis

Regression analysis incorporated an investigation of any possible relationship between Orapa Slurry Dam 2 CPTu measured variables (Cone Tip Resistance, Sleeve Friction and Pore Pressure) and depth along slurry dam walls. The investigation involved a selection of upstream CPTu test points, one was sampled from each dam wall. An upstream test point is a point located at the top of the dam wall as shown in Figure 4.50. Test points at this location have established evidence in the ability to delineate a complete stratigraphic section of the dam walls (see Figure 4.4). North dam wall point North010 was chosen for north dam wall, east dam wall point East008 was chosen for east dam wall, south dam wall point South004 was chosen for south dam wall and west dam wall point West004 was chosen for west dam wall. Data as described in Section 3.5 was imported into the Regression Learner App for training and selection of the best model.

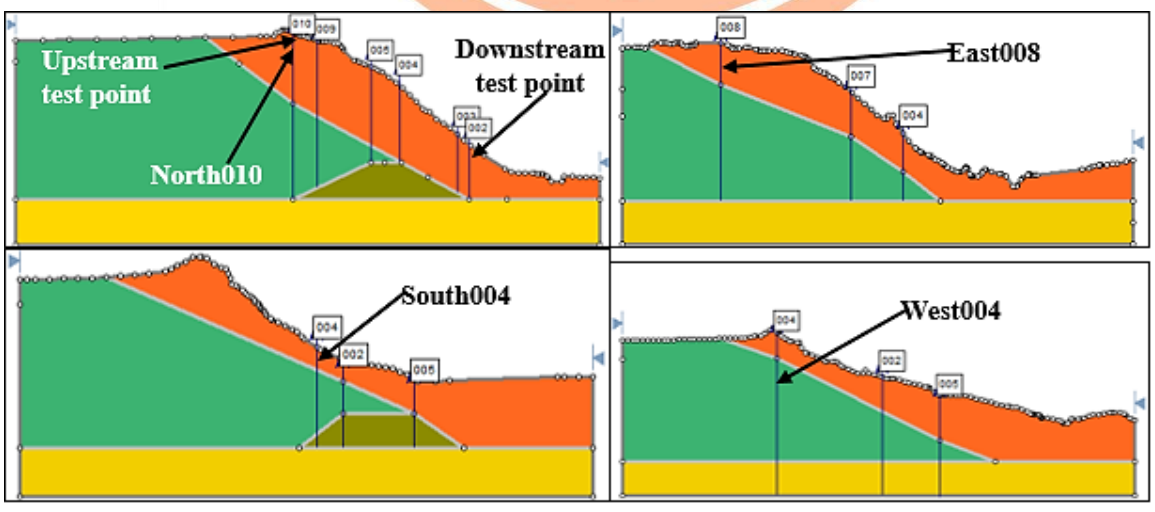

Figure 4.50 Selected Upstream Points for Regression Analysis

The model that provided a higher R-Squared value and lower validation errors belonged to the Gaussian Process group of regression models. Specifically, Rational Quadratic and Exponential Gaussian Process regression models responded well to the training than any other model. A sample MATLAB R2020a generated GPR model for test point EAST008 is shown in Appendix E2 for depth versus pore pressure. These Gaussian Process types of regression models are very complex, therefore, the mathematical underpinnings of these models are out of context of this research. The only interest was that they became the best predictive models such that it was possible to export them to MATLAB workspace for prediction of responses with new data.

Each dam wall had nine plots (three for each CPTu variable) giving a total of thirty-six plots. These plots as explained in Section 2.7.3 were used for qualitative assessment of the model to evaluate goodness of fit of the regression model. However, qualitative analysis does not provide enough information and judgement might be based on viewer's discretion. Only cone tip resistance regression models for east dam wall were used in this section to demonstrate the methodology used in qualitatively assessing the models. Furthermore, a table containing model evaluation parameters for quantitative assessment is presented (Table 4.7). This table was used in support of the model plots to quantify the performance of regression models. Figures 4.51 to 4.53 are the Response plot (Figure 4.51), the Predicted versus Actual plot (Figure 4.52) and the Residuals plot (Figure 4.53) for east dam wall respectively.

Figure 4.51 shows a Rational Quadratic Gaussian Process Regression (GPR) model that proved to be the perfect fitting model for Cone Tip Resistance versus depth in the east dam wall. It displays the response variable (Cone Tip Resistance, Qc) versus the predictor variable (depth). The plot with blue markers represents true response, it was obtained when plotting the data that was imported from excel. The plot with orange markers represents the predicted response, this is the regression (or predictive) model that resulted from the training.

A 100% perfect model (which probably does not exist) would result in the orange markers perfectly overlapping with the blue markers, causing the orange markers to hide the blue markers. This would occur when the differences between observed known values and the predicted values are close to zero and/or equal to zero, this is when the errors are close to

zero and/or equal to zero and the R-Squared value would be close to and/or equal to 100%. However, it can be observed from the plot that the difference between the observed values and the fitted values is very small hence an R-Squared value of 99% (quantitative assessment). The presented model statistics from comparisons with other models, proved that this particular model would be the best for accurate predictions.

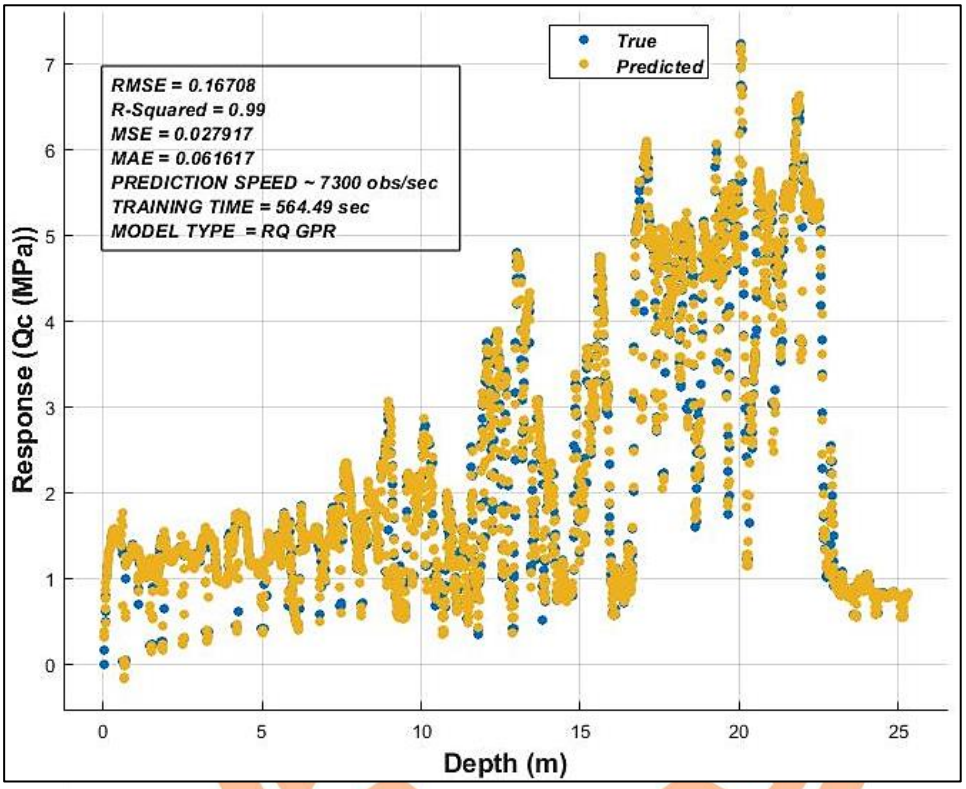

Figure 4.51 Response Plot showing Cone Tip Resistance versus Depth from CPTu Test Point EAST008

The Predicted versus Actual plot was used for model performance evaluation, to understand better how well the chosen model is able to make predictions for different response values. In a Predicted versus Actual plot, the model's predicted response plotted against the actual response. In a perfect regression model, the predicted response equals the actual response, and the values are along a diagonal as shown by a black solid line in Figure 4.52. The prediction error of an observation point is the vertical distance from the black solid line to that specific point (the blue marker). A good model has small errors, therefore the points of observations (predictions) should be scattered near the black line. This can be seen from Figure 4.52, almost all predictions are scattered around the line with just a few points

standing a small distance away from the line. Therefore, it is safe to rate this model as a good model.

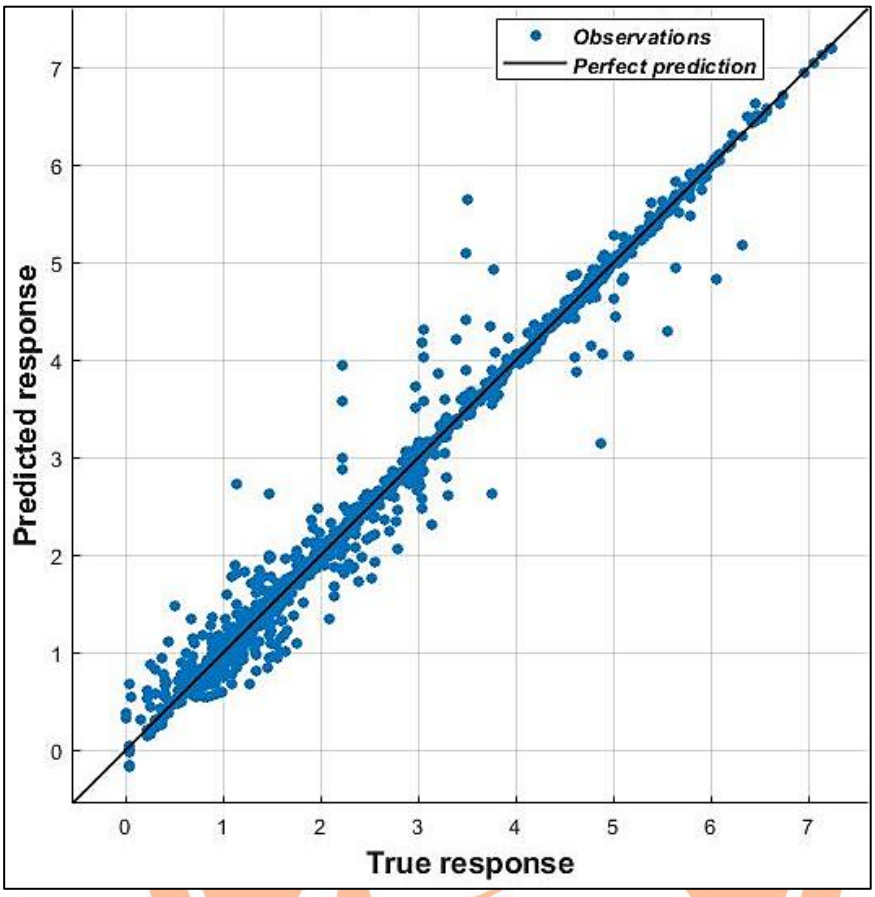

Figure 4.52 Predicted versus Actual Plot for Cone Tip Resistance versus Depth from CPTu Test Point EAST008

A Residual plot has residuals (residual values) on the vertical axis and an independent variable on the horizontal axis. It is also used for model performance evaluation to show differences between predicted and actual true responses. A good model has residuals roughly scattered symmetrically around zero. The model in Figure 4.53 has almost all points scattered around the y=0 line, just a few points are dispersed away (large residuals/errors) from the line. This model is reasonably good and can make predictions with very small errors.

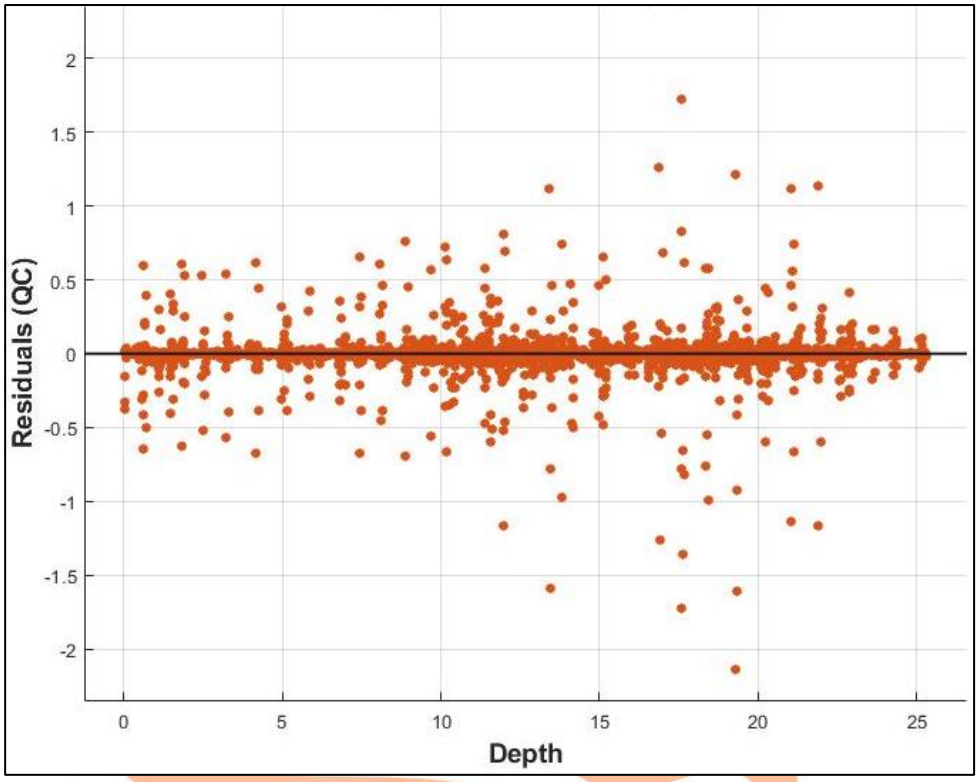

Figure 4.53 Residuals Plot for Cone Tip Resistance versus Depth from CPTu Test Point EAST008

These regression model plots are subjective, decisions on which model is better are based on the discretion of the person viewing the model. Decisions based on qualitative analysis can be unreliable since they differ according to knowledge and experience. In engineering design, decisions are mostly based on measurements and calculations because this type of analysis produces results that are supported by concrete evidence. Model evaluation statistic parameters described in Table 2.2, were used to assess model performance in support of the model plots. Table 4.7 provides a summary of these parameters, obtained for each dam wall.

Table 4.7 Regression Analysis Results for All Four Slurry Dam Walls

Dam Wall	Model Statistic	Cone Tip Resistance Versus Depth	Sleeve Friction Versus Depth	Pore Pressure Versus Depth
EAST 008	Model Type	RQ GPR	RQ GPR	RQ GPR
	RMSE	0.17	1.99	18.00
	R-Squared	0.99	0.99	0.98
	MSE	0.03	3.95	322.25
	MAE	0.06	0.87	6.57
	Training Time (s)	564.49	464.81	549.81
NORTH 010	Model Type	EXP GPR	EXP GPR	RQ GPR
	RMSE	0.21	5.21	20.09
	R-Squared	0.98	0.96	0.99
	MSE	0.04	27.11	403.67
	MAE	0.07	1.35	7.30
	Training Time (s)	234.04	257.67	327.88
SOUTH 004	Model Type	EXP GPR	RQ GPR	EXP GPR
	RMSE	0.23	2.31	2.03
	R-Squared	0.98	0.99	0.99
	MSE	0.05	5.33	4.12
	MAE	0.09	1.25	0.39
	Training Time (s)	13.88	29.44	21.40
WEST 004	Model Type	RQ GPR	RQ GPR	RQ GPR
	RMSE	0.11	2.54	17.58
	R-Squared	0.99	0.99	0.99
	MSE	0.01	6.45	309.01
	MAE	0.04	1.06	6.90
	Training Time (s)	572.25	541.95	576.04

Regression models that proved to be better for all the dam walls were Rational Quadratic and Exponential GPR models. Specifically, west dam wall data for cone tip resistance produced a perfect Rational Quadratic GPR model with the lowest validation errors. Validation errors (RSME, MSE and MAE) were in overall very high for pore pressure models as shown in Table 4.4a, with the RMSE reaching values close to and over 20kPa. With such high values of errors, even when the R-Squared value is high enough, this makes

the model less able to make accurate predictions, and therefore cannot be used for such. Therefore, a Gaussian Process Regression algorithm when trained with Slurry Dam 2 piezocone data produces a good model which could be used to predict unknown values of cone tip resistance at specified depths with minimum errors.

CHAPTER 5

CONCLUSIONS AND RECOMMENDATIONS

Continuous tailings dam failure events worldwide confirm the need for continued stability analysis and intensive research on tailings dam operations, maintenance and management. This research has focused on slope stability analysis of Orapa Mine Slurry Dam 2, which is one of the oldest slurry dams for this mine. The basis of this research was data obtained from Cone Penetration Testing with pore pressure measurements (CPTu). This is a closing chapter that presents main findings and minor findings of this study including recommendations for future research.

5.1 Conclusions

This section presents the findings obtained from this study which have been subdivided into main findings and minor findings as follows.

5.1.1 Main Findings

i. Orapa Mine Slurry Dam 2 walls are made up of alternating layers of clay, silt and sand sized material as obtained from piezocone data interpretation.

ii. Dissipation test results estimated the phreatic surface elevation to ~978 meters above mean sea level (± 5 m), with high pore water pressures trapped within the clay material.

iii. LE and FE analysis results presented Factors of Safety less than and /or marginally above 1.5 for north, south and east dam walls. Therefore, these were considered unsafe in terms of the recommended minimum Factor of Safety of 1.5.

iv. The optimum machine learning model was the Rational Quadratic Gaussian Process Regression model, with R-Squared of 99% and RMSE of 0.11.

5.1.2 Minor Findings

i. Generally, the LE and FE analyses results were in good agreement in terms of slip circle path and the Factor of Safety. The Strength Reduction Factors (SRFs) were slightly lower than the LE factors of safety with differences averaging at 0.09 or 5.28%.

ii. There is need for further research into why the north, south and east dam walls do not offer satisfactory factors of safety.

iii. Probabilistic analysis results have stated that overall Probability of Failure of the slurry dam is zero (0). This simply implies that of all the samples analysed, no sample produced a Factor of Safety which was less than 1 (FoS of 1 represents the brink of collapse/failure).

iv. The reliability indices for north, south and west dam walls were over and above 3 which is a minimum value recommended for a safe slope design. Therefore, the east dam wall's reliability index which stands at 2.8, means that the slope may be unsafe.

v. From the sensitivity analysis, it was apparent that the results were influenced by the critical slip/failure surface path. In each case the governing parameter was the friction angle of materials through which the failure surface passes. In some cases, where the slip circle was deep seated (located at high depths), the Factor of Safety became more sensitive towards unit weight of the material. This was as a result of an increase in overburden pressure, whereby the vertical force could increase the susceptibility to failure at the slip/failure surface.

vi. Cohesion was very low (≤ 5) for all Slurry Dam 2 materials, this meant that friction angle would be the governing strength parameter in the stability of the dam.

vii. Generally, cone tip resistance data with respect to depth produced good models with maximum RMSE of 0.23 and minimum R-Squared of 98%. High validation errors were encountered for pore pressure and sleeve friction data.

5.2 Recommendations

The research has highlighted the need for close attention to factors that may affect the Orapa Mine Slurry Dam 2. This is highlighted by current height (~ 1000 meters above mean sea level) as well as lower Strength Reduction Factors presented for east, south and north dam walls. It is recommended as follows regarding the slurry dam and future research work.

i. The mine should maintain a smooth drainage system to allow the dam to dry and consolidate, hence increasing the overall Factor of Safety of the slurry dam.

ii. North, east and south dam walls have lower factors of safety, hence, any form of deposition into the dam will trigger destabilizing mechanisms.

iii. The mine should allow for closure of Slurry Dam 2 and execution of aftercare plan.

iv. Slurry Dam 2 Piezocone data can be trained with Gaussian Process Regression algorithms in MATLAB and the best performing model can predict unknown values to the highest possible accuracy.

REFERENCES

1. Abramson, L. W., Lee, T. S., Sharma, S. and Boyce, G. M. (2002), *Slope Stability and Stabilization Methods* (2nd ed.), John Wiley and Sons, Inc, New York, 649 pp.
2. Alkalaj, S. (2014), *Safety guidelines and good practices for tailings management facilities*, United Nations Economic Commission for Europe, New York, 42 pp.
3. Amazon Web Services (2020), "Training ML Models", www.docs.aws.amazon.com. Accessed: April 29, 2020.
4. ANCOLD (Australian National Committee of Large Dams) (1969), *Current Technical Practices for the Design, Construction, Operation and Maintenance of Large Dams*, Australian National Committee on Large Dams, 233 pp.
5. FrontlineSolvers (2021), "Regression Trees", www.solver.com/regression-trees. Accessed: May 18, 2021.
6. ArcMap (2016), "What is a TIN surface?", www.desktop.arcgis.com /en/arcmap/10.3/manage-data/tin/fundamentals-of-tin-surfaces.htm. Accessed: May 04, 2021.
7. Ashcroft, I. A., Mubashar, A. (2011), "Numerical Approach: Finite Element Analysis", *Handbook of Adhesion Technology*, Springer, pp. 629-660.
8. Autodesk (2019), "About Creating a TIN Surface", www.knowledge.autodesk.com/support/civil-3d/learn-explore. Accessed: May 18, 2021.
9. Autodesk (2021), "Civil Infrastructure Design and Documentation Software", www.autodesk.in/products/civil-3d/overview. Accessed: May 18, 2021.
10. Bachoc, F., Gamboa, F., Loubes, J., Venet, N. (2017), "A Gaussian Process Regression Model for Distribution Inputs", *IEEE Transactions on Information Theory*, 99 pp.
11. Bolton, H. P., Heymann, G. and Groenwold, A. A. (2010), "Global Search for Critical Failure Surface in Slope Stability Analysis", *Engineering Optimization, 35*(1), pp. 51-65.
12. Brownlee, J. (2016), "Machine Learning Mastery", www.machinelearning mastery.com. Accessed: May 1, 2020.
13. Ryzhkov, I. B. and Isaev, O. N. (2015), "Current Status and Trends in Cone Penetration Testing of Soil", *Proceedings of the 3rd International Symposium on*

Cone Penetration Testing, Soil Mechanics Foundation Engineering, Spain, pp. 171-173.

14. Carter, J., Schmid, K., Waters, K., Betzhold, L., Hadley, B., Mataosky, R. and Halleran, J. (2012), *Lidar 101: An Introduction to Lidar Technology, Data, and Applications*, National Oceanic and Atmospheric Administration (NOAA) Coastal Services Center, Charleston, 72 pp.
15. Chioba, T. B. (2015), "A study on internal dilution in the Orapa 2125 A/K1 Kimberlite based on 2D quantitative textural analysis data", University of the Witwatersrand, Johannesburg, pp. 10-15.
16. Chiwaye, H. and Stacey, T. (2010), "A comparison of limit equilibrium and numerical modelling approaches to risk analysis for open pit mining", *Journal of the Southern African Institute of Mining and Metallurgy, 110(10)*, pp. 571-580.
17. CIVILAX (Civil Engineering Knowledge Base) (2018), "Limit Equilibrium Methods of Slope Stability Analysis ─ Fundamentals", www.CIVILAX.com/limit-equilibrium-methods-of-slope-stability-analysis. Accessed: July 12, 2020.
18. De Beers UK, L. (2019), "De Beers Group", www.debeersgroup.com/the-group/about-debeers-group/mines/botswana/orapa. Accessed: June 11, 2019.
19. deWolfe, G. F., Griffiths, D. V. and Huang, J. (2011), "Probabilistic and Deterministic Slope Stability Analysis by Random Finite Elements", *Conference on Geotechnical Practice Publication*, Colorado, 22 pp.
20. Educba (2020), "What is Supervised Learning?", www.educba.com/what-is-supervised-learning. Accessed: July 16, 2020.
21. Ellis, M., Ogee, A. and Scibilia, B. (2013), "The Minitab Blog", www.blog.minitab.com/blog/adventures-in-statistics-2/regression-analysis-how-do-i-interpret-r-squared-and-assess-the-goodness-of-fit. Accessed: January 10, 2020.
22. Elprocus. (2020), "All You Know About LIDAR Systems and Applications", www.elprocus.com/lidar-light-detection-and-ranging-working-application. Accessed: July 23, 2020.
23. El-Reedy, M. A. (2017), *Onshore Structural Design Calculations*. Elsevier Ltd., pp. 345 - 385.
24. Envi (2012), "Envi logger C1 & CS1 User Manual", Environmental Mechanics AB, www.envi.se/Manuals/CPT%20software%20manual. Accessed: May 18, 2021.

25. Expert.ai (2020), "What is Machine Learning? A Definition", www.expert.ai/blog/machine-learning-definition. Accessed: May 18, 2021.
26. Fallah, S., Yousefpour, N. (2018), "Application of Machine Learning in Geotechnics", University College, Dublin, 11 pp.
27. Geologismiki (2018), "Geologismiki", www.geologismiki.gr/products/cpet-it. Accessed: November 19, 2019.
28. Golder Associates Africa (Pty) Ltd. (2002), "No. 2 Slurry Dam Design Report", *Unpublished Mine Report*, Orapa Diamond Mine, Orapa, 77 pp.
29. Gonzalez De Vallejo, L. I. and Ferrer, M. (2011), *Geological Engineering*, Taylor and Francis Group, London, pp. 10-559.
30. Google (2020), "Google Maps", www.google.cm/maps/place/Orapa. Accessed: July 23, 2020.
31. Hamade, T. and Mitri, H. (2013), "Reliability-based approach to the geotechnical design of tailings dams", *International Journal of Mining, Reclamation and Environment, 27*(6), pp. 377-392.
32. Hayes, A. (2021), "Linear Relationship Definition", www.investopedia.com/terms/I/linearrelationship.asp. Accessed: May 18, 2021.
33. Herza, J., Ashley, M. and Thorp, J. (2017), "Factor of Safety? - Do we use it correctly?", *Conference on Factor of Safety*, ANCOLD, Hobart, 11 pp.
34. Huang, Y. H. (2014), *Slope Stability Analysis by the Limit Equilibrium Method: Fundamentals and Methods*, ASCE Press, Lexington, pp. 1-360.
35. International Council on Mining Metals (2020), "International Council on Mining Metals (ICMM)", www.icmm.com/en-gb/environment/tailings. Accessed: July 8, 2020.
36. Jones and Wagener (2016), "Orapa and Damtshaa Slurry and Storm Water Dams Stability and dam break Analyses", *Unpublished Mine Report*, Orapa Diamond Mine, Orapa, 200pp.
37. Kanda, M. J. and Stacey, T. R. (2016), "The influence of various factors on the results of stability analysis of rock slopes and on the evaluation of risk", *The journal of the South African Institute of Mining and Metallurgy, 116*(11), pp. 1075-1081.
38. Kossoff, D., Dubbin, W., Alfredsson, M., Edwards, S. J., Macklin, M. G. and Hudson-Edwards, K. A. (2014), "Mine tailings dams: Characteristics, failure, environmental impacts, and remediation", *Applied Geochemistry, 51*, pp. 229 - 245.

39. Krahn, J. (2003), "The limits of limit equilibrium analysis", *Canadian Geotechnical Journal, 44*, pp. 643-660.
40. Kujawa, C. (2011), "Cycloning of Tailing for the Production of Sand as TSF Construction Material", *Tailings and Mine Waste*, Paterson and Cooke Ltd., Golden, pp. 1-11.
41. Laçasse, S. (1994), "Reliability and Probabilistic Methods", *International Society for Soil Mechanics and Geotechnical Engineering*, New Delhi, pp. 225-227.
42. Leao, T. F. (2019), *Development of an Educational Tool for Deterministic and Probabilistic Slope Stability Analysis*, Purdue University Graduate School, Hammond, pp. 1-102.
43. Lindquist, A. and Törnqvist, S. (2015), *Stability analysis on a planned Mexican tailings dam.* Uppsala Unversity, Ångströmlaboratoriet, pp. 1-52.
44. Luiz , R. H., Alcântara, E., Park, E., Rogério, N. G. and Lin, N. Y. (2020), "The 2019 Brumadinho tailings dam collapse: Possible cause and impacts of the worst human and environmental disaster in Brazil", *International Journal of Applied Earth Observation and Geoinformation, 90*, pp. 102-119.
45. Lunne, T., Robertson, P. K. and Powell, J. J. (1997), *Cone Penetration Testing in Geotechnical Practice.* E and FN Spon, New York, pp. 1-203.
46. Lyu , Z., Chai, J., Xu, Z., Qin, Y. and Cao, J. (2019), "A Comprehensive Review on Reasons for Tailings DamFailures Based on Case History", *Advances in Civil Engineering, 9*, pp. 1-18.
47. MathWorks, Inc. (2020), "MathWorks", www.mathworks.com/help/stats/ regression-learner-app. Accessed: May 4, 2020.
48. McPhail, G. I. and Wagner, J. C. (1989)," Disposal of Residues", *The Extractive Metallurgy of Gold in South Africa*, Stanley, pp. 655-706.
49. Memon, M. Y. (2018), "A Comparison Between Limit Equilibrium and Finite Element Methods for Slope Stability Analysis', *Unpublished Project Report*, Missouri University of Science & Technology, Rolla, Missouri, 15 pp.
50. Mosquera, J., Hamade, T. and Mitri, H. (2013), *Comparative Stability Analysis of Tailings Storage Facilities*, McGill University, Canada, pp. 1-11.
51. Mustafa, M. R., Rezaur, R. B., Saiedi, S. and Rahardjo, H. (2013), "Evaluation of MLP-ANN Training Algorithms for Modeling Soil Pore-Water Pressure Responses to Rainfall", *Journal of Hydrologic Engineering, 1*(18), pp. 50-57.

52. Naeini, M. and Akhtarpour, A. (2018), "Numerical analysis of seismic stability of a high centerline tailings dam", *Soil Dynamics and Earthquake Engineering, 107*, pp. 179-194.
53. Penner, D. (2014), "How tailings dams work", www.vancouversun.com/technology/ tailings. Accessed: May 4, 2020.
54. Ponce-Zambrano, M. R. and Gordon, D. P. (2014), "Geotechnical Characterization of the Site and Stability of a Tailings Dam in Ecuador", *Rock Engineering and Rock Mechanics: Structures in and on Rock Masses*, 1166p.
55. Pricop, M., Oncica, V., Cristian, I. (2013), "Factor of Safetyin Offshore Structures Design According to Environmental Loads", *Scientific Bulletin of Naval Academy, Vol 16, No. 2,* pp. 152-157.
56. Pupale, R. (2018), "Support Vector Machines (SVM) - An Overview", www.towardsdatascience.com/https-medium-com-pupalerushikesh-svm. Accessed: May 18, 2021.
57. Queiroz, I. M. (2016), "Comparison between Deterministic and Probabilistic Stability Analysis, Featuring Consequent Risk Assessment", *International Journal of Geotechnical and Geological Engineering, 10(6)*, pp. 636-643.
58. Reale, C., Gavin, K., Libric, L., Juric-Kacunic, D. (2018), "Automatic classification of fine-grained soils using CPT measurements and Artificial Neural Networks", *Advanced Engineering Informatics*, pp. 207-215.
59. Rico, M., Benito, G. and Díez-Herrero, A. (2018), "Floods from tailings dam failures", *Journal of Hazardous Materials, 154*(1-3), pp. 79-87.
60. Robertson , P. K. (2010), *Soil behaviour type from the CPT: an update*, Gregg Drilling and Testing Inc., California, pp. 1-128.
61. Robertson, P. K. and Cabal, K. L. (2010), *Guide to Cone Penetration Testing for Geotechnical Engineering*, Gregg Drilling and Testing, Inc., Signal Hill, California 90755, pp. 842-853.
62. Rocscience (2018), "Rocscience", www.rocscience.com. Accessed: December 9, 2019.
63. Sabatini, R., Richardson, M. A., Gardi, A., Ramasamy, S. (2015), "Airborne Laser Sensors and Integrated Systems", *Progress in Aerospace Sciences 79*, pp. 15-63.
64. Schreiber, D. (2007), "Matrix Laboratory", *Scholarpedia, 2*(7), 2929 pp.

65. Serra, M. P. (2013), "Geotechnical Stability Analysis Using Student Versions of Flac, Plaxis, and Slope/w", University of Southern Queensland, Southern Queensland, pp. 1-81.
66. Shai , S.-S. and Shai, B.-D. (2014), *Understanding Machine Learning: From Theory to Algorithms*, Cambridge University Press, New York, pp. 1-434.
67. Souza, E. D. (2010), *Designing safe and stable tailings dam structures with centrifuge modelling*, WIT Press, Canada, pp. 615-625.
68. Spring (2004), "Notes on the Cone Penetrometer Test", *Advanced Engineering Geology and Geotechnics*, 9 pp.
69. Steiner, A., Kopf, A. J., Henry, P., Stegmann, S. (2015), "Cone Penetration Testing to Assess Slope Stability in the 1979 Nice Landslide Area", *Marine Geology*, pp. 162-181.
70. Sternik, K. (2013), "Comparison of Slope Stability Predictions by Gravity Increase and Shear Strength Reduction Methods", *Technical Transactions Environment Engineering*, pp. 121-130.
71. Taormina, R., Sethi, R. and Chau, K. W. (2012), "Artificial Neural Network Simulation of Hourly Groundwater Levels in a Coastal Aquifer System of the Venice Lagoon", *Engineering Applications of Artificial Intelligence*, *25*(8), pp. 1670-1676.
72. Thygesen, K. (2017), "Causes of tailing dams failures 1915-2016", www.grida.no/resources/11424. Accessed: June 19, 2018.
73. Tiemann, T. K., Mahbobi, M. (2010), "Regression Basics", In Chap. 8 of *Introductory Business Statistics with Iterative Spreadsheets - 1st Canadian Edition*, *BCcampus*, 69 pp.
74. Ural, N. (2018), "Importance of Clay in Geotechnical Engineering", In Chap. 5 of *Current Topics in the Utilization of Clay in Industrial and Medical Applications*, Zoveidavianpoor, M. (ed.), IntechOpen, pp. 758.
75. U.S. Environmental Protection Agency, EPA (1994), "Design and Evaluation of Tailings Dams", U.S. Environmental Protection Agency, EPA, Washington, pp. 1-59.
76. Vaseekaran, G. (2018), "Machine Learning: Supervised Learning vs Unsupervised Learning", www.medium.com/@gowthamy/machine-learning-supervised-learning-vs-unsupervised-learning. Accessed: May 1, 2020.

77. Vick, S. (1990), *Planning, Design and Analysis of Tailings Dams*, BiTech Publishers Ltd., Vancourver, pp. 1-369.
78. Yabbarova, E. N., Zaikin, A. A., Latypor, A. I. (2021), " Application of Machine Learning for Prediction of Cone Penetretion Test Data", *IOP Conference Series: Earth and Environmental Science*, IOP Publishing Ltd., pp. 1-6.
79. Yin, G. Z., Li, G. Z., Wei, Z., Wan, L., Shui, G. and Jing, X. (2011), "Stability analysis of a copper tailings dam via laboratory model tests: A Chinese case study", *Minerals Engineering*, 24(2), pp. 122-130.

APPENDICES

APPENDIX A

CONE PENETRATION TEST RESULTS

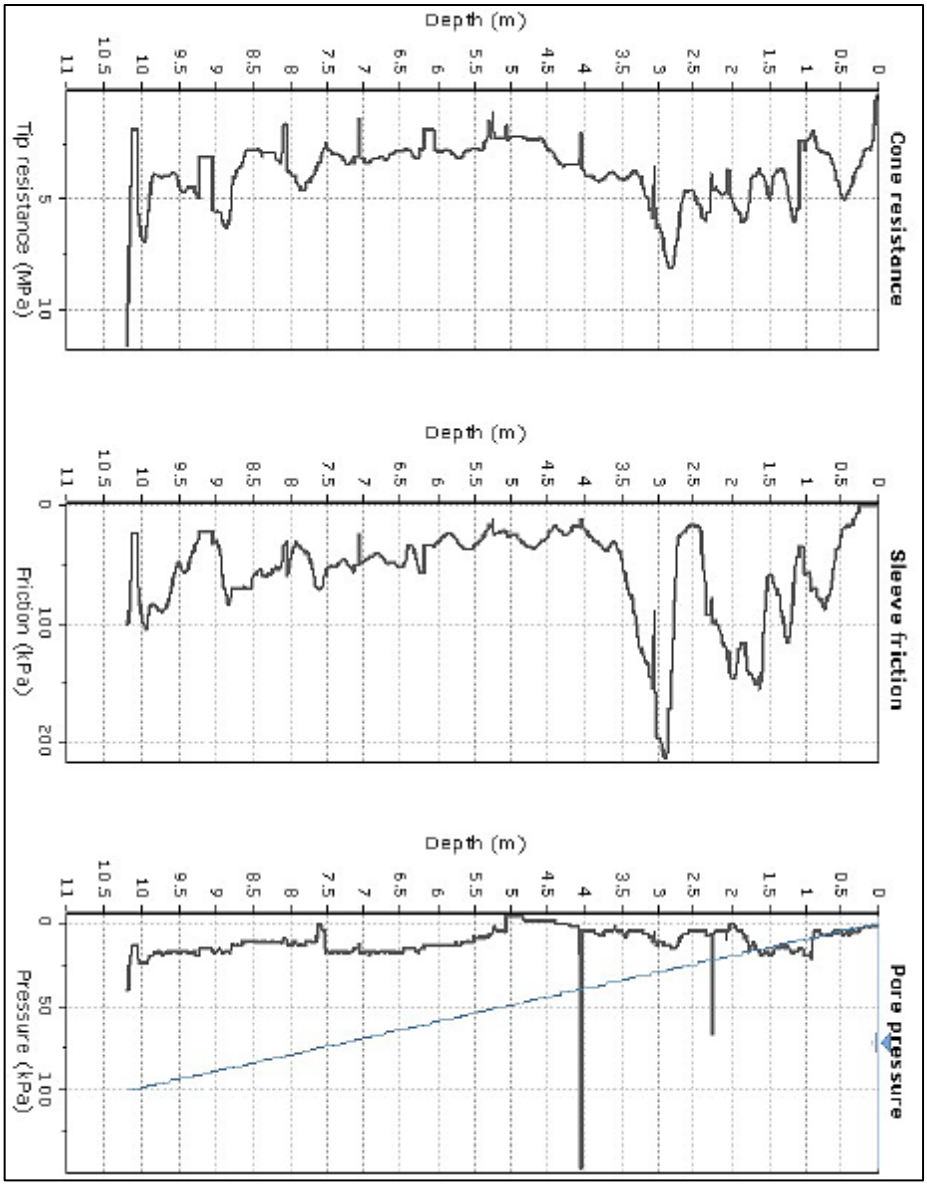

Appendix A1 CPTu Parameter Profiles for North Dam Wall CPTu Test Point 002

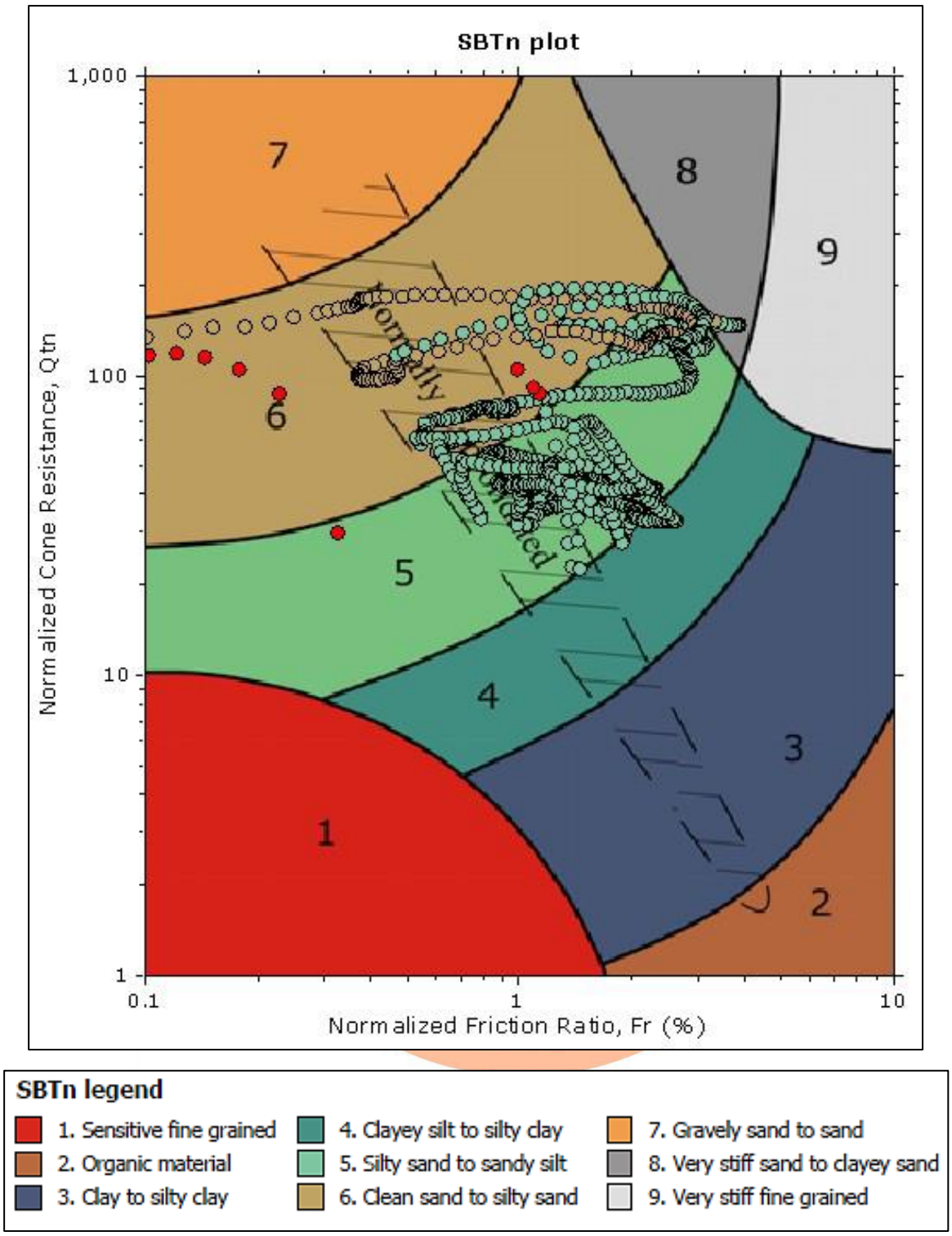

Appendix A2 Normalized SBT Plot for North Dam Wall CPTu Test Point 002

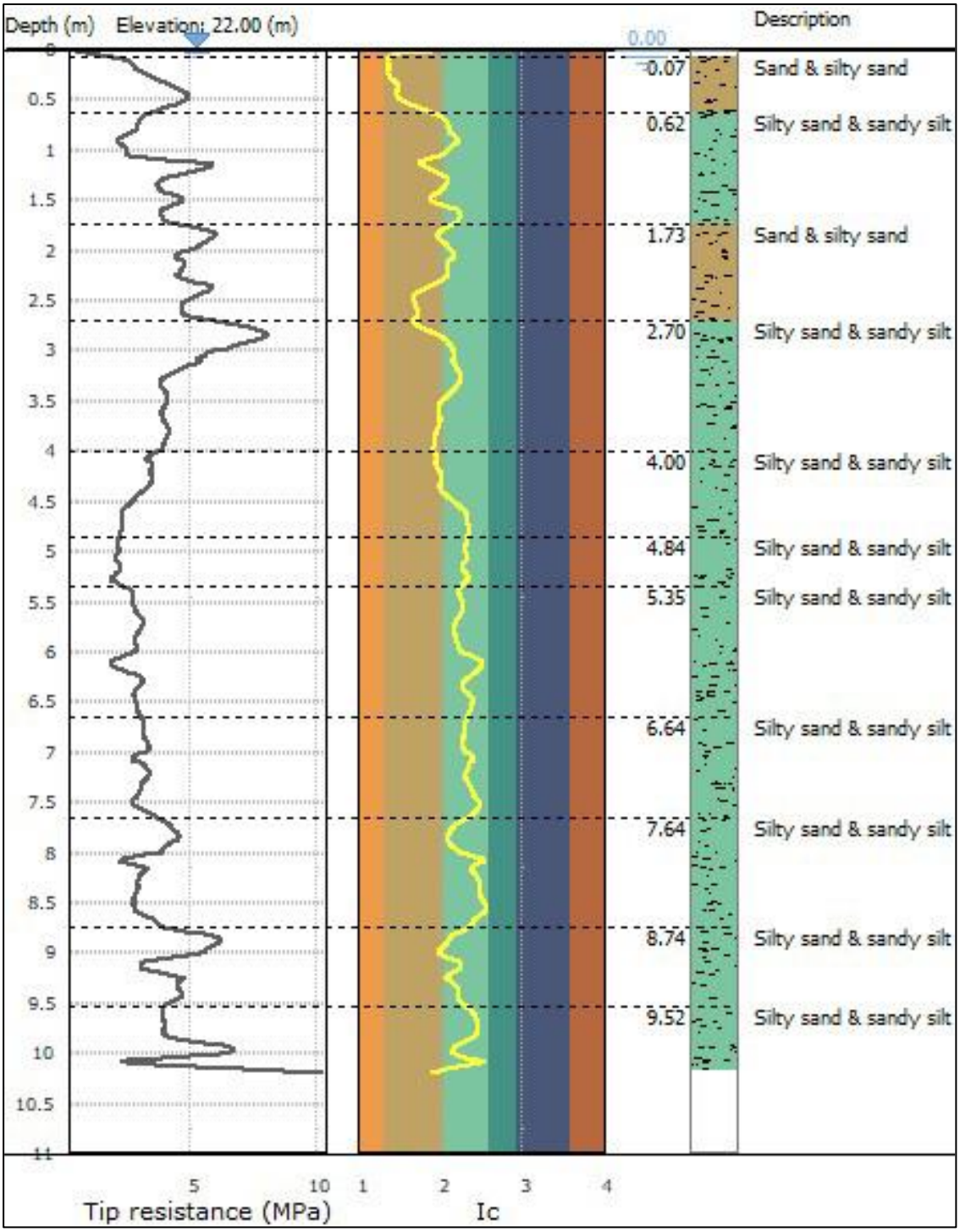

Appendix A3 Geotechnical cross section alongside Cone Tip Resistance Profile for North Dam Wall CPTu Test Point 002

Summary table of mean values

From depth To depth (m)	Thickness (m)	Permeability (m/s)	SPT_{N60} (blows/30cm)	E_s (MPa)	D_r	Friction angle	Constrained modulus, M (MPa)	Shear modulus, G_0 (MPa)	Undrained strength, S_u (kPa)	Undrained strength ratio	OCR	Unit weight (kN/m³)
0.07	0.55	2.81E-04	7.3	21.6	70.1	42.2	22.5	22.5	0.0	0.0	0.0	19.0
0.62		(±1.71E-04)	(±2.0)	(±3.9)	(±2.9)	(±0.4)	(±7.5)	(±7.5)	(±0.0)	(±0.0)	(±0.0)	(±0.0)
0.62	1.11	9.00E-06	10.1	34.4	65.4	41.5	42.7	43.1	0.0	0.0	0.0	19.0
1.73		(±1.02E-05)	(±2.2)	(±7.4)	(±4.8)	(±0.7)	(±8.7)	(±9.2)	(±0.0)	(±0.0)	(±0.0)	(±0.0)
1.73	0.97	2.43E-05	13.2	42.8	61.7	40.9	53.7	53.7	0.0	0.0	0.0	19.0
2.70		(±2.75E-05)	(±1.7)	(±8.7)	(±5.8)	(±0.9)	(±10.9)	(±10.9)	(±0.0)	(±0.0)	(±0.0)	(±0.0)
2.70	1.30	1.07E-05	13.6	46.2	54.4	39.6	57.3	57.9	0.0	0.0	0.0	19.0
4.00		(±1.51E-05)	(±3.6)	(±13.4)	(±8.7)	(±1.5)	(±16.7)	(±16.8)	(±0.0)	(±0.0)	(±0.0)	(±0.0)
4.00	0.84	5.49E-06	8.5	29.6	38.7	36.5	34.8	37.1	0.0	0.0	0.0	19.0
4.84		(±4.31E-06)	(±0.5)	(±1.1)	(±3.2)	(±0.8)	(±2.6)	(±1.4)	(±0.0)	(±0.0)	(±0.0)	(±0.0)
4.84	0.51	9.22E-07	7.0	27.5	32.4	34.8	29.2	34.5	0.0	0.0	0.0	19.0
5.35		(±1.41E-07)	(±0.3)	(±1.1)	(±1.0)	(±0.3)	(±1.5)	(±1.4)	(±0.0)	(±0.0)	(±0.0)	(±0.0)
5.35	1.29	1.18E-06	9.1	35.3	35.0	35.5	37.9	44.1	0.0	0.0	0.0	19.0
6.64		(±6.46E-07)	(±0.8)	(±3.4)	(±1.5)	(±0.4)	(±4.3)	(±4.3)	(±0.0)	(±0.0)	(±0.0)	(±0.0)
6.64	1.00	7.26E-07	10.6	42.2	34.6	35.4	42.3	52.9	0.0	0.0	0.0	19.0
7.64		(±2.76E-07)	(±0.6)	(±2.5)	(±1.3)	(±0.4)	(±3.0)	(±3.2)	(±0.0)	(±0.0)	(±0.0)	(±0.0)
7.64	1.10	1.14E-06	11.6	45.6	34.8	35.5	44.9	57.3	0.0	0.0	0.0	19.0
8.74		(±1.34E-06)	(±1.1)	(±3.1)	(±3.2)	(±0.9)	(±7.7)	(±4.0)	(±0.0)	(±0.0)	(±0.0)	(±0.0)
8.74	0.78	3.09E-06	13.8	48.9	37.9	36.3	59.0	61.3	0.0	0.0	0.0	19.0
9.52		(±2.19E-06)	(±2.2)	(±7.7)	(±3.9)	(±1.0)	(±10.0)	(±9.6)	(±0.0)	(±0.0)	(±0.0)	(±0.0)
9.52	0.64	1.04E-06	15.0	58.8	36.4	35.9	60.6	73.7	0.0	0.0	0.0	19.0
10.16		(±1.02E-06)	(±2.8)	(±8.1)	(±4.7)	(±1.2)	(±15.5)	(±10.2)	(±0.0)	(±0.0)	(±0.0)	(±0.0)

Depth values presented in this table are measured from free ground surface

Appendix A4 Mean Values of Acquired Parameters for North Dam Wall CPTu Test Point 002

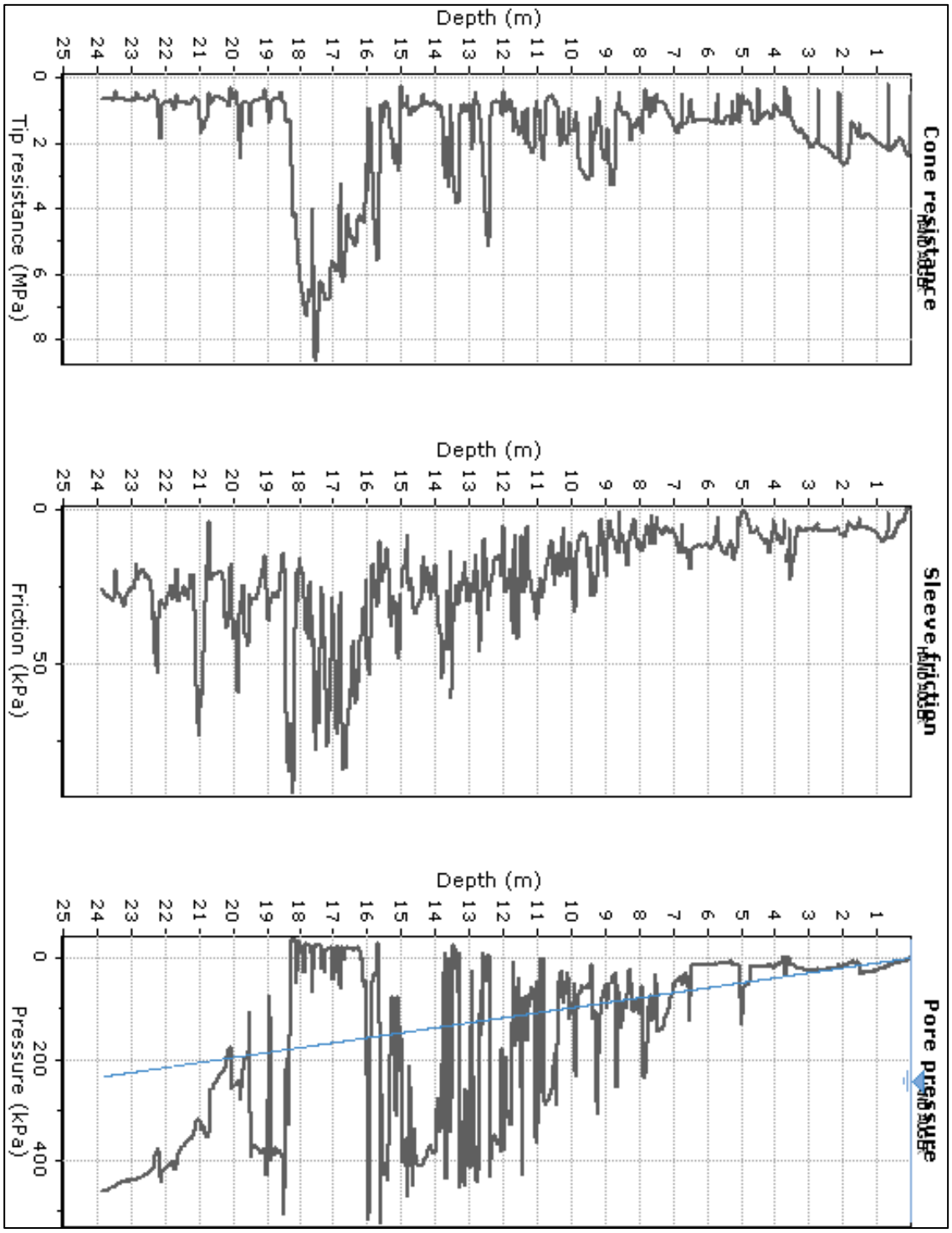

Appendix A5 CPTu Parameter Profiles for North Dam Wall CPTu Test Point 009

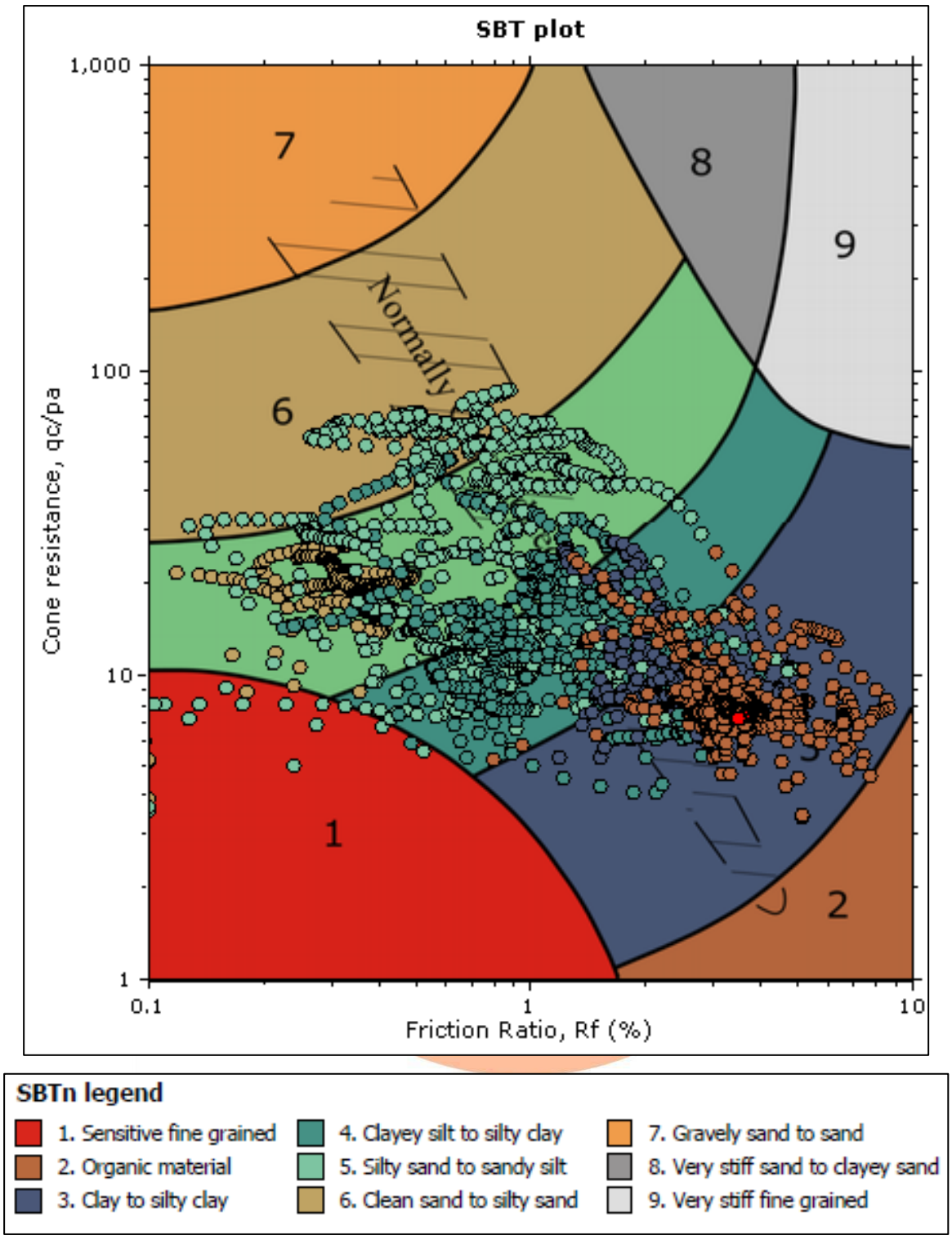

Appendix A6 Normalized SBT Plot for North Dam Wall CPTu Test Point 009

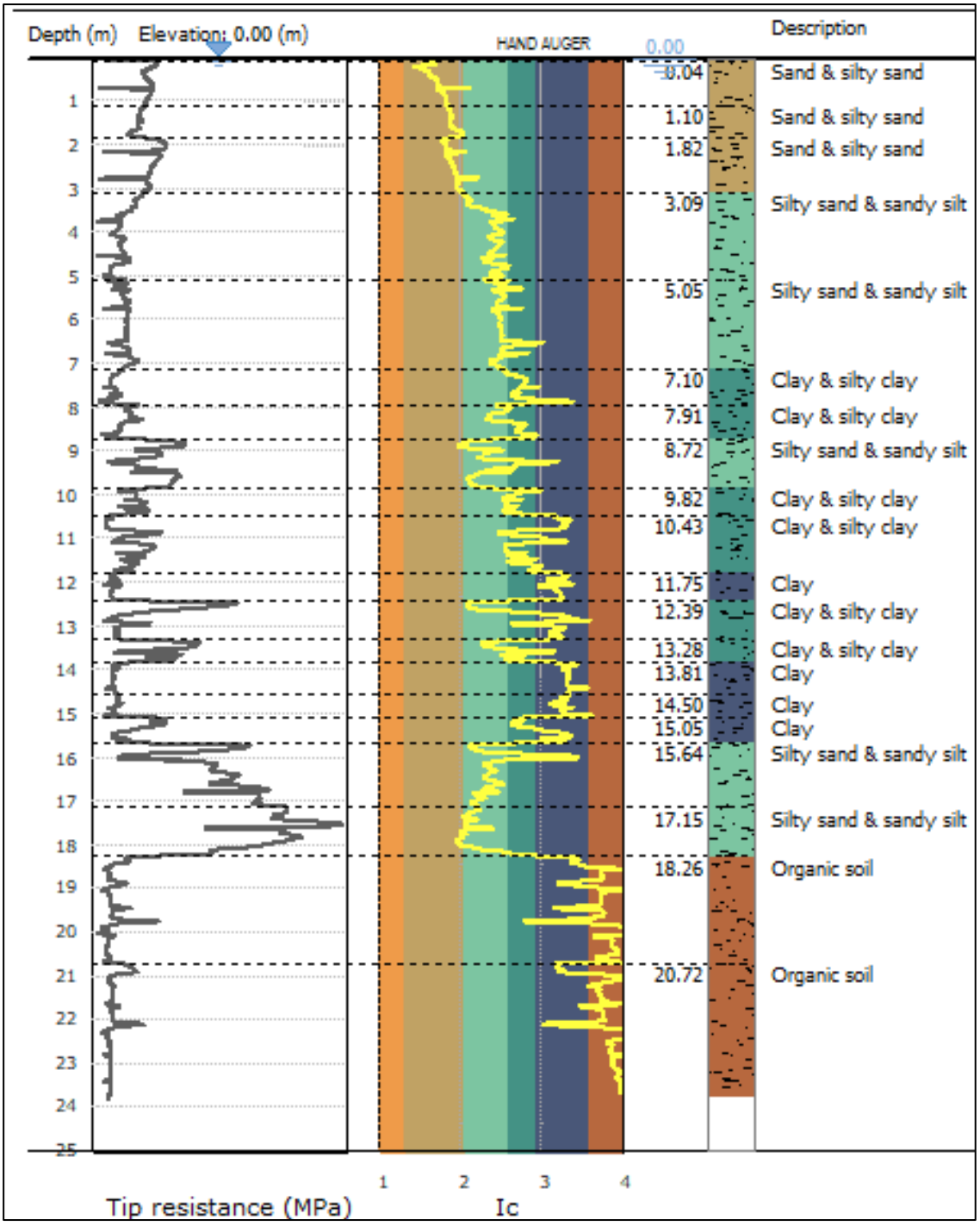

Appendix A7 Geotechnical Cross Section alongside Cone Tip Resistance Profile for North Dam Wall CPTu Test Point 009

Summary table of mean values

From depth To depth (m)	Thickness (m)	Permeability (m/s)	SPT_{N60} (blows/30cm)	E_s (MPa)	D_r (%)	Friction angle	Constrained modulus, M (MPa)	Shear modulus, G_0 (MPa)	Undrained strength, S_u (kPa)	Undrained strength ratio	OCR	Unit weight (kN/m³)
0.04	1.06	6.95E-05	4.5	12.7	49.2	36.1	25.1	15.7	0.0	0.0	0.0	19.0
1.10		(±6.18E-05)	(±0.7)	(±2.1)	(±4.3)	(±0.9)	(±4.1)	(±2.6)	(±0.0)	(±0.0)	(±0.0)	(±0.0)
1.10	0.72	1.57E-05	4.2	13.3	39.2	33.7	26.7	16.7	0.0	0.0	0.0	19.0
1.82		(±5.12E-06)	(±0.4)	(±0.4)	(±2.5)	(±0.6)	(±0.7)	(±0.4)	(±0.0)	(±0.0)	(±0.0)	(±0.0)
1.82	1.27	1.75E-05	5.6	17.0	38.3	33.4	33.4	21.0	0.0	0.0	0.0	19.0
3.09		(±9.14E-06)	(±0.7)	(±1.5)	(±3.5)	(±0.7)	(±5.4)	(±3.2)	(±0.0)	(±0.0)	(±0.0)	(±0.0)
3.09	1.96	1.09E-06	4.0	15.7	26.2	32.6	16.7	19.1	0.0	0.0	0.0	19.0
5.05		(±1.49E-06)	(±0.8)	(±2.3)	(±4.0)	(±0.7)	(±8.2)	(±3.8)	(±0.0)	(±0.0)	(±0.0)	(±0.0)
5.05	2.05	2.60E-07	4.8	20.1	23.7	32.4	16.2	24.9	0.0	0.0	0.0	19.0
7.10		(±1.58E-07)	(±0.6)	(±1.7)	(±1.0)	(±0.3)	(±3.0)	(±2.5)	(±0.0)	(±0.0)	(±0.0)	(±0.0)
7.10	0.81	5.90E-08	3.8	0.0	0.0	0.0	7.8	20.7	48.0	0.7	3.1	19.0
7.91		(±5.08E-08)	(±0.6)	(±0.0)	(±0.0)	(±0.0)	(±3.8)	(±2.4)	(±12.9)	(±0.2)	(±0.8)	(±0.0)
7.91	0.81	2.20E-07	5.0	0.0	0.0	0.0	14.6	26.6	65.6	0.8	3.8	19.0
8.72		(±2.41E-07)	(±0.8)	(±0.0)	(±0.0)	(±0.0)	(±5.5)	(±3.4)	(±12.6)	(±0.2)	(±0.8)	(±0.0)
8.72	1.10	2.12E-06	7.6	28.6	27.9	32.2	38.1	35.4	0.0	0.0	0.0	19.0
9.82		(±2.23E-06)	(±1.4)	(±3.8)	(±2.9)	(±0.4)	(±18.0)	(±5.2)	(±0.0)	(±0.0)	(±0.0)	(±0.0)
9.82	0.61	1.57E-07	6.7	0.0	0.0	0.0	20.2	36.5	97.5	1.0	4.8	19.0
10.43		(±2.31E-07)	(±0.8)	(±0.0)	(±0.0)	(±0.0)	(±5.3)	(±4.3)	(±18.5)	(±0.2)	(±0.9)	(±0.0)
10.43	1.32	5.28E-08	6.4	0.0	0.0	0.0	14.0	37.8	77.7	0.8	3.5	19.0
11.75		(±6.80E-08)	(±1.6)	(±0.0)	(±0.0)	(±0.0)	(±9.6)	(±7.6)	(±35.3)	(±0.3)	(±1.6)	(±0.0)
11.75	0.64	2.01E-09	5.2	0.0	0.0	0.0	4.0	33.4	46.3	0.4	1.9	19.0
12.39		(±1.58E-09)	(±0.5)	(±0.0)	(±0.0)	(±0.0)	(±1.7)	(±3.8)	(±9.3)	(±0.1)	(±0.4)	(±0.0)
12.39	0.89	7.46E-07	7.8	0.0	0.0	0.0	25.3	42.9	64.9	0.5	2.5	19.0
13.28		(±1.41E-06)	(±2.8)	(±0.0)	(±0.0)	(±0.0)	(±31.8)	(±7.9)	(±29.0)	(±0.3)	(±1.2)	(±0.0)

Appendix A8 Mean Values of Acquired Parameters for North Dam Wall CPTu Test Point 009

Summary table of mean values

From depth To depth (m)	Thickness (m)	Permeability (m/s)	SPT_{N60} (blows/30cm)	E_s (MPa)	D_r (%)	Friction angle	Constrained modulus, M (MPa)	Shear modulus, G_0 (MPa)	Undrained strength, S_U (kPa)	Undrained strength ratio	OCR	Unit weight (kN/m³)
13.28	0.53	3.0E-07	10.1	0.0	0.0	0.0	32.0	54.5	125.0	1.0	4.7	19.0
13.81		(±3.7E-07)	(±2.1)	(±0.0)	(±0.0)	(±0.0)	(±14.4)	(±7.9)	(±46.9)	(±0.4)	(±1.8)	(±0.0)
13.81	0.69	1.0E-09	5.9	0.0	0.0	0.0	3.5	39.8	46.9	0.4	1.7	19.0
14.50		(±1.47E-09)	(±0.8)	(±0.0)	(±0.0)	(±0.0)	(±2.5)	(±5.3)	(±11.9)	(±0.1)	(±0.4)	(±0.0)
14.50	0.55	1.1E-09	5.9	0.0	0.0	0.0	3.6	38.8	48.7	0.4	1.7	19.0
15.05		(±6.42E-10)	(±0.7)	(±0.0)	(±0.0)	(±0.0)	(±1.3)	(±5.4)	(±9.6)	(±0.1)	(±0.3)	(±0.0)
15.05	0.59	2.4E-08	8.0	0.0	0.0	0.0	15.3	48.3	97.8	0.7	3.3	19.0
15.64		(±3.02E-08)	(±2.1)	(±0.0)	(±0.0)	(±0.0)	(±12.1)	(±10.9)	(±48.3)	(±0.4)	(±1.7)	(±0.0)
15.64	1.51	9.7E-07	15.1	61.0	30.5	33.8	65.0	73.7	0.0	0.0	0.0	19.0
17.15		(±8.68E-07)	(±3.5)	(±9.5)	(±3.0)	(±1.0)	(±30.5)	(±13.9)	(±0.0)	(±0.0)	(±0.0)	(±0.0)
17.15	1.11	4.0E-06	18.6	63.9	35.1	33.7	109.8	81.0	0.0	0.0	0.0	19.0
18.26		(±2.70E-06)	(±2.5)	(±9.1)	(±3.3)	(±1.0)	(±32.1)	(±11.5)	(±0.0)	(±0.0)	(±0.0)	(±0.0)
18.26	2.46	9.4E-10	6.7	0.0	0.0	0.0	2.4	42.8	36.5	0.2	1.0	19.0
20.72		(±3.22E-09)	(±1.4)	(±0.0)	(±0.0)	(±0.0)	(±4.3)	(±12.2)	(±26.9)	(±0.2)	(±0.7)	(±0.0)
20.72	3.06	3.9E-10	7.2	0.0	0.0	0.0	1.5	43.5	30.9	0.2	0.7	19.0
23.78		(±7.46E-10)	(±0.8)	(±0.0)	(±0.0)	(±0.0)	(±1.9)	(±8.9)	(±18.8)	(±0.1)	(±0.5)	(±0.0)

Depth values presented in this table are measured from free ground surface

Appendix A8 Mean Values of Acquired Parameters for North Dam Wall CPTu Test Point 009

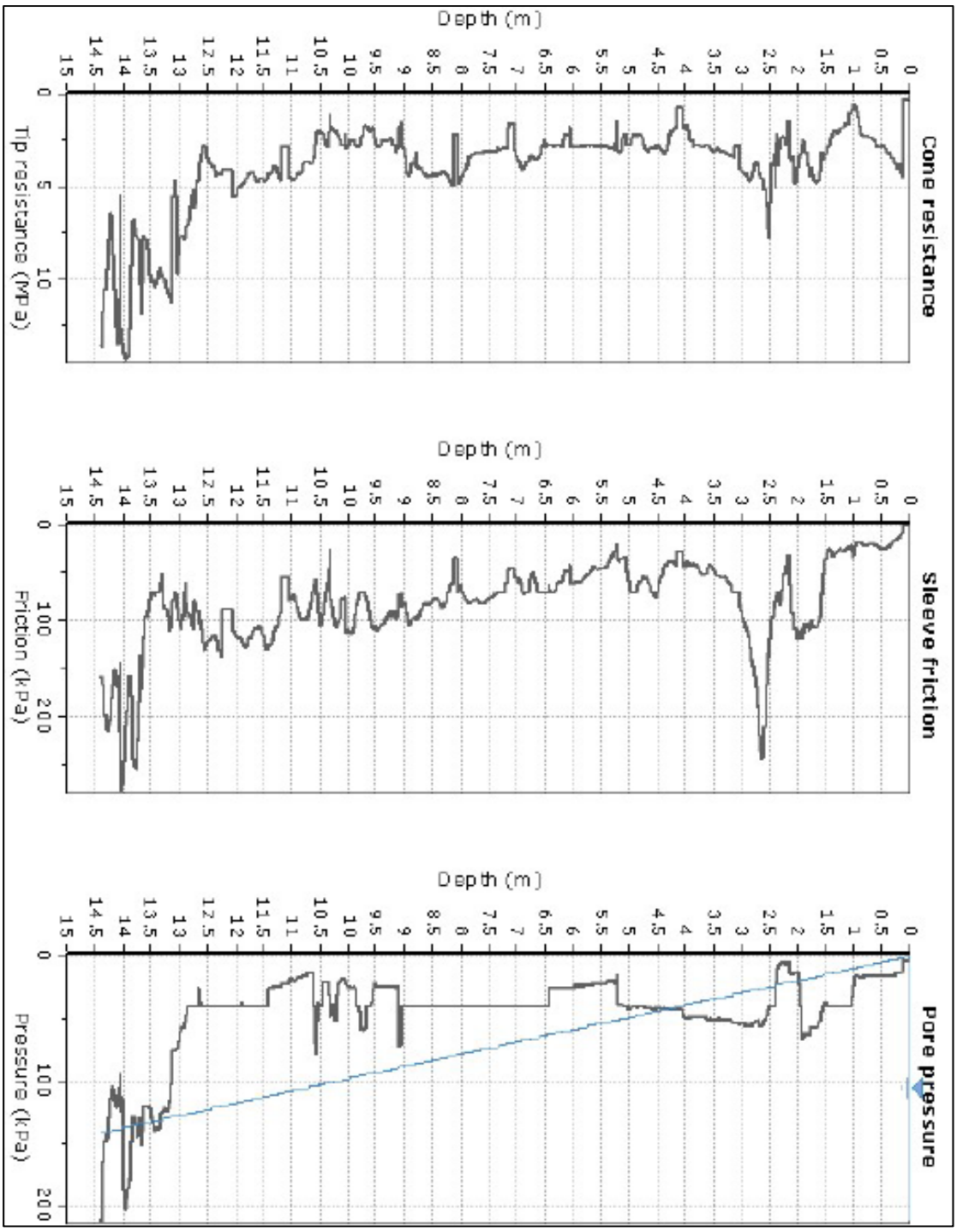

Appendix A9 CPTu Parameter Profiles for East Dam Wall CPTu Test Point 004

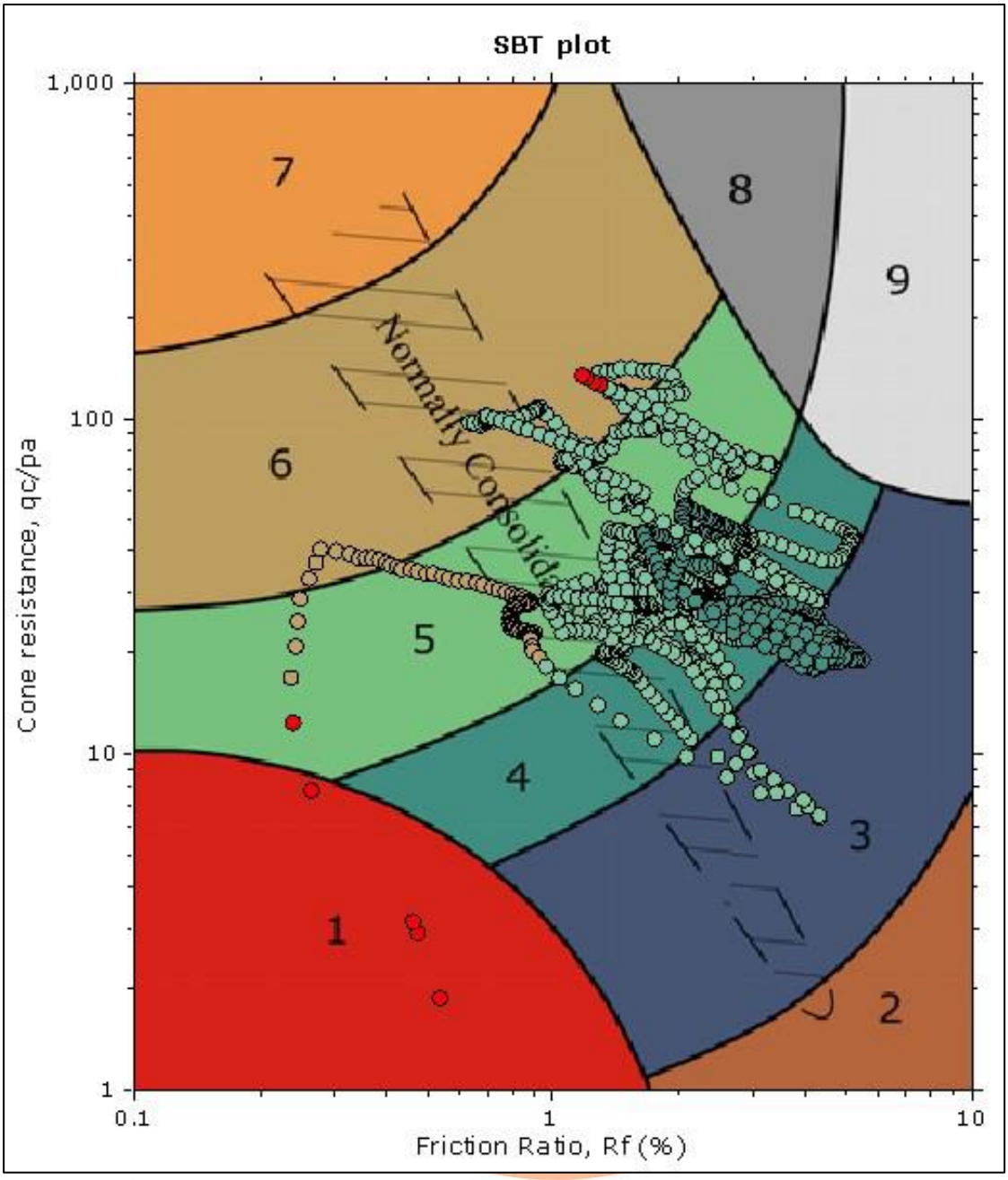

Appendix A10 Normalized SBT Plot for East Dam Wall CPTu Test Point 004

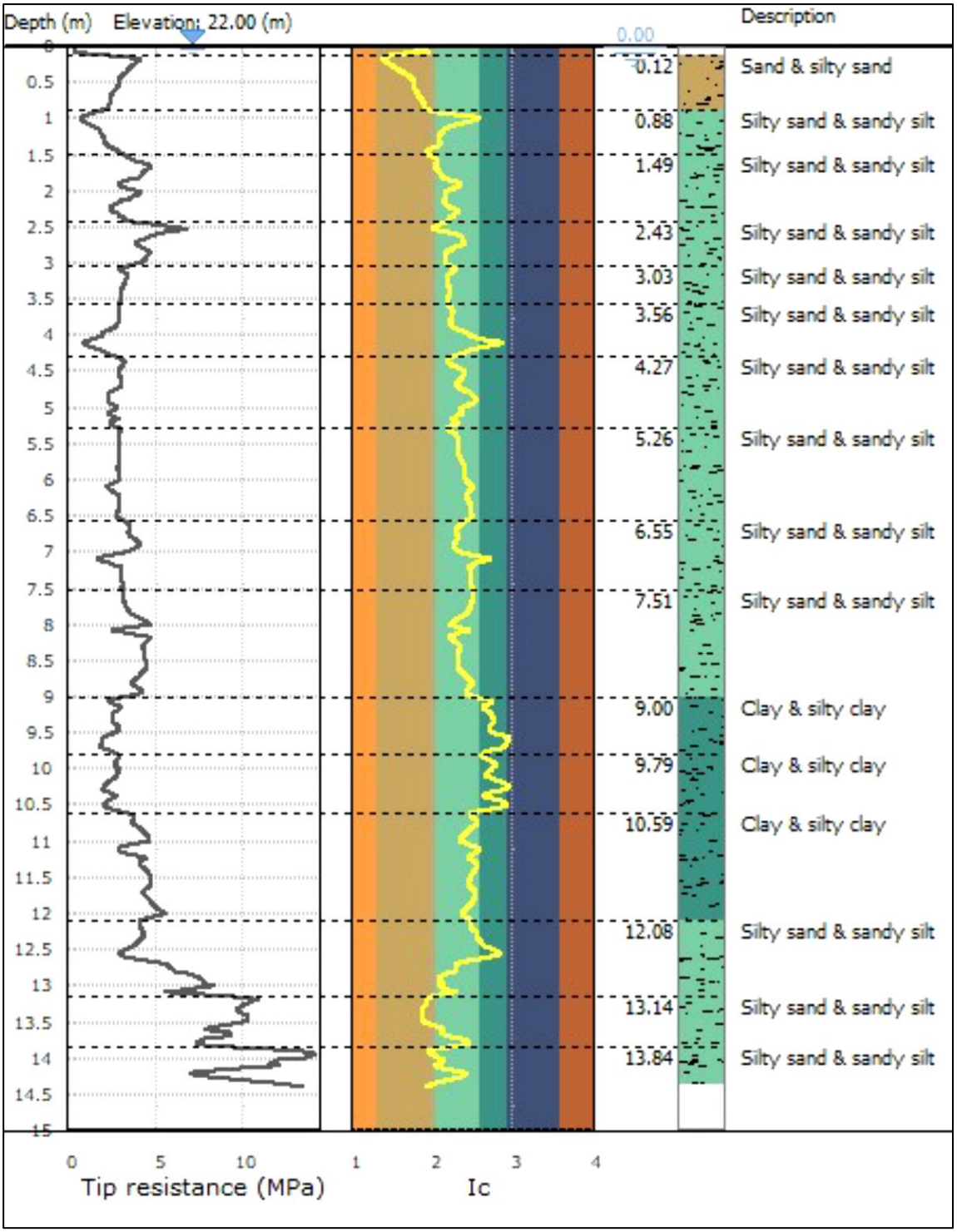

Appendix A11 Geotechnical Cross Section alongside Cone Tip Resistance Profile for East Dam Wall CPTu Test Point 004

Summary table of mean values

From depth (m)	To depth (m)	Thickness (m)	Permeability (m/s)	SPT_{N60} (blows/30cm)	E_s (MPa)	D_r	Friction angle	Constrained modulus, M (MPa)	Shear modulus, G_0 (MPa)	Undrained strength, S_u (kPa)	Undrained strength ratio	OCR	Unit weight (kN/m^3)
0.12	0.88	0.76	1.24E-04 (±1.56E-04)	6.4 (±0.8)	17.4 (±1.9)	62.3 (±6.9)	41.0 (±1.1)	21.8 (±2.3)	21.8 (±2.3)	0.0 (±0.0)	0.0 (±0.0)	0.0 (±0.0)	19.0 (±0.0)
0.88	1.49	0.61	4.19E-06 (±3.64E-06)	5.0 (±1.5)	18.8 (±3.3)	46.9 (±3.4)	38.3 (±0.7)	21.1 (±6.5)	22.4 (±4.7)	0.0 (±0.0)	0.0 (±0.0)	0.0 (±0.0)	19.0 (±0.0)
1.49	2.43	0.94	3.12E-06 (±2.40E-06)	10.3 (±1.6)	37.7 (±5.4)	56.2 (±6.2)	40.0 (±1.1)	45.3 (±7.5)	47.3 (±6.6)	0.0 (±0.0)	0.0 (±0.0)	0.0 (±0.0)	19.0 (±0.0)
2.43	3.03	0.60	2.32E-06 (±1.86E-06)	14.2 (±1.9)	51.2 (±6.5)	58.5 (±5.4)	40.4 (±0.9)	61.8 (±7.4)	67.3 (±8.9)	0.0 (±0.0)	0.0 (±0.0)	0.0 (±0.0)	19.0 (±0.0)
3.03	3.56	0.53	1.80E-06 (±3.17E-07)	9.5 (±0.6)	35.8 (±1.9)	45.0 (±1.7)	38.0 (±0.4)	43.3 (±2.4)	44.9 (±2.4)	0.0 (±0.0)	0.0 (±0.0)	0.0 (±0.0)	19.0 (±0.0)
3.56	4.27	0.71	8.81E-07 (±6.38E-07)	7.4 (±1.7)	31.7 (±2.0)	38.8 (±3.2)	36.5 (±0.8)	29.9 (±9.7)	37.1 (±5.5)	0.0 (±0.0)	0.0 (±0.0)	0.0 (±0.0)	19.0 (±0.0)
4.27	5.26	0.99	8.02E-07 (±4.99E-07)	9.1 (±0.8)	35.9 (±3.7)	37.8 (±2.5)	36.3 (±0.6)	36.2 (±4.4)	45.3 (±4.3)	0.0 (±0.0)	0.0 (±0.0)	0.0 (±0.0)	19.0 (±0.0)
5.26	6.55	1.29	6.02E-07 (±4.13E-07)	9.5 (±0.6)	38.7 (±3.2)	35.3 (±1.0)	35.6 (±0.3)	37.2 (±2.2)	49.1 (±4.3)	0.0 (±0.0)	0.0 (±0.0)	0.0 (±0.0)	19.0 (±0.0)
6.55	7.51	0.96	5.40E-07 (±3.56E-07)	10.9 (±1.4)	45.9 (±2.2)	36.5 (±2.1)	35.9 (±0.6)	42.0 (±8.0)	56.4 (±5.0)	0.0 (±0.0)	0.0 (±0.0)	0.0 (±0.0)	19.0 (±0.0)
7.51	9.00	1.49	6.30E-07 (±3.83E-07)	13.3 (±1.3)	54.5 (±4.9)	37.0 (±2.1)	36.1 (±0.6)	52.2 (±7.4)	67.7 (±6.0)	0.0 (±0.0)	0.0 (±0.0)	0.0 (±0.0)	19.0 (±0.0)
9.00	9.79	0.79	4.62E-08 (±3.22E-08)	10.7 (±1.0)	54.0 (±1.3)	0.0 (±0.0)	0.0 (±0.0)	31.6 (±5.1)	66.2 (±4.5)	161.3 (±26.1)	1.9 (±0.3)	8.6 (±1.5)	19.0 (±0.0)

Appendix A12 Mean Values of Acquired Parameters for East Dam Wall CPTu Test Point 004

Summary table of mean values

From depth To depth (m)	Thickness (m)	Permeability (m/s)	SPT_{N60} (blows/30cm)	E_s (MPa)	D_r	Friction angle	Constrained modulus, M (MPa)	Shear modulus, G_0 (MPa)	Undrained strength, S_u (kPa)	Undrained strength ratio	OCR	Unit weight (kN/m³)
9.79	0.80	4.61E-08	11.0	50.8	0.0	0.0	32.0	67.5	163.5	1.7	8.0	19.0
10.59		(±3.14E-08)	(±0.9)	(±0.5)	(±0.0)	(±0.0)	(±4.4)	(±4.2)	(±22.6)	(±0.3)	(±1.2)	(±0.0)
10.59	1.49	2.92E-07	15.6	66.7	0.0	0.0	56.6	83.4	273.6	2.6	12.2	19.0
12.08		(±1.36E-07)	(±1.9)	(±8.4)	(±0.0)	(±0.0)	(±8.1)	(±9.7)	(±39.3)	(±0.3)	(±1.5)	(±0.0)
12.08	1.06	1.14E-06	17.6	73.9	40.1	36.8	67.4	89.9	0.0	0.0	0.0	19.0
13.14		(±1.38E-06)	(±3.0)	(±3.9)	(±3.4)	(±0.8)	(±20.4)	(±5.1)	(±0.0)	(±0.0)	(±0.0)	(±0.0)
13.14	0.70	9.61E-06	25.6	84.9	47.5	38.5	102.5	108.4	0.0	0.0	0.0	19.0
13.84		(±7.08E-06)	(±1.4)	(±11.7)	(±2.9)	(±0.6)	(±9.0)	(±16.4)	(±0.0)	(±0.0)	(±0.0)	(±0.0)
13.84	0.52	3.94E-06	31.9	113.0	49.9	38.9	134.4	141.7	0.0	0.0	0.0	19.0
14.36		(±2.91E-06)	(±4.1)	(±8.7)	(±5.8)	(±1.1)	(±20.0)	(±10.9)	(±0.0)	(±0.0)	(±0.0)	(±0.0)

Depth values presented in this table are measured from free ground surface

Appendix A12 Mean Values of Acquired Parameters for East Dam Wall CPTu Test Point 004

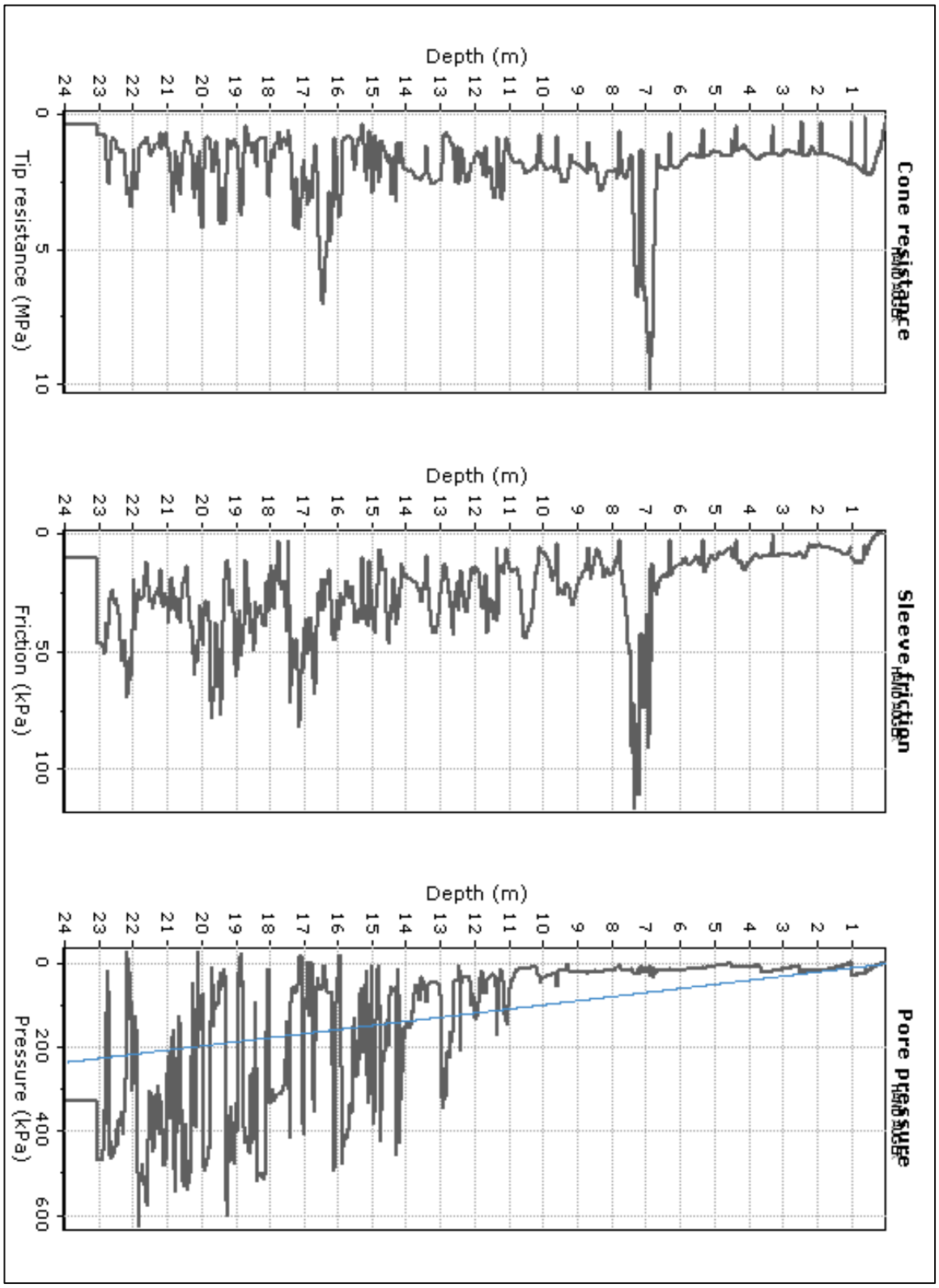

Appendix A13 CPTu Parameter Profiles for East Dam Wall CPTu Test Point 007

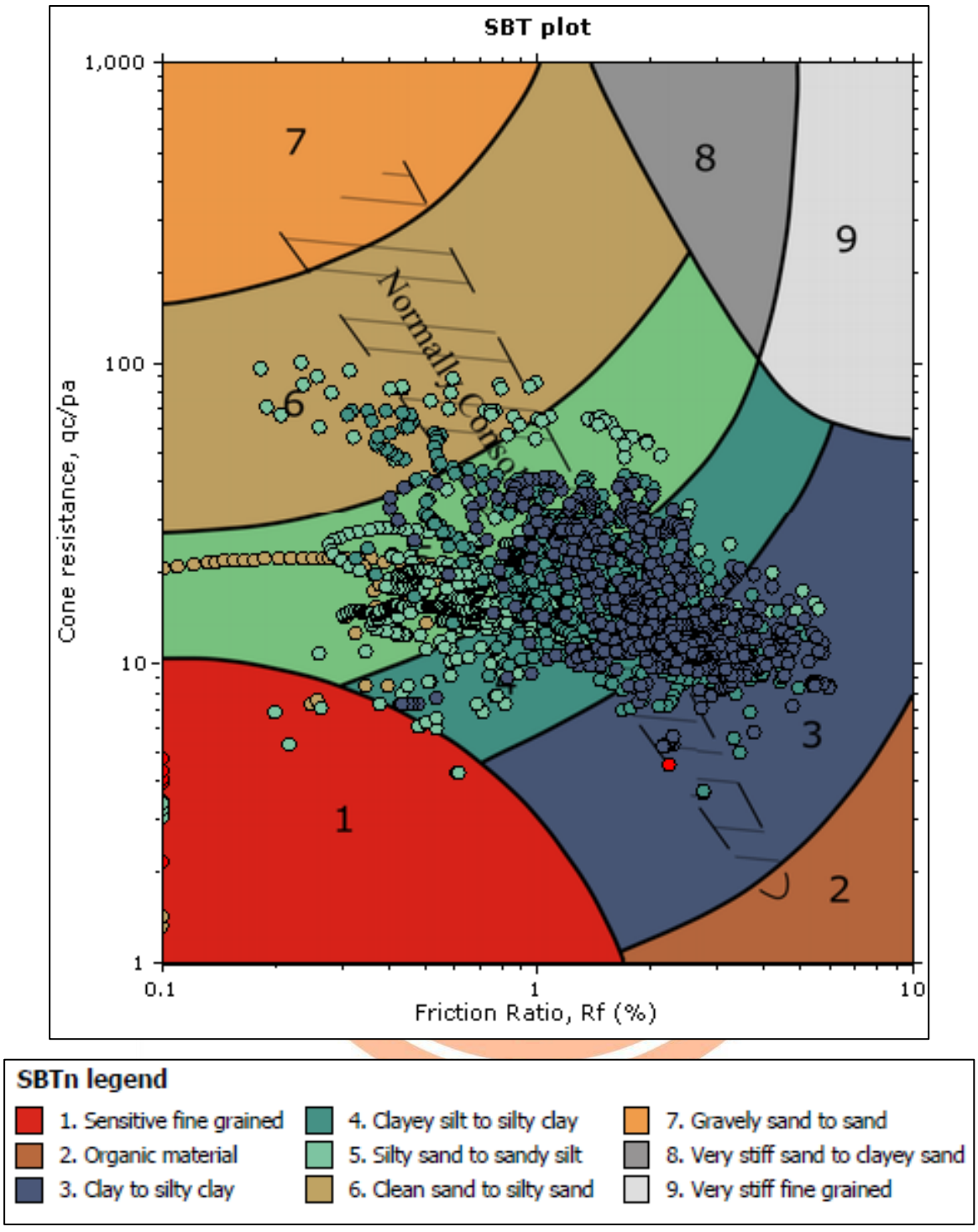

Appendix A14 Normalized SBT Plot for East Dam Wall CPTu Test Point 007

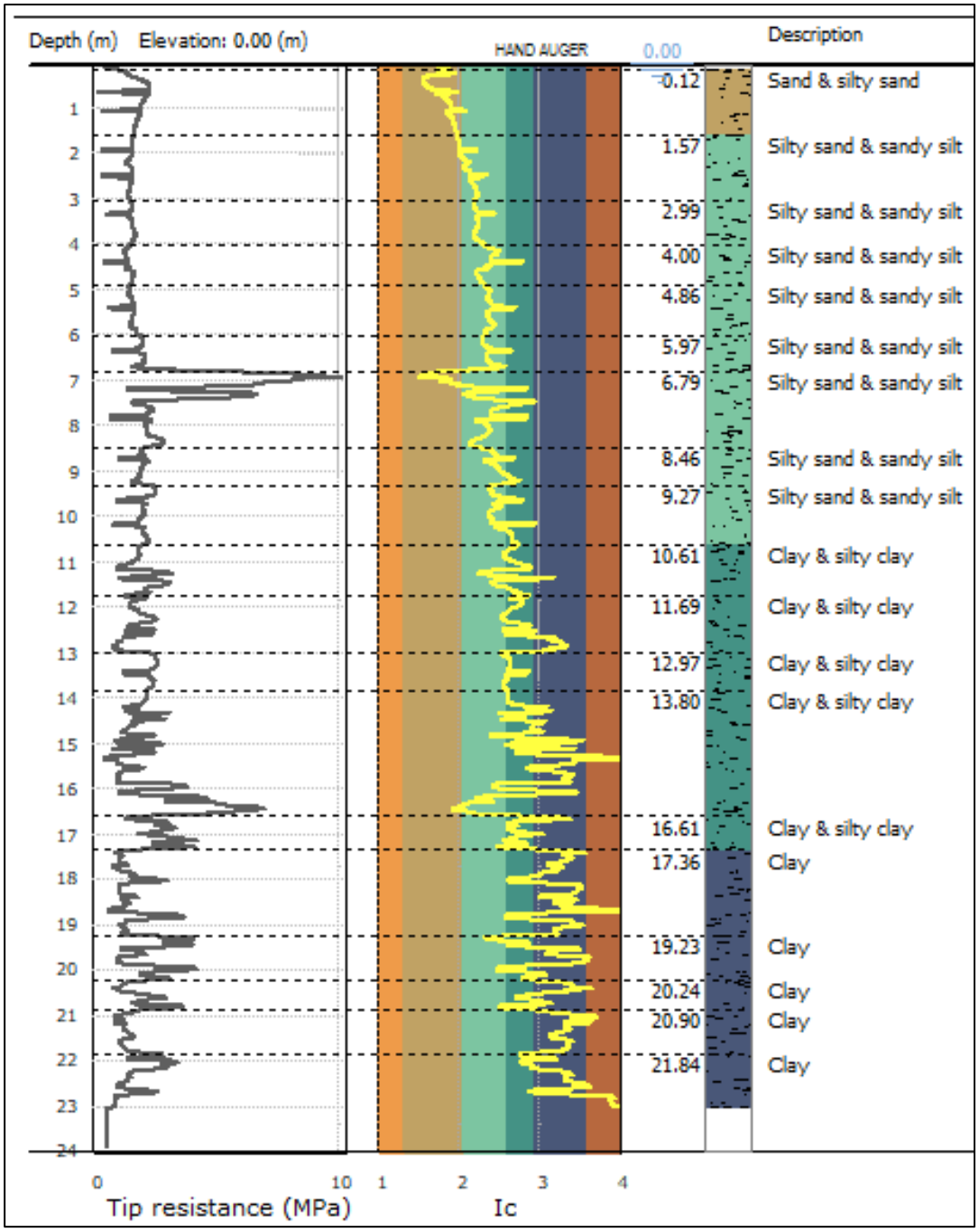

Appendix A15 Geotechnical Cross Section alongside Cone Tip Resistance Profile for East Dam Wall CPTu Test Point 007

Summary table of mean values

From depth To depth (m)	Thickness (m)	Permeability (m/s)	SPT_{N60} (blows/30cm)	E_s (MPa)	D_r (%)	Friction angle	Constrained modulus, M (MPa)	Shear modulus, G_0 (MPa)	Undrained strength, S_u (kPa)	Undrained strength ratio	OCR	Unit weight (kN/m^3)
0.12	1.45	3.58E-05	4.2	13.4	44.6	35.2	24.4	15.3	0.0	0.0	0.0	19.0
1.57		(±4.47E-05)	(±0.9)	(±1.6)	(±5.1)	(±1.1)	(±6.1)	(±3.8)	(±0.0)	(±0.0)	(±0.0)	(±0.0)
1.57	1.42	4.40E-06	4.0	14.0	33.1	32.9	24.0	16.5	0.0	0.0	0.0	19.0
2.99		(±2.54E-06)	(±0.4)	(±1.6)	(±2.5)	(±0.4)	(±7.9)	(±4.6)	(±0.0)	(±0.0)	(±0.0)	(±0.0)
2.99	1.01	1.62E-06	4.8	17.0	30.2	32.7	23.8	21.2	0.0	0.0	0.0	19.0
4.00		(±3.65E-07)	(±0.6)	(±1.5)	(±1.7)	(±0.2)	(±7.4)	(±2.3)	(±0.0)	(±0.0)	(±0.0)	(±0.0)
4.00	0.86	7.64E-07	4.7	18.1	27.1	32.7	17.5	22.1	0.0	0.0	0.0	19.0
4.86		(±4.94E-07)	(±0.7)	(±0.7)	(±0.9)	(±0.7)	(±3.7)	(±2.6)	(±0.0)	(±0.0)	(±0.0)	(±0.0)
4.86	1.11	5.36E-07	5.0	20.2	26.1	32.4	18.8	24.8	0.0	0.0	0.0	19.0
5.97		(±1.72E-07)	(±0.6)	(±1.4)	(±0.9)	(±0.4)	(±3.3)	(±2.9)	(±0.0)	(±0.0)	(±0.0)	(±0.0)
5.97	0.82	1.04E-06	6.4	25.7	28.4	33.0	26.3	31.3	0.0	0.0	0.0	19.0
6.79		(±2.09E-06)	(±1.5)	(±3.4)	(±3.1)	(±0.6)	(±12.2)	(±5.7)	(±0.0)	(±0.0)	(±0.0)	(±0.0)
6.79	1.67	1.23E-05	10.3	38.9	36.3	34.5	52.3	47.0	0.0	0.0	0.0	19.0
8.46		(±3.64E-05)	(±5.0)	(±14.0)	(±11.2)	(±2.4)	(±37.9)	(±17.2)	(±0.0)	(±0.0)	(±0.0)	(±0.0)
8.46	0.81	3.20E-07	6.7	27.5	24.5	32.4	23.1	35.5	0.0	0.0	0.0	19.0
9.27		(±3.09E-07)	(±0.8)	(±2.3)	(±1.1)	(±0.4)	(±4.0)	(±4.5)	(±0.0)	(±0.0)	(±0.0)	(±0.0)
9.27	1.34	2.61E-07	7.4	29.9	24.4	32.5	24.3	38.8	0.0	0.0	0.0	19.0
10.61		(±1.85E-07)	(±1.4)	(±3.6)	(±1.8)	(±0.6)	(±6.9)	(±8.3)	(±0.0)	(±0.0)	(±0.0)	(±0.0)
10.61	1.08	2.12E-07	7.7	0.0	0.0	0.0	23.5	41.2	101.9	1.0	4.6	19.0
11.69		(±3.12E-07)	(±1.7)	(±0.0)	(±0.0)	(±0.0)	(±9.8)	(±7.8)	(±27.7)	(±0.3)	(±1.2)	(±0.0)
11.69	1.28	5.26E-08	7.0	0.0	0.0	0.0	16.2	41.0	91.1	0.8	3.8	19.0
12.97		(±5.42E-08)	(±1.4)	(±0.0)	(±0.0)	(±0.0)	(±9.2)	(±6.0)	(±33.4)	(±0.3)	(±1.4)	(±0.0)
12.97	0.83	1.07E-07	9.1	0.0	0.0	0.0	27.8	49.9	143.9	1.2	5.5	19.0
13.80		(±3.92E-08)	(±1.1)	(±0.0)	(±0.0)	(±0.0)	(±6.6)	(±6.9)	(±27.4)	(±0.2)	(±1.1)	(±0.0)

Appendix A16 Mean Values of Acquired Parameters for East Dam Wall CPTu Test Point 007

Summary table of mean values

From depth To depth (m)	Thickness (m)	Permeability (m/s)	SPT_{N60} (blows/30cm)	E_F (MPa)	D_r (%)	Friction angle	Constrained modulus, M (MPa)	Shear modulus, G_0 (MPa)	Undrained strength, S_U (kPa)	Undrained strength ratio	OCR	Unit weight (kN/m^3)
13.80 16.61	2.81	6.18E-07 (±1.89E-06)	8.9 (±3.1)	0.0 (±0.0)	0.0 (±0.0)	0.0 (±0.0)	25.9 (±28.7)	49.4 (±10.6)	90.8 (±40.8)	0.7 (±0.3)	3.1 (±1.5)	19.0 (±0.0)
16.61 17.36	0.75	6.22E-08 (±5.68E-08)	11.8 (±2.0)	0.0 (±0.0)	0.0 (±0.0)	0.0 (±0.0)	32.0 (±12.7)	69.6 (±7.7)	166.9 (±49.5)	1.1 (±0.3)	5.0 (±1.5)	19.0 (±0.0)
17.36 19.23	1.87	1.23E-08 (±2.97E-08)	7.9 (±1.9)	0.0 (±0.0)	0.0 (±0.0)	0.0 (±0.0)	8.3 (±10.7)	50.1 (±10.9)	74.7 (±46.4)	0.4 (±0.3)	2.1 (±1.3)	19.0 (±0.0)
19.23 20.24	1.01	8.46E-08 (±1.59E-07)	11.1 (±2.8)	0.0 (±0.0)	0.0 (±0.0)	0.0 (±0.0)	23.5 (±18.5)	66.4 (±13.6)	119.0 (±65.8)	0.7 (±0.4)	3.1 (±1.7)	19.0 (±0.0)
20.24 20.90	0.66	2.92E-08 (±5.26E-08)	9.5 (±2.1)	0.0 (±0.0)	0.0 (±0.0)	0.0 (±0.0)	14.8 (±13.0)	56.7 (±9.9)	99.9 (±48.0)	0.5 (±0.3)	2.5 (±1.2)	19.0 (±0.0)
20.90 21.84	0.94	1.29E-09 (±1.62E-09)	7.9 (±0.8)	0.0 (±0.0)	0.0 (±0.0)	0.0 (±0.0)	3.8 (±2.3)	49.2 (±5.7)	58.9 (±18.0)	0.3 (±0.1)	1.4 (±0.4)	19.0 (±0.0)
21.84 23.07	1.23	7.53E-09 (±1.10E-08)	9.9 (±2.3)	0.0 (±0.0)	0.0 (±0.0)	0.0 (±0.0)	11.0 (±11.9)	62.1 (±14.0)	90.3 (±57.8)	0.4 (±0.3)	2.0 (±1.3)	19.0 (±0.0)

Depth values presented in this table are measured from free ground surface

Appendix A16 Mean Values of Acquired Parameters for East Dam Wall CPTu Test Point 007

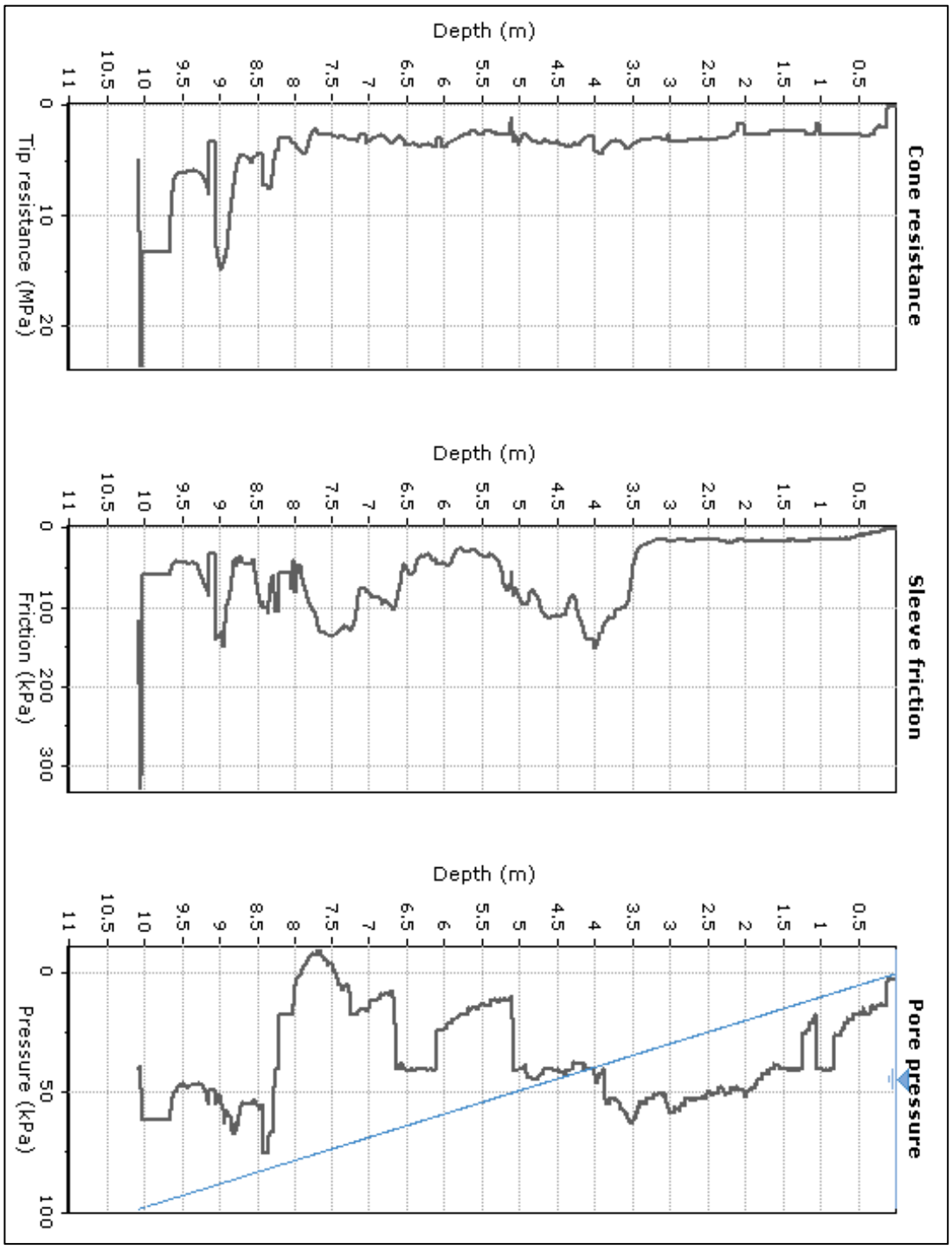

Appendix A17 CPTu Parameter Profiles for South Dam Wall CPTu Test Point 002

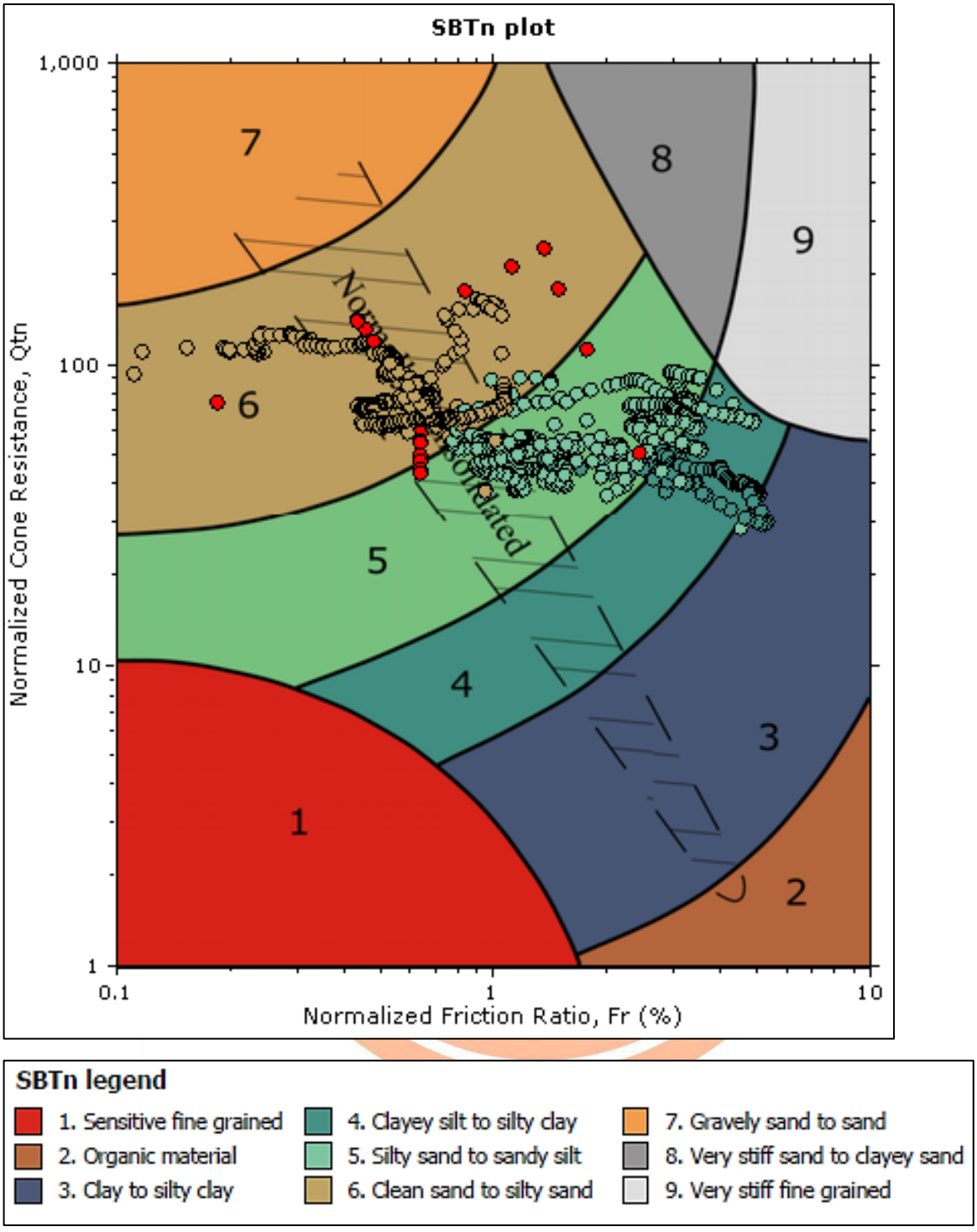

Appendix A18 Normalized SBT Plot for South Dam Wall CPTu Test Point 002

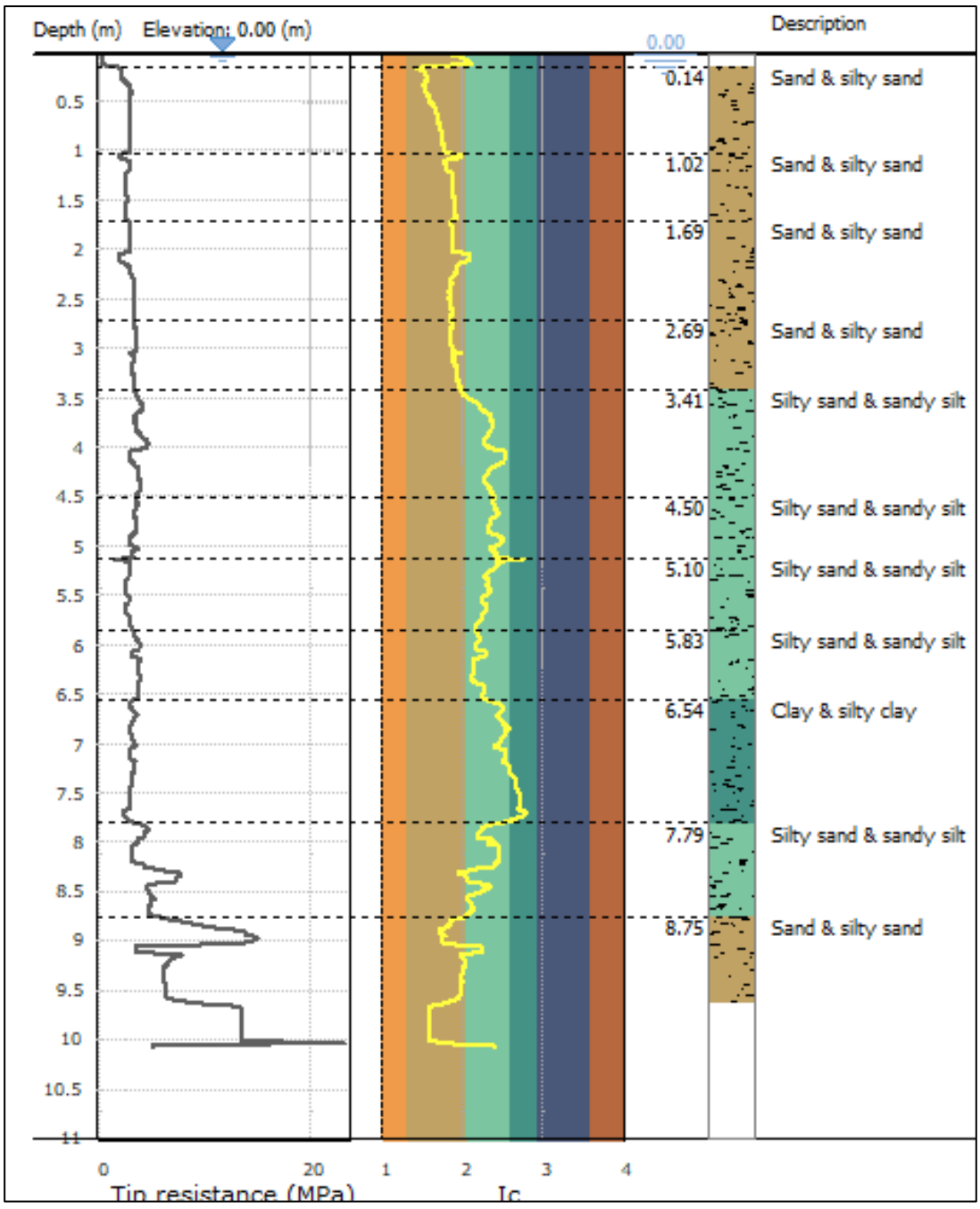

Appendix A19 Geotechnical Cross Section alongside Cone Tip Resistance Profile for South Dam Wall CPTu Test Point 002

Summary table of mean values

From depth To depth (m)	Thickness (m)	Permeability (m/s)	SPT_{N60} (blows/30cm)	E_s (MPa)	D_r (%)	Friction angle	Constrained modulus, M (MPa)	Shear modulus, G_0 (MPa)	Undrained strength, S_u (kPa)	Undrained strength ratio	OCR	Unit weight (kN/m³)
0.14	0.88	1.13E-04	5.7	15.6	56.1	37.6	30.9	19.3	0.0	0.0	0.0	19.0
1.02		(±7.23E-05)	(±0.9)	(±2.9)	(±2.0)	(±0.4)	(±6.0)	(±3.8)	(±0.0)	(±0.0)	(±0.0)	(±0.0)
1.02	0.67	1.99E-05	6.1	19.0	48.1	36.4	38.0	23.8	0.0	0.0	0.0	19.0
1.69		(±7.11E-06)	(±0.5)	(±1.1)	(±1.8)	(±0.3)	(±2.2)	(±1.4)	(±0.0)	(±0.0)	(±0.0)	(±0.0)
1.69	1.00	1.79E-05	7.2	22.1	45.2	35.6	44.1	27.7	0.0	0.0	0.0	19.0
2.69		(±5.64E-06)	(±0.9)	(±1.6)	(±2.1)	(±0.3)	(±3.2)	(±2.0)	(±0.0)	(±0.0)	(±0.0)	(±0.0)
2.69	0.72	1.70E-05	8.1	25.1	43.8	35.2	50.3	31.5	0.0	0.0	0.0	19.0
3.41		(±4.79E-06)	(±0.3)	(±1.1)	(±1.3)	(±0.3)	(±2.1)	(±1.3)	(±0.0)	(±0.0)	(±0.0)	(±0.0)
3.41	1.09	1.40E-06	11.9	46.9	46.8	39.3	52.9	59.6	0.0	0.0	0.0	19.0
4.50		(±1.87E-06)	(±1.2)	(±6.8)	(±2.2)	(±1.3)	(±10.5)	(±8.0)	(±0.0)	(±0.0)	(±0.0)	(±0.0)
4.50	0.60	4.93E-07	11.4	47.2	42.0	38.8	44.4	59.3	0.0	0.0	0.0	19.0
5.10		(±1.74E-07)	(±0.8)	(±2.6)	(±1.8)	(±0.6)	(±3.7)	(±3.1)	(±0.0)	(±0.0)	(±0.0)	(±0.0)
5.10	0.73	9.85E-07	8.8	34.3	35.2	35.6	37.5	43.3	0.0	0.0	0.0	19.0
5.83		(±5.23E-07)	(±0.8)	(±3.9)	(±1.5)	(±1.2)	(±8.1)	(±5.0)	(±0.0)	(±0.0)	(±0.0)	(±0.0)
5.83	0.71	2.13E-06	11.0	39.8	38.4	35.7	65.2	49.8	0.0	0.0	0.0	19.0
6.54		(±7.61E-07)	(±0.8)	(±2.8)	(±1.1)	(±0.5)	(±15.4)	(±3.5)	(±0.0)	(±0.0)	(±0.0)	(±0.0)
6.54	1.25	1.99E-07	11.7	0.0	0.0	0.0	40.0	66.5	200.5	2.9	13.2	19.0
7.79		(±2.21E-07)	(±0.8)	(±0.0)	(±0.0)	(±0.0)	(±4.0)	(±6.3)	(±18.7)	(±0.3)	(±1.4)	(±0.0)
7.79	0.96	2.26E-06	14.2	52.9	39.0	36.4	76.4	66.4	0.0	0.0	0.0	19.0
8.75		(±2.14E-06)	(±2.8)	(±7.8)	(±4.9)	(±1.0)	(±31.9)	(±9.6)	(±0.0)	(±0.0)	(±0.0)	(±0.0)
8.75	0.89	1.64E-05	19.7	61.2	48.2	36.7	119.7	76.7	0.0	0.0	0.0	19.0
9.64		(±1.51E-05)	(±6.4)	(±15.4)	(±9.6)	(±1.9)	(±35.5)	(±19.3)	(±0.0)	(±0.0)	(±0.0)	(±0.0)

Depth values presented in this table are measured from free ground surface

Appendix A19 Mean Values of Acquired Parameters for South Dam Dall CPTu Test Point 002

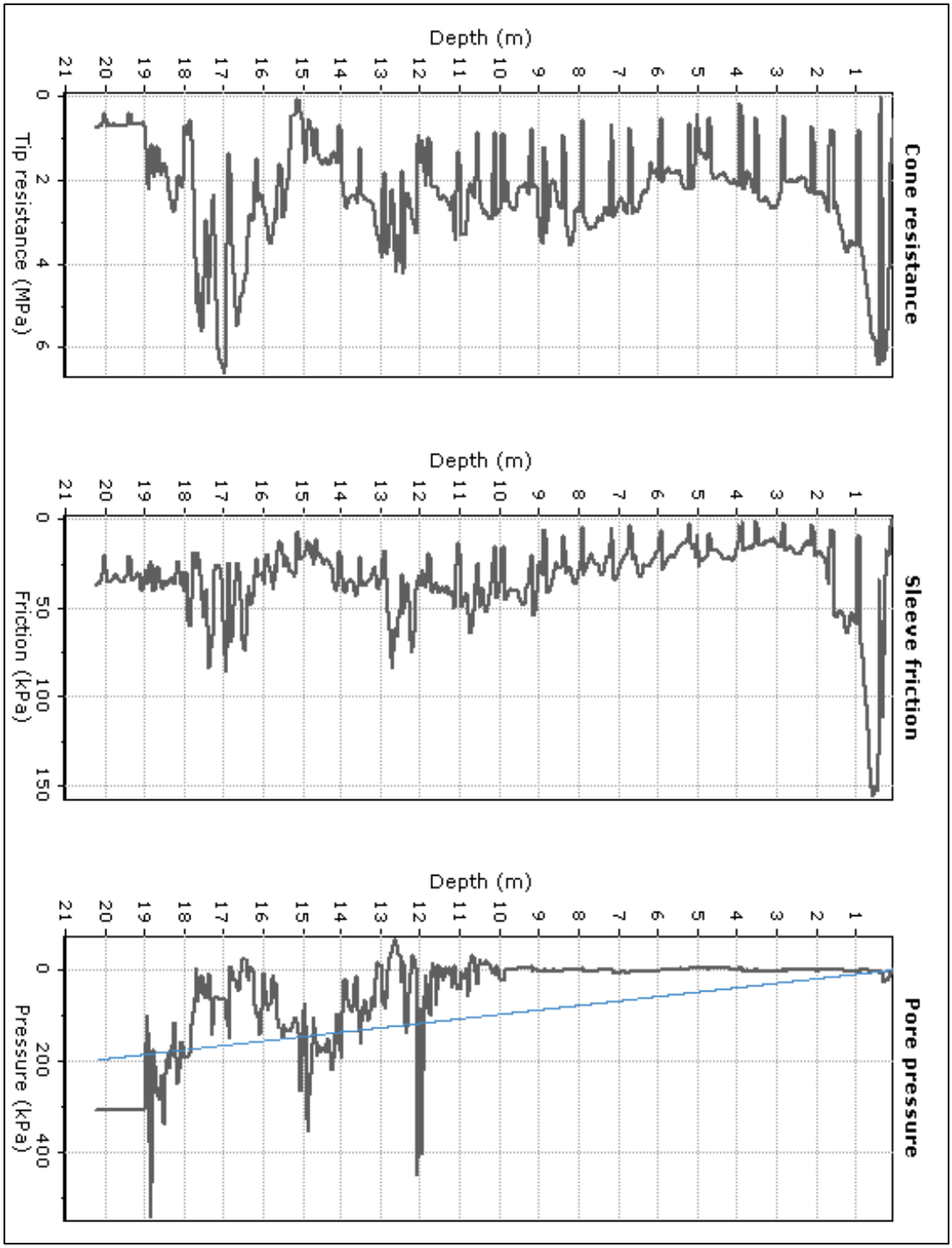

Appendix A20 CPTu Parameter Profiles for West Dam Wall CPTu Test Point 002

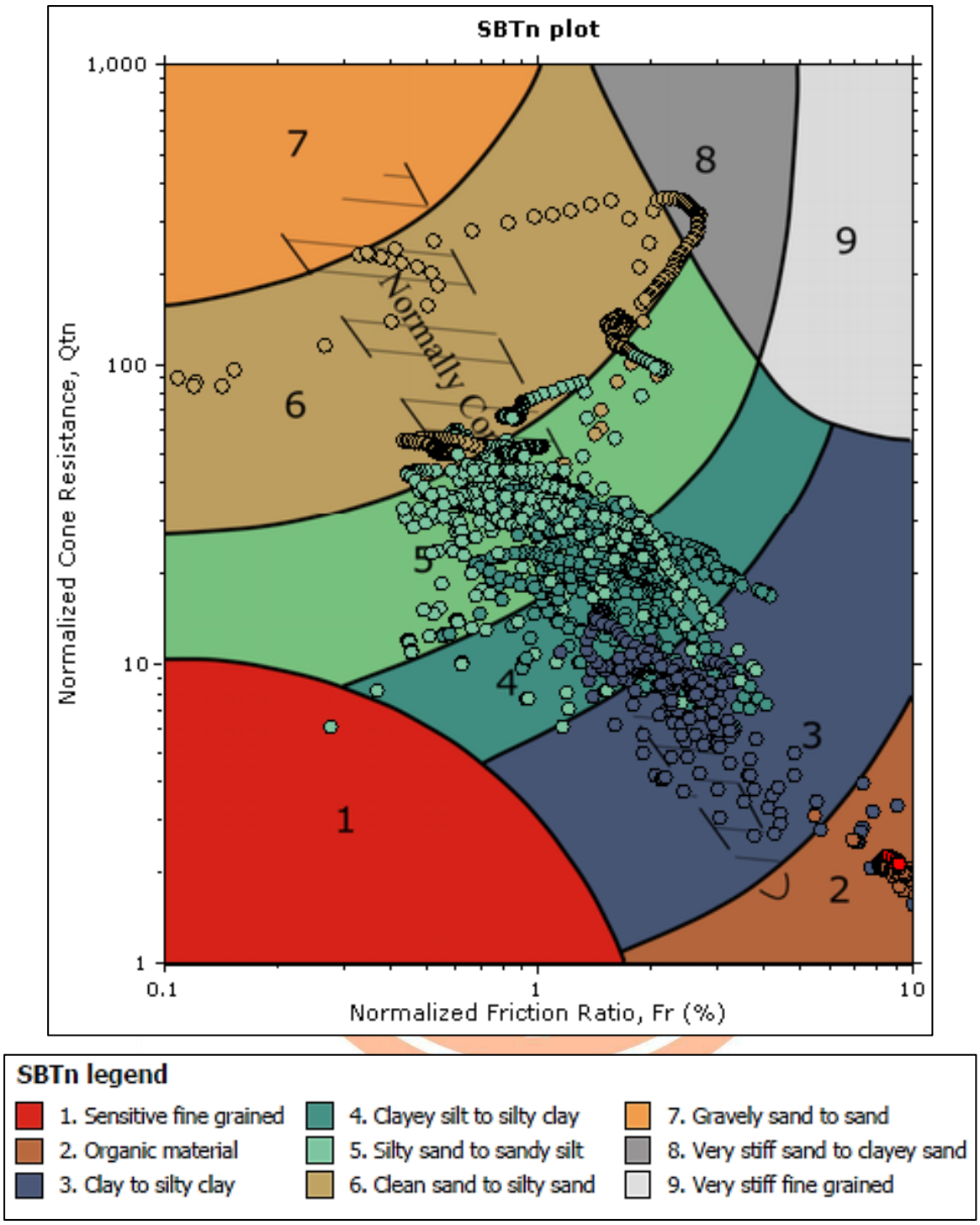

Appendix A21 Normalized SBT Plot for West Dam Wall CPTu Test Point 002

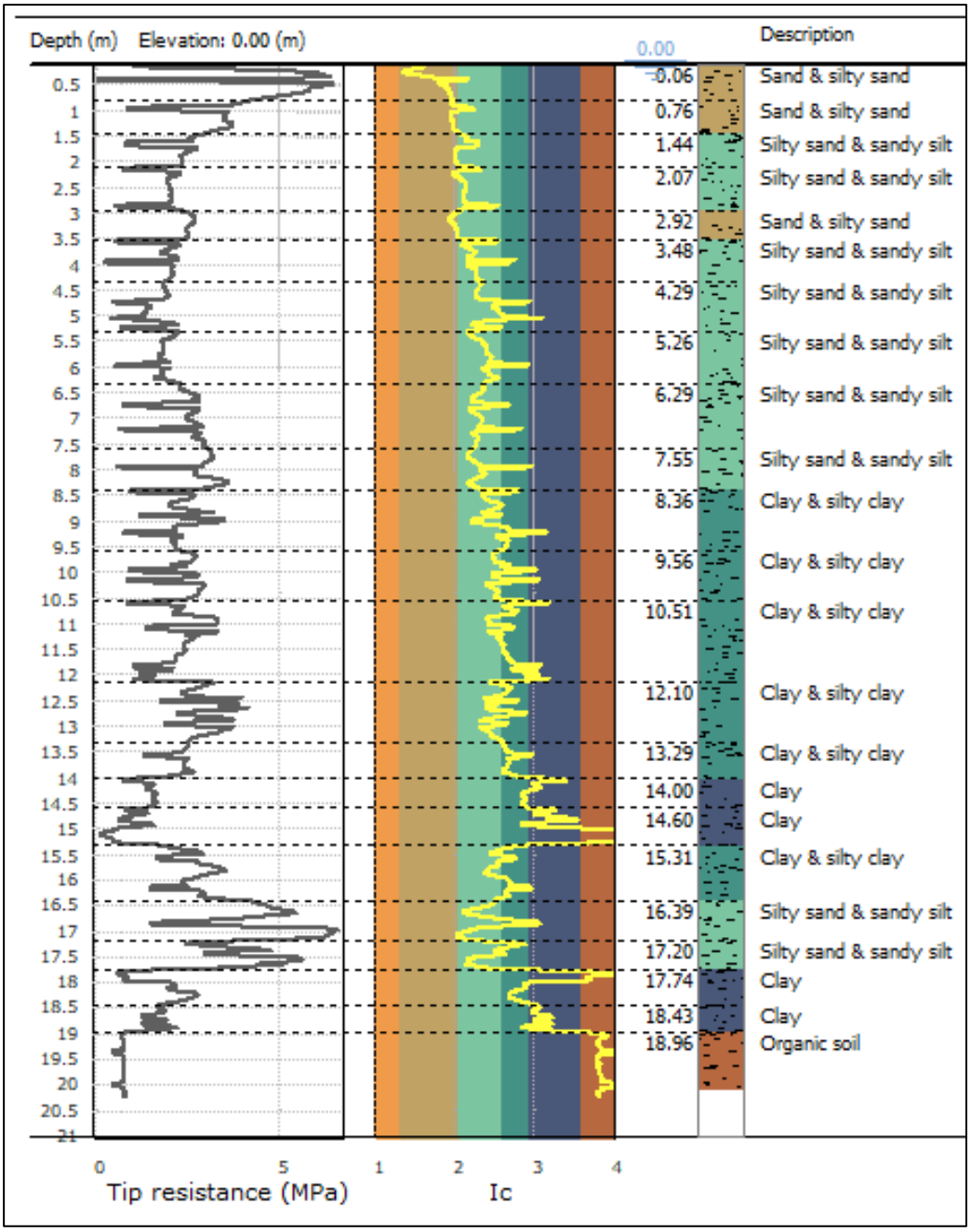

Appendix A22 Geotechnical Cross Section alongside Cone Tip Resistance Profile for West Dam Wall CPTu Test Point 002

Summary table of mean values

From depth To depth (m)	Thickness (m)	Permeability (m/s)	SPT_{N60} (blows/30cm)	E_s (MPa)	D_r (%)	Friction angle	Constrained modulus, M (MPa)	Shear modulus, G_0 (MPa)	Undrained strength, S_U (kPa)	Undrained strength ratio	OCR	Unit weight (kN/m³)
0.06	0.70	1.30E-04	10.8	32.1	83.9	43.6	59.9	37.6	0.0	0.0	0.0	19.0
0.76		(±1.99E-04)	(±4.5)	(±14.6)	(±15.4)	(±3.4)	(±32.2)	(±20.2)	(±0.0)	(±0.0)	(±0.0)	(±0.0)
0.76	0.68	8.2E-06	8.7	28.6	60.8	40.2	56.6	35.9	0.0	0.0	0.0	19.0
1.44		(±2.80E-06)	(±2.2)	(±6.8)	(±9.9)	(±1.9)	(±15.3)	(±8.5)	(±0.0)	(±0.0)	(±0.0)	(±0.0)
1.44	0.63	5.0E-06	6.2	21.4	44.5	36.6	41.0	26.8	0.0	0.0	0.0	19.0
2.07		(±2.51E-06)	(±1.6)	(±5.4)	(±7.0)	(±1.9)	(±14.1)	(±6.7)	(±0.0)	(±0.0)	(±0.0)	(±0.0)
2.07	0.85	3.6E-06	5.4	18.5	36.3	34.4	35.3	23.1	0.0	0.0	0.0	19.0
2.92		(±2.17E-06)	(±1.3)	(±3.9)	(±5.4)	(±1.0)	(±11.4)	(±4.9)	(±0.0)	(±0.0)	(±0.0)	(±0.0)
2.92	0.56	8.0E-06	6.9	22.1	38.9	34.2	44.3	27.7	0.0	0.0	0.0	19.0
3.48		(±2.12E-06)	(±0.2)	(±0.4)	(±0.8)	(±0.2)	(±0.7)	(±0.5)	(±0.0)	(±0.0)	(±0.0)	(±0.0)
3.48	0.81	1.7E-06	5.7	21.5	32.3	33.9	28.5	25.1	0.0	0.0	0.0	19.0
4.29		(±1.11E-06)	(±1.5)	(±4.5)	(±4.5)	(±0.8)	(±13.9)	(±8.3)	(±0.0)	(±0.0)	(±0.0)	(±0.0)
4.29	0.97	5.8E-07	5.2	22.4	29.4	33.8	19.7	26.9	0.0	0.0	0.0	19.0
5.26		(±4.72E-07)	(±1.2)	(±3.6)	(±4.0)	(±0.8)	(±7.1)	(±5.1)	(±0.0)	(±0.0)	(±0.0)	(±0.0)
5.26	1.03	6.5E-07	6.1	25.5	28.8	33.7	24.9	30.9	0.0	0.0	0.0	19.0
6.29		(±6.07E-07)	(±1.0)	(±2.0)	(±1.3)	(±0.6)	(±8.8)	(±4.4)	(±0.0)	(±0.0)	(±0.0)	(±0.0)
6.29	1.26	9.5E-07	8.0	32.1	31.3	34.0	32.9	38.5	0.0	0.0	0.0	19.0
7.55		(±4.87E-07)	(±1.7)	(±3.1)	(±2.0)	(±0.6)	(±10.0)	(±7.1)	(±0.0)	(±0.0)	(±0.0)	(±0.0)
7.55	0.81	1.3E-06	9.3	36.0	32.2	33.9	46.8	43.8	0.0	0.0	0.0	19.0
8.36		(±7.05E-07)	(±1.6)	(±2.2)	(±1.6)	(±0.4)	(±17.8)	(±6.1)	(±0.0)	(±0.0)	(±0.0)	(±0.0)
8.36	1.20	3.1E-07	8.2	0.0	0.0	0.0	27.7	44.1	123.7	1.4	6.7	19.0
9.56		(±4.01E-07)	(±1.8)	(±0.0)	(±0.0)	(±0.0)	(±9.5)	(±8.0)	(±34.6)	(±0.4)	(±1.8)	(±0.0)
9.56	0.95	1.8E-07	9.2	0.0	0.0	0.0	29.9	49.6	131.3	1.4	6.5	19.0
10.51		(±1.07E-07)	(±1.8)	(±0.0)	(±0.0)	(±0.0)	(±10.0)	(±8.2)	(±49.7)	(±0.5)	(±2.4)	(±0.0)

Appendix A23 Mean Values of Acquired Parameters for West Dam Wall CPTu Test Point 002

Summary table of mean values

From depth To depth (m)	Thickness (m)	Permeability (m/s)	SPT_{N60} (blows/30cm)	E_s (MPa)	D_r (%)	Friction angle	Constrained modulus, M (MPa)	Shear modulus, G_0 (MPa)	Undrained strength, S_u (kPa)	Undrained strength ratio	OCR	Unit weight (kN/m^3)
10.51	1.59	1.09E-07	9.0	0.0	0.0	0.0	26.3	50.8	126.0	1.2	5.6	19.0
12.10		(±1.15E-07)	(±1.9)	(±0.0)	(±0.0)	(±0.0)	(±10.9)	(±7.9)	(±38.5)	(±0.4)	(±1.8)	(±0.0)
12.10	1.19	2.28E-07	11.3	0.0	0.0	0.0	37.8	60.7	166.5	1.5	6.7	19.0
13.29		(±1.87E-07)	(±1.5)	(±0.0)	(±0.0)	(±0.0)	(±8.3)	(±8.1)	(±31.8)	(±0.3)	(±1.3)	(±0.0)
13.29	0.71	7.08E-08	9.7	0.0	0.0	0.0	28.4	55.1	147.7	1.2	5.5	19.0
14.00		(±2.82E-08)	(±0.9)	(±0.0)	(±0.0)	(±0.0)	(±6.3)	(±4.7)	(±24.5)	(±0.2)	(±0.9)	(±0.0)
14.00	0.60	1.16E-08	7.3	0.0	0.0	0.0	11.4	45.3	85.3	0.6	3.0	19.0
14.60		(±6.71E-09)	(±1.0)	(±0.0)	(±0.0)	(±0.0)	(±3.9)	(±4.8)	(±18.8)	(±0.1)	(±0.7)	(±0.0)
14.60	0.71	3.92E-09	5.5	0.0	0.0	0.0	3.4	33.2	40.5	0.3	1.4	19.0
15.31		(±5.05E-09)	(±0.9)	(±0.0)	(±0.0)	(±0.0)	(±3.5)	(±7.6)	(±25.8)	(±0.2)	(±0.9)	(±0.0)
15.31	1.08	1.44E-07	10.3	0.0	0.0	0.0	30.6	56.0	141.5	1.0	4.6	19.0
16.39		(±1.32E-07)	(±1.7)	(±0.0)	(±0.0)	(±0.0)	(±10.8)	(±7.9)	(±39.0)	(±0.3)	(±1.2)	(±0.0)
16.39	0.81	1.62E-06	15.6	61.6	31.4	33.8	73.5	75.7	0.0	0.0	0.0	19.0
17.20		(±1.83E-06)	(±2.8)	(±7.4)	(±3.0)	(±0.9)	(±35.5)	(±10.2)	(±0.0)	(±0.0)	(±0.0)	(±0.0)
17.20	0.54	8.02E-07	14.2	55.4	29.0	32.8	60.1	72.5	0.0	0.0	0.0	19.0
17.74		(±9.05E-07)	(±2.1)	(±7.2)	(±3.0)	(±0.8)	(±28.2)	(±10.3)	(±0.0)	(±0.0)	(±0.0)	(±0.0)
17.74	0.69	2.27E-08	9.2	0.0	0.0	0.0	16.0	56.1	104.9	0.6	2.9	19.0
18.43		(±2.25E-08)	(±1.9)	(±0.0)	(±0.0)	(±0.0)	(±11.5)	(±7.6)	(±51.7)	(±0.3)	(±1.4)	(±0.0)
18.43	0.53	5.50E-09	8.9	0.0	0.0	0.0	10.3	56.2	92.8	0.5	2.5	19.0
18.96		(±4.34E-09)	(±0.8)	(±0.0)	(±0.0)	(±0.0)	(±4.2)	(±4.8)	(±20.0)	(±0.1)	(±0.5)	(±0.0)
18.96	1.16	1.75E-10	6.6	0.0	0.0	0.0	0.8	40.0	24.5	0.1	0.6	19.0
20.12		(±5.17E-11)	(±0.7)	(±0.0)	(±0.0)	(±0.0)	(±0.2)	(±8.2)	(±6.6)	(±0.0)	(±0.2)	(±0.0)

Depth values presented in this table are measured from free ground surface

Appendix A23 Mean Values of Acquired Parameters for West Dam Wall CPTu Test Point 002 (continued)

APPENDIX B

LIDAR SURVEY DATA

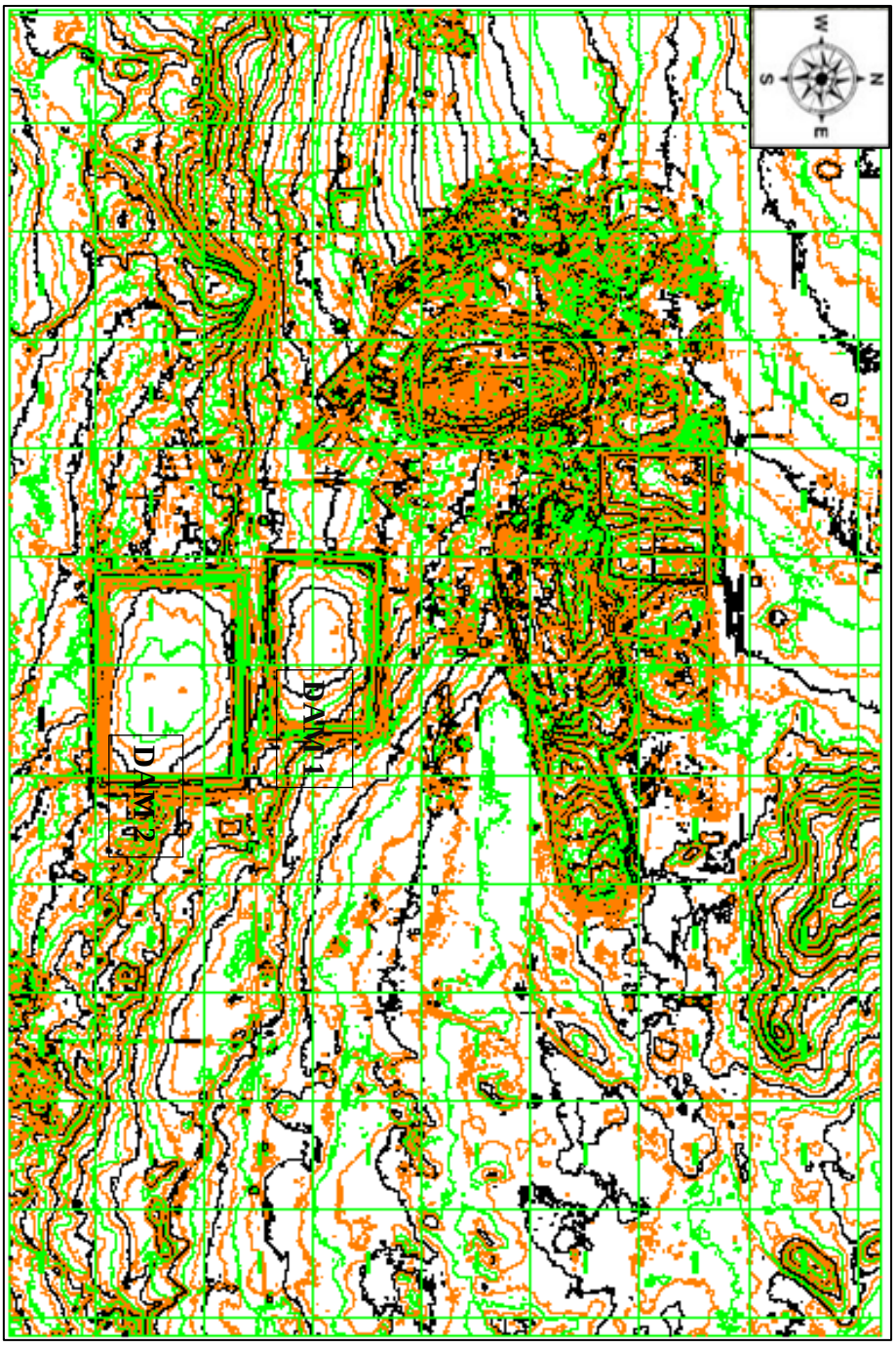

Appendix B1 2018 Contour Map of Orapa Area Produced through Lidar Survey

APPENDIX C

ORAPA SLURRY DAM WALLS' EXTERNAL BOUNDARY COORDINATES

Appendix C1 External Boundary Coordinates for North Dam Wall Geometry

			CONTINUED 1			CONTINUED 2	
HD	**E**		**HD**	**E**		**HD**	**E**
0	995.042		22.29	994.95		32	975.681
2	995.155		22.4	994.885		32.5	974.307
4	995.254		22.6	994.797		33	972.952
6	995.345		22.8	994.792		33.5	971.772
8	995.433		23.45	994.467		34	970.639
10	995.496		23.75	994.451		34.5	969.712
12	995.591		23.82	994.134		36	966.671
14	995.696		24	993.607		36.5	965.943
16	995.809		24.05	993.515		37	965.813
18	995.931		24.12	993.087		37.5	965.727
18.5	995.951		24.18	992.951		38	965.781
19	996.123		24.91	990.759		38.2	965.773
19.2	996.609		25	990.653		38.4	965.6
19.4	997.001		25.2	990.373		38.5	965.58
19.6	997.303		25.4	990.132		38.7	965.546
19.63	997.451		25.6	989.883		38.8	965.456
19.8	997.472		25.8	989.655		39.1	965.13
20	997.475		26.2	989.234		39.2	964.863
20.29	997.451		26.4	988.985		39.4	963.954
20.4	997.121		26.6	988.673		40.2	963.953
20.5	996.678		26.8	988.348		40.25	964.198
20.6	996.497		27	988.009		40.4	964.952
20.62	996.45		27.5	986.998		41	964.953
20.8	996.231		28	985.863		41.5	964.938
21	996.053		28.5	984.569		42	964.798
21.2	995.912		29	983.056		42.5	964.732
21.4	995.791		29.5	981.52		43	964.688
21.6	995.669		30	979.88		43	940

21.7	995.593		30.2	979.454		0	940
21.8	995.491		30.49	979.196		0	995.042
22	995.267		31	977.739			
22.2	995.048		31.5	976.802			
HD = Horizontal distance		E = Elevation					

Appendix C2 External Boundary Coordinates for East Dam Wall Geometry

		CONTINUED 1		CONTINUED 2		CONTINUED 3	
HD	**E**	**HD**	**E**	**HD**	**E**	**HD**	**E**
0	996.099	10.76	995.451	21.68	977.625	28.08	966.265
0.5	996.257	11	995.447	21.69	997.452	28.2	966.645
1	996.257	11.23	995.451	22	976.091	28.24	966.929
1.25	996.205	11.51	995.581	22.5	974.334	28.245	966.933
1.5	996.19	12	995.518	23	972.52	28.25	966.923
1.8	996.166	12.5	995.394	23.1	972.26	28.255	966.935
2	996.231	12.85	995.204	23.33	971.713	28.26	967.055
2.3	997.181	13.17	994.952	23.48	971.623	28.4	967.456
2.5	997.265	13.22	994.882	23.52	971.623	28.51	967.567
3	997.403	13.5	994.771	24	970.928	28.9	967.049
3.2	997.442	14.08	994.451	24.08	970.869	29.54	966.524
3.5	997.3	14.2	994.231	24.21	970.639	29.7	966.43
3.77	997.063	14.27	994.15	24.22	970.581	30.1	965.965
4	997.225	14.47	994.014	24.23	970.514	30.11	965.953
4.2	997.312	14.52	994.007	24.5	969.95	30.65	963.453
4.32	997.312	14.68	993.452	24.75	969.635	31	963.927
4.58	997.249	15	991.578	25	969.122	31.91	966.407
4.72	996.951	15.18	991.008	25.18	968.989	31.93	966.442
4.75	996.905	15.5	990.599	25.25	968.686	32.08	966.114
4.98	996.451	15.78	990.32	25.5	968.232	32.2	966.207
5.21	996.451	15.95	990.094	25.82	967.528	32.45	966.216
5.33	996.655	16.28	989.452	26	967.35	32.52	966.198
5.35	996.747	16.48	989.093	26.28	967.03	36	967.609
5.5	996.821	16.7	988.952	26.35	967.03	36.53	967.953
5.7	996.951	17	988.143	26.5	967.084	36.7	968.034
5.76	997.451	17.5	987.034	26.73	967.412	37	968.297

7.78	997.451	18	985.784	26.75	967.345	37.35	968.525
8.27	996.858	18.5	984.464	26.9	967.952	37.43	968.505
8.46	996.45	19	983.048	26.93	967.976	37.5	968.515
8.6	996.129	19.5	981.645	27	967.979	38	968.678
8.7	996.201	20	980.42	27.05	967.952	38.4	968.895
8.9	995.994	20.49	979.452	27.27	966.574	38.78	968.934
9.15	996.017	20.76	979.452	27.35	966.194	39.5	969.402
9.7	996.237	20.9	980.452	27.37	966.043	40	969.72
10	996.203	21.2	980.452	27.39	966.001	40	950
10.5	995.899	21.5	978.151	27.5	965.983	0	950
10.58	995.877	21.55	977.952	27.9	965.977	0	996.099
HD = Horizontal distance				E = Elevation			

Appendix C3 External Boundary Coordinates for South Dam Wall Geometry

			CONTINUED 1	
HD	**E**		**HD**	**E**
0	995.214		16.75	989.324
0.5	995.244		16.81	989.191
1	995.272		17.01	988.952
2	995.333		17.1	988.271
3	995.403		17.2	987.952
4	995.462		17.5	987.095
5	995.583		17.6	986.951
6	995.747		18	986.388
7	995.917		18.5	985.68
8	996.219		19	984.945
9	996.559		19.3	984.443
10.1	996.951		19.65	983.449
10.52	997.451		19.77	982.952
11	998.181		20.75	981.218
11.5	999.112		21	980.765
12.05	999.951		21.5	979.918
12.5	999.971		22.25	978.863
12.73	999.951		22.5	978.657
13	999.645		23	978.245

13.55	998.451		23.5	977.91
14	997.861		24	977.561
14.38	997.451		24.5	977.34
14.55	996.578		25	977.144
14.65	995.453		25.5	976.935
14.8	994.314		26	976.606
15	994.069		26.5	976.051
15.2	993.683		27	975.546
15.5	992.946		27.18	975.452
15.7	992.453		27.6	974.56
15.85	991.949		27.78	973.952
16	991.792		29	974
16.2	991.451		30	974.101
16.3	990.948		37.5	974.952
16.32	990.621		38	974.952
16.5	990.452		39	974.893
16.6	990.147		40	974.828
16.65	989.952		40	950
16.73	989.454		0	950
			0	995.214

Appendix C4 External Boundary Coordinates for West Dam Wall Geometry

			CONTINUED 1		CONTINUED 2		CONTINUED 3	
HD	**E**		**HD**	**E**	**HD**	**E**	**HD**	**E**
0	995.506		15	998.258	26.5	984.315	40.28	973.744
0.5	995.535		15.1	997.95	27	984.009	40.5	973.814
1	995.562		15.13	997.875	27.5	983.584	40.6	973.851
1.5	995.588		15.5	996.834	28	983.215	40.63	973.898
2	995.614		15.8	996.106	28.5	982.897	40.8	973.453
2.5	995.639		16	995.905	29	982.479	40.85	973.227
3	995.665		16.29	995.452	29.5	982.011	40.9	972.952
3.5	995.693		16.5	995.342	29.7	981.877	41	972.95
4	995.719		17	995.062	29.8	981.786	41.5	972.703
4.5	995.746		17.25	994.951	30	981.654	42	972.41
5	995.773		17.5	993.311	30.05	981.594	42.5	972.155

5.5	995.8	17.9	991.952	30.5	980.464	42.78	971.952
6	995.828	18	991.932	30.75	979.828	42.9	971.639
6.5	995.856	18.5	991.389	31	979.467	43	971.446
7	995.884	19	990.746	31.1	979.416	43.5	971.421
7.5	995.913	19.5	989.925	31.5	979.371	43.6	971.453
8	995.939	19.75	989.453	32	979.418	43.78	972.453
8.5	995.97	20	989.419	32.5	979.469	44	972.406
9	996.038	20.5	989.452	33	979.459	44.5	972.437
9.5	996.105	20.8	989.452	33.5	979.275	44.6	972.454
10	996.172	21	989.094	34	978.949	45	972.785
10.5	996.238	21.3	988.229	34.5	978.598	45.5	973.357
11	996.291	21.5	987.855	35	978.289	46	973.649
11.5	996.331	22	987.134	35.5	977.943	46.5	973.874
12	996.394	22.5	986.572	36	977.434	47	974.102
12.48	996.451	23	986.041	36.5	977.038	47.5	974.377
12.5	996.476	23.5	985.877	37	976.68	47.7	974.453
12.92	996.757	23.75	986.799	37.5	976.29	48	974.453
13	996.772	24	985.802	37.75	976.144	48.5	974.412
13.49	996.951	24.5	985.661	38	976.067	49	974.075
13.5	996.972	24.75	985.526	38.5	975.838	49.1	973.752
13.86	997.451	25	985.333	39	975.451	49.5	972.806
14	997.682	25.25	985.107	39.5	974.789	49.7	972.454
14.5	998.775	25.5	984.807	39.8	974.191	50	972.264
14.65	998.951	25.76	984.475	39.9	974.155	50	950
14.8	998.951	26	984.383	40.05	974.008	0	950
14.92	998.258	26.25	984.371	40.1	973.874	0	995.506
HD = Horizontal distance				E = Elevation			

APPENDIX D

LIMIT EQUILIBRIUM-PROBABILISTIC ANALYSIS RESULTS

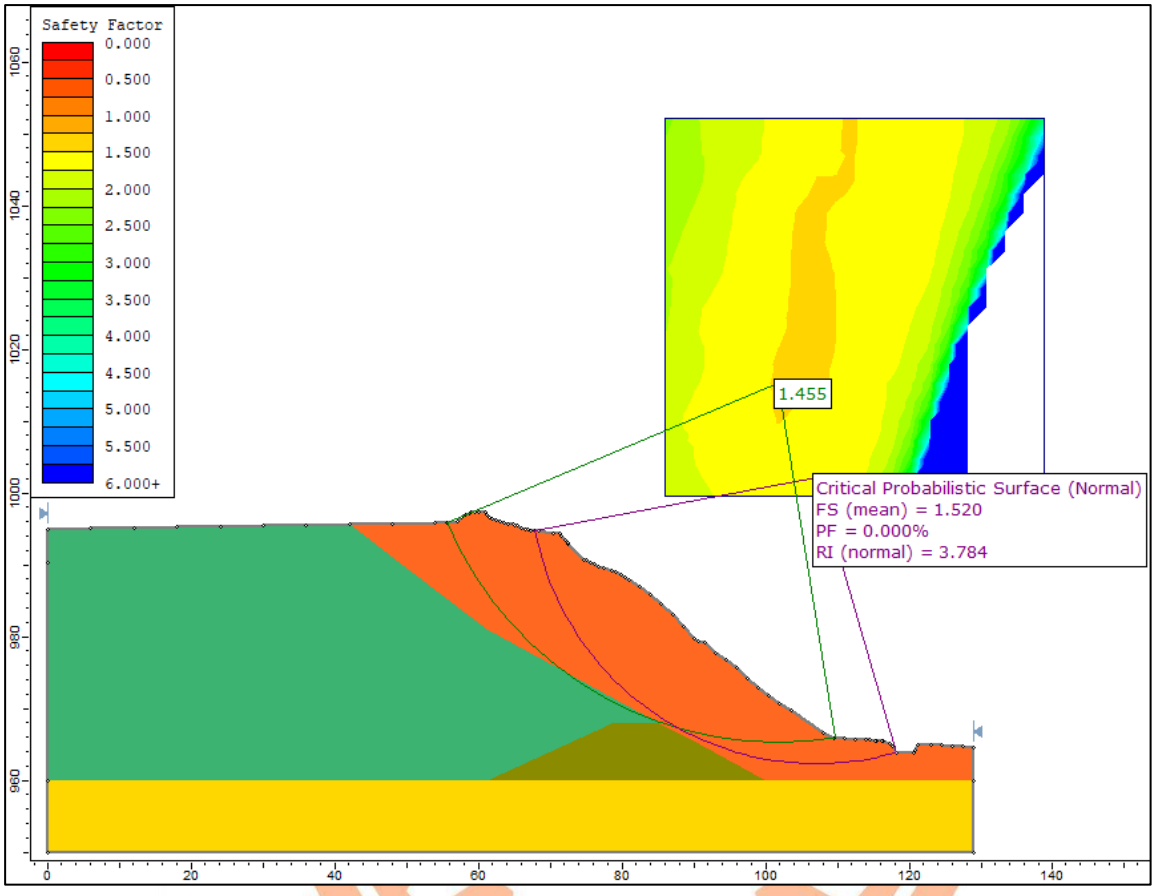

Appendix D1 Limit Equilibrium Probabilistic Analysis Results for North Dam Wall

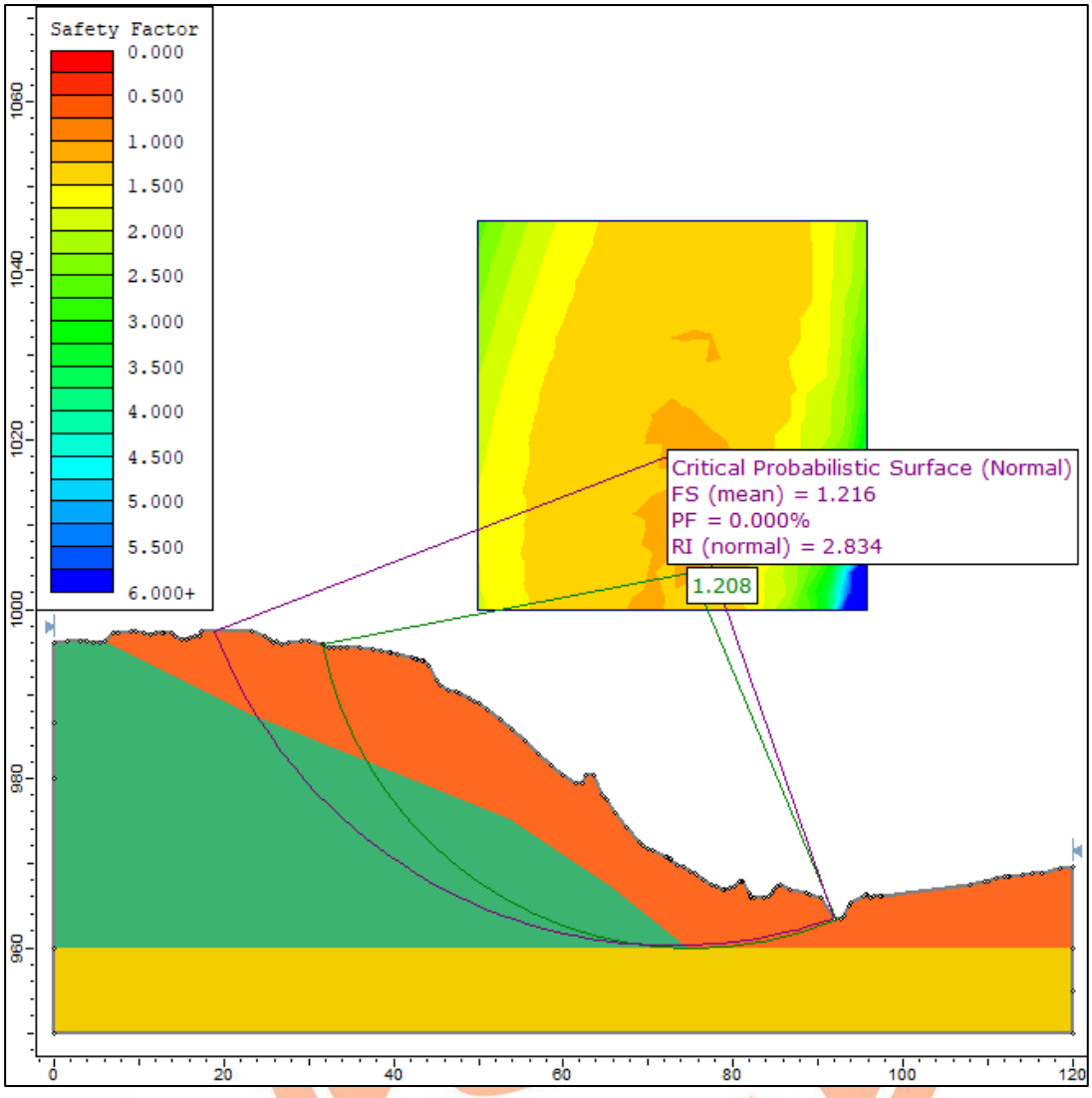

Appendix D2 Limit Equilibrium Probabilistic Analysis Results for East Dam Wall

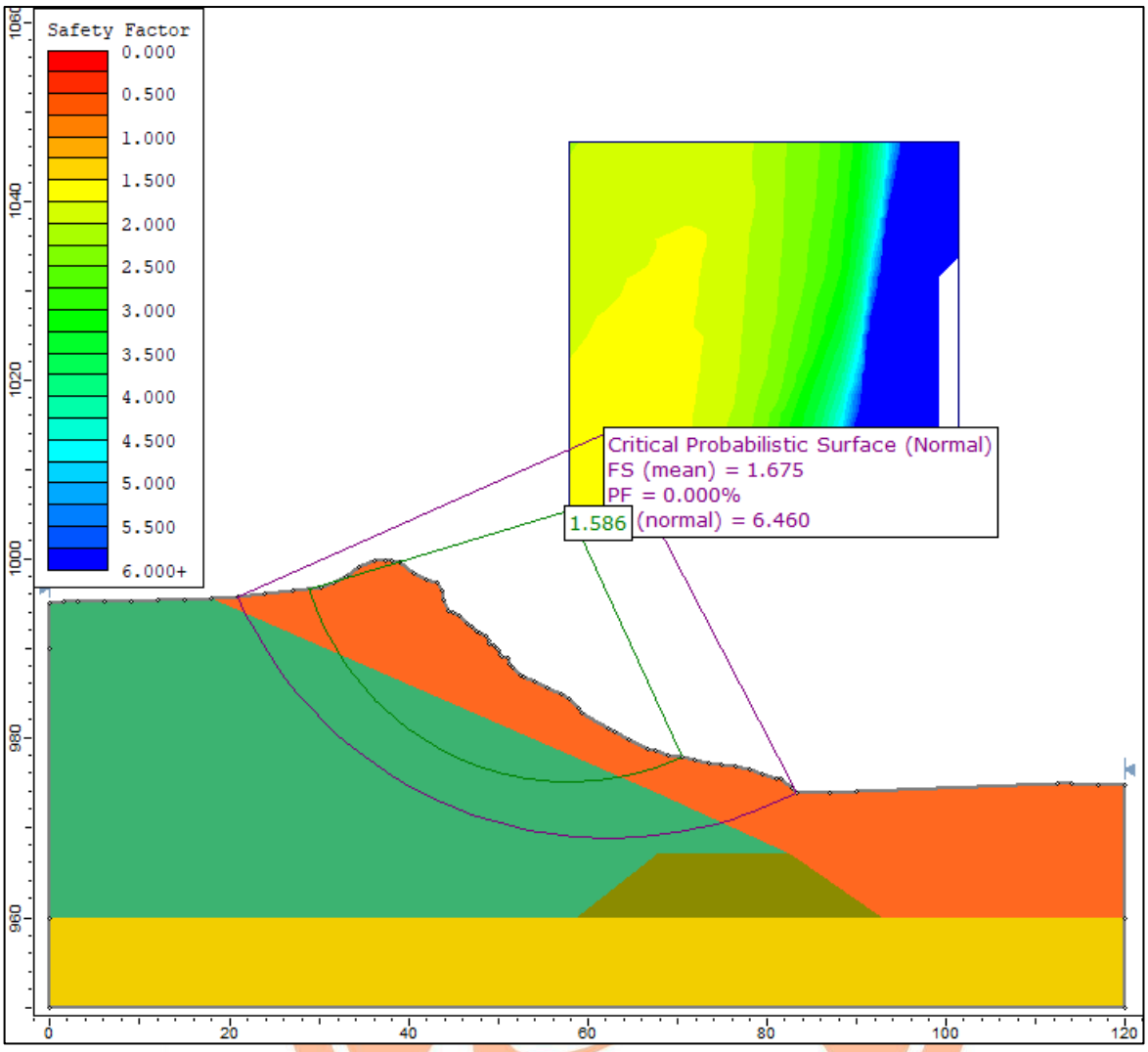

Appendix D3 Limit Equilibrium Probabilistic Analysis Results for South Dam Wall

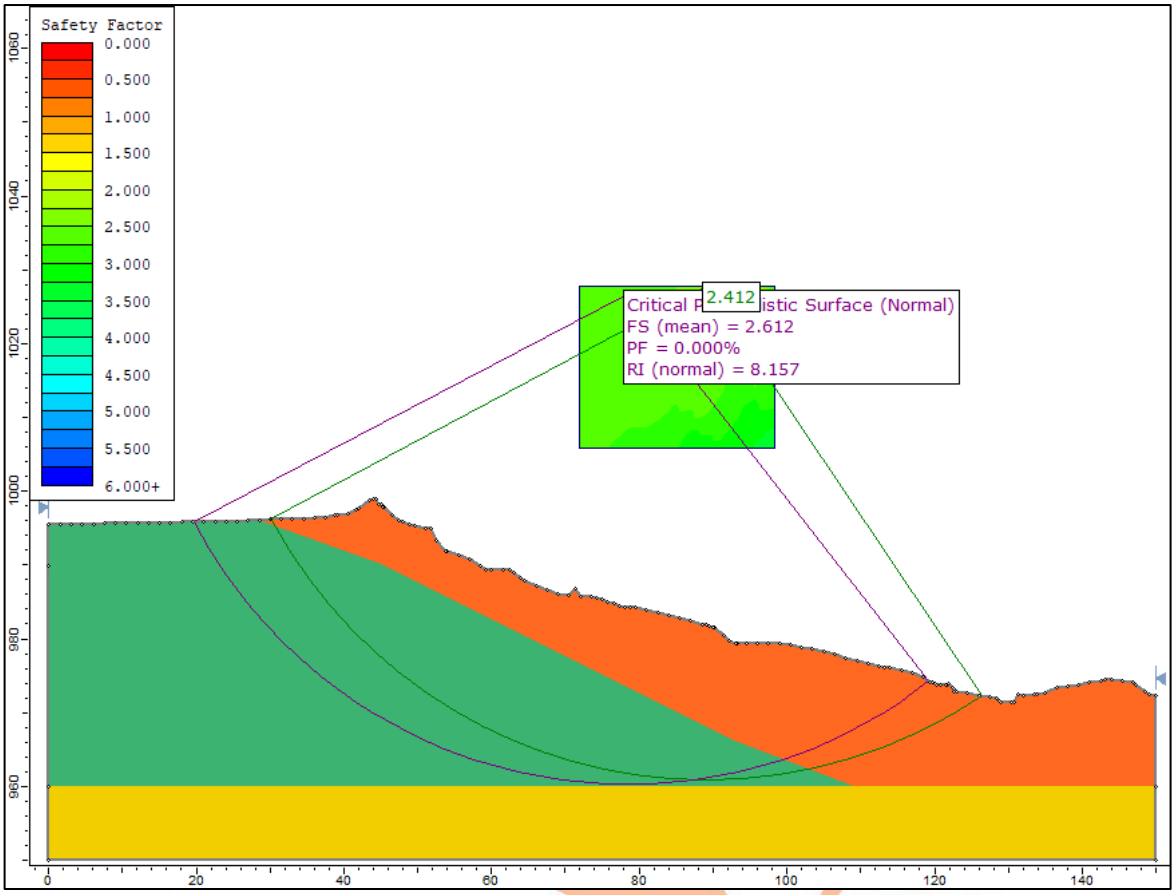

Appendix D4 Limit Equilibrium Probabilistic Analysis Results for West Dam Wall

APPENDIX E

GAUSSIAN PROCESS REGRESSION

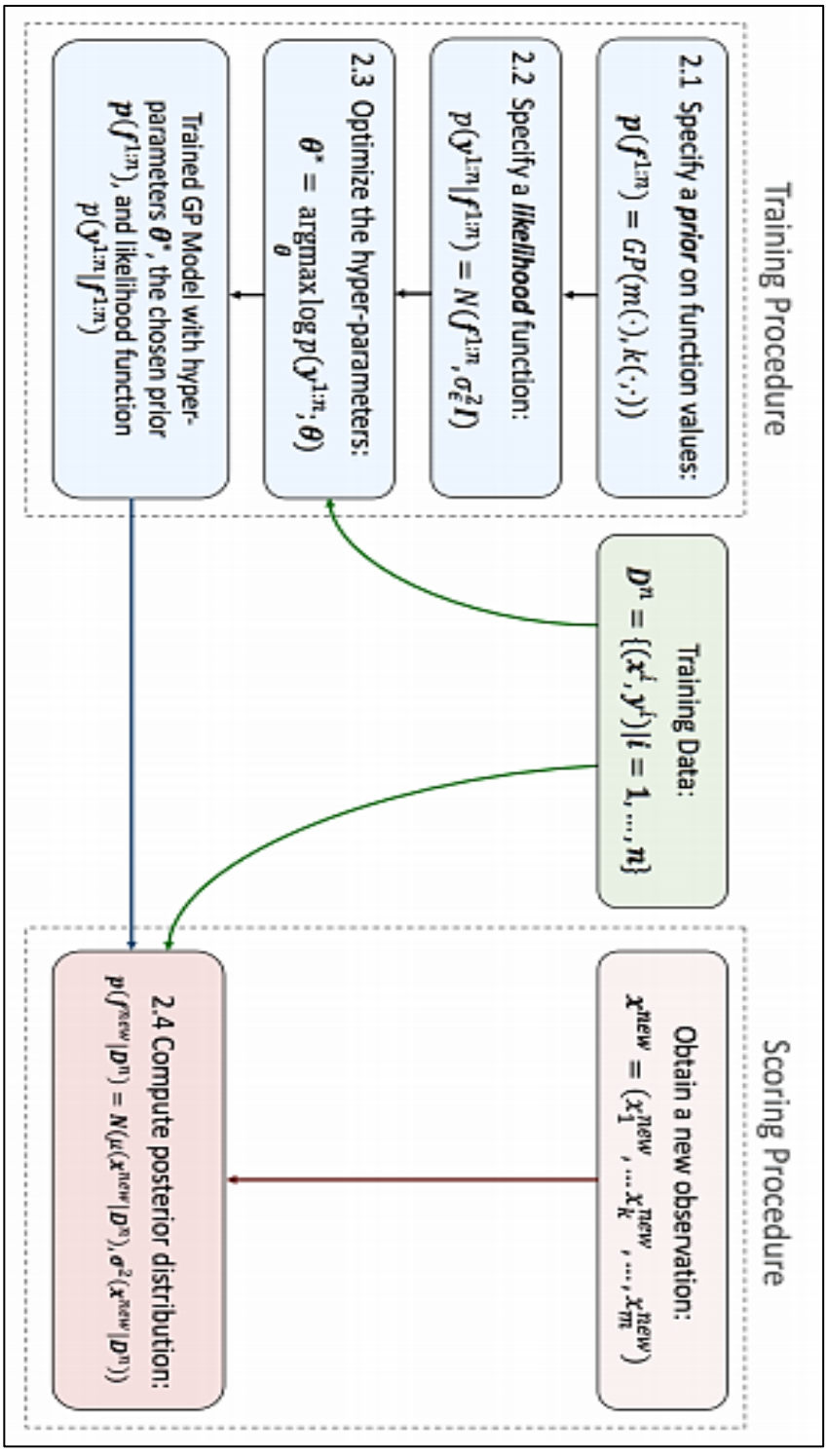

Appendix E1 Flowchart showing GPR Training and Scoring Procedure

Appendix E2 MATLAB R2020a Generated Gaussian Process Regression Model for EAST008-Depth versus Pore Pressure

```
function [trainedModel, validationRMSE] = trainRegressionModel(trainingData)
% [trainedModel, validationRMSE] = trainRegressionModel(trainingData)
% Returns a trained regression model and its RMSE. This code recreates the
% model trained in Regression Learner app. Use the generated code to
% automate training the same model with new data, or to learn how to
% programmatically train models.
%
%  Input:
%      trainingData: A table containing the same predictor and response
%       columns as those imported into the app.
%
%  Output:
%      trainedModel: A struct containing the trained regression model. The
%       struct contains various fields with information about the trained
%       model.
%
%      trainedModel.predictFcn: A function to make predictions on new data.
%
%      validationRMSE: A double containing the RMSE. In the app, the
%       History list displays the RMSE for each model.
%
% Use the code to train the model with new data. To retrain your model,
% call the function from the command line with your original data or new
% data as the input argument trainingData.
%
% For example, to retrain a regression model trained with the original data
% set T, enter:
%   [trainedModel, validationRMSE] = trainRegressionModel(T)
%
% To make predictions with the returned 'trainedModel' on new data T2, use
%   yfit = trainedModel.predictFcn(T2)
%
% T2 must be a table containing at least the same predictor columns as used
% during training. For details, enter:
%   trainedModel.HowToPredict

% Auto-generated by MATLAB on 19-May-2021 09:02:18


% Extract predictors and response
% This code processes the data into the right shape for training the
% model.
inputTable = trainingData;
predictorNames = {'DEPTH'};
```

```
predictors = inputTable(:, predictorNames);
response = inputTable.U2;
isCategoricalPredictor = [false];

% Train a regression model
% This code specifies all the model options and trains the model.
regressionGP = fitrgp(...
    predictors, ...
    response, ...
    'BasisFunction', 'constant', ...
    'KernelFunction', 'rationalquadratic', ...
    'Standardize', true);

% Create the result struct with predict function
predictorExtractionFcn = @(t) t(:, predictorNames);
gpPredictFcn = @(x) predict(regressionGP, x);
trainedModel.predictFcn = @(x)
gpPredictFcn(predictorExtractionFcn(x));

% Add additional fields to the result struct
trainedModel.RequiredVariables = {'DEPTH'};
trainedModel.RegressionGP = regressionGP;
trainedModel.About = 'This struct is a trained model exported from
Regression Learner R2020a.';
trainedModel.HowToPredict = sprintf('To make predictions on a new
table, T, use: \n  yfit = c.predictFcn(T) \nreplacing ''c'' with the
name of the variable that is this struct, e.g. ''trainedModel''. \n
\nThe table, T, must contain the variables returned by: \n
c.RequiredVariables \nVariable formats (e.g. matrix/vector, datatype)
must match the original training data. \nAdditional variables are
ignored. \n \nFor more information, see <a
href="matlab:helpview(fullfile(docroot, ''stats'', ''stats.map''),
''appregression_exportmodeltoworkspace'')">How to predict using an
exported model</a>.');

% Extract predictors and response
% This code processes the data into the right shape for training the
% model.
inputTable = trainingData;
predictorNames = {'DEPTH'};
predictors = inputTable(:, predictorNames);
response = inputTable.U2;
isCategoricalPredictor = [false];

% Perform cross-validation
partitionedModel = crossval(trainedModel.RegressionGP, 'KFold', 5);

% Compute validation predictions
validationPredictions = kfoldPredict(partitionedModel);

% Compute validation RMSE
validationRMSE = sqrt(kfoldLoss(partitionedModel, 'LossFun', 'mse'));
```